Supramolecular Helical Arrangement of Porphyrins Along DNA

A thesis submitted in the partial fulfilment
of the requirements for the degree of

Doctor of Philosophy
in Chemistry

Massey University,
Palmerston North, New Zealand

Adam Wayne Ian Stephenson

2010

Abstract

Porphyrins are useful chromophores and have been used in numerous biological applications including light harvesting, oxygen transport and energy transfer. DNA is a perfect template for the controlled assembly of organic chromophores. By combining DNA and porphyrins in a controlled manner we have developed a novel range of porphyrin-DNA supramolecular constructs for future applications in nanobiotechnology.

A number of β-pyrrolic functionalised porphyrin precursors were synthesised to be used as building blocks in the construction of both covalently and non-covalently modified DNAs. Using these porphyrins we have created several lipophilic porphyrin-DNA complexes through non-covalent attachment methods. Using a Cu^{I} catalysed azide alkyne cycloaddition (CuAAC) reaction of azido functionalised porphyrins we have developed a versatile approach for the covalent, site specific internal porphyrin insertion into oligonucleotides in a post-synthetic manner. We have investigated a number of duplex structures where porphyrins were located in the major or minor grooves of the duplex. Additionally, porphyrins were studied as intercalating moieties when they were inserted as a bulge in the middle of the duplexes or parallel triplexes. Additionally, when porphyrins were placed in both strands of the duplex they formed a zipper type structure in the minor groove. This resulted in a significant increase in the duplex thermal stability due to the formation of porphyrin H-aggregates. UV-Vis and CD spectroscopy as well as molecular modelling were used to help understand the interactions between porphyrins in the duplex.

These findings lay the foundation for the future design of artificial DNA-chromophore supramolecular architectures and for their applications in material science and nanotechnology.

Acknowledgements

I would like to firstly thank my supervisors Associate Professor Ashton Partridge and Dr Vyacheslav Filichev for their support and assistance throughout the duration of this project. Especially Vyacheslav for the enthusiasm he showed towards the project and the time taken to show me various techniques used in DNA chemistry. Thanks also to Niels Bomholt for his assistance with the DNA modelling of porphyrin modified oligonucleotides.

Thanks to all former and present colleagues in the NRC and MacDiarmid Centre of Advanced Materials and Nanotechnology for their assistance over the years. Especially Dr Wayne Campbell for his help with DSSCs and Dr Pawel Wagner for solving X-ray crystal structures. I am also grateful for the assistance of departmental staff over the years I have been at Massey University.

I would like to acknowledge important financial support from the Marsden grant administrated by the Royal Society of New Zealand (grants MAU0407, MAU0704).

Finally, a big thanks to family and friends for their support over the past few years and putting up with the mood swings associated with research and writing.

Table of Contents

Chapter 4: Construction of Lipophilic Porphyrin-DNA Complexes

Chapter 5: Covalent Attachment of Porphyrins to DNA

Chapter 6: Porphyrin H-Aggregate Formation in the Minor Groove of the Duplex

List of Figures

List of Tables

Abbreviations

A	adenosine
ACN	acetonitrile
AcOH	acetic acid
aq	aqueous
Ar	aromatic
ATR	Attenuated total reflection
BHT	2,6-bis(1,1-dimethylethyl)-4-methylphenol
BIAB	[bis(acetoxy)iodo]benzene
bp	base pair
br	broad
C	cytosine
Calcd	calculated
CD	circular dichroism spectroscopy
$CDCl_3$	deuterated chloroform
conc	concentrated
COSY	correlation spectroscopy
CPG	controlled porous glass
CTAB	cetyl trimethylammonium bromide
CuAAC	Cu^I catalysed Huisgen 1,3-dipolar azide alkyne cycloaddition
d	doublet
dA	2′-deoxyadenosine
Da	daltons
DBU	1,8-diazabicyclo[5.4.0]undec-7-ene
dC	2′-deoxycytosine
DCE	1,2-dichloroethane
DCM	dichloromethane
DDQ	2,3-dichloro-5,6-dicyanobenzoquinone
DFT	density functional theory
dG	2′-deoxyguanosine
DMAP	4-dimethylaminopyridine
DMEA	N,N'-Dimethyl-1,2-ethanediamine

DMF	*N*,*N*-dimethylformamide
DMT	4,4′-dimethoxytrityl
DMSO	dimethyl sulfoxide
DNA	deoxyribonucleic acid
DSSC	dye sensitised solar cell
EDC	1-ethyl-3-(3-dimethylaminopropyl) carbodiimide
EDTA	ethylenediaminetetraacetate acid
eq	equivalent
ESI	electrospray ionisation
EtOH	ethanol
FAB	fast atom bombardment
FF	fill factor
G	guanosine
GQ	guanosine quadruplex
h	hour(s)
HOMO	Highest occupied molecular orbital
HPLC	high preformance liquid chromatography
HRMS	high resolution mass spectrometry
IR	infra-red spectroscopy
ITO	indium tin oxide
J_{sc}	short circuit current
L	litres
LHCP	left hand circularly polarised
LNA	locked nucleic acid
LRMS	low resolution mass spectrometry
LUMO	Lowest unoccupied molecular orbital
m	multiplet
M	mol/L
MALDI	matrix assisted laser desorption ionisation
MeOH	methanol
min	minute
mL	millilitres
mmol	millimole
NBS	*N*-bromosuccinimide

NMR	nuclear magnetic resonance
ON	oligodeoxynucleotide
PAGE	polyacrylamide gel electrophoresis
PCC	pyridinium chlorochromate
Ph	phenyl
ppm	parts per million
R_f	retention factor
RHCP	right hand circularly polarised
RT	room temperature
s	singlet
t	triplet
T	thymidine
T_a	annealing temperature
TBAF	tetrabutyl ammonium fluoride
T_d	denaturing temperature
TFO	triplex forming oligonucleotide
TEAA	triethylammonium acetate
TEMPO	2,2,6,6-tetramethylpiperidine-1-oxyl
THF	tetrahydrofuran
TINA	twisted intercalating nucleic acid
TLC	thin layer chromatography
T_m	melting temperature
TMPyP	tetrakis[4-(*N*-methylpyridiumyl)]porphyrin
TMS	tetramethylsilane
TOF	time of flight
TPP	5,10,15,20-tetraphenylporphyrin
$TPPCH_3$	2-methyl-5,10,15,20-tetraphenylporphyrin
TPPCHO	2-formyl-5,10,15,20-tetraphenylporphyrin
TPPps	TPP phosphonium salt
U	uridine
UV-Vis	ultraviolet-visible spectroscopy
V_{oc}	open circuit voltage
µL	microlitres
µmol	micromole

Chapter 1 Introduction

1.1 Porphyrins

Porphyrin type compounds are found throughout nature where they are employed in a myriad of biological roles such as oxygen transport, reaction catalysts, electron transfer, energy transfer and light harvesting.[1] Porphyrins consist of four pyrrole rings linked *via* methylene groups to give a fully conjugated ring system. The most simple version of the porphyrin family is the porphin molecule depicted in Figure 1.1 including the standard nomenclature (A) used to locate the substituents attached to the porphyrin structure, and the standard numbering system (B). A commonly used porphyrin is 5,10,15,20-tetraphenylporphyrin (TPP, C), consisting of four phenyl rings in the *meso* positions, which are orthogonal to the plane of the porphyrin core.

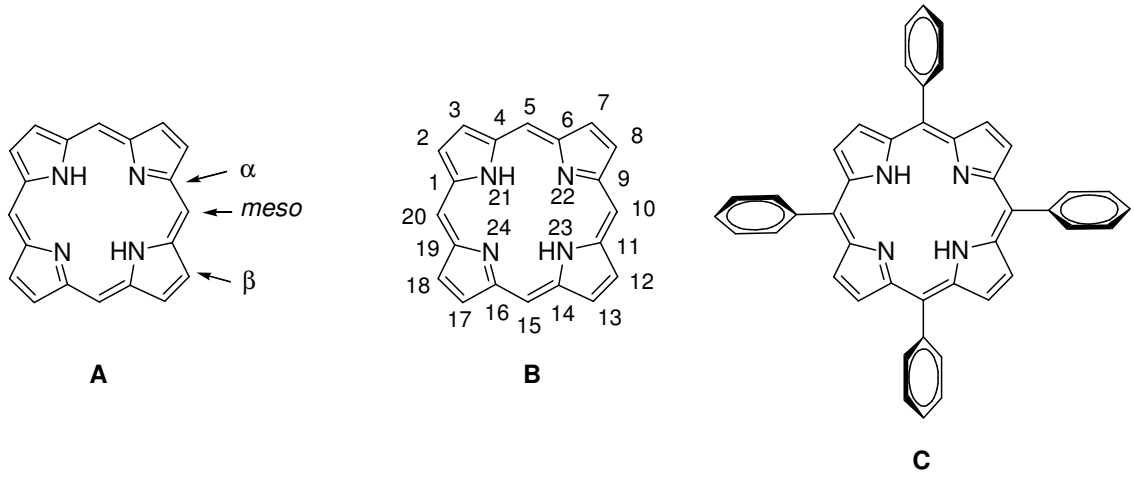

Figure 1.1 Structure of the porphyrin showing labelling (A) IUPAC numbering (B) the orthogonal *meso* rings (C).

The nitrogens of the porphyrin can either be protonated (more commonly known as the free base, Figure 1.2, A) or deprotonated (Figure 1.2, C) and exist in two tautomeric forms (Figure 1.2, A and B). On deprotonation, a cavity is formed that is of the ideal size to allow the binding of most metals. Porphyrins, which are approximately flat, are highly aromatic, however, only 18 of the π electrons can exist in an internal aromatic ring, with the peripheral double bonds being isolated. On metallation (Figure 1.2, D), there exists both an internal and an external aromatic ring system. It is the aromaticity of

the porphyrin molecule that gives it its high thermodynamic stability, a high molar absortivity coefficient and the ability to have its electronic properties tuned by the binding of different metals.

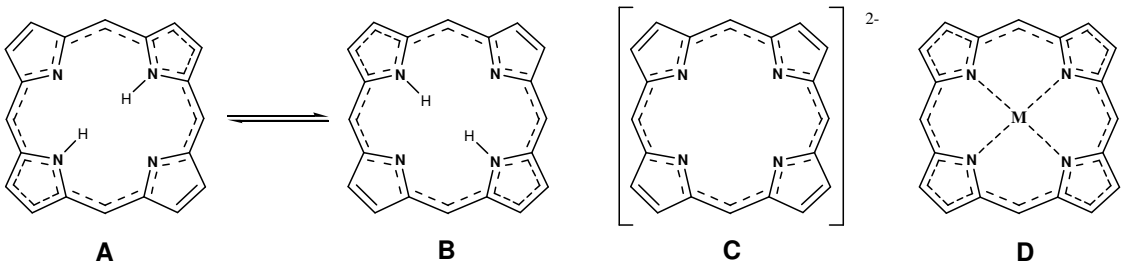

Figure 1.2 Aromaticity and tautomeric forms in the free-base (A and B), dianionic (C) and metallated (D) forms of the porphyrin.

Porphyrins are highly coloured and have characteristic electronic absorption spectra. Figure 1.3 shows the UV-visible spectrum for 5,10,15,20-tetraphenylporphyrin (TPP) and its Zn^{II} analogue, as an example of a typical electronic spectrum for a porphyrin molecule. The components include a strong Soret (or B) band (due π-π^* transitions) commonly between 400 – 420 nm and weaker Q bands (four in free base porphyrins and two in metalled porphyrins) between 520-600 nm. Modification of the porphyrin at one of the β-pyrrolic positions results in decreased intensity and broadening of the Soret band.[2] In general, porphyrins are also strongly fluorescent. This fluorescence (which usually occurs at approximately 650 nm) is dependent on a number of factors including metallation, for example, Zn^{II} and free base porphyrins are highly fluorescent while Ni^{II} porphyrins are virtually non-fluorescent.

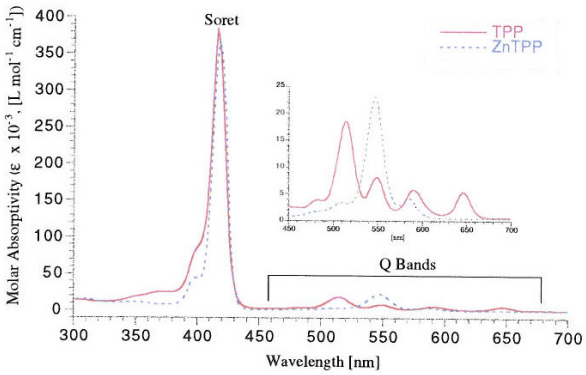

Figure 1.3 UV-Vis absorption spectrum of ZnTPP in dichloromethane showing the Soret and Q bands (reproduced from Campbell).[3]

1.1.1 Porphyrins and DNA

DNA is a perfect template or scaffold for the creation of functional π systems as it has a number of favourable characteristics such as:[4-6]

- The spontaneous self assembly of oligonucleotides with complementary sequences.
- The duplex has a well known and characteristic structure. In B DNA the base pair distances along the helical array is 3.4 Å providing the ideal basis with for π stacking.
- DNA is relatively easy to synthesise with predictable positioning of organic chromophores in various DNA secondary structures.
- There are a number of alternative methods to covalently and non-covalently bind molecules to the DNA structure.

Porphyrins make an ideal π system to be incorporated into DNA due to the large aromatic structure and the ability to tune the electronic properties of the complex by implementing small variations in the porphyrin. Therefore, in this thesis we discuss the construction of novel porphyrin-DNA supramolecular structures for the future development of various nanotechnological applications.

1.2 Deoxyribose Nucleic Acids - DNA

Nucleic acids consist of simple units called nucleotides which consist of a phosphate group and nucleosides (Figure 1.4). The latter consists of a pentafuranose ring which is ribofuranose for RNA and 2′-deoxyribofuranose for DNA. The four bases found in DNA are heterocyclic compounds of two types: purines and pyrimidines. Adenine (A) and guanine (G) are purines, and cytosine (C) and thymine (T) are pyrimidines. A fifth base called uracil (U) replaces thymine in RNA. Nucleosides are joined together by phosphate groups that form phosphodiester bonds between the third and fifth carbon atoms in the sugar ring. It is this asymmetry around the phosphates that gives directionality to the strands.[4]

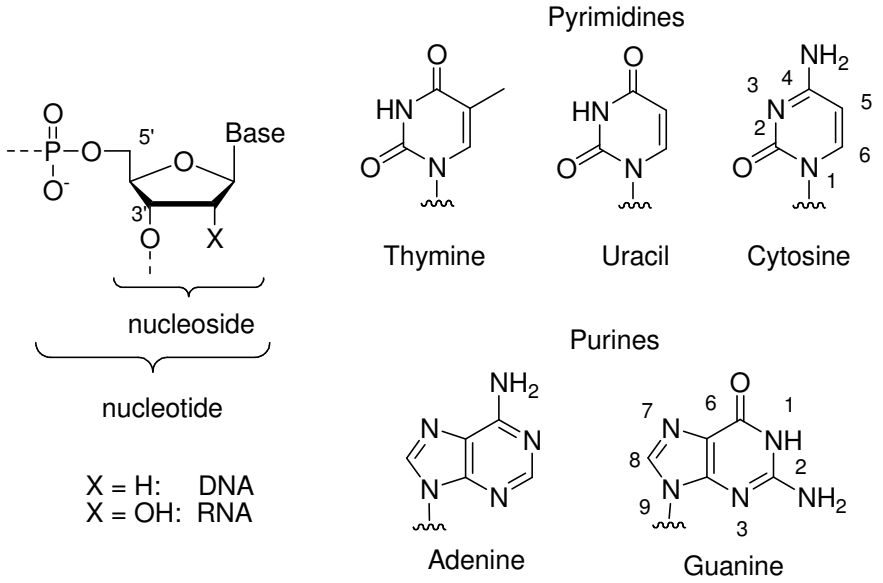

Figure 1.4 Nucleotides in DNA and RNA.

As a result of Watson-Crick hydrogen bonds (Figure 1.5), π-π stacking and electrostatic repulsion between the negatively charged phosphates in the DNA forms a helical structure. Depending on the sequence and the media, the duplex can exist in various conformations from the most commonly found right handed spiral B form, to the compact A form and the left handed Z form (Figure 1.6). The B form duplex forms two grooves, the major groove (22 Å wide) and the minor groove (12 Å wide). The size of the grooves means that the bases are more accessible in the major groove.

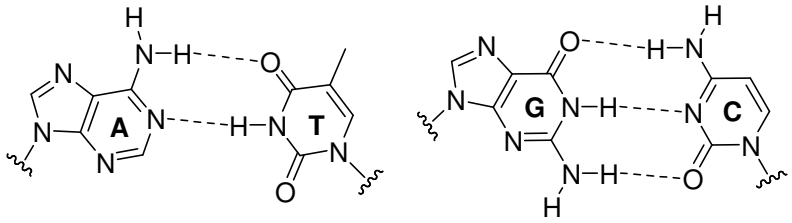

Figure 1.5 Watson-Crick hydrogen bonding in DNA.

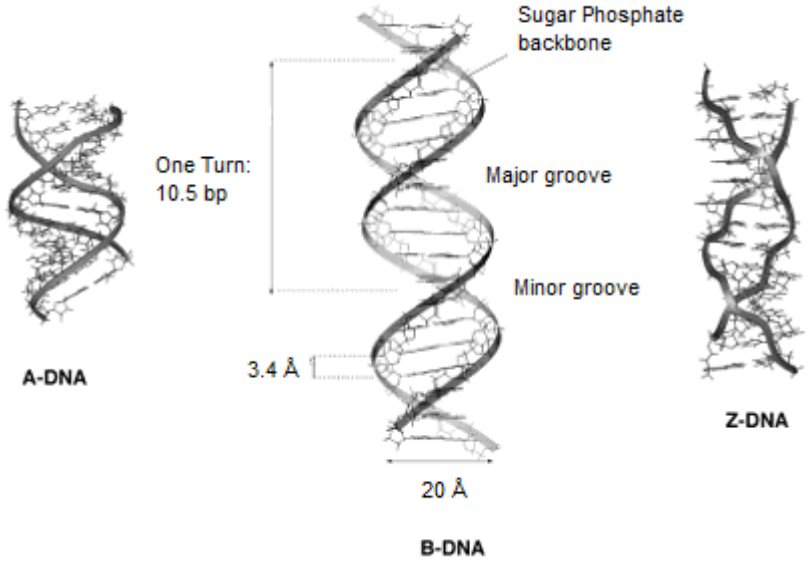

Figure 1.6 A, B and Z DNA.

DNA does not exist exclusively as a duplex but can also form various secondary structures. Watson-Crick hydrogen bonds form the above mentioned antiparallel duplex but alternative Hoogsteen base pairing allows for the formation of triplex and quadruplex structures. It is these structures that might be responsible for the regulation of some genes.[7]

A triple helix is formed when a third single stranded oligonucleotide binds in the major groove of the duplex (Figure 1.7). This third strand is commonly referred to as the triplex-forming oligonucleotide or TFO strand. As illustrated in Figure 1.7, triplexes are formed when the bases of the TFO strand form Hoogsteen or reverse Hoogsteen hydrogen bonds with the purine bases already involved in Watson–Crick base pairs. The directionality of the TFO strand gives rise to parallel and anti-parallel triplexes.[4] A homopyrimidine TFO binds in a parallel fashion (*i.e.* the same 5′ to 3′ orientation) to the homopurine strand in a DNA duplex. This is achieved by forming T-A··T and C-G··C^+ Hoogsteen interactions (··), and requires the protonation of the N-3 atom of cytosine in the TFO. The pK_a of the imino group of the cytosine (5.2) is well below that of physiological pH making parallel triplex formation pH dependent. Alternatively, triplexes can be formed from a homopurine (GA) TFO strand in a parallel or antiparallel fashion.

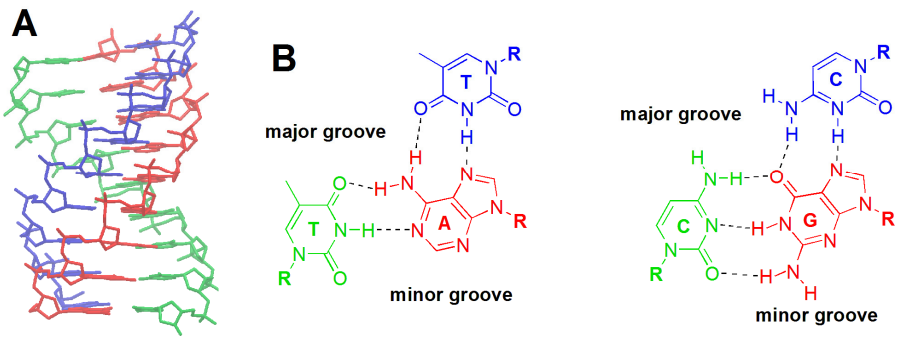

Figure 1.7 Structure of triplex DNA showing the TFO strand in blue (A), and the Hoogsteen base pairing in the TFO strand (B).

Guanosine quadruplex (GQ) is a unique secondary structure that can form at physiological pH and salt concentrations in sequences containing adjacent guanine residues (Figure 1.8). Hoogsteen interactions allow for the formation of intra or intermolecular quadruplexes that can exist in a variety of topologies based on strand polarity, the concentration of metal ions, length of sequence *etc*.[7]

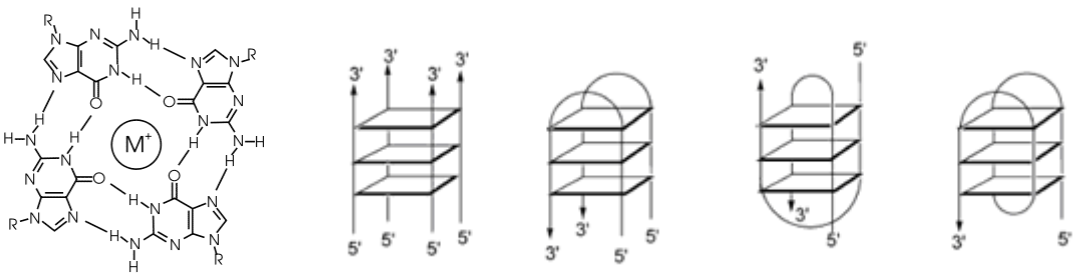

Figure 1.8 Hoogsteen type hydrogen bonding in a G-quartet (left) and different topologies of G-quadruplexes.

1.3 Methods for Studying DNA Secondary Structures

There are three main techniques for the investigation and characterisation of oligonucleotides: gel electrophoresis, UV-Vis spectroscopy and circular dichroism (CD) spectroscopy.

1.3.1 Gel Electrophoresis

Gel electrophoresis is a technique used for the separation and characterisation of DNA. DNA will migrate through a gel towards the positive electrode in the presence of a current, based on size, charge and topology of the strands. Shorter oligonucleotides

migrate faster through the gel than longer ones as it is easier for them to travel through the pores of the gel. Gels can be constructed from various polymers depending on the size of the DNA, the most common being agarose (> 150 nucleotides) and polyacrylamide (< 150 nucleotides) gels. Polyacrylamide gel electrophoresis (PAGE) can be performed under denaturing or non-denaturing conditions depending on the information that is desired. The addition of urea and formamide to a gel and oligonucleotide results in the loss of secondary structure of the DNA (denaturing), whereas non-denaturing gels retain the structure and topology on the DNA strands. As DNA only absorbs in the UV region, visualisation is generally achieved through the staining of the oligonucleotides with a visible dye.

1.3.2 UV-Vis Spectroscopy

The main tool for determining the effect of a modification on DNA is to measure the thermal stability of the secondary structure. On heating of a structure, be it a duplex, triplex or other secondary structure, disordering of the DNA occurs resulting in hyperchromicity at 260 nm. From the change in absorbance, we are able to determine the temperature of melting (T_m), or more accurately, the temperature of midtransition. This is the point at which half the oligonucleotides exist as a single strands and half as the secondary structure (Figure 1.9).

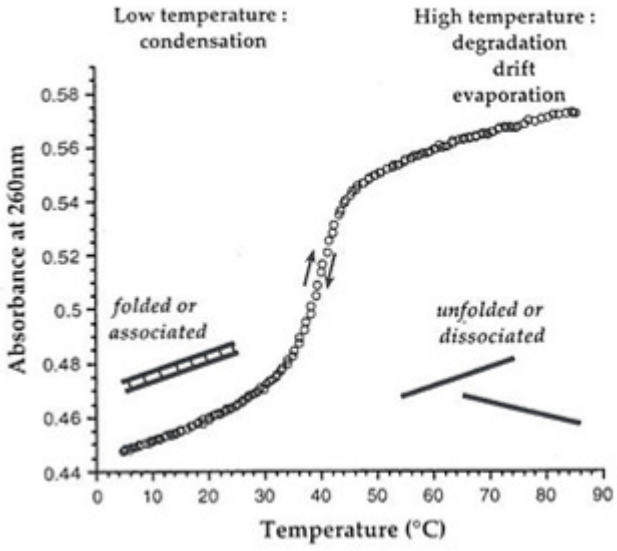

Figure 1.9 UV melting of duplex DNA (reproduced from Mergny *et al.*).[8]

There are a number of methods to determine the T_m of DNA secondary structure and two of these are shown in Figure 1.10A. In this report we employed the most common of the two methods where the T_m is the maximum of the first derivative of the melting curve. This is the more effective method when complex transitions, such as the melting of a triplex, is being determined (Figure 1.10B). An alternative method involves drawing baselines at the top and the bottom of the curve, a median line is then placed between these lines. The point at which the median line intersects the melting curve is the T_m. In general, only small difference in the calculated T_m is produced using either method.

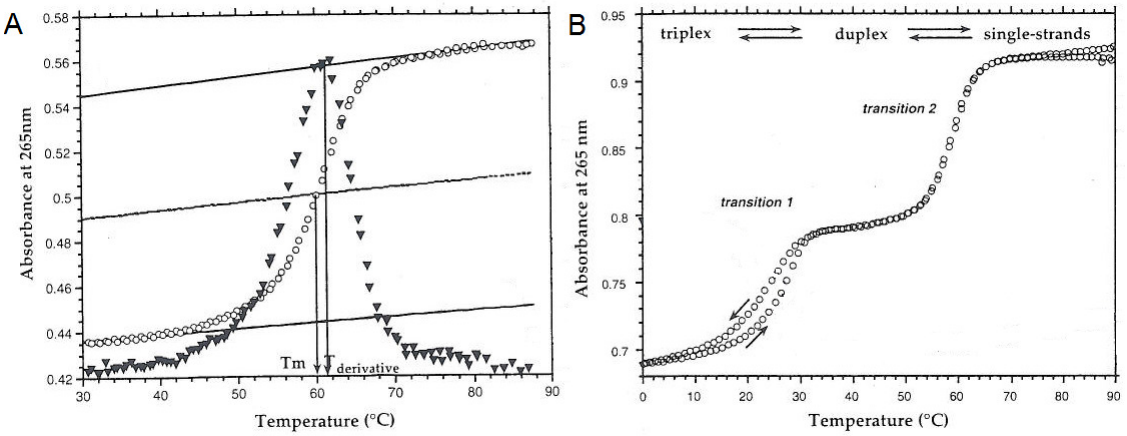

Figure 1.10 A) Determination of the T_m value using either the maximum of the first derivative (triangles) or the median method. B) Typical melting curve of a parallel triplex. (Reproduced and adapted from Mergny *et al.*).[8]

In some instances the DNA does not always display the same midtransition temperature during the melting and annealing processes, giving rise to hysteresis. Hysteresis is common in some secondary structures more than others, such as in the melting and annealing of triplexes. Generally, hysteresis can be overcome by heating and cooling the duplex at a slower rate. It is possible to gather thermodynamic information on a duplex by measuring T_m values at various DNA concentrations, providing no hysteresis occurs.[8]

Insertion of organic chromophores into DNA leads to the formation of additional peaks in the UV-Vis spectra at the wavelengths of chromophoric absorption. Attachment of several chromophores onto DNA gives rise to complex interacts between aromatic moieties, such as H- and J-aggregates, resulting from excitonic coupling.

1.3.3 Exciton Coupling

Exciton coupling is an important tool for understanding the relative conformation of closely located molecules, especially when combined with UV-Vis and circular dichroism spectroscopy. According to exciton coupling theory,[12] a molecule can be excited from the ground state (GS) to an excited state (E) by a photon of an appropriate wavelength. As a result, the distribution of electrons in the excited state differs to that of the ground state thus creating an electric transition dipole (μ). This dipole is described by a vector that corresponds to the direction of the electron movement and its strength is dependent on the nature of the transition occurring.

Although the direction of the transition dipole has been well studied in *meso* functionalised porphyrins,[9] the direction is less well defined in β-pyrrolic substituted porphyrins. Thus in the absence of DFT calculations we must make assumptions to determine the direction of the dipole. By observing the relative contributions and location of the HOMO and LUMO levels in similar β-pyrrolic modified porphyrins,[10, 11] where the HOMO is located on the porphyrin core and the LUMO is located on the β-pyrrolic phenyl moiety, we can assume that the electric dipole vector runs along the axis of the β-pyrrolic modification as shown in Figure 1.11.

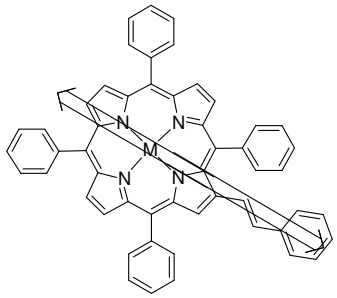

Figure 1.11 Proposed direction for the transition dipole moment (μ) vector in a β-pyrrolic modified porphyrin.

If multiple molecules are located in close proximity and are of similar energy levels then the excitation can be delocalised over both molecules, resulting in exciton coupling. As a result of this interaction, a pair of degenerate excited states results in two nondegenerate excited states (E′ and E″) which are of higher and lower energies compared to the original excited state (Figure 1.12).

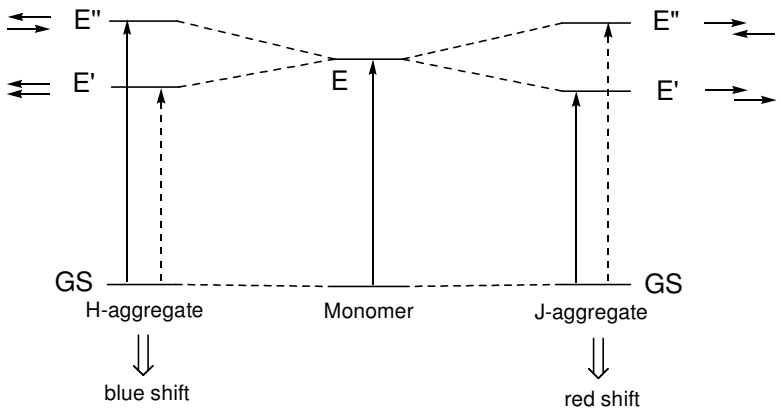

Figure 1.12 Schematic representation of the relationship between chromophore arrangement and spectral shift based on the molecular exciton theory. The solid arrow represents allowed transitions and the dashed arrow represents forbidden transitions.

These excited states are a combination of the relative directions of the dipoles in the excited molecules, either being in phase or out of phase, with out of phase motions being forbidden on electrostatic grounds. The difference between the excited and the ground states energy levels results in either a hypsochromic shift (H-aggregates, Figure 1.13A) or a bathochromic shift (J-aggregates, Figure 1.13B) in the UV-Vis spectra.[12]

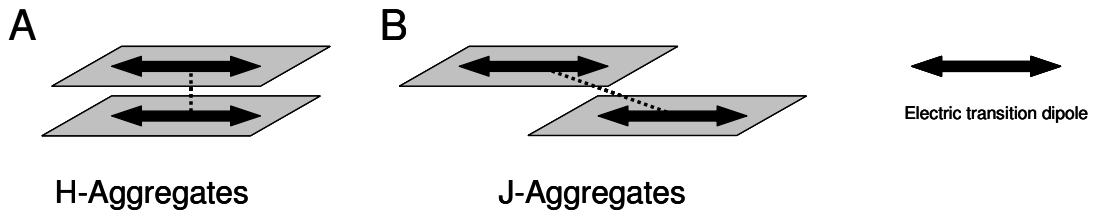

Figure 1.13 A) Schematic representation of H-aggregates showing face-to-face stacking of molecules with the transition dipoles located parallel to the lines joining their centres. B) Schematic representation of J-aggregates showing head-to-tail stacking of molecules with the transition dipoles located parallel to each other but perpendicular to the lines joining their centres.

1.3.4 Circular Dichroism (CD) Spectroscopy

Circular dichroism (CD) spectroscopy is a key technique for obtaining information into the structure of DNA.[13] This is achieved by studying the shape and intensity of the UV region (200-350 nm) where the DNA bases absorb the light. Information can be gathered to give an indication about the conformation of the DNA, such as B, Z, or A duplexes, G-quadruplexes, triplexes or other DNA secondary structures.[13] Circular

dichroism spectroscopy is a system that measures the difference in absorption of left handed (LHCP) and right handed circularly polarised (RHCP) light that originates from the interactions of chiral molecules (or molecules that have induced chirality) with circularly polarised electromagnetic radiation.[14] The difference in the absorption of LHCP and RHCP light can give rise to either positive or negative peaks in the CD spectrum (Figure 1.14A, Soret band region) which occur at the wavelength that the light is absorped. These positive and negative CD signals are called Cotton effects. Like those observed in UV-Vis spectroscopy, exciton coupling can occur when two chromophores with similar excited state energy levels are located in close proximity. Both the E′ and E″ excited states absorb LHCP and RHCP light to different extents resulting in two Cotton peaks of opposite signs, centered at λ_{max} of the monomer. The resulting observed signal is the sum of the Cotton effects which gives rise to bisignate curves as shown in Figure 1.14B and C. The sign of which is dependent on the relative orientation of the transition dipoles.

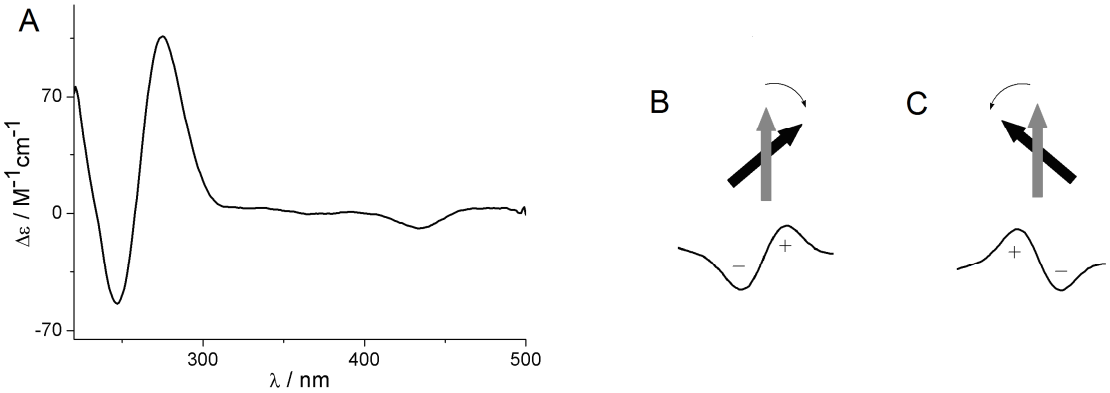

Figure 1.14 A) CD spectra of duplex B DNA exhibiting a Cotton effect signal in the porphyrin Soret band region. B) A positive CD bisignate curve resulting from exciton coupling of dipoles that are in a clockwise orientation. C) A negative CD bisignate curve resulting from exciton coupling of dipoles that are in an anticlockwise orientation.

1.4 Automated DNA Synthesis

Automated DNA synthesis allows for the rapid production of oligonucleotides up to 200 bases in length. Unlike DNA synthesis in nature, automated DNA synthesis occurs in the 3′ to 5′ direction and is achieved through the stepwise addition of nucleoside phosphoramidites or H-phosphonates to each other in a controlled manner. Construction is based on controlled porous glass (CPG) or polystyrene supports, which allows for removal of excess reagents by filtration and eliminates the need for purification steps between base additions.

The synthetic cycle is shown in Figure 1.15 and begins with a 3'-hydroxyl nucleoside attached to the support by a base sensitive linker. This nucleoside contains a 4,4′-dimethoxytrityl (DMT) protecting group which is cleaved with trichloroacetic acid, providing a free 5'-hydroxyl for the next coupling reaction (step 1). An activated trivalent phosphoramidite derivative is then added reacting with the free 5'-hydroxyl on the primary nucleotide to create a phosphite bond (step 2). Activation occurs with the simultaneous addition of 1H-tetrazole, protonation the 3′-*O*-phosphoramidite and promoting faster coupling with the 5′-OH of the nucleoside on the support. Self condensation of the activated nucleotide is prevented by the protection of the 5′-OH with DMT. Generally the elongation occurs in a quantitative yield, however, any chains that do not undergo coupling are capped with acetic anhydride and 1-methylimidazole (step 3). The phosphite linker is then oxidised to phosphotriester by the addition of iodine and water (step 4), and the cycle is continued until the desired chain length is obtained (step 5). When the desired length is obtained the oligonucleotide is cleaved from the support with a strong base (usually concentrated NH_4OH), which also removes the 2′-cyanoethyl groups from the phosphates and any protecting groups that are on the nucleobases (step 6). This desired oligonucleotide can be purified from any short oligonucleotide sequences using techniques such as reverse-phase or ion-exchange HPLC or denaturing gel electrophoresis.

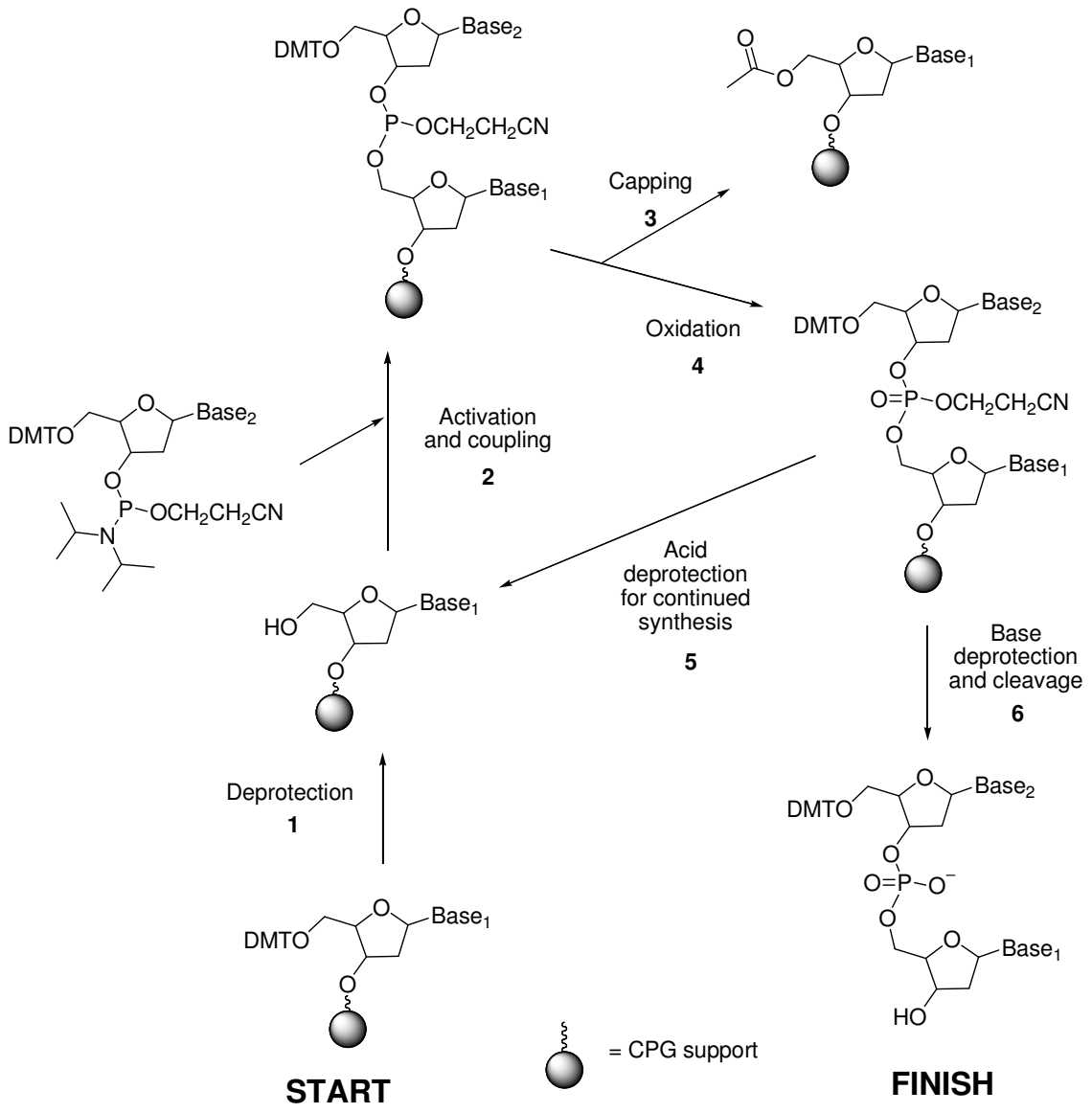

Figure 1.15 Automated DNA synthesis.

1.5 Incorporation of Porphyrins into DNA

Many organic molecules have already been incorporated into DNA using various chemical techniques as covered in the reviews of Filichev,[4] Wagenknecht[5] and Häner.[15] In this thesis we focus specifically on the incorporation of porphyrins into DNA.

The incorporation of porphyrins into DNA is not a novel concept. Various methods have been used successfully to construct supramolecular DNA-porphyrin complexes using two basic approaches – covalent and non-covalent attachment. Non-covalent

attachment of cationic porphyrins to DNA is a reasonably well investigated field, however, covalent attachment has been studied less extensively. Current covalent methods are scarce and focus on the attachment of porphyrins *via* the *meso* position. It is thus the goal of this thesis to lay the foundation for the development of novel *β*-pyrrolic functionalised porphyrins-DNA supramolecular structures for the use in future nanotechnological applications. This will be achieved through the synthesis of porphyrin precursors which can then be incorporated into the DNA structure through either non-covalent or covalent attachments.

1.6 Non-covalent Attachment of Porphyrins to DNA

The most commonly used porphyrin for non-covalent interactions with DNA is the water soluble *meso*-tetrakis[4-(*N*-methylpyridiumyl)]porphyrin, TMPyP (Figure 1.16). This cationic porphyrin has a natural affinity for DNA.[16] The four pyridiumyl salts allow for interaction with the negative phosphates of DNA. Intercalation of the porphyrin between base pairs has also been observed[17] along with groove binding and stacking along the exterior of the DNA.[18] Variation of the metal ions (such as the incorporation of metals with axial ligands),[19, 20] porphyrin loading and DNA base sequence allow for some degree of control over the type of interaction that occurs.

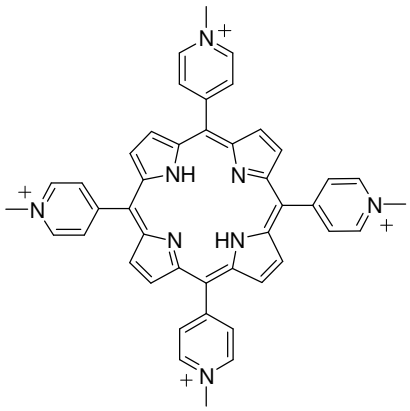

Figure 1.16 The cationic porphyrin *meso*-tetrakis[4-(*N*-methylpyridiumyl)]porphyrin, TMPyP.

Interaction of cationic porphyrins such as TMPyP have been shown to result in the photo cleavage of the DNA in the presence of light, and has been employed in photodynamic therapy for the treatment of cancer cells.[21, 22] Formation of complexes containing three, two[23] and one[24] charged *meso* derivatives have also been produced for

use in photodyanamic therapy studies. Unfortunately, reducing the number of cationic groups also reduces the solubility of the porphyrins in water.

The interaction of cationic porphyrins with DNA is not limited to duplexes. Studies have shown that cationic porphyrins such as TMPyP can bind to G-quadruplexes. Binding can occur in three modes, either binding to the top and bottom of quadruplexes (capping),[25] binding between strands of G-quadruplexes[26] or intercalation between guanine tetrads within a quadruplex.[27] All of these binding modes have been shown to increase the stability of the G-quadruplex structure. Of particular interest is the capping of porphyrins to the end of G-quadruplexes resulting in increased stability of the G-quadruplexes. This is biologically important as telomeric ends, which exist at the ends of chromosomal DNA protecting the DNA from degradation, consist of G rich sequences. Stabilising the telomeric G-quadruplex structure, for example by capping it with a porphyrin (Figure 1.17), inhibits the activity of telomerase, an enzyme responsible for the elongation of the telomeres. Inhibiting the elongation of telomeres can help restrict the growth of cancer cells.[28-30]

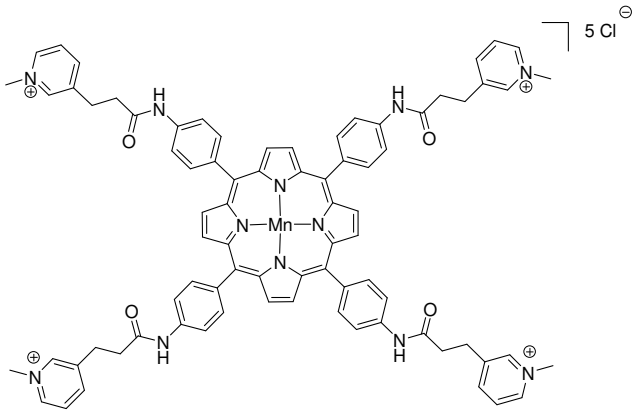

Figure 1.17 An example of a porphyrin that binds selectively to the top and bottom of the G-quadruplex preventing telomere extension.[25]

A slight variation on non-covalent attachment is the production of lipophilic DNA complexes. DNA is normally soluble in aqueous solution, however by exchanging the Na^+ or Li^+ ions along the phosphate backbone for quaternary ammonium salts possessing a long lipophilic chain (Figure 1.18), it is possible to create a complex that is soluble in organic solutions.[31, 32] Slow evaporation of organic solvents can produce lipophilic DNA films with aligned DNA strands that have shown to be important in the

production of batteries,[33] liquid crystals,[34] drug release systems,[35] photodynamic devices[36] and many other systems. Although many materials have been incorporated into DNA-lipid complexes, the incorporation of lipophilic porphyrins is a novel approach. If successful it may allow for the simple construction of porphyrin based arrays.

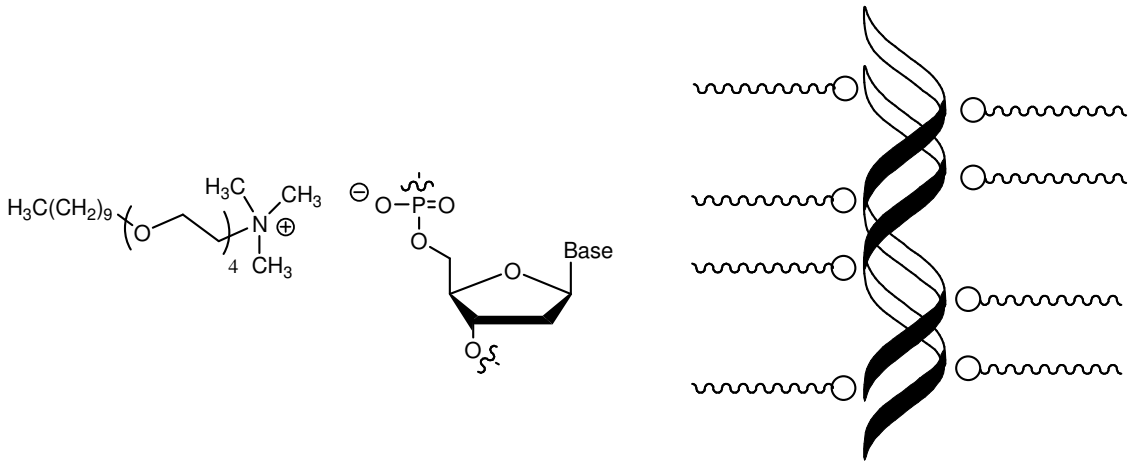

Figure 1.18 Illustration of one of the first lipophilic DNA complexes.[31]

1.7 Covalent Attachment of Porphyrins to DNA

The covalent attachment of porphyrin moieties to DNA can be realised through the use of either pre- or post-synthetic approaches (Figure 1.19). Currently there are only a few examples of post-synthetic porphyrin modifications[37-39] (Figure 1.20A and B) although there are many examples of post-synthetic modification involving other chromophores.[4, 15, 40] A pre-synthetic approach involves the attachment of a porphyrin to a nucleoside which is then converted to the appropriate porphyrin phosphoramidites or H-phosphonates. These are then incorporated into the DNA structure during DNA synthesis. The pre-synthetic approach can allow for the incorporation of many functionalised nucleotides on a single DNA strand using automated DNA synthesis only if high yielding coupling reactions occur.

Post-synthetic modification means that a special functional group of the porphyrin reacts specifically with a pre-synthesised oligonucleotide carrying a complementary functional group. In order to screen different substituents in nucleic acid structures, a post-synthetic approach is more convenient than the time-consuming preparation of an individual phosphoramidite or an H-phosphonate for each modification.

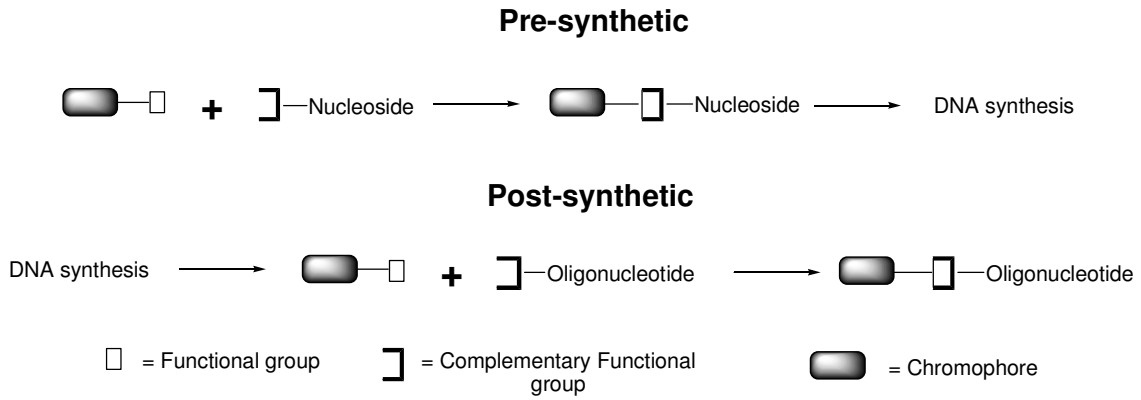

Figure 1.19 Pre- and post-synthetic DNA modifications.

Covalent attachment of porphyrin moieties to DNA has been achieved using a variety of methodologies including: the modification of nucleobases,[38, 41-44] ribofuranose residues,[37, 45-49] phosphate backbone[39, 50-52] and using acyclic linkers.[53, 54] This provided structures having porphyrin residues as 3′- or 5′-molecular caps,[47, 54-56] introducing them instead of a nucleobase in the middle of the helix[53] or as a label in the minor[39, 46] and major[38, 43, 44] grooves. These porphyrins have been attached to DNA using numerous linkers (Figure 1.20) including maleimido-thiol,[38, 39] amide,[46-49] phosphate[50-52] and alkyne bonds,[41-44] the latter being incorporated using the Sonogashira reaction. All of the current methods for covalent attachment are obtained through the *meso* position of the porphyrin.

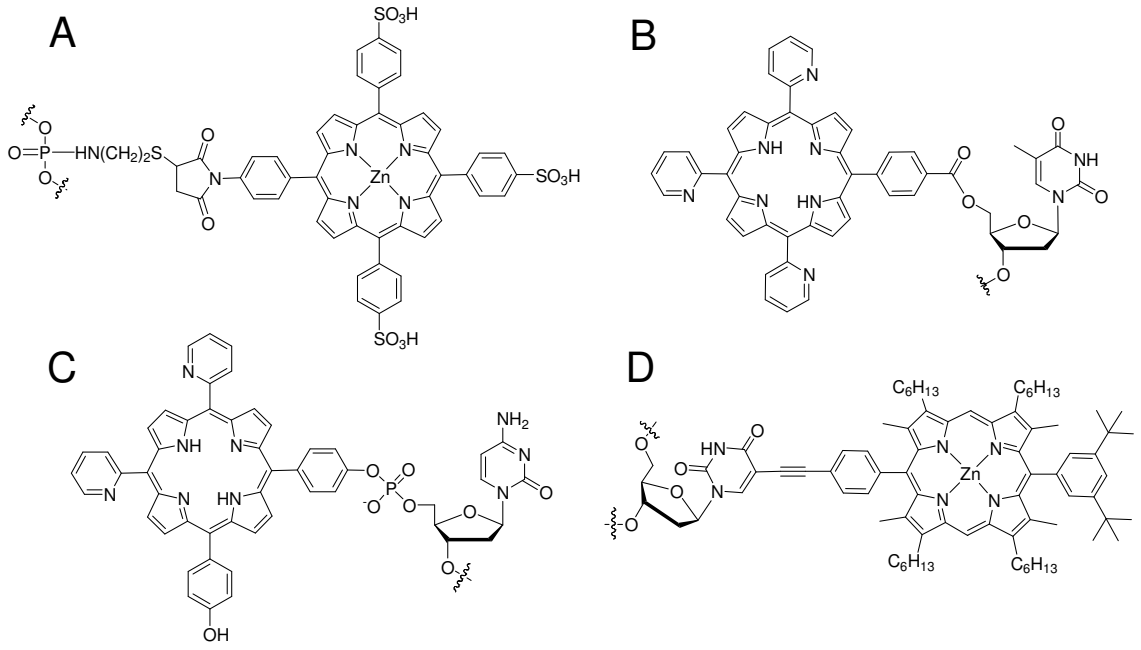

Figure 1.20 Examples of porphyrins incorporated into DNA. A) maleimido-thiol linkage,[39] B) amide bond,[37] C) phosphate attachment[51] and D) alkyne bond.[42]

There are many other routes available for the incorporation of organic chromophores into DNA.[40] Of particular interest is the use of Cu^{I} catalysed Huisgen 1,3-dipolar cycloaddition reaction between azides and alkynes (Figure 1.21).[57] This reaction is so efficient and reliable that the copper catalysed azide–alkyne cycloaddition (CuAAC) reaction is classified as a "click reaction". There has been a tremendous number of applications for use of this reaction since the recent discovery that azide–alkyne cycloadditions can be catalysed by Cu^{I}.[58, 59] The CuAAC reaction has been widely used for the attachment of organic chromophores and biomolecules to DNA.[60, 61] This is due to the relatively easy ways at which azide and alkyne functional groups can be incorporated into compounds, the inexpensive Cu^{I} catalyst (usually obtained from the reduction of stable sources of Cu^{II} such as $CuSO_4$) and the stability of the resulting 1,4-regioisomeric triazoles. The CuAAC reaction has not yet been applied for the attachment of porphyrins to DNA, and those reports on CuAAC reactions involving porphyrins hve been published on *meso* functionalised porphyrins only.[62-69]

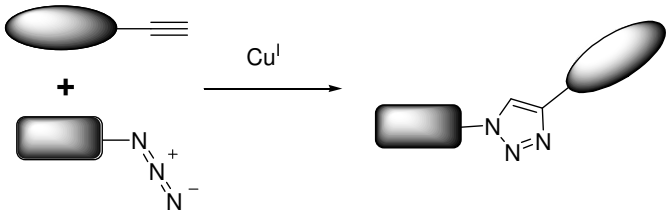

Figure 1.21 The Cu^{I} catalysed azide–alkyne cycloaddition (CuAAC) reaction.

1.7.1 External Modification

Covalent attachment can be achieved through internal or external attachment of porphyrins to DNA. The external modification of DNA, *i.e.* modification at the at the 5′ and or 3′ ends, has been shown to stabilise duplexes[45, 50] and even G-quadruplexes[70] by forming a molecular cap. This cap provides thermodynamic stability as a result of stacking with the nearest nucleobases,[71, 72] protecting their hydrogen bonds from the aqueous environment.[73] Depending on the modifications made to the porphyrin and the position of attachment to the DNA, various levels of stabilisation have been observed. It has been shown that even noncanonical GA base pairs can be stabilised over Watson-Crick base pairing.[50] For example, when the tetraaryl porphyrin shown in Figure 1.22 was placed at the 5′ end of a $d(GA)_4$ sequence, formation of a duplex consisting of GA base pairs was detected. In contrast, similar positioning in a duplex consisting of GC

base pairs resulted in thermal destabilisation. This is a result of the better overlap of the porphyrin with GA pairs than GC pairs. Other uses of a cap include extensive work by Berova and others[47, 49, 51] in the development of UV and CD detectors of B to Z transitions in DNA, where different CD exciton couplings were observed between porphyrins at either end of the duplex depending on the DNA conformation.

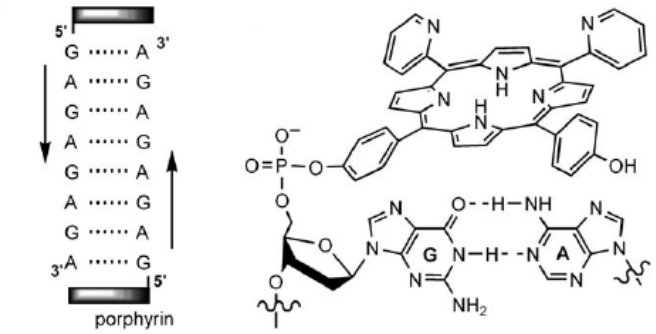

Figure 1.22 A porphyrin molecular cap that stabilises noncanonical DNA (reproduced from Berova *et al.*).[50]

Recently, it has been observed that porphyrin to porphyrin interactions were responsible for the aggregation of duplexes possessing porphyrins as a 5′ cap (Figure 1.23).[54, 56] Head to tail interduplex aggregates were observed at high salt concentrations at low temperature. This was shown by the conversion of a bisignate CD curve in the Soret region to a multisignate curve on increased salt concentration, suggesting porphyrin-porphyrin stacking. The strongest signals were observed in DNA containing Zn^{II} porphyrin but were also recorded for Cu^{II} and free base porphyrins.

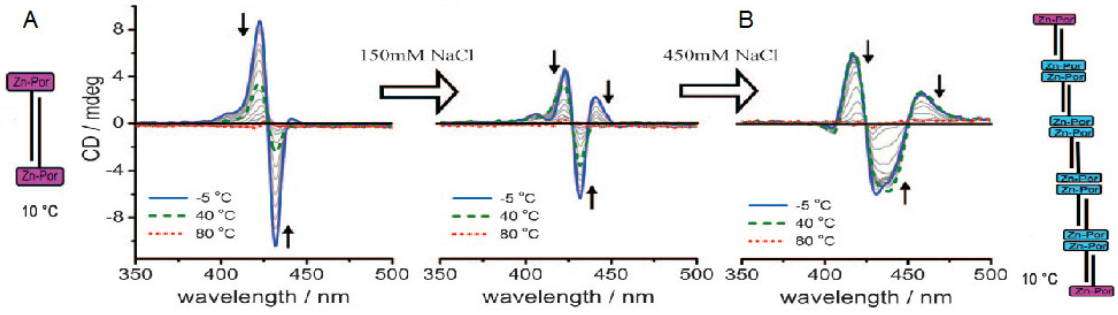

Figure 1.23 Stacking of 5′ porphyrin capped DNA by Berova *et al.*[56] A) Duplex representation and CD spectroscopy in the absence of NaCl showing no duplex stacking, B) Duplex representation and CD spectroscopy in 450 mM NaCl and the proposed porphyrin DNA stacking (reproduced and adapted from Berova *et al.*)[56]

1.7.2 Internal Modification

With exception to some early work by Richert[53] and Kool[45] where porphyrins were used as base replacements in DNA duplexes, the internal modification of nucleobases with porphyrins is a relatively new field. Prior to 2007, only work by Stulz[74, 75] and Sessler[76, 77] existed which focused on the development of *meso* porphyrin modified nucleosides and dinucleotides (Figure 1.24).

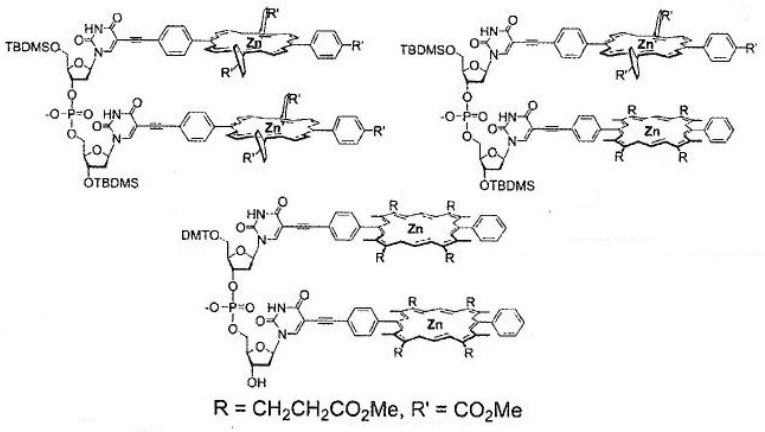

Figure 1.24 Example of porphyrin modified dinucleotides (reproduced and adapted from Stulz *et al.*)[74]

However, it was not until 2007/2008 that the synthesis of a DNA containing the internal modification of *meso* functionalised porphyrins was reported, placing the porphyrins in the major[38, 43, 44] and minor[39, 46] grooves of duplexes. This included work by Stulz's group where up to eleven porphyrins were incorporated into a single strand using a pre-synthetic approach.[43] This allowed for contiguous stacking of porphyrins in single stranded oligonucleotide (Figure 1.25A) and within the major groove of duplexes (Figure 1.25B). In addition, porphyrins based on the modification of 2′-deoxy-5-ethynyluridine showed significant thermal destabilisation of the resulting duplexes by 5-7 °C per porphyrin modification.

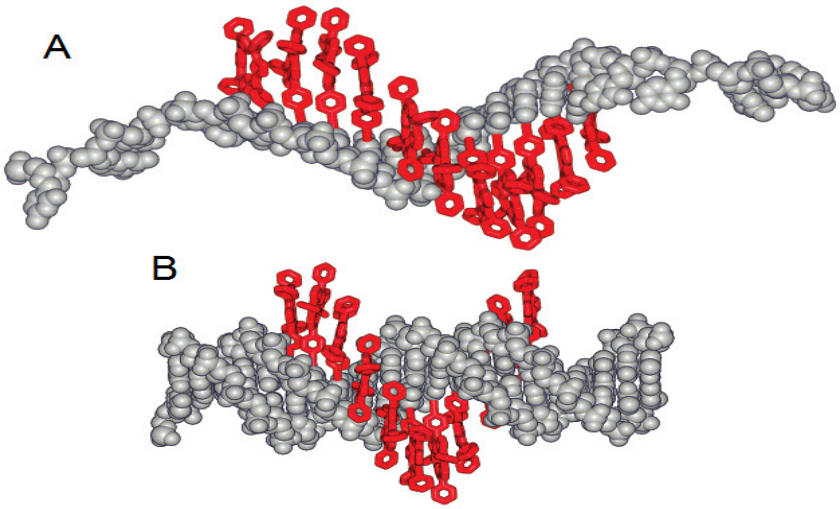

Figure 1.25 Molecular modelling of a *meso* linked porphyrin DNA complex by Stulz *et al.* showing porphyrin stacking in singled stranded (A) and duplex (B) DNA. (Reproduced from Stulz *et al.*)[43]

Further work showed a stabilising effect of +0.5 °C per porphyrin modification when the *meso* linked porphyrins were placed adjacently in complementary strands, forming a zipper in the major groove of the duplex. The placement of Zn^{II} and free base porphyrins in complementary strands allowed for effective energy transfer between a zinc porphyrin and a free-base porphyrin as shown in Figure 1.26.[44]

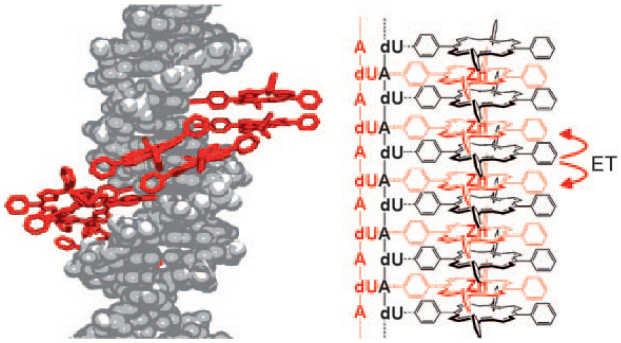

Figure 1.26 A porphyrin zipper in the major groove that when formed allowed for energy transfer between porphyrins (reproduced from Stulz *et al.*)[44]

1.8 Thesis Objectives

As porphyrins are interesting chromophores and DNA is a perfect template for chromophore scaffolding it was thus the aim of this thesis to create and study DNA-porphyrin supramolecular architectures based on *β*-pyrrolic modified porphyrins. Investigations into these complexes will be separated into two categories of modification: covalent and non-covalent attachment.

For the non-covalent approach we aim to synthesise lipophilic porphyrins and use them to create lipophilic porphyrin-DNA complexes. This may provide DNA porphyrin complexes or films with interesting spectroscopic properties.

For the covalent attachment we aim to design and construct a versatile approach for the site specific internal modification of oligonucleotides with multiple porphyrins. Both pre- and post-synthetic Sonogashira and CuAAC reactions will be investigated to modify oligonucleotides using pre-synthesised *β*-pyrrolic porphyrin building blocks. This work will differentiate from other recently published approaches by incorporating *β*-pyrrolic modified porphyrins in a *post*-synthetic manner using Sonogashira and CuAAC reactions. We have also focused on internal modification rather than modification of the 3′ and 5′ ends. Once oligonucleotides have been constructed we can investigate the effect of porphyrin modifications when incorporated in various positions of single stranded, duplex and triplex DNA. This should provide information for the future application of porphyrin modified ONs.

1.9 Thesis Structure

This thesis discusses the development of novel porphyrin-DNA complexes using *β*-pyrrolic modified porphyrins.

Chapter 2 describes the development of synthetic methods for the synthesis of porphyrin derivatives to be used in the creation of porphyrin-DNA supramolecular constructs. This includes the synthesis of lipophilic porphyrins for the non-covalent

attachment to DNA as well as porphyrin precursors for the covalent attachment to DNA.

Chapter 3 discusses the development of a modified Horner-Emmons reaction as a new synthetic method for creation of alkyne bonds in the β-pyrrolic position of porphyrins. This project allowed us to synthesise porphyrins for covalent attachment to DNA as well a series of novel alkyne linked porphyrinic acids for photovoltaic devices. This work has been published in *Tetrahedron Letters* (Stephenson, A. W. I.; Wagner, P.; Partridge, A. C.; Jolley, K. W.; Filichev, V. V.; Officer, D. L., *Tetrahedron Letters* **2008**, 49, (39), 5632-5635) .

Chapter 4 develops a method for the construction of novel supramolecular DNA-porphyrin complexes using the non-covalent attachment of lipophilic porphyrins. A manuscript discussing this work is under preparation for submission to *Tetrahedron Letters*.

Chapter 5 uses the porphyrin precursors developed in Chapter 2 to create covalently modified oligonucleotides containing a single internal modification of a β-pyrrolic porphyrin using CuAAC and Sonogashira reactions. The effect of porphyrin modification on the thermal stability of the resulting duplexes and triplexes is discussed. A manuscript involving this work has been prepared for submission to *Chemistry – A European Journal*.

Chapter 6 investigates the effect of porphyrin aggregate formation on the thermal stability of porphyrin modified duplexes. A range of duplexes were formed containing up to four porphyrins in a zipper fashion in the minor groove of the duplex. Thermal stability of each duplex was determined by UV-Vis spectroscopy. CD spectroscopy and molecular modelling was used to help to understand the high thermal stabilities observed for these complexes. This work has been published in *ChemBioChem* (Stephenson, A. W. I.; Bomholt, N.; Partridge, A. C.; Filichev, V. V., *ChemBioChem*, **2010**, 11, (13), 1833-1839).

Future work and applications are discussed in Chapter 7 and experimental procedures are included in Chapter 8.

Chapter 2 Synthesis of β-Pyrrolic Porphyrin Derivatives for DNA Modification

2.1 Introduction

The structure of the porphyrin allows for two main locations for the extension of the molecule, the β-pyrrolic position and the *meso* position (Figure 2.1). In this thesis we focus on the synthesis of β-pyrrolic functionalised porphyrins as they have advantages over *meso* functionalisation. Derivatives attached to the *meso* phenyl ring have been shown to result in the disruption of the conjugation between the porphyrin core and the attached group as a result of the phenyl *meso* ring sitting orthogonal to the plane of the porphyrin core. This is a result of steric interactions between the adjacent β-pyrrolic hydrogens and *meso* phenyl ring which twists the phenyl ring in relation to the porphyrin core. In contrast, alkene and alkyne modifications at the β-pyrrolic position result in a system that is in the same plane as the porphyrin core.

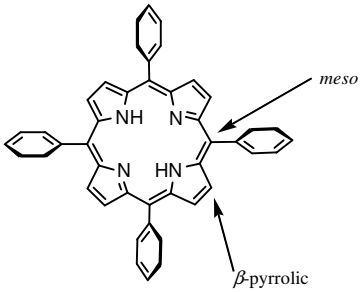

Figure 2.1 5,10,15,20-Tetraphenylporphyrin (TPP) showing the β-pyrrolic and *meso* positions.

To allow for β-pyrrolic modification, a functional group needs to be added to the β-pyrrolic position. This is usually achieved *via* the synthesis of β-pyrrolic formyl and bromo derivatives which act as building blocks for the extension of the porphyrin core. Formylation, such as that in 2-formyl-5,10,15,20-tetraphenylprophyrin, provides a starting material for the synthesis of many derivatives including 2-alkenes *via* the Wittig reaction[78, 79] and 2-alkynes *via* the Horner-Emmons reaction[80] (see Chapter 3). Bromination, as in 2-bromo-5,10,15,20-tetraphenylporphyrin, allows for the synthesis of 2-alkynes *via* Sonogashira and related reactions.

2-Bromo-5,10,15,20-tetraphenylporphyrin (**1**) is generally synthesised through the reaction of TPP with NBS in an organic solvent, usually chloroform.[81-86] Synthesis of 2-bromo-5,10,15,20-tetraphenylporphyrin is difficult and requires significant care to limit the quantity of the di- and tri-brominated species, and yet still maximise the yield of 2-bromo-5,10,15,20-tetraphenylporphyrin (Figure 2.2). There are a number of publications detailing the synthesis of **1**,[81-86] however, these results were generally difficult to reproduce. Purification of the 2-bromo-5,10,15,20-tetraphenylporphyrin from the di- and tri-species is difficult due to the similar R_f of the brominated species and the smearing of bands that occurs during column purification on silica gel. As a result only a small quantity of 2-bromo-5,10,15,20-tetraphenylporphyrin can be purified at one time and purities of above 95% are difficult to achieve. Scaling up to multi-gram quantities of 2-bromo-5,10,15,20-tetraphenylporphyrin, which is required for the synthesis of large quantities of porphyrins, is practically difficult to achieve.

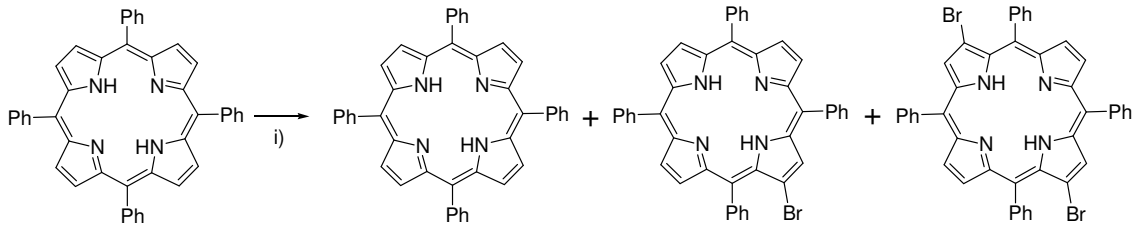

Figure 2.2 The synthesis of 2-bromo-5,10,15,20-tetraphenylporphyrin **1**. Reagents and conditions: i) $CHCl_3$, NBS, RT.

As an alternative to bromination, 2-formyl-5,10,15,20-tetraphenylporphyrin (TPPCHO, **2**) provides an excellent building block for β-pyrrolic functionalisation as it is easy to synthesise in high yields and multi-gram quantities without the need for difficult silica gel chromatography. Synthesis of **2** is achieved in three steps from 5,10,15,20-tetraphenylporphyrin (TPP) in high yields (Figure 2.3).[87] The aldehyde can be used in many different reactions for the synthesis of alkene and alkyne derivatives. Conversion of TPPCHO in three steps to the phosphonium salt (TPPps, **3**) provides a building block for the synthesis of alkenes using Wittig chemistry[87] (Figure 2.3). Thus, due to the ease of synthesis, 2-formyl-5,10,15,20-tetraphenylporphyrin was used as a building block for the development of porphyrin compounds in this thesis.

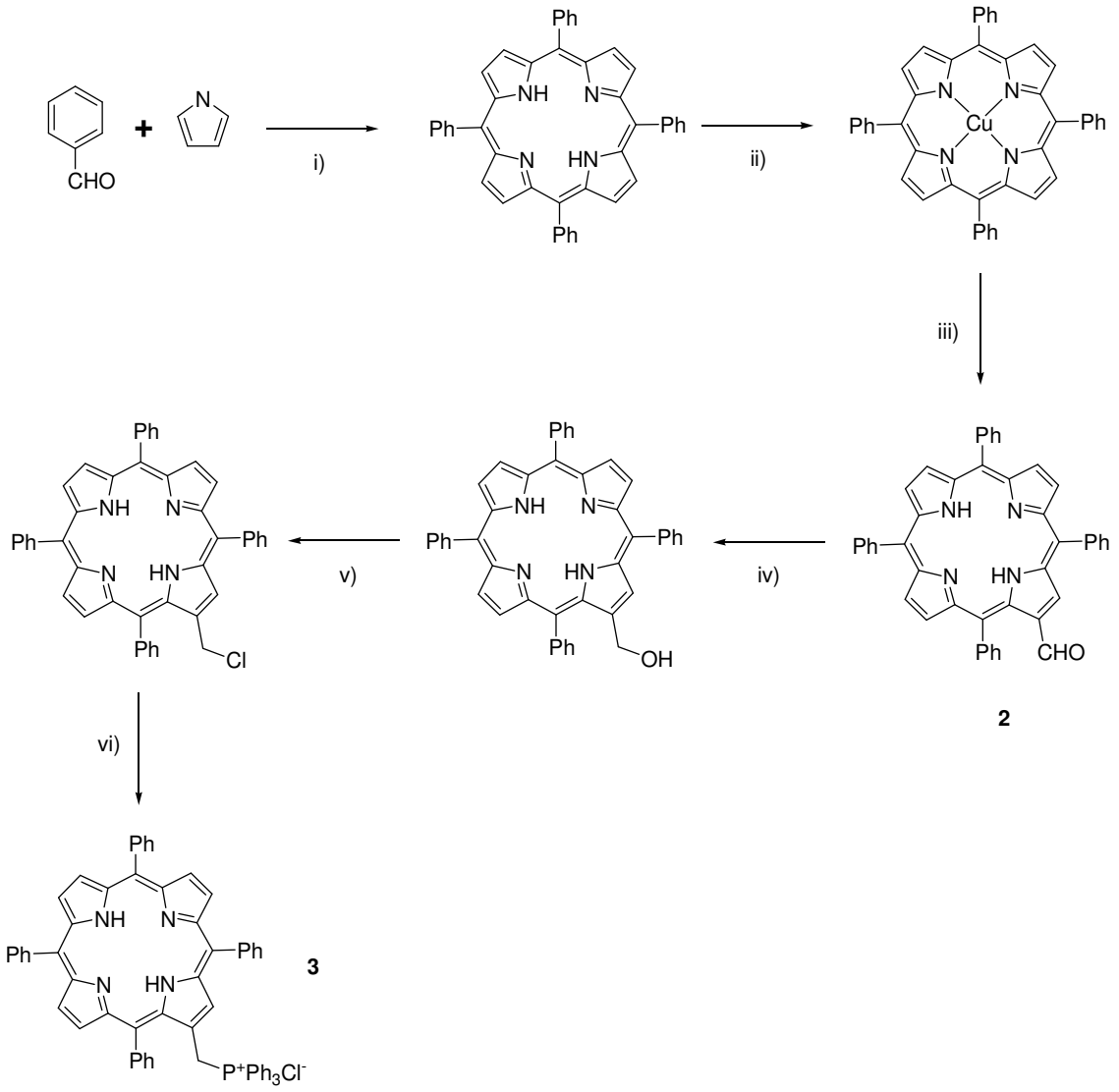

Figure 2.3 The synthesis of TPPps. Reagents and conditions: i) Propionic acid, reflux, 15-20% ii) $Cu(OAc)_2 \cdot H_2O$, $CHCl_3$, MeOH, reflux, 100% iii) $POCl_3$, DMF, 1,2-DCE, reflux then H_2SO_4, 90-95% iv) $NaBH_4$, THF, H_2O, RT, 85-100% v) $SOCl_2$, pyridine, DCM, 0 °C to RT, 95-100% vi) PPh_3, $CHCl_3$, reflux, 80-90%.

2.2 Chapter Summary

In this chapter, we have synthesised alkane, alkene and alkyne β-pyrrolic derivatives from 2-formyl-5,10,15,20-tetraphenylporphyrin for the development of DNA-porphyrin supramolecular structures (Figure 2.4).

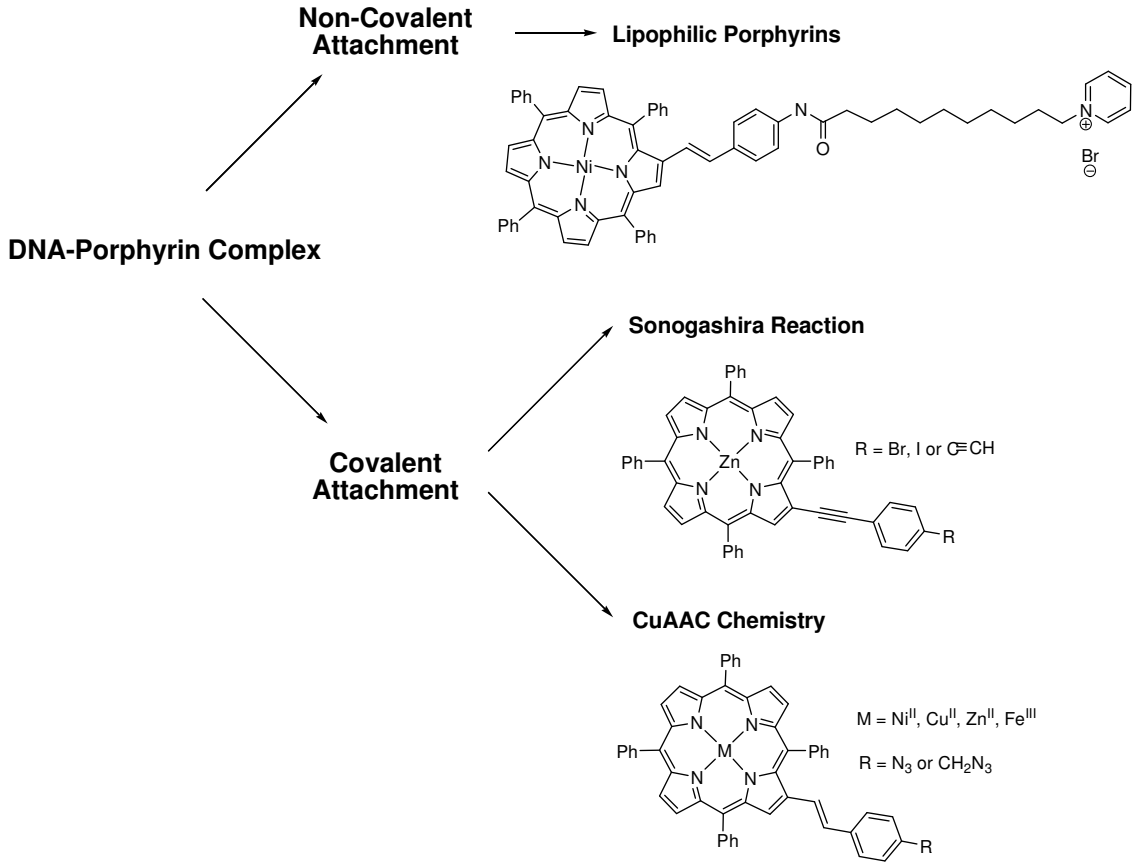

Figure 2.4 Synthetic plan for the development of DNA-porphyrin supramolecular structures.

The DNA-porphyrin complexes are divided into two groups based on the method of attachment - covalent or non-covalent. For the non-covalent attachment (lipophilic porphyrins) we have created several pyridinium salts of TPP, discussed in section 2.3. The covalent attachment involved the synthesis of precursors for pre- and post-synthetic attachment to DNA. This includes azido porphyrins as starting materials for Huisgen 1,3-dipolar cycloaddition reactions (CuAAC reactions), and ethylene, bromo and iodo porphyrin derivatives as starting materials for Sonogashira chemistry. All compounds were derived from 2-formyl-5,10,15,20-tetraphenylporphyrin for the reasons covered above. All compounds were characterised using ^{1}H NMR, HRMS, UV-Vis and IR spectroscopy, where required, as discussed in Chapter 8 - Experimental.

2.3 Synthesis of Porphyrins for Development of Non-Covalently Attached Lipophilic Porphyrin-DNA Complexes

This work focused on the creation of a lipophilic porphyrin that could interact with DNA *via* electrostatic interactions with the negatively charged phosphate backbone. This is a novel approach that could be used to create DNA that is soluble in organic solutions, aligned DNA films for use in light harvesting devices,[88, 89] or fluorescent labelling of DNA. To ensure solubility of the lipophilic complex in organic solvents an aliphatic chain of C_{10} or greater is generally required. This may not be required for porphyrins due to the intrinsic solubility of porphyrins in organic solvents, however, there appeared to be little advantage to deviate from this length. Three different synthetic routes were investigated for the synthesis of the novel lipophilic porphyrins (Figure 2.5). These routes are classified by the key reactions used: Route A – Wittig reaction, Route B – Schiff base formation and Route C – amide bond formation. Route C was found to be the most successful method for the large scale synthesis of lipophilic porphyrins. Route A also provided lipophilic porphyrins, however, in a lower yield.

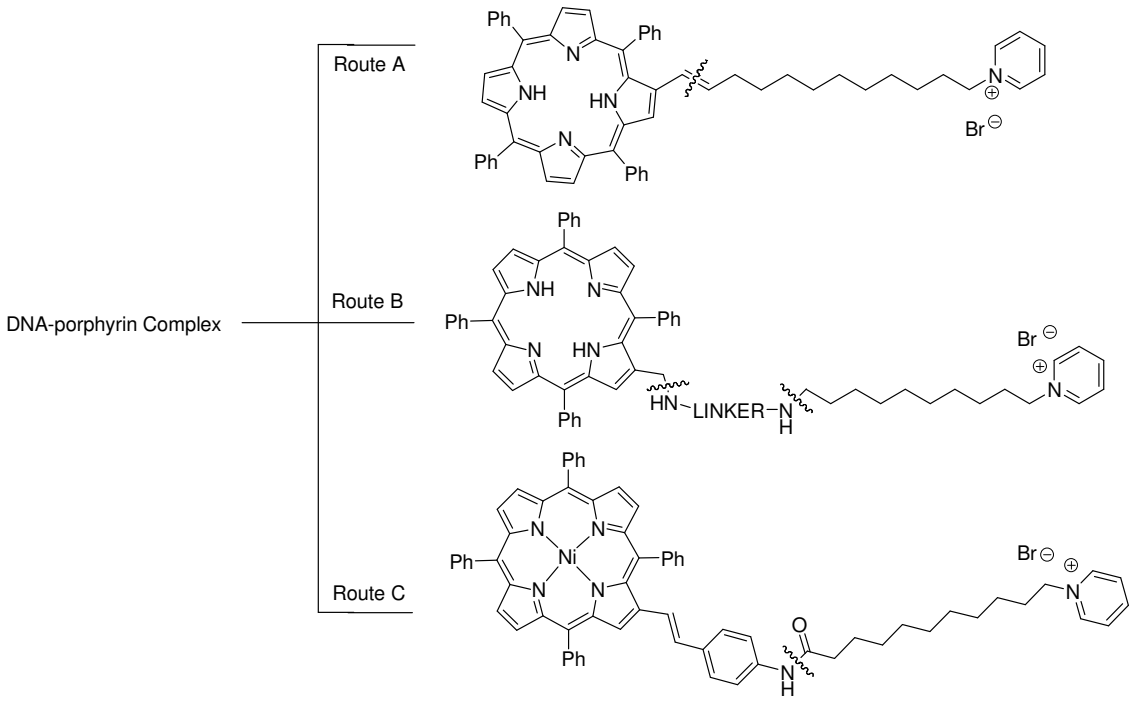

Figure 2.5 Routes to lipophilic porphyrins.

2.3.1 Route A – Wittig Reaction

The Wittig reaction was the key synthetic step to link the aliphatic 11-bromoundecanal (**4**) with TPPps (**3**) allowing for the overall synthesis of the lipophilic compound **6** as shown in Figure 2.6. 11-Bromoundecanal (**4**) was chosen as it was easily synthesised from the inexpensive 11-bromoundecanol, in 83% yield using PCC.[90] 11-Bromoundecanal must be prepared freshly as it is difficult to prevent the oxidation of the aldehyde to the acid, which occurs in hours if the compound is left open to air. Additionally, the terminal bromine allows for the easy synthesis of pyridinium salts (**6**). The synthesis of **6** was broken down into three steps; the Wittig reaction, isomerisation and the pyridinium salt formation.

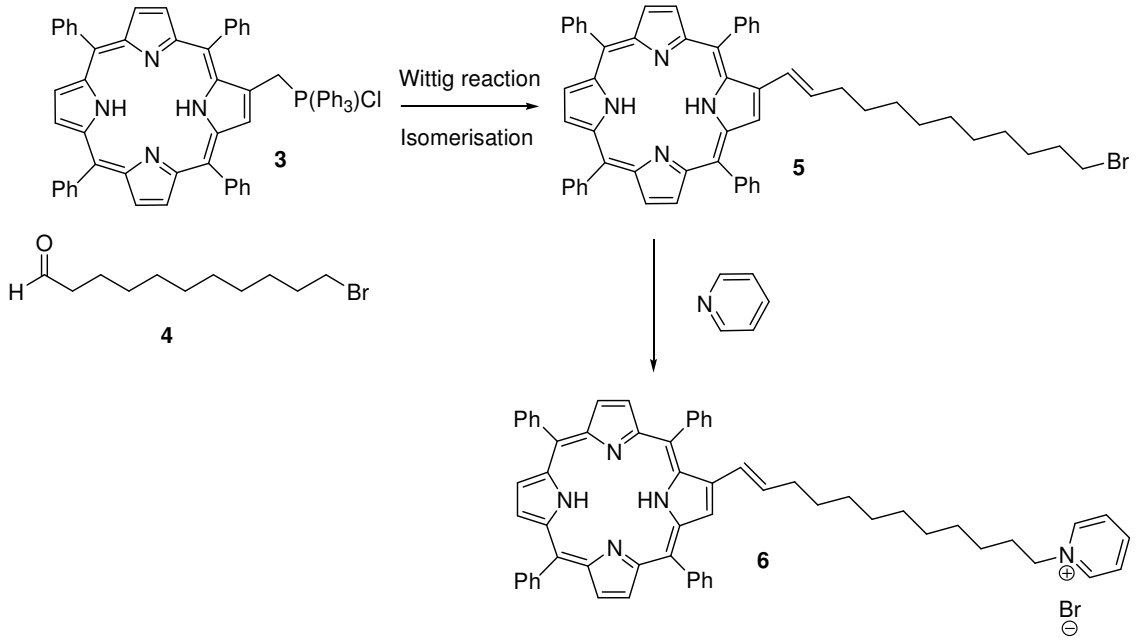

Figure 2.6 Synthesis of lipophilic porphyrin **6** *via* the Wittig reaction and pyridinium salt formation.

2.3.1.1 The Wittig Reaction

The first step in the synthesis of lipophilic porphyrins using route A was the Wittig reaction. Wittig reactions on porphyrins are generally carried out using conditions developed by Bonfantini *et al.*[78, 87] This involves the combination of the phosphonium salt in dry solvent (usually chloroform or toluene) with approximately three equivalents of an aldehyde and DBU. This reaction is completed very quickly and in general produces a *cis/trans* mixture of the desired porphyrin that can be isomerised to the *trans*

product with iodine. Using minor adjustments on the above method (DCM, 3.75 eq of **1**, 9 eq of DBU, RT, 20 min, Figure 2.7), the reaction of TPPps **3** with aldehyde **4** produced a *cis/trans* mixture of **5** and a common by-product of the Wittig reaction, 2-methyl-5,10,15,20-tetraphenylporphyrin[91] ($TPPCH_3$, **7**). This was observed in a ratio of 1:2:5 (**7**:**5***cis*:**5***trans*) as judged by ^{1}H NMR spectroscopy with an overall reaction yield of 67%. This by-product of the Wittig reaction generally occurs as a result of a competitive reaction when the aldehyde is slow to react with the ylid. $TPPCH_3$ can usually be separated from the desired compound using silica gel or alumina chromographic techniques. Unfortunately, the by-product **7** moved at the same R_f to the *cis:trans* mixture of **5** in various solvent combinations on silica and alumina media, therefore, could not be separated from the *cis/trans* mixture of **5**.

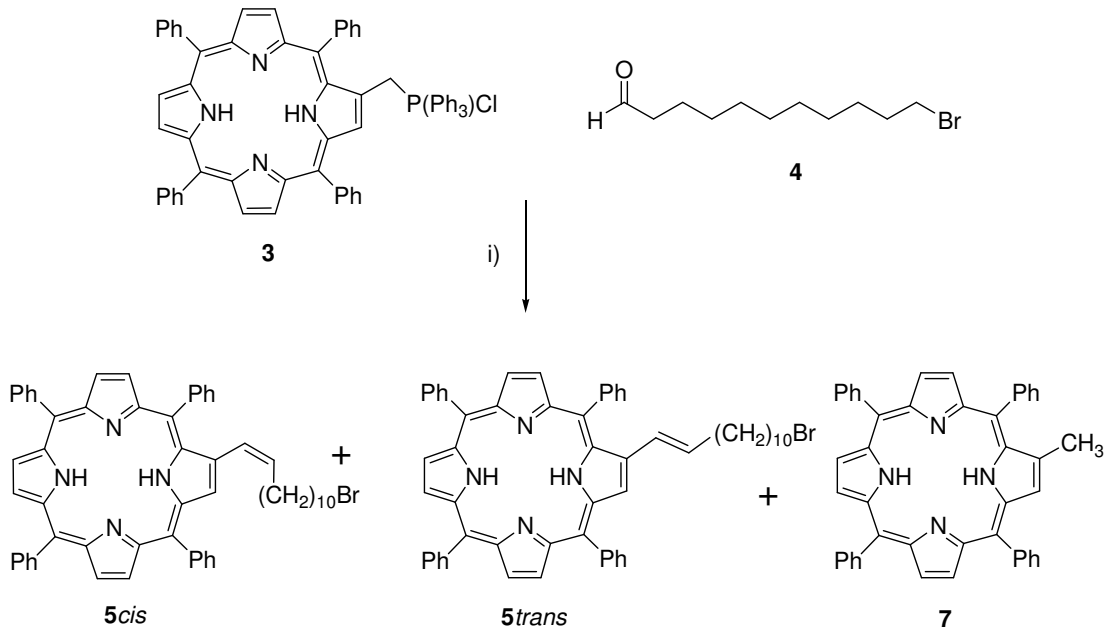

Figure 2.7 Synthesis of compound **5** *via* the Wittig reaction. Reagents and conditions: i) DCM, DBU, RT, 20 min, 67%.

Previous results have shown that by carrying out the reaction in dry refluxing toluene, the production of **7** could be limited and the formation of the *trans* product favoured.[92] When these conditions were tried results showed little change in the *cis:trans* ratio, however, the production of **7** was reduced but not completely eliminated. Unfortunately, the overall yield of the reaction decreased from 67% to 43% as well. Although pure **5** could not be obtained, the synthesis was continued on the hope that purification would be more achievable after isomerisation and/or pyridinium salt formation.

2.3.1.2 Isomerisation

Two options are commonly used for the isomerisation of alkene bonds to the thermodynamically stable *trans* orientation, stirring with iodine in complete darkness or refluxing for long periods in a high boiling, inert solvent such as toluene. Both methods were attempted on the *cis:trans* mixture of **5** with varying results. Refluxing the diastereomeric mixture in toluene for 72 hours showed no change in the ratio of *cis:trans* by ^{1}H NMR spectroscopy, suggesting that the energy required to isomerise the mixture is greater than that supplied in refluxing toluene. The treatment of the *cis:trans* mixture with three equivalents of I_2 at RT in chloroform for three hours successfully isomerised the mixture as could be observed in the ^{1}H NMR spectrum. This resulted in **5***trans* that still contained **7**, but now the ratio was 6:1 (**5***trans*:**7**). Attempts to purify this mixture using various chromatographic techniques were unsuccessful.

2.3.1.3 Pyridinium Salt Formation

The pyridinium salt **6** was formed by refluxing **5***trans* in neat pyridine for two days followed by silica gel column purification to remove TPP-CH_3 **7**. This allowed for the formation of the lipophilic porphyrin **6** in an overall yield of 19% from TPPps (Figure 2.8).

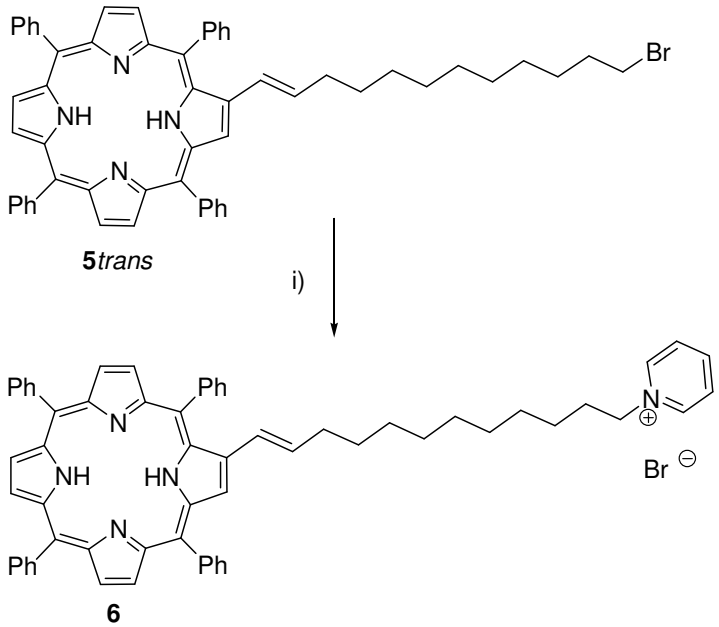

Figure 2.8 Synthesis of compound **6**. Reagents and conditions: i) pyridine, reflux, 2 days, 74%.

^{1}H NMR spectroscopic analysis in $CDCl_3$ of the obtained pyridinium salt showed what appeared to be a multiple porphyrin mixture in equal molar concentrations. (Figure 2.9B). As an impure compound was not suitable for the construction of lipophilic porphyrin-DNA constructs, alternative methods for the synthesis of lipophilic porphyrins were investigated (see reduction, route B and route C). It was not until different routes were investigated that high resolution ESI mass spectrometry confirmed the presence of the desired compound **6**. Further NMR spectroscopic analysis showed that what appeared to be multiple porphyrin products was in fact a pure single compound. When the solvent was changed to d_6-DMSO, the two signals appear to coalesce into one (Figure 2.9A). It is unlikely this is a result of aggregation in $CDCl_3$ as the characteristic broad NMR signals are not present. Due to the limited amount of compound no further studies were undertaken to explain the unusual NMR spectrum (*i.e.* variable temperature NMR studies in $CDCl_3$).

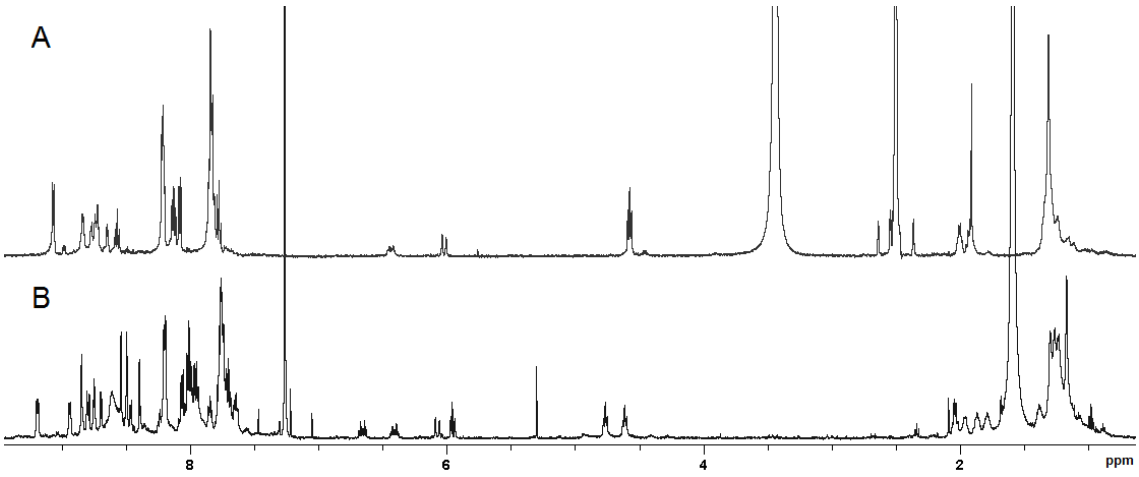

Figure 2.9 ^{1}H NMR spectrum of the pyridinium salt **6** in $CDCl_3$ (B) and d_6-DMSO (A). Note the two sets of signals in $CDCl_3$.

2.3.1.4 Alkene to Alkane Reduction and Pyridinium Salt Formation

Because of the initial thoughts that the pyridinium salt **6** may not be pure, reduction of the *cis/trans* mixture of alkene **5** to an alkane bond (**8**) was carried out using 10% Pd on carbon under and atmosphere of H_2 (Figure 2.10)[3] This resulted in an intractable mixture of the reduced material **8** and the starting impurity $TPPCH_3$ (**7**). Due to the low yield of the reduction reaction (*ca.* 40%), the ratio of the desired product (**8**) to $TPPCH_3$ (**7**) decreased from 6:1 to 1:1 as judged by ^{1}H NMR spectroscopy.

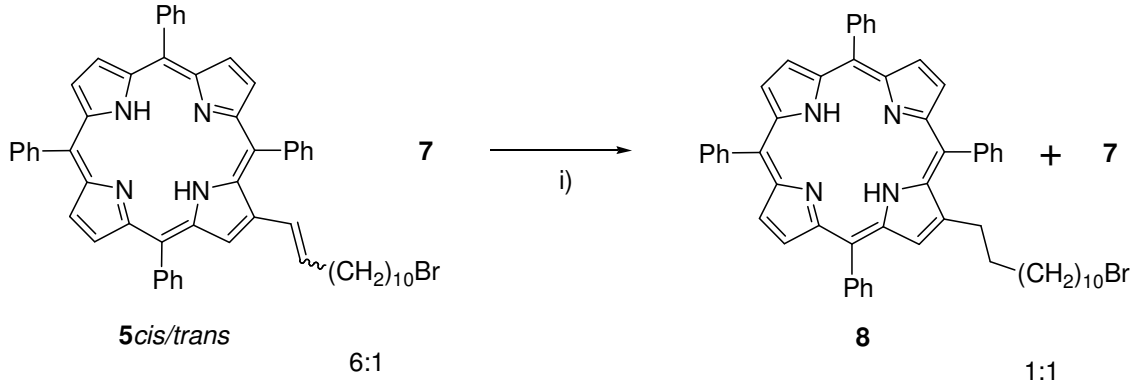

Figure 2.10 Reduction of the alkene (**5**) to an alkane (**8**). Reagents and conditions: i) 10% palladium on carbon, formic acid, H_2, 50°C, 3.5 h then NaOH, *ca.* 40%.

The pyridinium salt **9** was formed in 30% yield by refluxing the product of the Pd catalysed reduction reaction in pyridine for 48 hours. This was followed by purification through silica gel to remove $TPPCH_3$ **7** (Figure 2.11), eluting the desired salt in MeOH:DCM (1:4). Interestingly, no changes were observed when comparing ^1H NMR spectra in DMSO and $CDCl_3$, which contrasts to the alkene derivative (Figure 2.9).

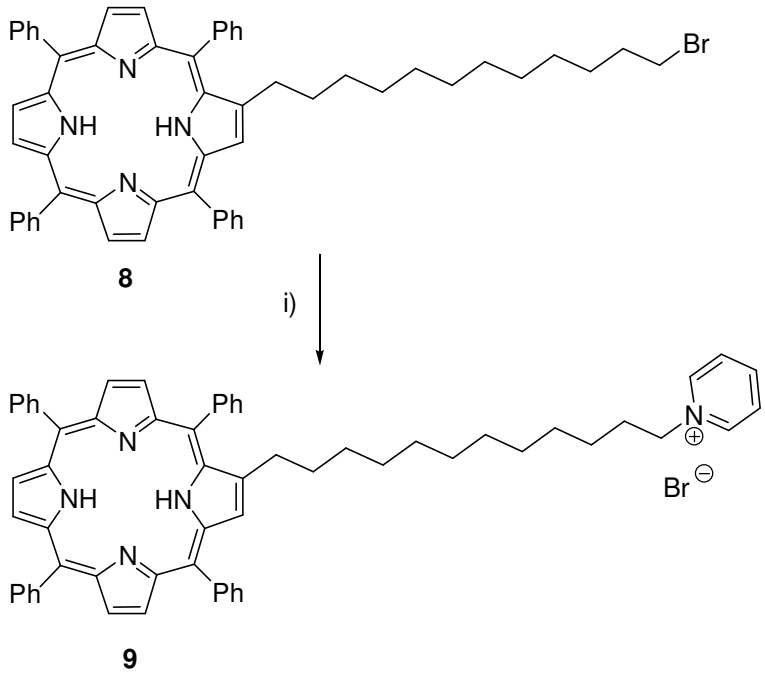

Figure 2.11 Synthesis of pyridine salt **9**. Reagents and conditions: i) pyridine, reflux, 2 days, 30%.

Due to the problems associated with the Wittig chemistry (*i.e.* the formation of significant quantities of $TPPCH_3$) its use for the large scale synthesis of lipophilic

porphyrins would not be feasible. Although enough material was prepared for the possible construction of a limited range of porphyrin-DNA constructs, alternative methods were investigated for the large scale synthesis of lipophilic porphyrins.

2.3.2 Route B – Schiff Base Formation

Route B was investigated as an alternative method for the construction of lipophilic porphyrins. This involved the synthesis of Schiff base or imine linkages between the porphyrin and the aliphatic chain (Figure 2.12). Schiff bases or imine forming reactions at the β-pyrrolic position of porphyrins have been scarcely reported.[93-95] Schiff bases have been prepared in refluxing toluene under Dean-Stark conditions with the use of the Lewis acid catalyst lanthanum^{II} triflate.[95] Reduction of the imine to the stable tertiary amine was performed with $NaBH_4$.

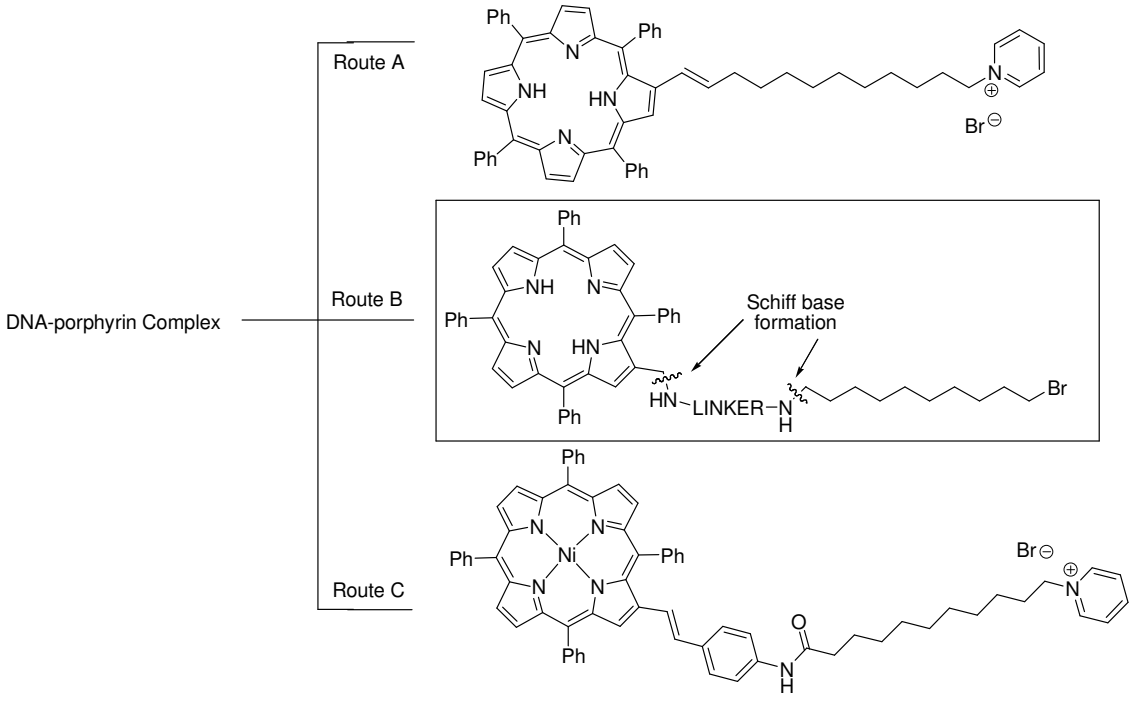

Figure 2.12 Route B.

Unfortunately, lanthanum^{II} triflate was not available therefore acetic acid was used as this is a common catalyst for the formation of Schiff bases. Reactions were initially performed using an ethylenediamine (**10**) linker. This allowed for the formation of an imine bond with TPPCHO, leaving a free amino group to be reacted with an appropriate aldehyde such as 11-bromoundecanal. Reaction of TPPCHO (**2**) with 10 eq of

ethylenediamine (**10**) in chloroform or THF at 50 °C, using catalytic amounts of acetic acid, showed the production of imine **11** by ^{1}H NMR and MALDI-TOF spectroscopic analysis (Figure 2.13). Purification of imine **11** using silica and alumina columns was unsuccessful as the imine was labile, resulting in the isolation of TPPCHO starting material. However, the imine could be isolated as a 1:1 mixture of imine **11** and TPPCHO by direct precipitation of the reaction mixture from MeOH. The insertion of the Ni^{II} ion into the porphyrin core is known to stabilise previously reactive compounds, however, the imine formed from NiTPP-CHO (obtained from the reaction of TPP-CHO and $Ni(OAc)_2 \cdot 4H_2O$) and ethylenediamine showed the same labile properties as the free base.

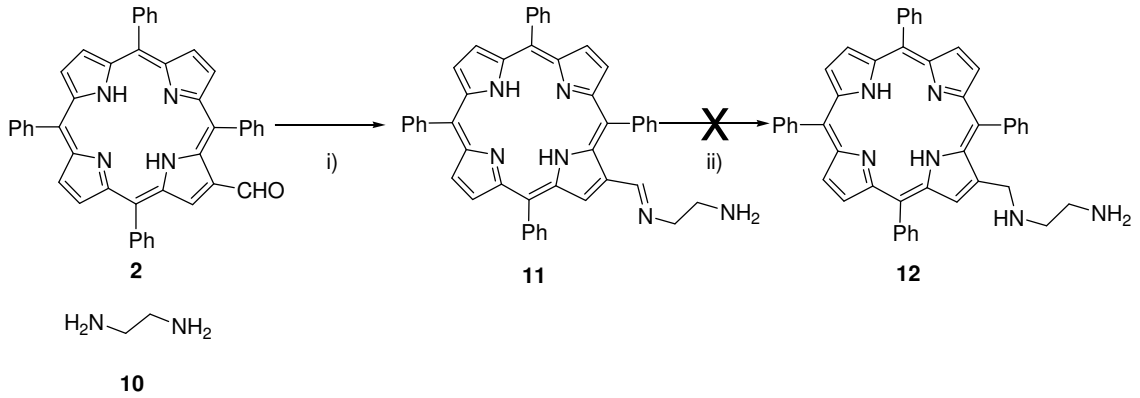

Figure 2.13 Attempted synthesis of Schiff base **12**. Reagents and conditions: i) $CHCl_3$, AcOH, 50 °C, 1 h ii) $NaBH_4$ or $NaCNBH_3$, THF, RT.

Reduction of imine **11** to the corresponding amine (**12**) was attempted using $NaBH_4$ or $NaCNBH_3$ in THF. TLC analysis of the resulting reaction mixtures suggested that no reaction had occurred. This was confirmed by MALDI-TOF analysis where only the starting imine was detected. The inability to reduce the imine was unexpected as literature has shown that the reduction of porphyrin Schiff bases could successfully be performed using $NaBH_4$.[93, 95] Attempts to react the unreduced imine (**12**) with 11-bromoundecanal (**3**) without catalytic amounts of acid showed no reaction. The addition of acetic acid to the reaction resulted in production of TPPCHO (**2,** Figure 2.14).

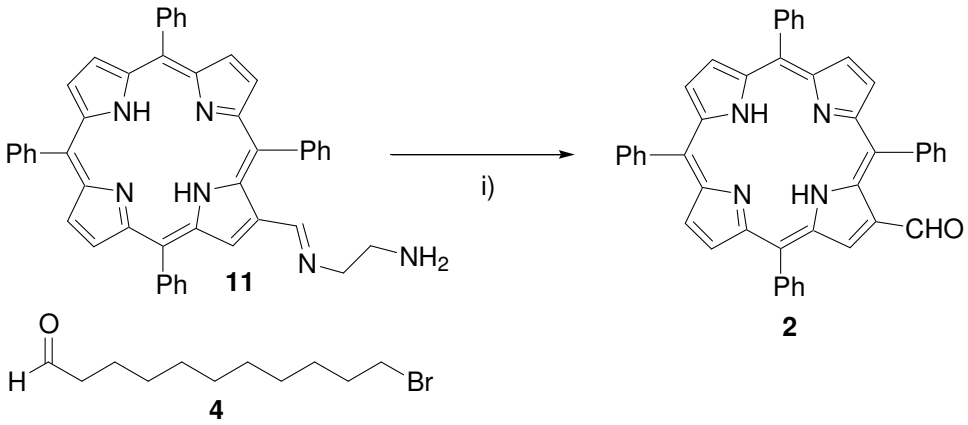

Figure 2.14 Failed Schiff base reaction. Reagents and conditions: i) $CHCl_3$, AcOH, 50 °C.

Due to the problems outlined above, 1,4-phenylenediamine (**13**) was used instead of ethylenediamine as it has the potential to produce a more stable imine due to electron delocalisation between the benzene ring and the porphyrin core. NiTPPCHO (**14**) was reacted with 1,4-phenylenediamine (**13**) in the presence of acetic acid (Figure 2.15). This showed, by TLC, the production of a band with lower R_f than the starting aldehyde, consistent with the production of imine **15**. Attempts to purify the material through neutral alumina resulted in the decomposition to NiTPPCHO, though unlike **11** some of the suspected imine remained. A ^{1}H NMR spectrum of the resulting solid confirmed the existence of NiTPPCHO and another porphyrin in a 1:1 ratio. Although it was suspected that the other compound was the imine due to the presence of appropriate aromatic signals, its presence could not be confirmed by MALDI and ESI mass spectrometry. Attempts to reduce the imine **15** to the corresponding amine using $NaBH_4$ or $NaCNBH_3$ failed to produce any sign of the desired product.

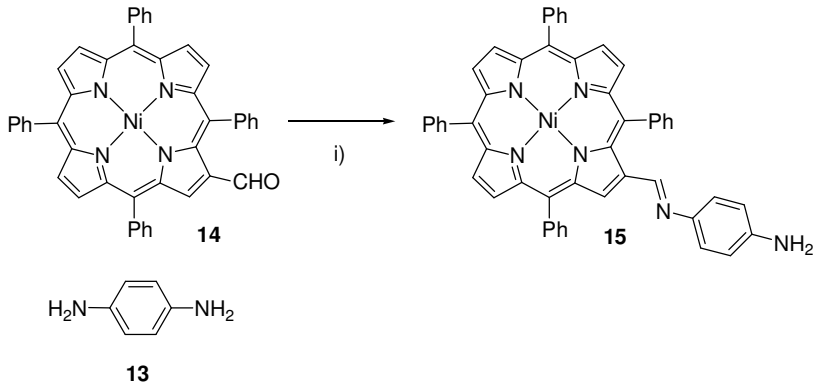

Figure 2.15 Attempted synthesis of imine **15**. Reagents and conditions: i) THF, AcOH, RT, overnight.

Alternatively, the reaction between 11-bromoundecanal (**4**) and a large excess of 1,4-phenylenediamine (**13**) or ethylenediamine (**10**) showed the production of an uncharacterisable black tar. From these results we can conclude that the use of Schiff base reactions to produce lipophilic porphyrins is not possible using the conditions described.

2.3.3 Route C – Amide Bond Formation

Route C was the most successful route for the synthesis of lipophilic porphyrins and allowed for the multi-gram production of the desired compound **16** (Figure 2.16). This involved two major steps: the Wittig reaction to create a stable amino functionalised porphyrin and amide bond formation to add the lipophilic chain.

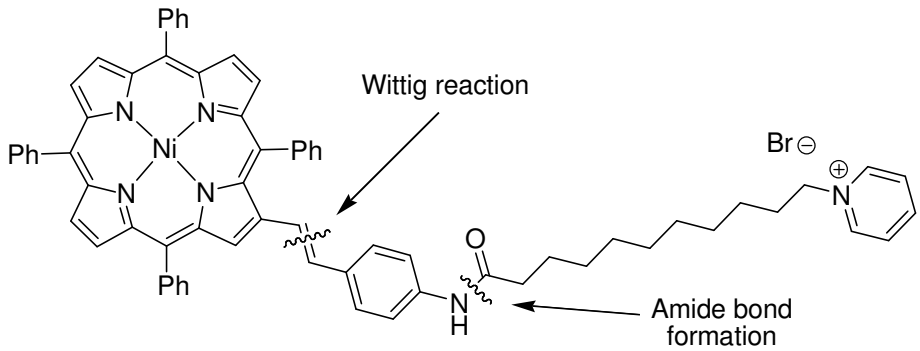

16

Figure 2.16 Lipophilic porphyrin from route C.

2.3.3.1 Synthesis of Amino Porphyrins

β-Pyrrolic modification was chosen over *meso* functionalisation as a *meso* derivative would require the synthesis of a new core porphyrin. Instead, the β-pyrrolic derivative can be obtained from TPP. Direct amine formation at the β-pyrrolic position (Figure 2.17) was avoided as previous attempts showed low stability of 2-amino-5,10,15,20-tetraphenylporphyrinato copper (II) (**17**).[96, 97] Instead, the Wittig reaction was used to indirectly attach an amino functionality to the porphyrin. This produced a more stable amine, particularly, when the Ni^{II} ion was located in the core of the porphyrin.

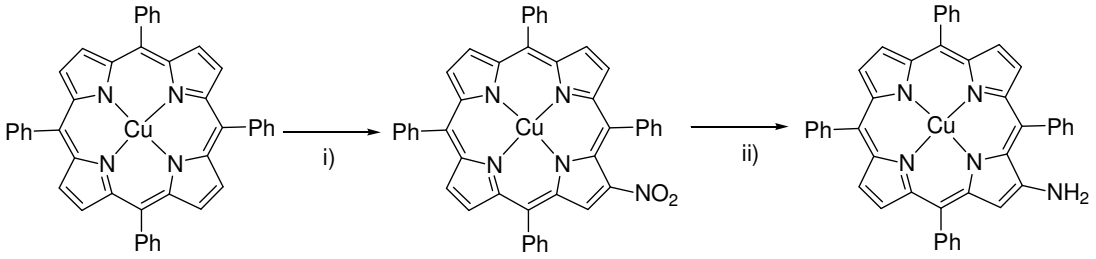

Figure 2.17 Synthesis of 2-amino-5,10,15,20-tetraphenylporphyrinato copper (II) from Zhu *et al.*[96] Reagents and conditions: i) $CHCl_3$, $Cu(NO_3)_2$, AcOH, Ac_2O, RT, 2 h, 30% ii) DCM, MeOH, 10% palladium on carbon, $NaBH_4$, RT, 2 h, 12%.

The treatment of a solution of TPPps (**3**) in dry DCM with 4-nitrobenzaldehyde (**18**) and DBU (Figure 2.18) resulted in the rapid formation of a *cis/trans* (1:2.3) mixture of **19**, which was converted exclusively to the *trans* isomer with iodine treatment. Reduction of compound **19** with $SnCl_2 \cdot 2H_2O$ and HCl[69] to **20** was found to be problematic. Occasionally, after the addition of Et_3N to the reaction, a highly polar material was produced rather than the desired amine. ESI mass spectrometry showed an ion with *m/z* of 950.24 which was consistent with the $M+H^+$ of the Sn^{IV} porphyrin **21**. It was not possible to obtain a crystal of the polar material, however IR spectroscopy showed signals consistent with N=O stretches at 1519 and 1640 cm^{-1} and no NH_2 signals. Furthermore, UV-Vis and ^1H NMR spectroscopy was consistent with a metalled species. Instead the Ni^{II} metal analogue of the nitro porphyrin **19** was prepared using $Ni(OAc)_2 \cdot 4H_2O$ in $CHCl_3$:MeOH (10:1). Ni^{II} was chosen as it is a stable metal ion that is able to be characterised using NMR spectroscopy. Compound **22** was easily converted to amine **23** without the production of any unwanted polar material. This was achieved by stirring **22** in $SnCl_2 \cdot 2H_2O$ and HCl for 48 hours at RT to give **23** in 78% yield, along with the starting material **22** (15% yield). As an aside, it was observed that Ni^{II} or Zn^{II} insertion into **20** resulted in the decomposition of the amine in the presence of the metal acetate.

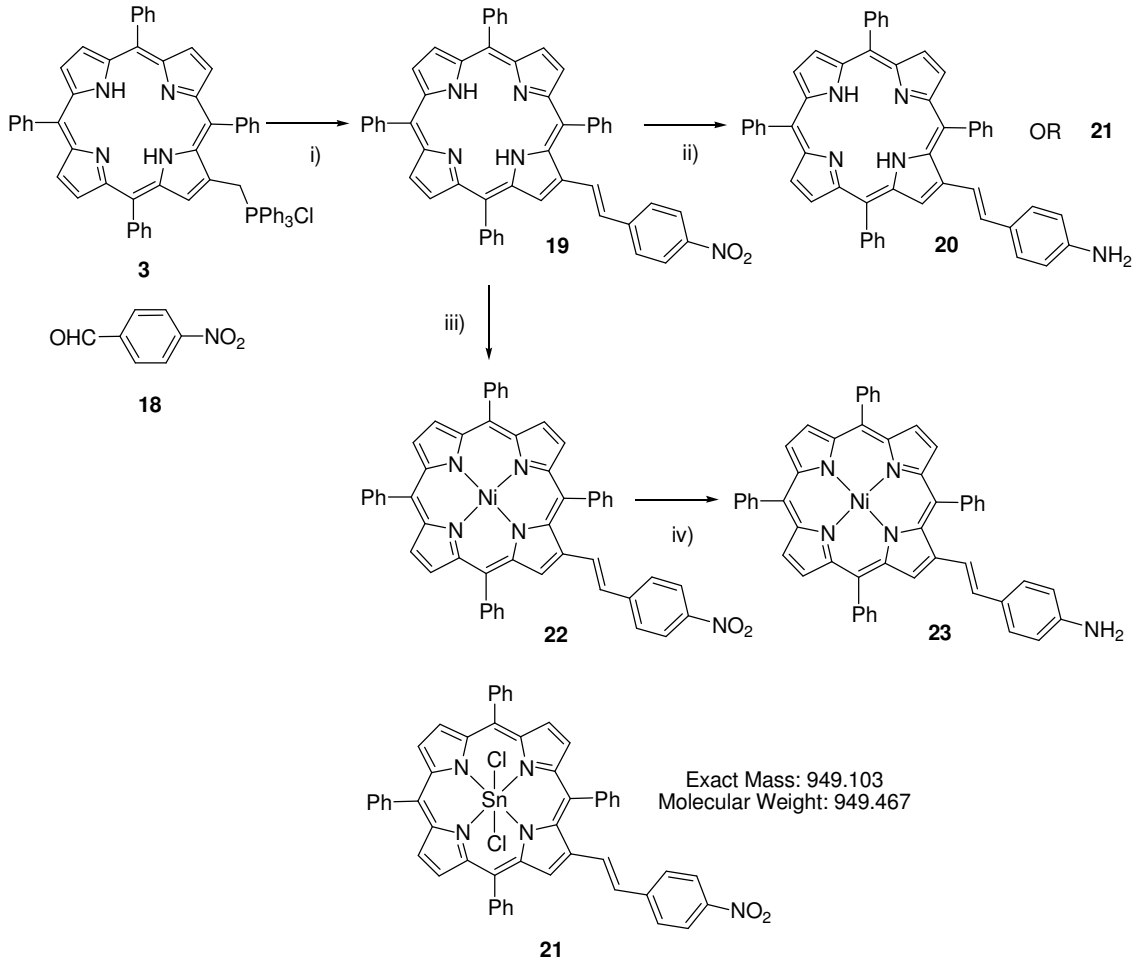

Figure 2.18 Synthesis of amino functionalised porphyrins. Reagents and conditions: i) DCM, DBU, RT, 30 min then I_2, $CHCl_3$, RT, 3 h, 85% ii) THF, $SnCl_2 \cdot 2H_2O$, HCl, RT, 24 h, Et_3N, 87% iii) DCM, MeOH, $Ni(OAc)_2 \cdot 4H_2O$, overnight, reflux, 100% iv) THF, $SnCl_2.2H_2O$, HCl, RT, 24 h, Et_3N, 78%.

2.3.3.2 Amide Bond and Pyridinium Salt Formation

Amide coupling between 11-bromoundecanoic acid **25** (synthesised from 11-bromoundecanol (**24**) as shown in Figure 2.19) and amino porphyrin **23**, to give amide **26**, was performed using adapted methods.[33, 98] This reaction was shown to proceed cleanly in 48 hours using 7.5 eq of EDC, DMAP and acid **25** in THF at RT, or slower over 96 hours using 2.5 eq of each reactant. Purification was achieved *via* silica gel chromatography to give **26** in 76% yield using a reaction that could be easily scaled up to multi-gram quantities. The pyridinium salt (**27**) was formed by refluxing **26** in neat pyridine overnight. Traces of pyridine were removed from **27** by storing the compound under high vacuum for five days.

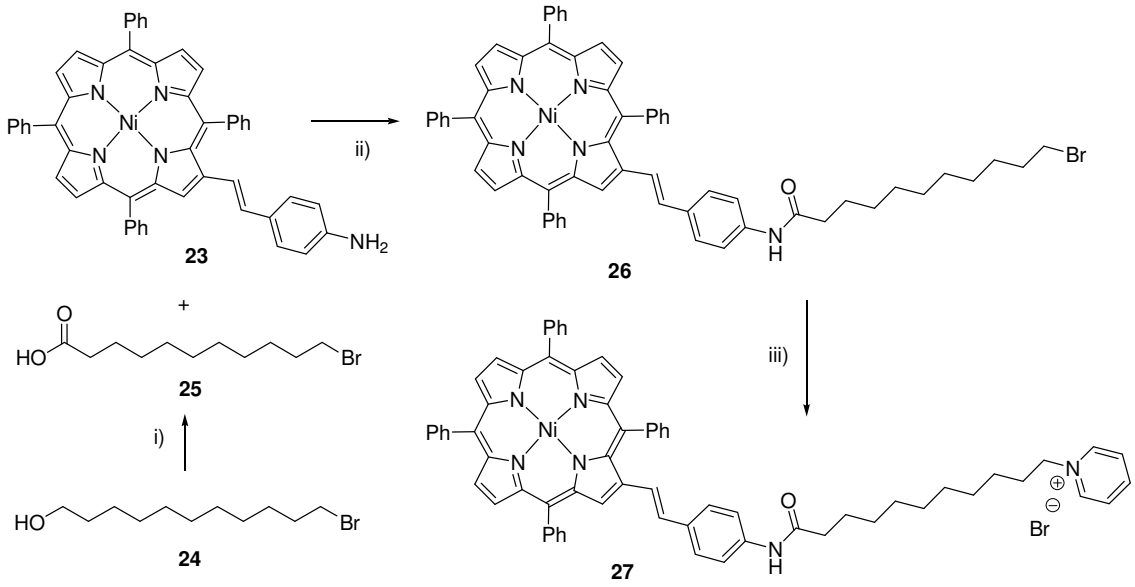

Figure 2.19 Synthesis of lipophilic porphyrin **27**. Reagents and conditions: i) acetone, H_2O, CrO_3, H_2SO_4, 0 °C, 2 h then RT, 12h, 43% ii) THF, EDC, DMAP, RT, 48 h, 76% iii) pyridine, reflux, overnight, 100%.

In summary, three routes were investigated to synthesise lipophilic porphyrins for the construction of DNA-porphyrin supramolecular assemblies. These provided three lipophilic porphyrins (Figure 2.20). Two of the porphyrins (**27** and **9**) were synthesised in a scale large enough to be useful for the development of supramolecular DNA-porphyrin structures, but only compound **27** could be produced in multi-gram quantities.

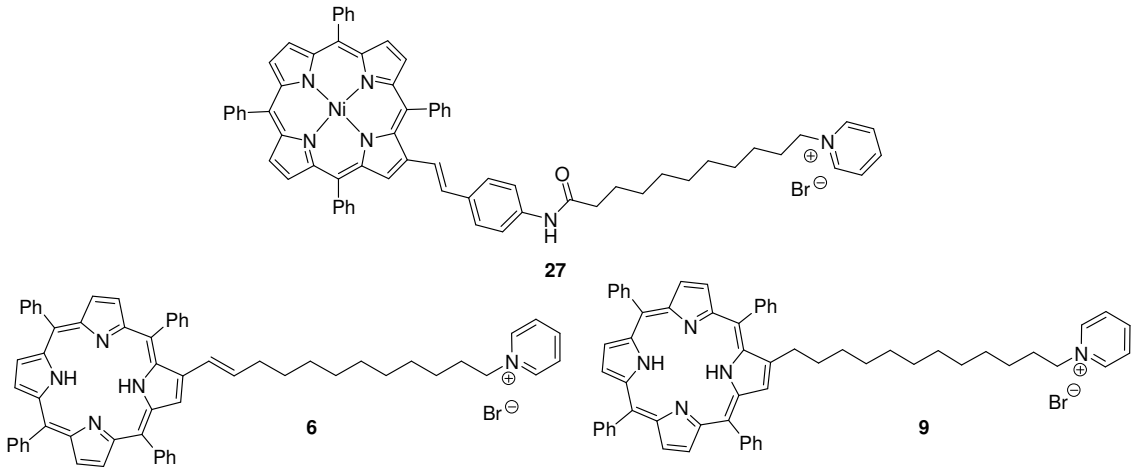

Figure 2.20 Summary of lipophilic porphyrins synthesised.

2.4 Synthesis of Porphyrins for the Covalent Attachment to Nucleosides and DNA

This work studied the covalent attachment of porphyrins to DNA for the development of supramolecular structures around a DNA scaffold. This required the site-specific covalent labelling of DNA. Various chemical coupling methods have been previously implemented to achieve this as discussed in Chapter 1.7. The covalent attachment of porphyrins to DNA can take place using either pre- or post-synthetic approaches (Figure 2.21). The pre-synthetic approach involves the synthesis of porphyrin containing phosphoramidites or H-phosphonates which are then incorporated into the DNA structure during DNA synthesis. The post-synthetic approach involves the synthesis of an oligonucleotide containing a functional group that the porphyrin moieties can be attached to later on. Pre-synthetic modification has advantages over post-synthetic modification, such as ability to incorporate large numbers of modifications into a single strand using automated DNA synthesis. Significant disadvantages also exist such as the time consuming preparation of phosphoramidites, which, in some cases may not be stable for long periods and may not necessary couple into DNA with the required high efficiencies. Post-synthetic modification avoids the synthesis of complex phosphoramidites and allows for the attachment of the porphyrins to functional groups that can be positioned in a number of locations in the oligonucleotide. To achieve pre- or post-synthetic modification a linker is required between the nucleotides and the porphyrin. We decided to use two linkers that have been used substantially in oligonucleotide chemistry. The 1,2,3-triazole linker, which is formed using Cu^{I} catalysed azide alkyne Huisgen 1,3-dipolar cycloaddition (CuAAC), and the alkyne linker formed using Pd^{0} catalysed Sonogashira reaction. The synthesis of the porphyrins used in these reactions is detailed below. The pre- and post-synthetic coupling reactions will be discussed in Chapter 5 and 6.

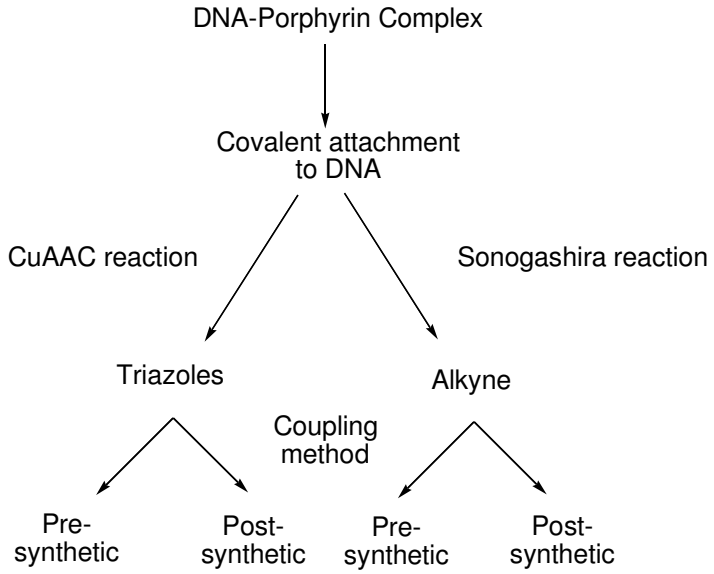

Figure 2.21 Synthetic outline for the development of DNA-porphyrin supramolecular structures using covalent attachment methods.

2.4.1 Synthesis of Porphyrin for Use in Pre- and Post-synthetic Sonogashira Chemistry

The Sonogashira reaction is a Pd^0 catalysed reaction between a terminal alkyne and a halide, preferably an iodo derivative. Three β-pyrrolic functionalised porphyrin derivatives were chosen as target compounds (Figure 2.22). The iodo **32**, the bromo **40** and the terminal alkyne **35** were synthesised using modified Horner-Emmons chemistry. The implementation of modified Horner-Emmons chemistry to create β-pyrrolic ethynyl modifications in porphyrins is a novel approach involving the reaction of a phosphonate and an aldehyde in basic conditions to give an alkyne. Further details of the modified Horner-Emmons reactions are discussed in depth in Chapter 3. Direct halogenation at the β-pyrrolic position of the porphyrin core was not considered for reasons discussed previously.

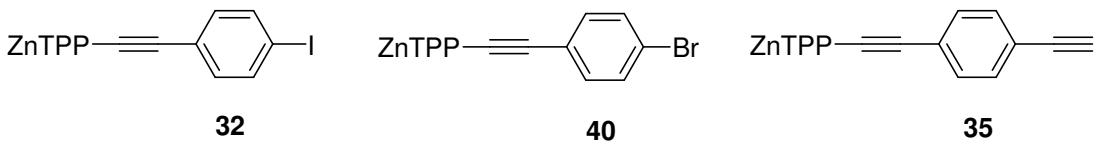

32 **40** **35**

Figure 2.22 Target compounds for use in Sonogashira chemistry.

Compounds **32** and **35** were synthesised from bromophosphonate **30** and TPPCHO (**2**) as shown in Figure 2.23. The bromophosphonate **30** was synthesised from phosphonate **29** using tetrabutylammonium bromide, DDQ and triphenylphosphine in a 84% yield using the method of Firouzabadi *et al.*[99] Phosphonate **29** was synthesised in a 90% yield using diphenylphosphite and 4-iodobenzaldehyde,[100] which in turn was synthesised in three steps from 4-iodobenzoic acid (**28**) in a 35% yield.[101, 102] The iodo functionalised porphyrin **31** was synthesised *via* a modified Horner-Emmons reaction[80] between the bromophosphonate **30** and TPP-CHO (**2**) in a 75% yield. This reaction could easily be scaled up to allow for the multi-gram production of **31**. Zn^{II} was inserted into the porphyrin core (**32**) in a quantitative yield in order to prevent copper insertion during the subsequent Sonogashira reactions, in which Cu^{I} is the co-catalyst.

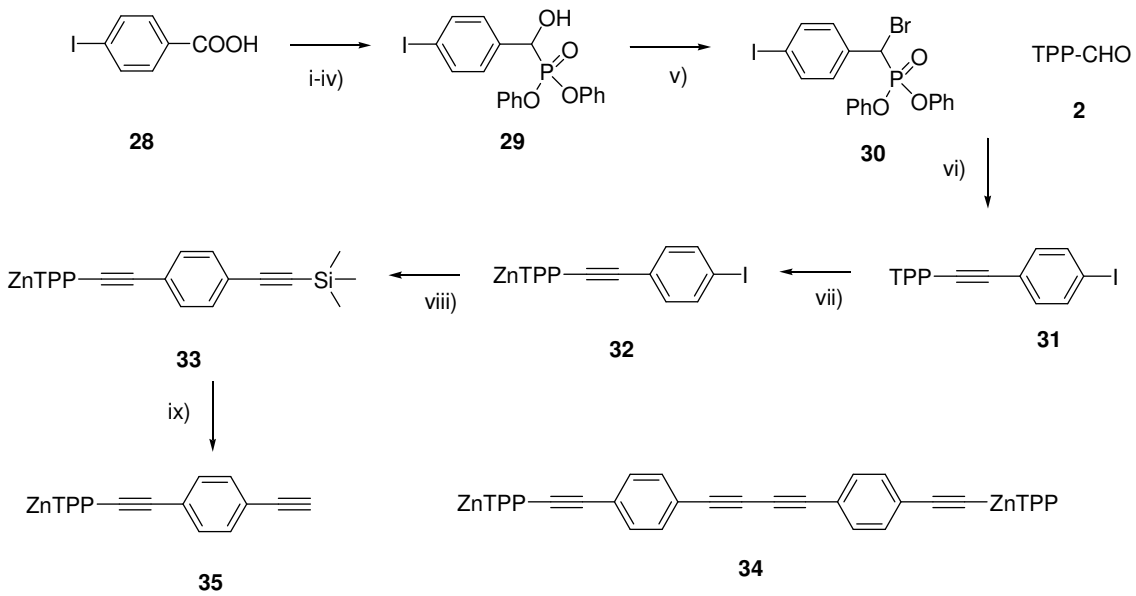

Figure 2.23 Synthesis of precursors for the Sonogashira reaction. Reagents and conditions: i) $SOCl_2$, reflux, overnight, 47% ii) CH_3CN, $LiClO_4$, $NaBH_4$, RT, overnight, 87% iii) DCM, BIAB, TEMPO, RT, 2 h, 85% iv) diphenylphosphite, MgO, RT, overnight, 90% v) DCM, DDQ, PPh_3, $n$$Bu_4NBr$, RT, overnight, 84% vi) THF, *t*-BuOK, RT, 3 h, 75% vii) $CHCl_3$, MeOH, $Zn(OAc)_2{\cdot}2H_2O$, RT, 1 h, 99% viii) Et_3N, trimethylsilylacetylene, $Pd(PPh_3)_4$, CuI, reflux 3 h, 93% ix) DCM, THF, TBAF, RT, 5 min, 97%.

Conversion of **32** to **33** was achieved in a 93% yield by refluxing a solution of 2-(4′-iodophenyl)ethynyl-5,10,15,20-tetraphenylporphyrinato zinc (II) (**33**) and trimethylsilylacetylene in Et_3N in the presence of 0.3 eq. of $Pd(PPh_3)_4$ and 0.5 eq. of CuI under argon overnight. The use of DMF as a solvent resulted in the isolation of the starting material. It was critical to remove trace quantities of copper and palladium salts by washing the trimethylsilyl protected porphyrin **33** repeatedly with a 5% aq

Na_2EDTA solution followed by 3M NH_4OH. Failure to do so resulted in the exclusive formation of the Glaser homodimer by-product **34** upon cleavage of the silyl protecting group. After washing, deprotection of **33** to **35** using TBAF was achieved with no sign of the unwanted Glaser homodimer **34**. This synthesis provided both a terminal alkyne and iodo derivatives for the use in pre- and post-synthetic Sonogashira coupling methods.

Alternatively, the bromo derivative of compound **32** was synthesised as shown in Figure 2.24. The synthesis of **40** was achieved using similar chemistry to that of **32**. Phosphonate **36** was synthesised from 4-bromobenzaldehyde and diphenylphosphate using MgO. The required halophosphonate for the modified Horner-Emmons chemistry was synthesised as the chlorophosphonate **37** and the bromophosphonate **38**. The chlorophosphonate **37** was prepared in a 22% yield using $POCl_3$/*N*,*N*-diethylaniline[103] and the bromophosphonate **38** in a 73% yield using milder reaction conditions of tetrabutylammonium bromide, DDQ and triphenylphosphine.[99] Phosphonates **37** and **38** were then reacted separately with TPPCHO (**2**) under modified Horner-Emmons conditions to produce alkyne **39**. Yields were moderately higher using the bromophosphate **38** than the chlorophosphonate **37**. Reactions from either phosphonate produced an inseparable mixture of **39** and the halovinyl intermediate (see Chapter 3). This could only be avoided by performing the Horner-Emmons reaction in refluxing THF but as a consequence the yield dropped to 15%. Zn^{II} was inserted into porphyrin **39** to prevent Cu insertion during the following Sonogashira reactions.

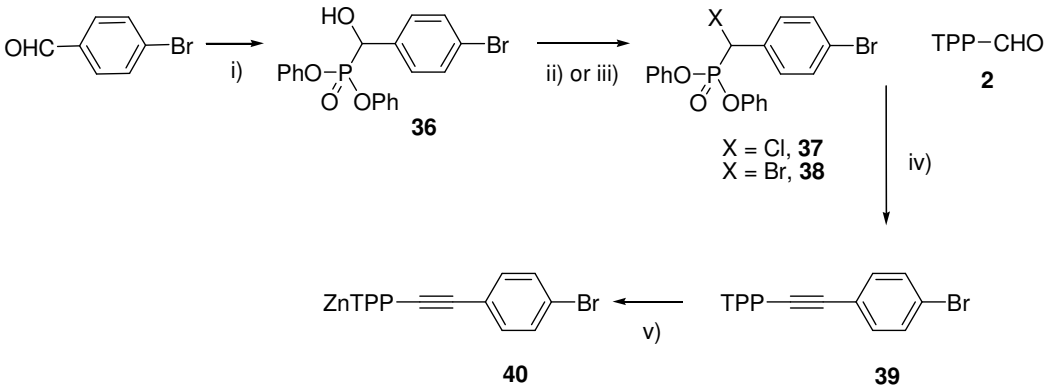

Figure 2.24 Synthesis of precursor **40** for the Sonogashira reaction. Reagents and conditions: i) diphenolphosphite, MgO, RT, overnight, 90% ii) $POCl_3$, *N*,*N*-diethylaniline, 90 °C, 1 h, 22% iii) DCM, DDQ, PPh_3, nBu_4NBr, RT, overnight, 73% iv) THF, *t*-BuOK, RT, 45 min, 81% from **37**, 40% from **38** v) $CHCl_3$, MeOH, $Zn(OAc)_2 \cdot 2H_2O$, RT, 1.5 h, 92%.

2.4.2 Synthesis of Porphyrin for Use in Pre- and Post-synthetic CuAAC Reactions

Huisgen 1,3-dipolar cycloaddition between an azide and a terminal alkyne (CuAAC reaction) as a variety of the "click reaction" and is an invaluable tool for the modification of DNA and other biomolecules.[60, 61] CuAAC chemistry has been used to couple a significant number of organic molecules to DNA.[104] Prior to this work coupling had not been achieved using porphyrins. It is difficult to synthesise an azido functionalised DNA, however, alkyne nucleosides are commercially available. Therefore a number of novel azido functionalised porphyrins were synthesised for the use in CuAAC reactions. Although few examples of azido porphyrins are present in literature, it was possible to tune existing chemistry and apply it for the synthesis of the desired compounds (Figure 2.25). The azido porphyrins were classed in two categories depending on the type of azide synthesised: aliphatic and aromatic azides. After purification the presence of the azides was confirmed by observing the IR azide asymmetric stretches at ~2015 cm^{-1} for aromatic azides and 2095 cm^{-1} for aliphatic azides.

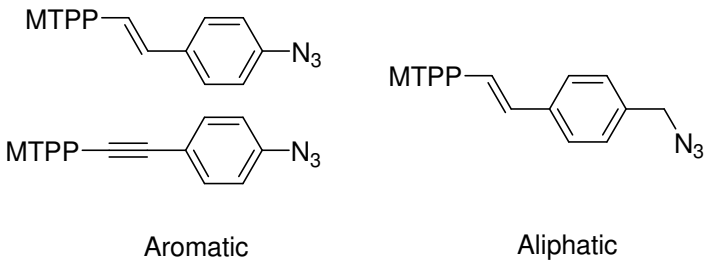

Figure 2.25 Target compounds for use in CuAAC reactions (M = H_2, Ni^{II}, Cu^{II}, Zn^{II}, Fe^{III}).

2.4.2.1 Synthesis of Aromatic Azides

The aromatic Ni^{II} azido porphyrin **41** was obtained in four steps from TPPps **3** and nitro benzaldehyde as shown in Figure 2.26. As discussed previously, the treatment of a DCM solution of **3** with 4-nitrobenzaldehyde and DBU, using a method adapted from Bonfantini *et al.*,[78, 87] resulted in the rapid formation of a *cis/trans* mixture of **19**. This was converted exclusively to the *trans* isomer by iodine treatment. Metallation of the nitro compound **19** with $Ni(OAc)_2 \cdot 4H_2O$ provided the Ni^{II} analogue **22** which was reduced to the amine **23** using $SnCl_2 \cdot 2H_2O$ and HCl. Azide formation (**41**) was

achieved *via* diazotisation with $H_2SO_4/NaNO_2$ in the dark followed by the addition of NaN_3.[68, 69] The formation of the β-functionalised free base aromatic azide **42** was achieved using a similar method to that described for the Ni^{II} porphyrin.

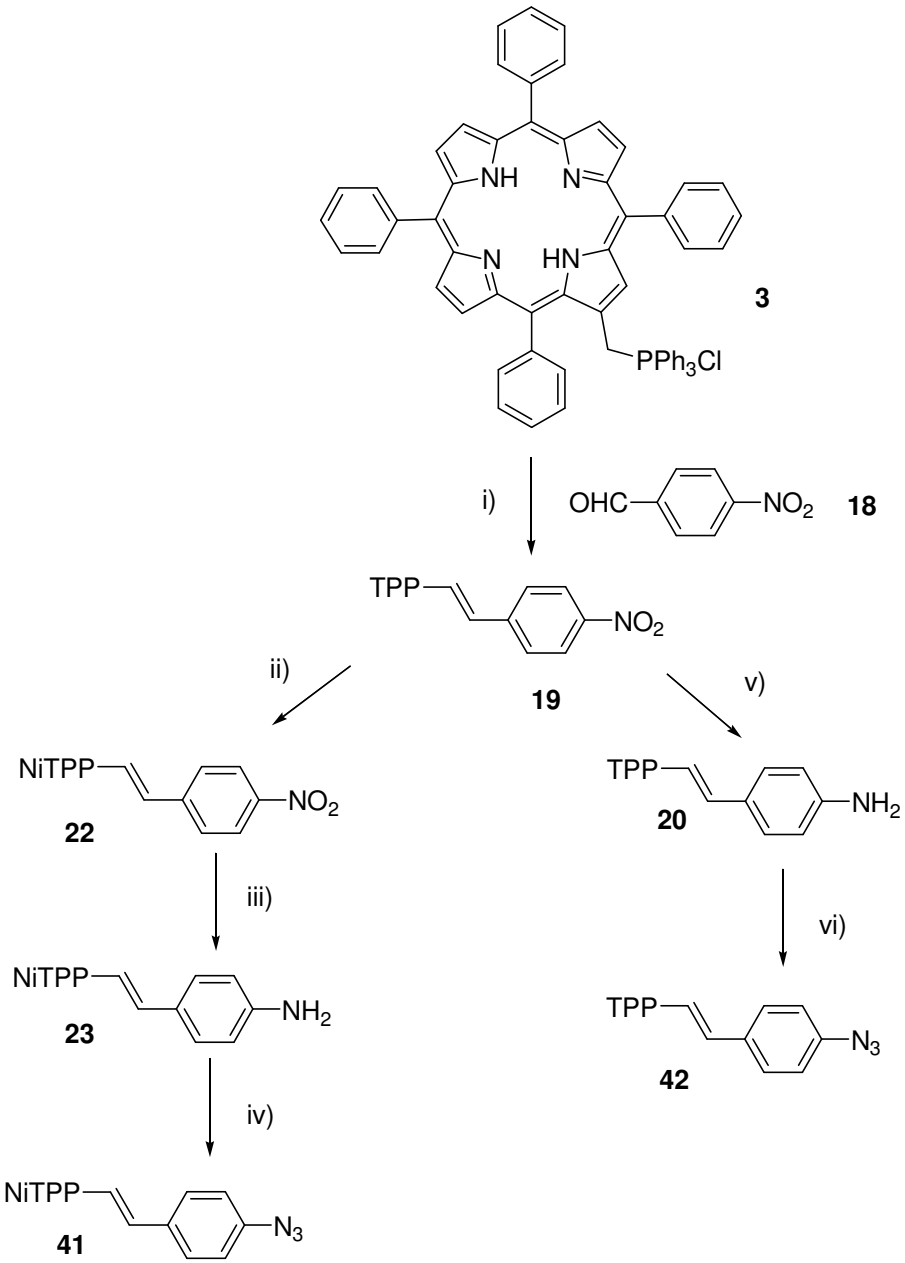

Figure 2.26 Synthesis of aromatic azides **41** and **42** for use in CuAAC reactions. Reagents and conditions: i) DCM, DBU, RT, 30 min then I_2, $CHCl_3$, RT, 3 h, 85% ii) DCM, MeOH, $Ni(OAc)_2 \cdot 4H_2O$, overnight, reflux, 100% iii) THF, $SnCl_2.2H_2O$, HCl, RT, 24 h, Et_3N, 78% iv) THF, H_2O, $NaNO_2$, H_2SO_4, RT, 2 h then NaN_3, RT, 20 min, 98% v) THF, $SnCl_2.2H_2O$, HCl, RT, 24 h, Et_3N, 78% vi) THF, H_2O, $NaNO_2$, H_2SO_4, RT, 2 h then NaN_3, RT, 20 min, 96%.

The alkyne linked aromatic azide **45** (Figure 2.27) was successfully synthesised after numerous unsuccessful reactions. Attempts to form azide **45** from nitro **44** (*via* the corresponding aniline derivative) failed as the nitro precursor (**44**) could not be obtained using Horner-Emmons chemistry. Attempts to synthesise the nitro porphyrin **44** from the appropriate bromophosphonate **43** and TPPCHO (**2**) using modified Horner-Emmons chemistry resulted in the isolation of an intractable mixture of unknown compounds. Alternatively, it was possible to obtain the azide from the corresponding iodo derivative **32**. The synthesis of the azide **45** was achieved in a 61% yield *via* the reaction of the iodo precursor **32** with NaN_3, sodium ascorbate, *N*,*N*-DMEA and $Cu(ACN)_4PF_6$ in dry DMSO. Alternative reaction conditions involving the bromo (**40**) or iodo (**32**) functionalised porphyrins, as listed in Table 2.1, resulted in the quantitative isolation of the starting material. It is interesting that although iodo **32** could be converted to azide **45**, reaction using the ethene equivalent of porphyrin **32** under identical reaction conditions only resulted in the isolation of the starting material.

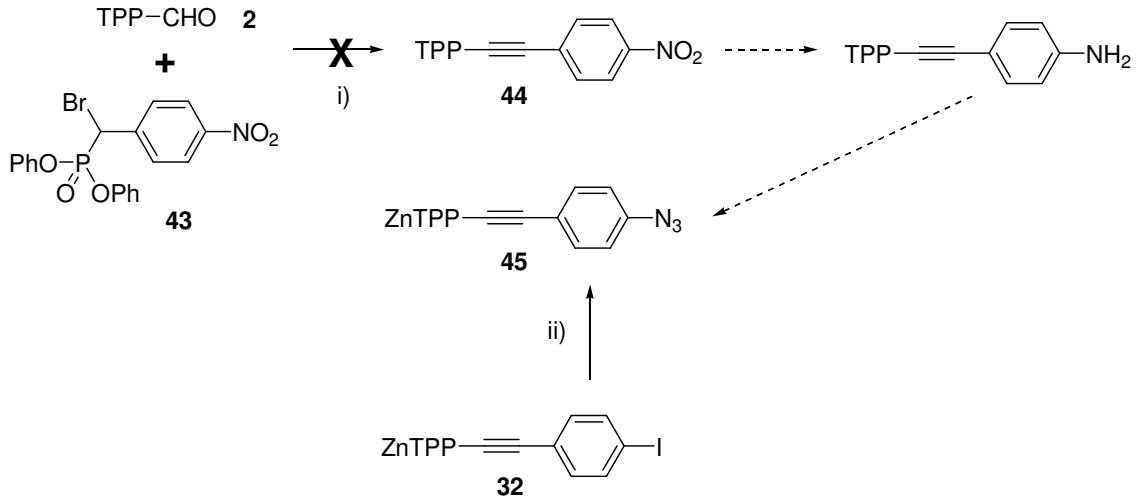

Figure 2.27 Synthesis of aromatic azide **45** for use in CuAAC reactions. Reagents and conditions: i) THF, *t*-BuOK, RT, 3 h ii) DMSO, NaN_3, sodium ascorbate, $Cu(ACN)_4PF_6$, *N*,*N*-DMEA, 70 °C, 48 h, 61%.

Table 2.1 Synthetic attempts for the synthesis of azide **45**.

Starting material	Reagents	Reaction Conditions	Result
Bromo **40**	NaN_3, sodium ascorbate, CuI, *N*,*N*-DMEA	DMSO, RT, overnight	No reaction
Bromo **40**	NaN_3, sodium ascorbate, CuI, *N*,*N*-DMEA	DMSO, 70 °C, overnight	No reaction
Iodo **32**	NaN_3, sodium ascorbate, CuI, *N*,*N*-DMEA	DMSO, 70 °C, overnight	No reaction
Bromo **40**	NaN_3, sodium ascorbate, CuI, *N*,*N*-DMEA	DMSO: H_2O (9:1), microwave, 1 h, 100 °C	No reaction
Iodo **32**	NaN_3, sodium ascorbate, CuI, *N*,*N*-DMEA	DMSO: H_2O (9:1), microwave, 1 h, 100 °C	No reaction
Iodo **32**	NaN_3, sodium ascorbate, CuI, *N*,*N*-DMEA	DMSO: H_2O (9:1), 70 °C, overnight	No reaction
Iodo **32**	NaN_3, sodium ascorbate, CuI, *N*,*N*-DMEA	Toluene, 70 °C, overnight	No reaction
Iodo **32**	NaN_3, L-proline, CuI, NaOH	DMSO, 70 °C, overnight	No reaction
Iodo **32**	*n*BuLi, tosyl azide	THF, -78 °C to RT	Unknown products
Iodo **32**	NaN_3, sodium ascorbate, $Cu(ACN)_4PF_6$, *N*,*N*-DMEA	DMSO, 70 °C, 48 h	61 %

2.4.2.2 Synthesis of Aliphatic Azides

The desired aliphatic azides (Figure 2.28) were synthesised from aldehyde **47** and TPPps **3** in two steps *via* the Wittig reaction followed by metal insertion. Aldehyde **47** was obtained from *para*-tolunitrile in three steps using methods of Schlenoff *et al.*[105] and Barbe *et al.*[106] The aliphatic azide **48** was synthesised in an overall yield of 60% *via* a Wittig reaction between phosphonium salt **3** and aldehyde **47** followed by iodine isomerisation. The Wittig reaction must be performed using the azido aldehyde **47** as the bromo aldehyde **46** was found to self polymerise in the presence of DBU. Importantly, the aliphatic azide **48** was stable to the conditions used for the insertion of various metal ions (Zn^{II} (**49**), Ni^{II} (**50**), and Fe^{III} (**51**)). Pt^{II} insertion, which requires refluxing in benzonitrile, could not be obtained as decomposition of the azide occurred at the elevated temperatures.

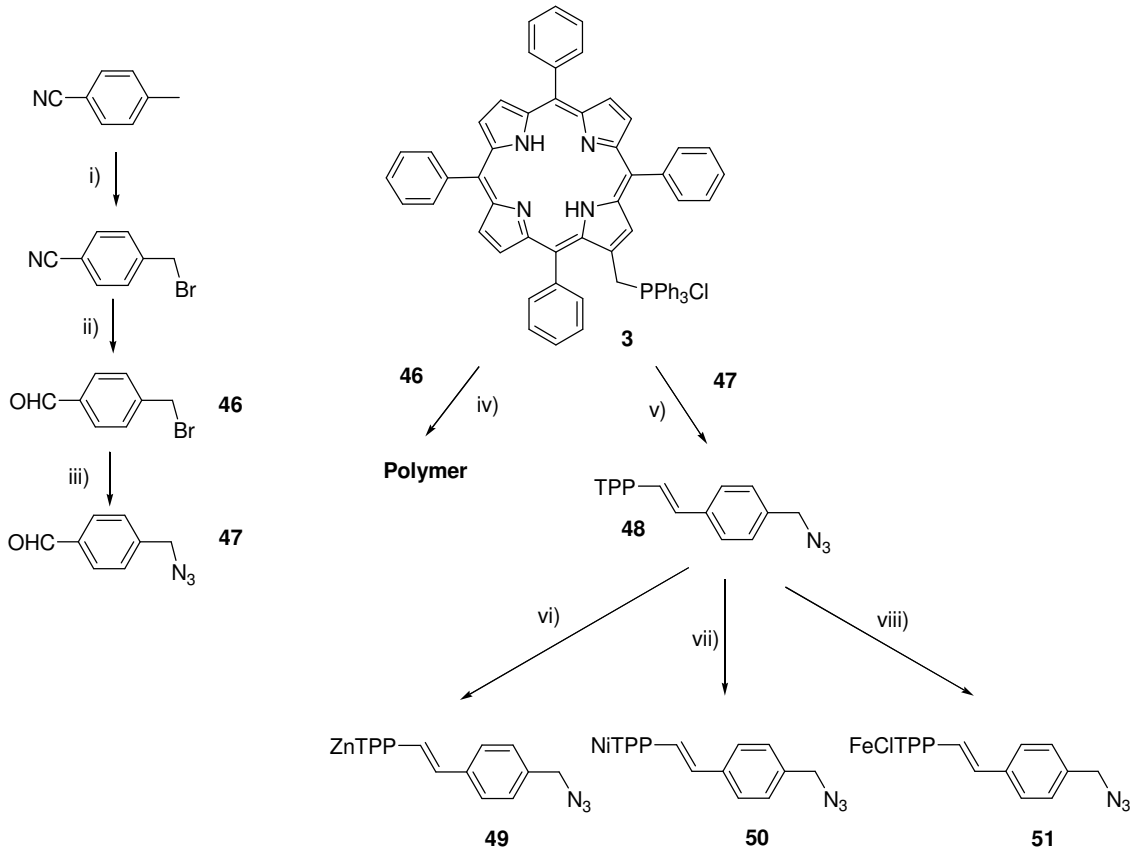

Figure 2.28 Synthesis of aliphatic azides **48-51** for use in CuAAC reactions. Reagents and conditions: i) CCl_4, NBS, light, reflux, 2 h, 62% ii) toluene, DIBAL, 0 °C, 1 h then $CHCl_3$, HCl, RT, 1 h, 72% iii) Acetone, H_2O, NaN_3, reflux, overnight, 100% iv) DCM, DBU, RT, 20 min v) DCM, DBU, RT, 20 min then $CHCl_3$, I_2, RT, overnight, 60% vi) DCM, MeOH, $Zn(OAc)_2 \cdot 2H_2O$, RT, 1 h, 97% vii) $CHCl_3$, MeOH, $Ni(OAc)_2 \cdot 4H_2O$, reflux, overnight, 99% viii) acetonitrile, $CHCl_3$, $FeCl_2 \cdot 4H_2O$, 70 °C, 5 h, then air, 70 °C, overnight, 90%.

2.5 Conclusion

In summary, we have synthesised a number of β-pyrrolic functionalised porphyrin precursors for the development of DNA-porphyrin supramolecular constructs. This includes the synthesis of lipophilic porphyrins for the construction of lipophilic DNAs, as well as building blocks required for pre- and post-synthetic Sonogashira and CuAAC reactions. The construction of these complexes will be discussed in Chapters 4-6.

Chapter 3 Synthesis of β-Pyrrolic Ethynyl Porphyrin Derivatives *via* the Modified Horner-Emmons Reaction

3.1 Introduction

An ethynyl bond is an important linkage for the development of chromophores for use in light harvesting devices[88, 89, 107] and supramolecular DNA-porphyrin systems. Molecular modelling calculations have shown that enhanced communication exists in β-pyrrolic ethynyl porphyrins over similar ethenyl compounds.[2] It has also been observed that a triple-bonded β-pyrrolic substituent stabilises the porphyrin ring toward oxidation more effectively than the equivalent double-bond systems, suggesting possible advantages of ethynyl linkages in light harvesting devices.[108]

The synthesis of porphyrins containing ethynyl substituents at the β-pyrrolic position is typically achieved *via* a Sonogashira[108-110] or other metal catalysed coupling reactions from the corresponding 2-bromoporphyrins.[81-86] However, Sonogashira coupling reactions on 2-bromo-5,10,15,20-tetraphenylporphyrin are relatively low yielding and restricted to small scales. [76, 7781, 109, 111-115] Sonogashira couplings also require the use of a copper co-catalyst which has the potential to metalate/transmetalate the porphyrin.[116] Alternative copper free coupling has been performed using Pd catalysts[81] and ligands such as $AsPh_3$.[81, 109, 117] However, the restriction imposed by the expense and toxicity of the reagents, together with the harsh reaction conditions (high reaction temperatures for extended times), limits the application of this approach in possible scaled-up reactions. Due to the importance of the ethynyl linkage we investigated a new method for the creation of β-pyrrolic ethynyl bonds in porphyrins. As an alternative, a modified Horner-Emmons (or Horner-Wadsworth-Emmons) reaction (Figure 3.1) was applied to porphyrins for the construction of β-pyrrolic ethynyl linkages.

The Horner-Emmons reaction is used for the synthesis of alkenes from an aldehyde and a phosphonate in the presence of a base. Modifying the phosphonate to introduce a

leaving group enables the synthesis of ethynyl linkages as shown in Figure 3.2. This modified Horner-Emmons reaction negates the need for a halogenated porphyrin and a metal catalyst. Target compounds could be produced in high yielding, scalable reactions from the readily synthesised 2-formyl-5,10,15,20-tetraphenylporphyrin (TPPCHO, **2**).

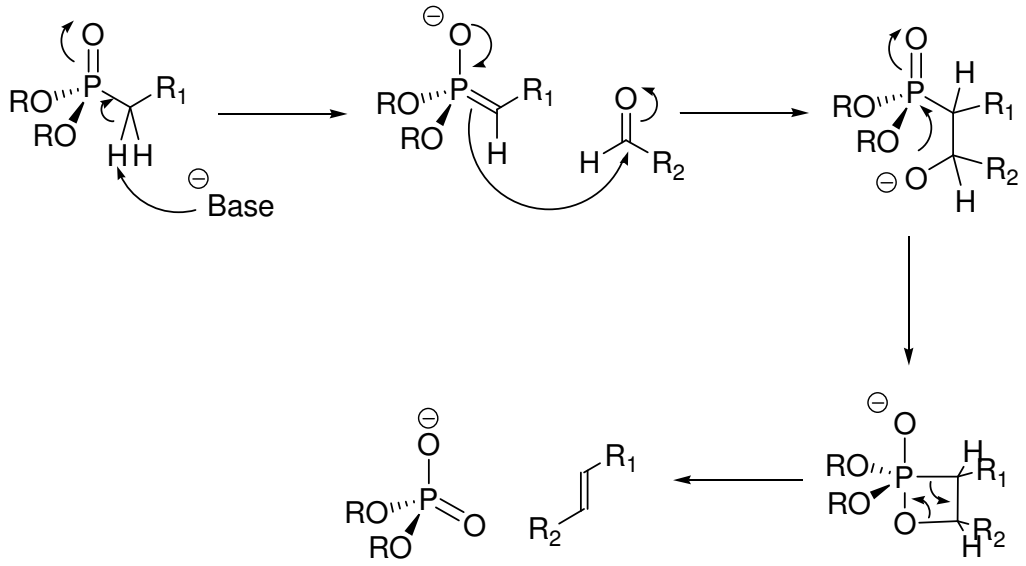

Figure 3.1 The mechanism of the Horner-Emmons reaction for the synthesis of alkenes.

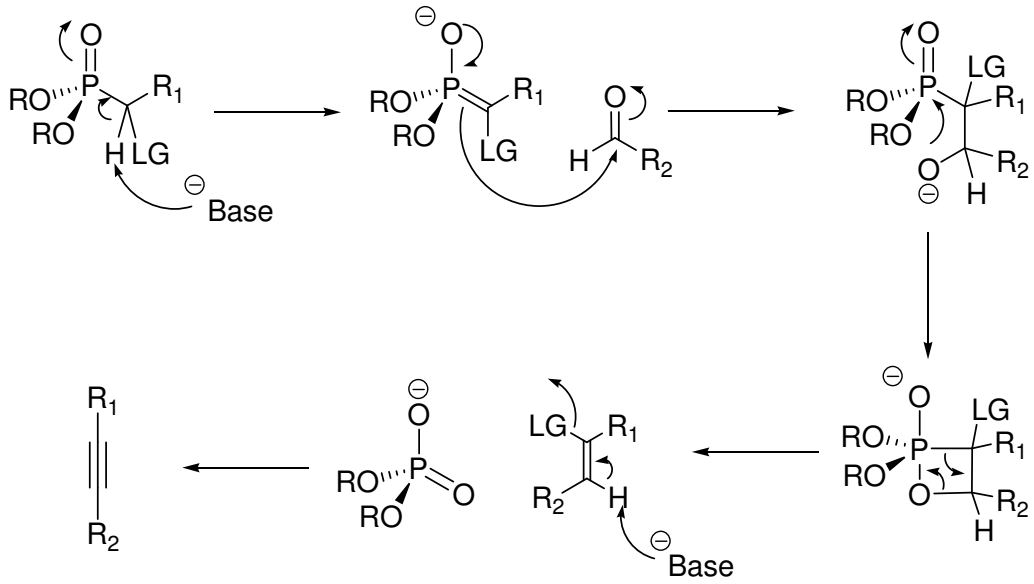

Figure 3.2 The mechanism of the modified Horner-Emmons reaction for the synthesis of alkynes.

The synthesis of β-pyrrolic substituted ethynyl porphyrins also gave us an opportunity to construct and investigate the performance of novel β-pyrrolic functionalised ethynyl

acid derivatives as light harvesting molecules in a dye sensitised solar cell (DSSC) device.

Dye sensitised solar cells are a relatively new class of low-cost photovoltaic devices that have been the focus of research here at Massey University and elsewhere for more than two decades. Porphyrins have shown promise as dyes in DSSCs.[88, 89, 107] DSSCs, most commonly known as Grätzel cells[118] after its inventor, consists of a layered structure comprising of (Figure 3.3):

- A conducting ITO covered glass electrode,
- A wide band gap semi-conductor, most commonly nanocrystalline anatase TiO_2,
- A monolayer of dye (porphyrin),
- A redox active electrolyte (usually I^-/I_3^- couple) and
- A counter ITO covered glass electrode with catalytic Pt coating.

Photo-excitation of the dye on the surface of the TiO_2 results in the injection of an electron from the dye into the conduction band of the TiO_2, which then perculates to the ITO electrode of the glass. The captured electrons can then be used by a device or stored. The electrons then flow back to the counter electrode where they are picked up *via* an I^-/I_3^- redox couple in the electrolyte. The redox couple then returns the charged dye back to the neutral state, allowing the whole process to repeat upon further excitation.

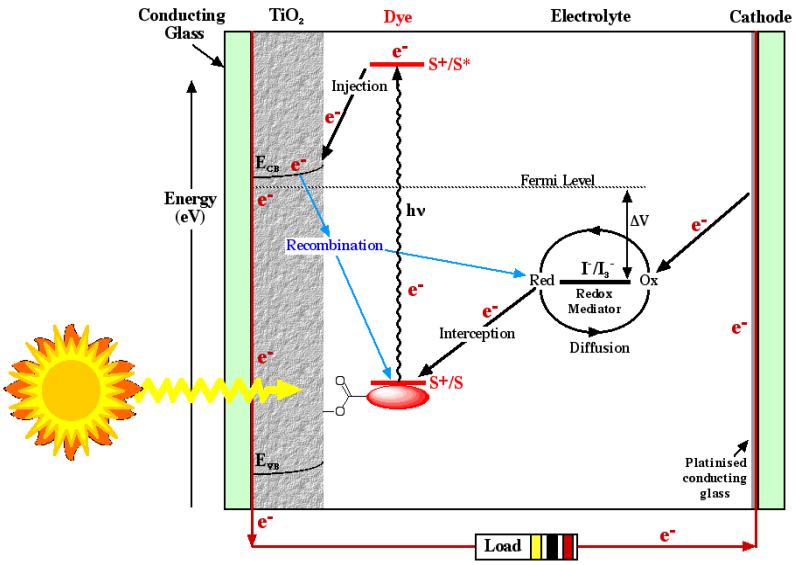

Figure 3.3 Schematic representation of a Grätzel cell (reproduced from Campbell).[3]

Previous research has found that three important aspects of the porphyrin dye affect the performance of the dye in light harvesting Grätzel cells: the chromophore, the linker and the binding group (Figure 3.4).[88] Previous studies have extensively tested a number of β-pyrrolic porphyrins containing a variety of conjugated and non conjugated linkers.[10, 88, 89, 119-121] None of these early studies explored the ethynyl linker in these molecules. As we have a route to the synthesis of ethynyl derivatives and the ability to test them it was decided to synthesise and to explore their efficiencies in a DSSC. Comparisons can then be made to the previously studied ethane and ethene linker derivatives.

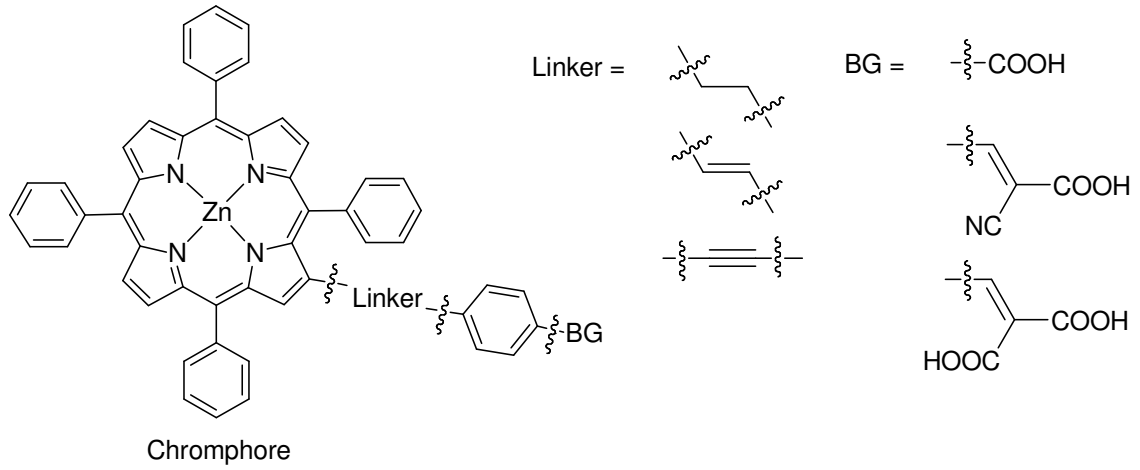

Figure 3.4 β-Pyrrolic substituted TPP showing various linkers and binding groups (BG) used for DSSCs.

3.2 Chapter Summary

This chapter discusses the development and limitations of modified Horner-Emmons chemistry for the synthesis of a number of novel β-pyrrolic substituted ethynyl porphyrins. From these we have synthesised several carboxylic acids dyes for use in light harvesting DSSC devices. Spectroscopic properties and application of these molecules in DSSC were investigated and discussed.

3.3 Synthesis of β-Pyrrolic Ethynyl Porphyrins

3.3.1 Phosphonate Synthesis

To synthesise the desired alkynes the modified Horner-Emmons reaction requires an aldehyde and a phosphonate containing an appropriate leaving group. We chose to use 2-formyl-5,10,15,20-tetraphenylporphyrin (TPPCHO, **2**) and an aromatic phosphate. There are many synthetic routes for the formation of phosphonates from the corresponding aldehydes. Phosphonates **29**, **36** and **52-58** (Figure 3.5 and Table 3.1) were obtained from the corresponding aromatic aldehydes using diphenolphosphite and MgO in high yields.[100, 122] Aldehydes required were either purchased or synthesised as in the case of 4-iodobenzaldehyde[101, 102] and 4-(5,5-dimethyl-2-phenyl-1,3-dioxane)benzaldehyde.

To prevent the reaction stopping at the production of the alkene the phosphonates must contain an appropriate leaving group. Previous work has shown the effective use of leaving group such as halogens,[122, 123] benzotriazoles and methylsulfonic acids.[100] Bromo and chloro leaving groups were selected as they are easy to prepare (Figure 3.5). Halophosphonates were either synthesised as the chlorophosphonates (**37**, **59-63** and **66**, Table 3.1) with phosphoroxychloride and *N,N*-diethylaniline[103] or as bromophosphonates (**30**, **38**, and **64**-**65**) using tetrabutylammonium bromide, DDQ and triphenylphosphine[99] (Table 3.1). Halophosphonates were easily purified *via* silica gel column chromatography or recrystallisation. Although the halophosphonates were present in an mixture of isomers this did not effect the Horner-Emmons reaction. Chlorophosphonates were obtained in a lower yield than the bromophosphonates due to the harsh acidic conditions involved in chlorination. Similarly, chlorination could not be used where the aromatic substituent was acid sensitive such as in **63** where the 1,3-dioxane ring was hydrolysed in acidic conditions.

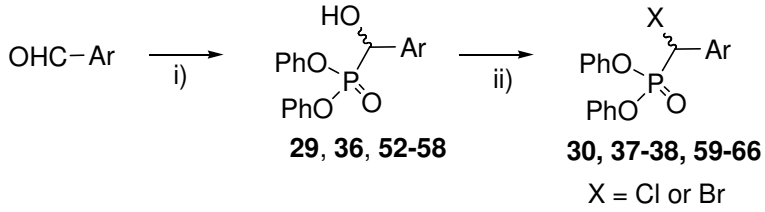

Figure 3.5 Synthesis of chloro and bromophosphonates from the appropriate aldehydes. Reagents and conditions: i) diphenylphosphite, MgO, RT, overnight ii) $POCl_3$, *N,N*-diethylaniline, 90 °C, 1 h or DCM, DDQ, PPh_3, nBu_4NBr, RT, overnight.

Table 3.1 Phosphonates synthesised and their yields.

Ar	X (compound)	Yield (%)	X (compound)	Yield (%)
4-Iodophenyl	OH (**29**)	84	Br (**30**)	84
4-Bromophenyl	OH (**36**)	90	Cl (**37**)	22
			Br (**38**)	84
Phenyl	OH (**52**)	73	Cl (**59**)	19
4-Methoxyphenyl	OH (**53**)	90	Cl (**60**)	25
4-Methoxycarbonylphenyl	OH (**54**)	82	Cl (**61**)	17
4-Pyridyl	OH (**55**)	40	Cl (**62**)	45
4-(5,5-Dimethyl-2-phenyl-	OH (**56**)	88	Cl (**63**)	0
1,3-dioxane)			Br (**64**)	64
4-Benzonitrile	OH (**57**)	69	Br (**65**)	69
4-Nitrophenyl	OH (**58**)	84	Cl (**66**)	35

3.3.2 Modified Horner-Emmons Reaction

Typically a Horner-Emmons reaction uses equimolar amounts of reactants and two equivalents of a strong base to convert the aldehyde and phosphonate to an ethene derivative. It was found that under these conditions the synthesis of ethynyl-functionalised porphyrins generally (exclusion of pyridine derivative **70** – refer to Table 3.2) resulted in the isolation of the starting material as well as an inseparable mixture of the halovinyl intermediate (**31a**, **39a**, **67a-72a**) and the desired product (**31**, **39**, **67-72**) (Figure 3.6). Unfortunately, the halovinyl intermediate could not be separated as it had an identical R_f to the ethynyl product on silica gel or alumina columns in various solvents.

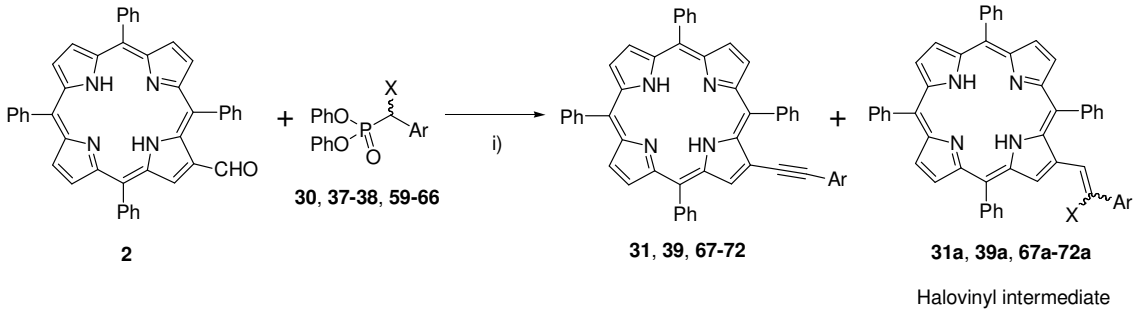

Figure 3.6 The modified Horner-Emmons reaction showing the formation of the ethynyl linkage and the undesired halovinyl intermediate (X = Br or Cl). Regents and conditions: i) THF, *t*-BuOK, RT, overnight.

Conformation of the structure of the halovinyl intermediate was achieved by X-ray crystallography (Figure 3.7). A single crystal of the halovinyl intermediate **39a** was obtained by the slow diffusion of MeOH into a mixture of halovinyl intermediate **39a** and ethynyl **39** in DCM.

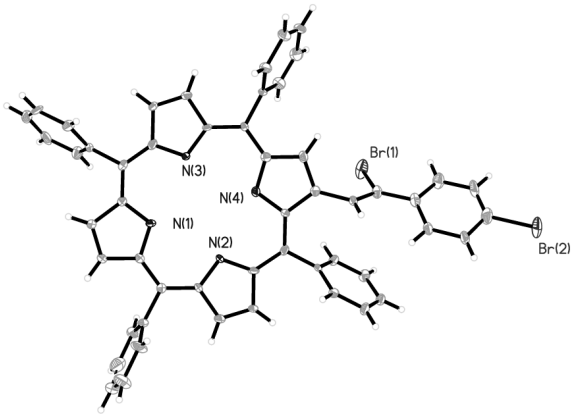

Figure 3.7 The molecular structure of the halovinyl intermediate **39a** as defined by defined by X-ray crystallography.

The removal of the halovinyl intermediate was overcome in moderate to high yields (Table 3.2) by significantly reducing the reaction time from overnight to 1.5 hours and dramatically increasing the concentration of a base to a 10% solution of *t*-BuOK (*ca*. 80 eq). This resulted in the formation of only trace amounts of the halovinyl intermediate as confirmed by the NH signal at -2.6 ppm in ^{1}H NMR spectra. Further treatment of the isolated products containing the halovinyl intermediate with *t*-BuOK in THF resulted in spectroscopically pure materials for all compounds excluding the bromo porphyrin **39**. Pure compound **39** could only be obtained in a very low yield by performing the reaction in refluxing THF.

Table 3.2 β-Pyrrolic alkyne porphyrins **31**, **39** and **67-72** and their yields.

Porphyrin	Ar	Phosphonate (X)	Yield (%)
31	4-Iodophenyl	**30** (Br)	75
39	4-Bromophenyl	**37** (Cl)	80
		38 (Br)	35
67	Phenyl	**59** (Cl)	54
68	4-Methoxyphenyl	**60** (Cl)	84
69	4-Methoxycarbonylphenyl	**61** (Cl)	0
70	4-Pyridyl	**62** (Cl)	70
71	4-(5,5-Dimethyl-2-phenyl-[1,3]dioxane)	**64** (Br)	88
72	4-Nitrophenyl	**66** (Cl)	0

Although the modified Horner-Emmons reaction provided a means of attaching a range of ethynyl-linked aromatic substituents, it was found to be restricted to aryl substituents that did not react with the *t*-BuOK. For example, the reaction of TPPCHO with diphenyl chloro(4-methoxycarbonylphenyl)methylphosphonate (**61**) or diphenyl chloro(4-nitrophenyl)methylphosphonate (**66**) failed to produce the desired products (**69** or **72**) but instead gave an intractable mixture of multiple products. Additionally, in the case of the cyano bromophosphonate **65** (Figure 3.8) the reaction afforded a readily separated mixture of the desired product **73** and the unexpected 2-(4′-benzamide)ethynyl-5,10,15,20-tetraphenylporphyrin **74**. Although not a common method, the use of base for the hydrolysis of nitriles to amides has been previously reported.[124-126]

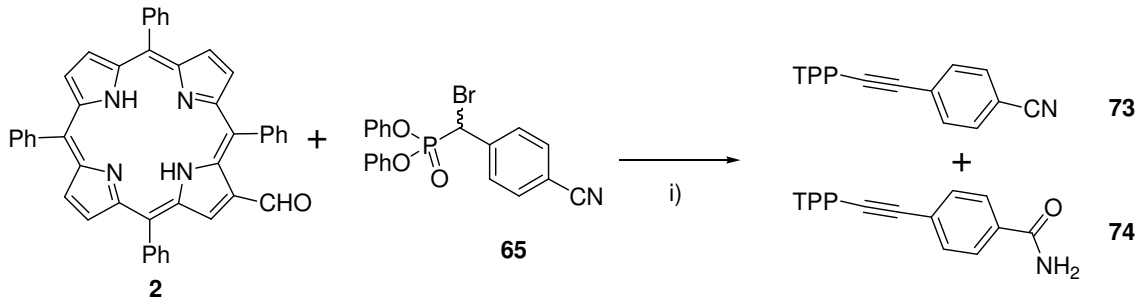

Figure 3.8 Synthesis of porphyrins **73** and **74**. Reagents and conditions: i) THF, *t*-BuOK, RT, 3 h, 36% for **73**, 26% for **74**.

Metallation of ethynyl porphyrins **31**, **39**, **67-68** and **70-71** was performed using $Zn(OAc)_2 \cdot 2H_2O$ to obtain Zn^{II} porphyrins **32**, **40**, **75-78**. These compounds were required for DFT studies in collaboration with Otago University. Although results are not included in this thesis, a manuscript is under preparation[11] and results will also be published in the PhD thesis of John Earles.[127]

3.3.3 Synthesis of β-Pyrrolic Ethynyl Dyes for Dye Sensitised Solar Cells

Porphyrins are strong chromophores and much effort has been put into their study as light harvesting complexes. Many different dyes, linkers and binding groups have been investigated for the use in DSSC devices. Currently no work has been published on the use of β-pyrrolic functionalised ethynyl porphyrin acids in DSSC applications. This is mainly due to the inherent problems associated with the synthesis of such compounds. The development of the modified Horner-Emmons chemistry in porphyrins has allowed us to easily synthesise the required acid derivatives and study their properties in light harvesting devices. Three commonly used acids for DSSCs - benzoic acid, malonic acid and cyanoacetic acid - were synthesised from the protected aldehyde **71** for the use in DSSCs.

Synthesis of the benzoic acid was achieved in five steps from the protected aldehyde in an overall yield of 51% (Figure 3.9). The protecting group was cleaved using trifluroacetic acid in DCM:H_2O at room temperature to give the aldehyde **79**. The protected (**71**) and unprotected (**79**) aldehydes had the same R_f on silica TLC, however, visualisation of the unprotected aldehyde was possible as it turned brown in the presence of 2,4-dinitrophenylhydrazine. Zn^{II} was inserted using $Zn(OAc)_2 \cdot 2H_2O$ in $CHCl_3$/MeOH to give **80** which was further oxidised to the methyl ester **81** using a procedure described by Campbell.[3] Porphyrin **80** was dissolved in a mixture of THF:MeOH and stirred in the presence of NaCN followed by oxidation with activated MnO_2. This reaction is assumed to proceed through the cyanohydrin which is oxidised to an α-keto nitrile (Figure 3.10). The α-keto nitrile is in turn converted to the methyl ester by MnO_2 in methanol. The product of the esterification still contained approximately 5% of the starting aldehyde judged by ^{1}H NMR spectroscopy. This was removed by silica gel column purification after hydrolysis of the methyl ester to the benzoic acid **82** using KOH.

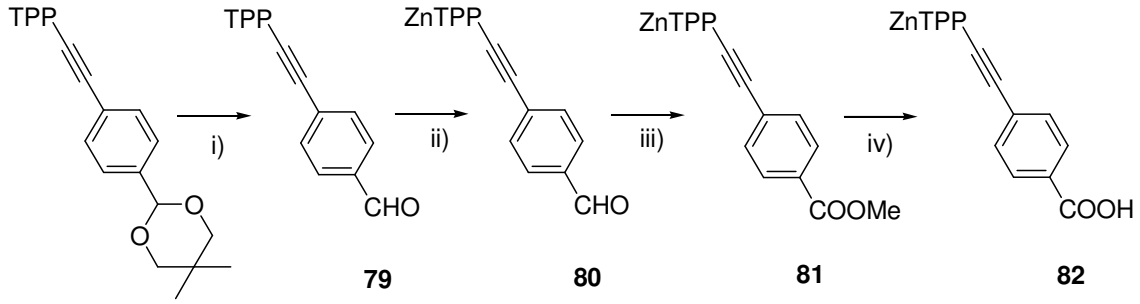

Figure 3.9 Synthesis of benzoic acid **82** for use in DSSCs. Reagents and conditions: i) DCM, TFA, H_2O, RT, 1 h, 81% ii) $CHCl_3$, MeOH, $Zn(OAc)_2 \cdot 2H_2O$, RT, 1 h, 99%, iii) THF, MeOH, NaCN, RT, 30 min then MnO_2, reflux 18 h, 88% iv) THF, MeOH, H_2O, KOH, reflux, 15 h, 73%.

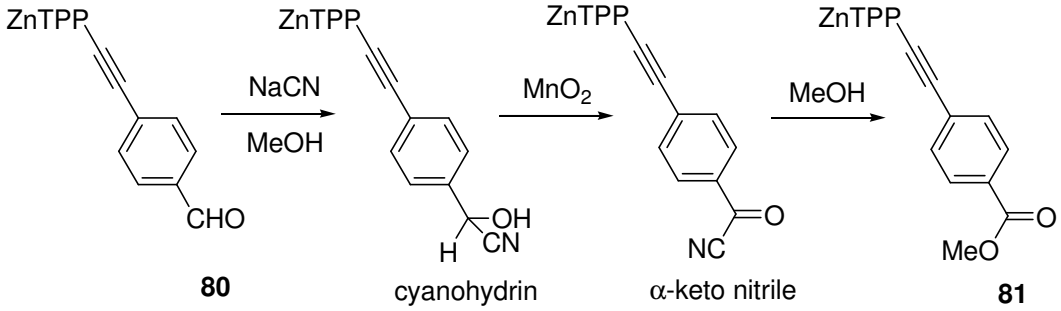

Figure 3.10 Proposed sequence for the conversion of the aldehyde **80** into the methyl ester **81**.

The cyanoacetic acid porphyrin derivative **83** was produced in a 97% yield from the aldehyde **80**. This was achieved using cyanoacetic acid and ammonium acetate in a mixture of acetic acid and THF (Figure 3.11).[128]

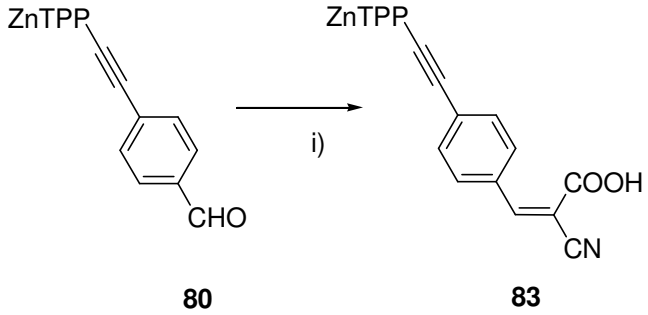

Figure 3.11 Synthesis of the cyanoacetic acid **83**. Reagents and conditions: i) THF, acetic acid, cyanoacetic acid, ammonium acetate, 60 °C, 5 h, 97%.

The malonic acid **84** shown in Figure 3.12 was problematic to synthesise. Porphyrin malonic acid derivatives are generally synthesised at 70 °C using 6 eq of malonic acid and ammonium acetate in THF:acetic acid.[120] Using these general conditions the desired

malonic **84** and the decarboxylated acid **85** were produced in a 10:90 ratio as determined by the ratio of the aromatic hydrogens to the adjacent β-pyrrolic hydrogens in the ^{1}H NMR spectrum. It was possible to observe the production of the malonic acid and the decarboxylated material by silica TLC, however due to the high polarity of the malonic acid, separation *via* silica gel column chromatography was not possible. Decarboxylation, which is undesirable as it provides an impure compound for DSSC testing, usually results from over heating the reaction mixture. It was possible to avoid the production of the decarboxylated product by performing the reaction at 40 °C with 20 eq of malonic acid and ammonium acetate. This reaction would not go to completion resulting in the isolation of the starting aldehyde (**80**) and the malonic acid (**84**) in a 40:60 ratio. By increasing the equivalents of the acid and the ammonium acetate to 40 eq we were able to push the reaction to completion but unfortunately both the malonic acid and the decarboxylated acid were obtained in a 70:30 ratio.

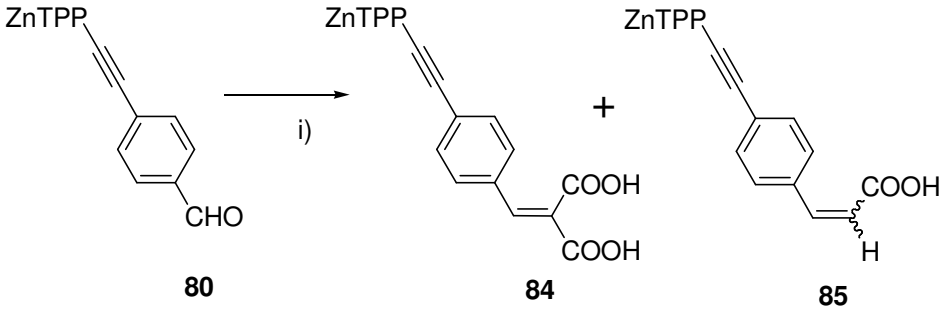

80 **84** **85**

Figure 3.12 Synthesis of malonic acid **84** showing the production of the decarboxylated product **85**. Reagents and conditions: THF, acetic acid, malonic acid, ammonium acetate, 40 °C, 4 h, 96%.

3.4 UV-Vis Spectroscopy and DSSC Testing

The synthesis of the new ethynyl modified porphyrins provided us the opportunity to investigate their spectroscopic and photovoltaic properties in DSSCs. Comparisons could be made to the previously synthesised and studied alkane and alkene porphyrin derivatives.

3.4.1 UV-Vis Absorption Spectroscopy

UV-Vis spectroscopy gave us an insight into the relative energy levels of the new ethynyl compounds. Figure 3.13 showed that both the Soret and the two Q bands of the ethynyl benzoic acid **82** were red shifted 1.5, 2.5 and 5.5 nm, respectively, relative to the equivalent ethene compound **87**. Shifts of 13.0, 12.5 and 14.5 nm were observed compared to ethane compound **86**.[88] This suggested that there was increased conjugation, or more precisely an increased electron withdrawing effect,[129] between the aromatic ring and the porphyrin core in the ethynyl derivative. This is consistent with observations in other β-alkyne porphyrins.[109, 130]

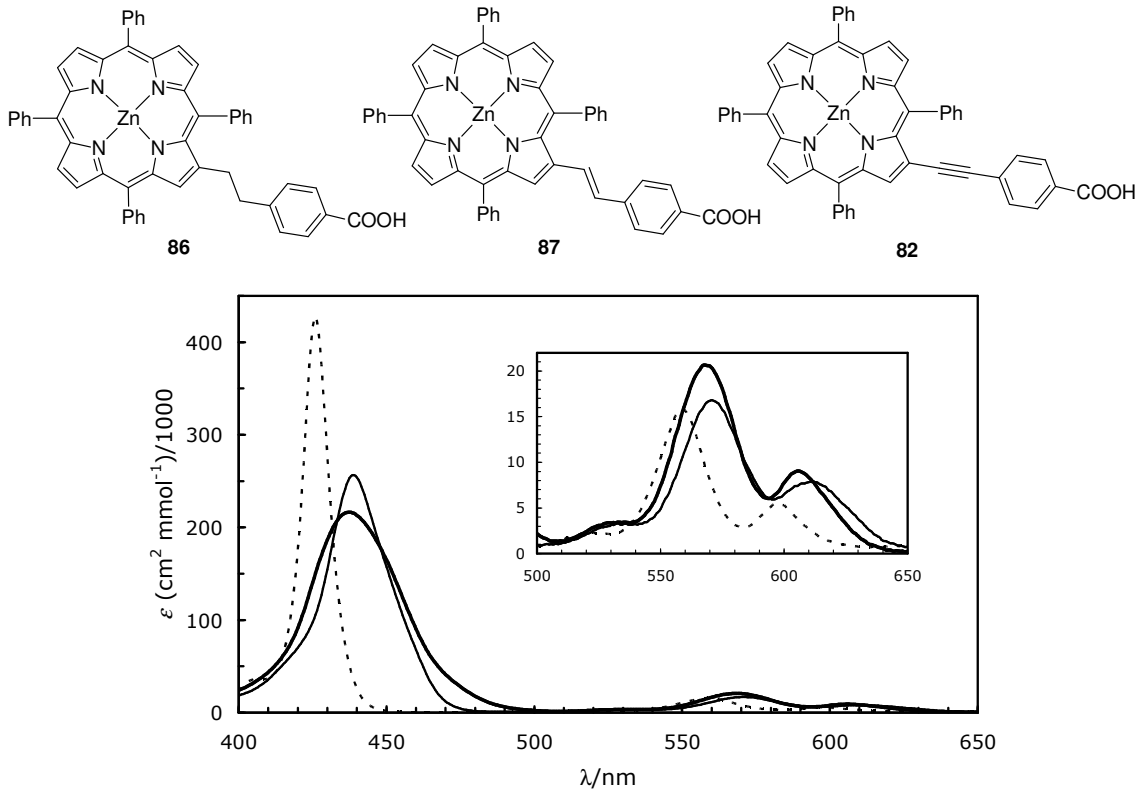

Figure 3.13 UV-Vis spectra of the ethynyl, alkene and alkane porphyrinic acids in DMF at 25 ˚C. Ethynyl **82** (thinner line), alkene **87** (thicker line) and alkane **86** (dotted line). Inserted is an expansion of the Q-band region.

3.4.2 X-ray Crystallography

It was not possible to obtain a single crystal of the acid **82**, but a crystal of aldehyde **80** suitable for X-ray diffraction was obtained by slow diffusion of methanol into a solution

of compound **80** in DCM (Figure 3.14). This could be compared to the crystal structure of the previously published Cu^{II} ethene derivative **88** (Figure 3.15).[78, 131]

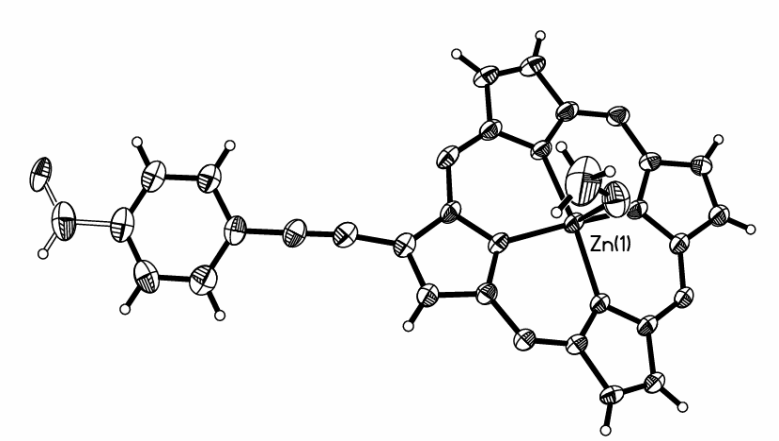

Figure 3.14 Crystal structure of 2-(4′-formyl)phenylethynyl-5,10,15,20-tetraphenylporphyrinato zinc (II) **80** with methanol coordinated to the zinc. The angle between the benzene ring and the plane of best fit made by the porphyrin ring is 31.98(16) degrees (phenyl rings omitted for clarity). The thermal ellipsoids were set at 50% probability level. The hydrogen atoms are drawn as spheres of arbitrary radii.

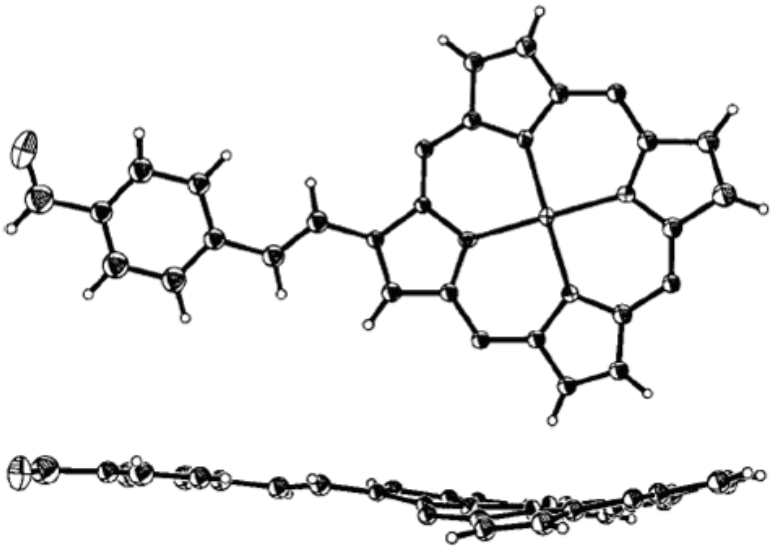

Figure 3.15 Crystal structure of 4-{*trans*-2′-[2″-(5″,10″,15″,20″-tetraphenylporphyrinato copper (II) yl) ethen-1′-yl]}-1-benzaldehyde **88** taken from Bonfantini *et al.*[78]

It has been shown that the extent of conjugation between the porphyrin and the β-pyrrolic substituent increases as the dihedral angle between the two moieties becomes more planar.[132] Thus, it would be expected from the UV-Vis spectroscopy that a more planar structure would exist in the ethynyl linkage compared to the alkene linkage. Against expectations, the dihedral angle between the plane of the benzene ring and the

plane of best fit made by the porphyrin core was 31.98(16) degrees, and almost twice that of the corresponding angle in **88** of 17(2) degrees. Interestingly, the increase in planarity that is suggested in the UV-Vis data is not supported by the crystal structure of compound **80**. Thus, it is difficult to draw conclusions relating to the relevant extent of the electronic communication in ethene and ethynyl derivatives. It is possible that this angular deformity may be a result of crystal packing forces.

3.4.3 Dye Sensitised Solar Cells (DSSCs)

The synthesised benzoic (**82**), cyanoacetic (**83**), and malonic acids (**84/85**) were tested under conditions as described by Campbell[3] and compared to the previously synthesised alkene and alkane acids **86**, **87**, and **89** (Figures 3.13 and 3.16).

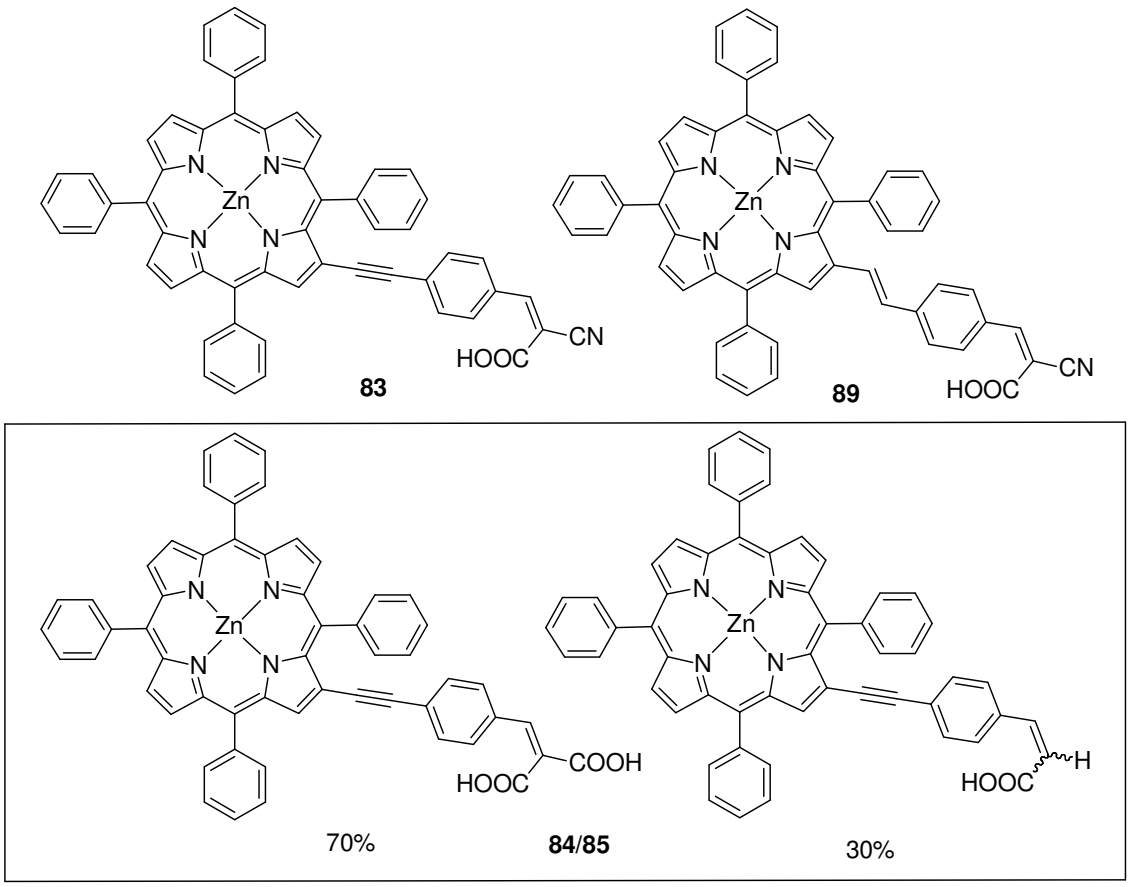

Figure 3.16 Malonic acid and cyanoacetic acid dyes tested in DSSCs.

Solutions of these porphyrin acids were prepared in THF (0.2 mM, BHT stabilised). Porphyrins were then absorbed onto sintered TiO_2 glass electrodes by soaking overnight

at RT in darkness. The TiO_2 electrodes with bound porphyrins were removed from the dye solutions, rinsed, dried under high vacuum and tested immediately. The cells were assembled and tested in an open unsealed cell holder shown in Figure 3.17. Introduction of an I^-/I_3^- redox electrolyte *via* capillary action between the working electrode and the counter electrode completed the working cell. Four identical cells for each acid were irradiated under the equal intensity of 1 sun and the average values calculated (Table 3.3). The efficiencies (η) presented using an unsealed cell have been shown to be approximately half of those expected in a sealed optimal cell.[121]

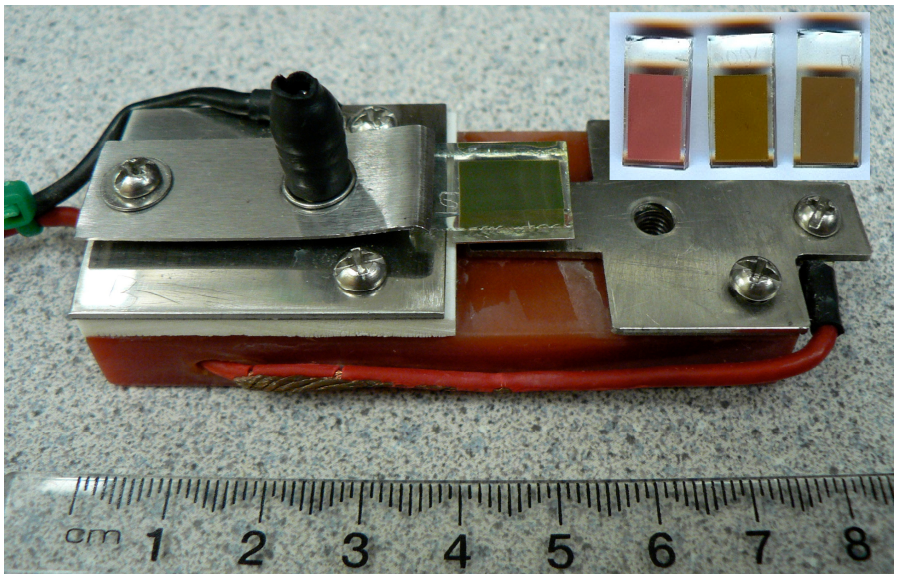

Figure 3.17 DSSC cell holder containing a TiO_2 cell with bound porphyrin. Insert is a photograph of TiO_2 cells with bound acids **86**, **87** and **82** respectively.

Table 3.3 Results of DSSC testing.

Compound	η (%)	FF	V_{oc} (V)	J_{sc} (mAcm^{-2})
86	1.29 (1)	0.55	0.555	4.20
87	2.12 (2)	0.52	0.583	6.97
82	1.86 (1)	0.50	0.577	6.39
89	2.65 (3)	0.52	0.611	8.41
83	2.80 (1)	0.53	0.624	8.58
84/85	2.64 (4)	0.57	0.665	7.09

η = cell efficiency (1 standard deviation), FF = fill factor, V_{oc} = open circuit voltage, J_{sc} = short circuit current.

The DSSC results can be separated into porphyrins possessing benzoic acids (**86**, **87** and **82**) and those containing cyanoacetic/malonic acids (**89**, **83** and **84/85**). The alkene linkage in compound **87** was found to be the best performing benzoic acid dye followed by the alkyne **82** and alkane **86** respectively, as shown by the higher cell efficiency (η). As can be seen in Table 3.3, the results show that dyes with cyanoacetic and malonic acid binding groups have higher efficiencies than benzoic acids. This is consistent with previously published porphyrinic acids using these binding groups.[89] The ethynyl cyanoacetic porphyrin **83** showed higher efficiencies than the alkene variant **89**. The malonic acid showed similar efficiency to that of the double bond cyanoacetic acid but it is difficult to compare these as the malonic acid was not pure.

It is plausible that variations in cell efficiencies could be the result of differences in dye loading on the TiO_2 surface, rather than due to the real efficiency of the chromophore. To investigate this we determined the dye loading of the three benzoic acids dyes (**86**, **87** and **82**) on the TiO_2 surface using UV-Vis spectroscopy (see experimental methods section for details). Results showed that varying the linker did not substantially affect the surface coverage of the dye on TiO_2 (Table 3.4). It can therefore be assumed that the trends in DSSC efficiency are not a direct result of different dye loading on the surface.

Table 3.4 Dye loading on TiO_2

Compound	Moles absorbed	Mass absorbed (g)	Dye loading (mol/g of TiO_2)
86	2.2×10^{-7}	1.8×10^{-4}	5.3×10^{-5}
87	2.3×10^{-7}	1.9×10^{-4}	5.5×10^{-5}
82	2.3×10^{-7}	1.9×10^{-4}	5.6×10^{-5}

To provide further insight into the acids used in DSSCs a DFT study is being undertaken in collaboration with Otago University (not discussed in the current thesis).[11, 127]

3.5 Conclusion

The use of modified Horner-Emmons conditions has provided a versatile method for the synthesis of ethyne linked substituents at the β-pyrrolic position of TPP. This high

yielding, scalable methodology negated the need of a metal catalyst and did not require the preparation of 2-bromo-5,10,15,20-tetraphenylporphyrin as the starting material. The X-ray crystallography data showed that the dihedral angle between the plane of the porphyrin core and the plane of the aryl substituent was greater in the ethynyl linked molecule compared to an ethylene analogue. Electronic properties indicated a bathochromic shift of the ethynyl linked porphyrin compared to the corresponding ethylene analogue which is in contrast to the information gained in the crystal structure. A number of porphyrin benzoic, cyanoacetic and malonic acids were synthesised and evaluated in DSSCs. Results showed that the obtained ethynyl dyes were effective in DSSCs, however no significant improvement over similar alkene acids was observed.

Chapter 4 Construction of Lipophilic Porphyrin-DNA Complexes

4.1 Introduction

A variation to general TmPyP cationic porphyrin used for the non-covalent attachment to DNA[16] is the production of lipophilic DNA complexes. DNA is normally soluble in aqueous solution, however by exchanging the Na^+ or Li^+ ions along the phosphate backbone for quaternary ammonium salts possessing a long lipophilic chain (Figure 1.15) it is possible to create an organically soluble complex.[31, 32] These complexes can be simply prepared by mixing of salmon testes or calf thymus DNA (*ca*. 1.3×10^6 Da, 2000 bp) and a lipophilic salt in an aqueous environment. A precipitate is formed which on filtration and drying can be resolubilised in an organic solvent. Slow evaporation of the organic solvent has been shown to produce lipophilic DNA films with aligned DNA strands.[133, 134] These have shown promise in the production of batteries,[33] liquid crystals,[34] drug release systems[35] and photodynamic devices.[36] Although many materials have been incorporated into DNA-lipid complexes, the incorporation of lipophilic porphyrins is a novel approach. If successful it may allow for the simple construction of porphyrin based arrays for use in nanotechnological applications such as light harvesting, fluorescent labelling or low-power photon upconversion.

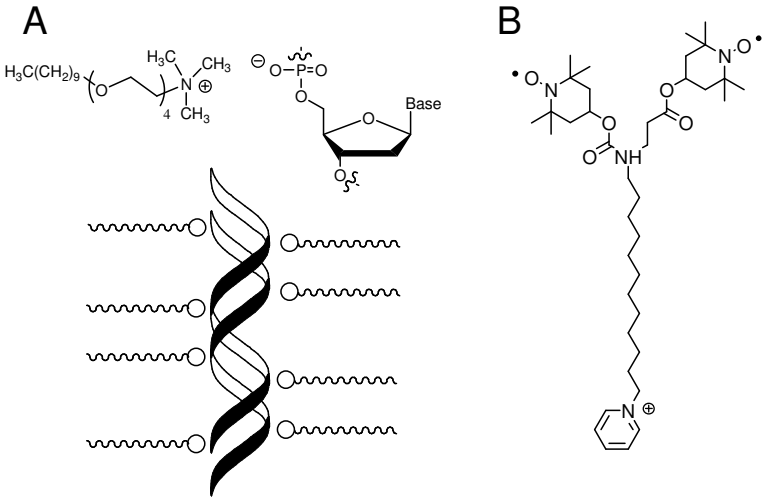

Figure 4.1 A) An illustration of one of the first lipophilic-DNA complexes[31] B) A TEMPO lipophilic salt used in the construction of DNA batteries.[33]

Lipophilic porphyrins were synthesised as discussed in Chapter 2. Three porphyrins were synthesised for the use in lipophilic arrays, compounds **6**, **9** and **27** (Figure 4.2). Due to the problems associated with the synthesis of compound **6**, not enough material was available for the construction of DNA-porphyrin complexes. Complexes were instead made from the more abundant porphyrins **27** and **9**. Along with porphyrin **9** and **27** we created lipophilic DNA using cetyl trimethylammonium bromide (CTAB).

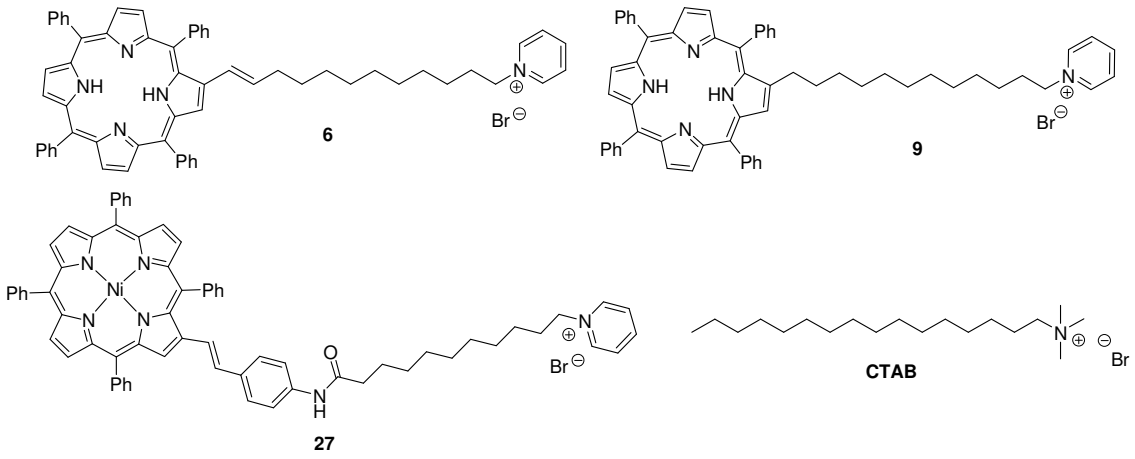

Figure 4.2 Lipophilic compounds used to create DNA-porphyrin complexes.

4.2 Chapter Summary

This chapter discusses the synthesis of novel porphyrin-DNA supramolecular assemblies around single and double stranded DNA as well as guanosine quadruplexes (GQ). Loading rates and solubility of such compounds were investigated.

4.3 Porphyrin Solubility

A critical feature of the lipophilic porphyrins is that they must be soluble in a solvent that is miscible with water, therefore allowing the lipophilic porphyrin to be properly mixed with the oligonucleotide. The porphyrin-DNA complexes were constructed by the addition of a solution containing porphyrin **9** or **27** to an oligonucleotide in water. Therefore the porphyrins must remain soluble on dilution with water. Failure to do so will result in the porphyrin rather than the porphyrin-DNA complex precipitating from solution. Solubility of **9** and **27** was investigated in water miscible solvents as shown in Table 4.1. Solubility tests were performed at room temperature on 1 mg of porphyrin and solubility properties were identical for both porphyrins.

Table 4.1 Solubility at RT of 1 mg of porphyrin **9** or **27**.

Solvent	**Solubility**
H_2O	Insoluble
THF	Soluble in 20 μL, remained soluble on dilution with water to 2 mL.
DMSO	Soluble in 20 μL, remained soluble on dilution with water to 2 mL.
DMF	Soluble in 20 μL, remained soluble on dilution with water to 2 mL.
EtOH	Partially soluble in 20 μL. Completely soluble on addition of 20 μL water. Remained soluble on further dilution with water to 3 mL.
Acetonitrile	Partially soluble in 20 μL. Completely soluble on addition of 20 μL water. Remained soluble on further dilution with water to 10 mL.

As can be observed from Table 4.1, porphyrins **9** and **27** were soluble in a number of solvents that could be implemented in the development of lipophilic complexes. The use of DMSO and DMF was avoided as it would be difficult to remove trace quantities of these solvents after the complex has been formed. Out of the remaining three solvents acetonitrile was chosen for the construction of lipophilic complexes. It is worth mentioning that to dissolve the porphyrins in a mixture of ACN:water, the acetonitrile must be added first to suspend the porphyrin followed by the addition of water. The addition of a solution of ACN:water (1:1) will not solubilise either porphyrin.

To investigate the possibility of reducing the lipophilic chain length compound **90** was synthesised by the reaction of porphyrin **70** with methyl iodide (Figure 4.3). It was observed that compound **90** was soluble in THF, DMSO or DMF but precipitation of the porphyrin occurred on addition of water. This result means that the formation of a lipophilic complex with a shorter tether is not feasible using the current protocol.

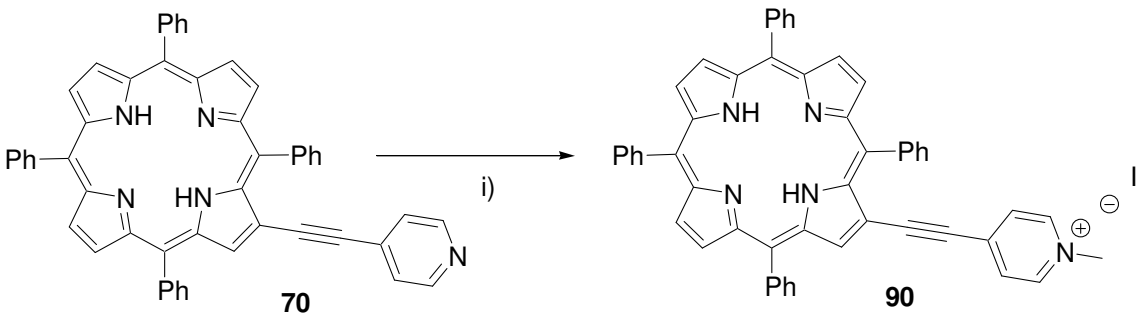

Figure 4.3 Synthesis of compound **90**. Reagents and conditions: i) DMF, CH_3I, overnight, 40 °C, 92%.

4.4 Complex Formation

Complexes were formed by the slow addition of a solution of porphyrin to a solution of oligonucleotide. For the creation of the porphyrin-DNA complexes a solution of oligonucleotide (Li^+ or Na^+ salt) was prepared in water (generally 100 μL, concentration of 100-500 μM). To the oligonucleotide solution either porphyrin **9** or **27** (2.5 mg in 80 μL ACN and then diluted with 920 μL water) was added in 2-5 μL fractions forming a red precipitate. Addition was continued until no more red precipitate was observed and a red colour developed in the solution. To see if any more precipitate was occurring, it was necessary to centrifuge the sample (5 seconds at 13500 rpm) between additions of the porphyrin. When no more precipitate was observed the sample was centrifuged (15 min at 13500 rpm) to form a red pellet of the porphyrin-DNA complex (Figure 4.4). The supernatant was then removed and the pellet was washed twice with H_2O (1 mL) then dried under high vacuum for two days to remove any traces of solvent.

Figure 4.4 Example of a DNA-porphyrin complex of compound **27**.

Initial complexes were formed from salmon testes DNA (*ca.* 1.3×10^6 Da, 2000 bp). This is a cheap DNA sample that can be obtained commercially in large quantities. A majority of lipophilic complexes have been constructed around this material and used to produce organically soluble complexes.[31, 33-36] On the addition of porphyrin **27** to the sodium salt of salmon sperm DNA, a precipitate was formed. This was washed with H_2O and dried under high vacuum for three days. When attempts were made to dissolve the resulting solid in various solvents (DCM, $CHCl_3$, DMSO, DMF, toluene or EtOH) the complex was found to be insoluble. This is most likely a result of the π stacking of porphyrins which can prevent the solvation, especially in porphyrins based on TPP. This insolubility was unfortunate as it makes the complexes unusable.

Because of the insolubility resulting from large DNA sequences, complex formation was investigated using short oligonucleotides (12-15 mers) in the hope that these would be more soluble in an organic media. Complexes formed from the single stranded 12 mer sequence (5′AGCTTGCTTGAG) were found to be completely soluble in DCM or chloroform. This allowed us to investigate some of the properties of these complexes.

4.4.1 Singe Stranded and Duplex DNA Porphyrin Loading Ratios

To determine the ratio of porphyrin to DNA we calculated the loading of porphyrin on DNA. In doing so it is assumed that all phosphate groups are charged and available to interact with the porphyrins. Loading rates were calculated on single strand and duplex oligonucleotides using a similar method to construct the complex to that described above. Through careful measurements we were able to calculate the approximate number of moles of the porphyrin used to precipitate the oligonucleotide.

To achieve this a solution of single stranded or duplex DNA was created at a concentration of approximately 100 μM in water (100 μL). 5 μL of this solution was added to 995 μL of water and the concentration of the oligonucleotide solution was accurately determined by UV-Vis spectroscopy. To the remaining 95 μL, a porphyrin solution of a known concentration (approximately 2.5 μmoles per mL) was added gradually until no more precipitation occurred. The pellet was centrifuged and the supernatant removed. Any remaining oligonucleotide in the supernatant was precipitated from $LiClO_4$ and acetone, dissolved in water and the concentration determined by UV-Vis spectroscopy.

From the initial and final concentrations of DNA and the moles of porphyrin added, it is possible to determine the ratio of porphyrin to DNA. The results represented in Table 4.2 showed that slight overloading of the DNA occurred for both porphyrins. This suggests that some porphyrin is not bound to the DNA *via* ionic interactions. This could be due to either the intercalation of the porphyrin between bases or, what is more likely, the stacking of porphyrins with each other creating a second layer of porphyrin around the DNA (Figure 4.5). The loading ratios of the free base porphyrin **9** were found to be slightly higher than that for the Ni^{II} porphyrin **27**. This may possibly suggest that porphyrin **9** stacks better with itself than porphyrin **27**.

Table 4.2 Loading ratios for porphyrins **9** and **27**.

Sequence	Porphyrin	Loading rate[a]
5′AGCTTGCTTGAG	**27**	1.2
5′AGCTTGCTTGAG	**9**	1.3
5′AGCTTGCTTGAG 3′TCGAACGAACTC	**27**	1.1
5′AGCTTGCTTGAG 3′TCGAACGAACTC	**9**	1.2

[a] Loading rate is calculated as porphyrins per phosphate and are the average of three titrations.

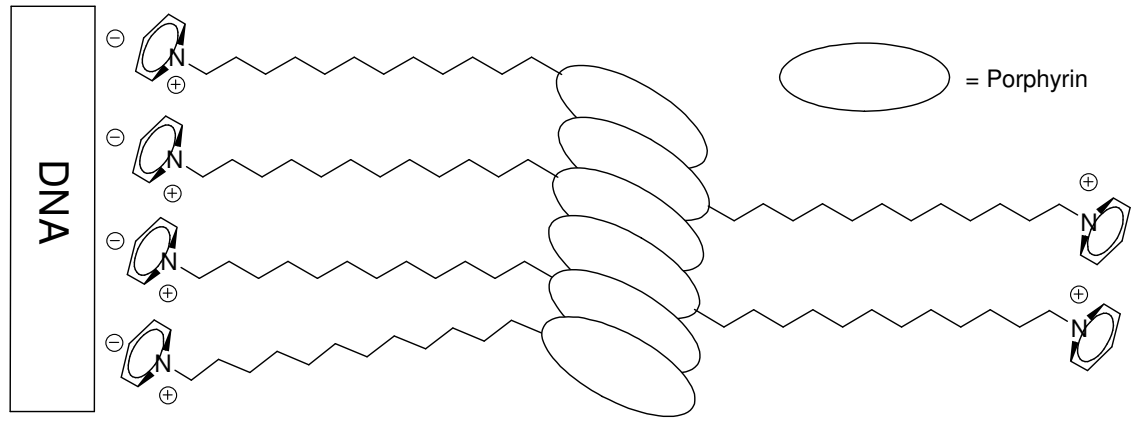

Figure 4.5 Possible stacking arrangement of lipophilic porphyrins on DNA.

It should be noted that the point at which precipitation was maximised was much harder to determine for compound **9** than it was for **27**. In the case of porphyrin **27** there was a distinct transition where the addition of more porphyrin only resulted in an increase of porphyrin in solution. The addition of many equivalents eventually resulted in the resolvation of the complex. In contrast, the transition for compound **9** is not as defined as there was always trace quantity of porphyrin in solution. The continued addition of porphyrin **9** well past the equivalence point (4-5 eq) did not result in an increase in the porphyrin concentration in the solution, however a significant increase in the amount of precipitate was observed without any sign of resolvation. This suggests different stacking of compound **9** and **27** around DNA.

4.4.2 G-Quadruplex (GQ) Complex Formation

To extend our study we investigated the formation of lipophilic 2′-deoxyguanosine quadruplexes of thrombin binding aptamer (5′-dGGTTGGTGTGGTTGG) using porphyrin **27** and CTAB. G-quadruplexes (GQ) are formed in G rich sequences in the presence of buffers containing potassium ions.[7] A standard buffer for the formation of GQ is 10 mM sodium phosphate and 100 mM KCl, pH 7.0. Unfortunately, the addition of **27** to a solution of the above buffer containing no DNA resulted in the precipitation of the porphyrin. Further investigation showed that the porphyrin was still semi insoluble in salt concentrations as low as 0.62 mM sodium phosphate and 6.25 mM KCl.

It was observed that the GQ-porphyrin supramolecular complex could be formed by pre-forming the GQ in 10 mM sodium phosphate, 100 mM KCl then precipitating the oligonucleotide in GQ form from $LiClO_4$ and acetone. It was found that when the DNA precipitate was redissolved in water the GQ structure was still preserved, as shown by a characteristic CD signal with minima at 260 nm and maxima at 292 nm.[135] On the addition of porphyrin **27** to the GQ solution a precipitate was formed which was isolated, dried and dissolved in $CHCl_3$. UV-Vis spectroscopy of the resulting solution showed a peak at 260 nm that was not present in porphyrin **27** therefore confirming the existence of both oligonucleotide and porphyrin in the chloroform solution (Figure 4.6). It was not possible to determining if the GQ structure still remained after complex formation as the CD spectrum of the porphyrin-DNA complex could not be measured due to the strong HT voltage rising from the porphyrin in the UV region. Dilution of the solution to give a reliable HT voltage showed no CD induced Cotton effects in the porphyrin region. This solution was also too dilute to observe any GQ CD signal. By repeating the experiment using CTAB, a precipitate was produced that could be dissolved in EtOH. This solution had an identical CD spectrum to the unmodified GQ which suggests that the GQ structure in the porphyrin modified GQ still remains.

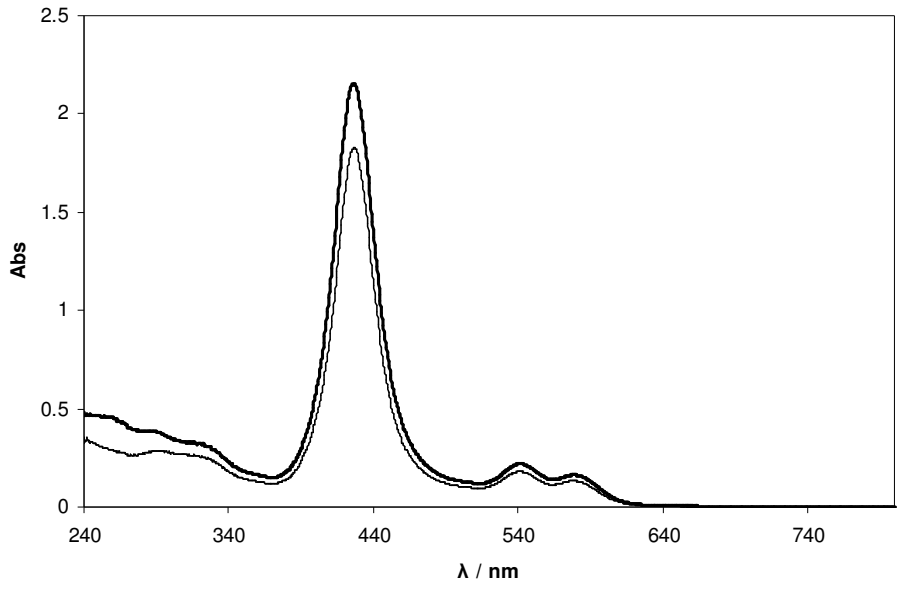

Figure 4.6 UV-Vis spectra of GQ-porphyrin complex (thicker line) and unreacted porphyrin **27** (thinner line) in $CHCl_3$.

4.5 Conclusion

Lipophilic porphyrin complexes could be synthesised using short sequences of single stranded, duplex and GQ oligonucleotides. Longer DNA sequences resulted in the formation of an insoluble complex. Loading studies on single stranded and duplex DNA showed slight overloading of porphyrins on DNA. Characterisation of the porphyrin-DNA supramolecular structure by CD spectroscopy was not possible due to the overpowering porphyrin signal.

Because the non-covalent complexes were either insoluble or unable to be fully characterised, focus switched to the covalent attachment of porphyrins to DNA as discussed in Chapters 5 and 6.

Chapter 5 Covalent Attachment of Porphyrins to DNA

5.1 Introduction

Porphyrin-DNA supramolecular assemblies are important for the development of functional π-systems with tunable optical properties. As discussed previously, we have chosen to focus on two coupling methods, Sonogashira and Cu^{I} catalysed azide alkyne Huisgen 1,3-dipolar cycloaddition reactions, also known as CuAAC reactions, as a means of the pre- or post-synthetic site-specific modification of oligonucleotides (Figure 5.1).

Contrary to the common functionalisation of the porphyrin through the *meso* positions[38, 41-44, 46, 55] which results in a system orthogonal to the porphyrin core, a *β*-pyrrolic modified porphyrin was used which provided a planar system between the porphyrin core and the adjacent benzene ring. To achieve site-specific modification *β*-pyrrolic substituted porphyrins containing halogens (Br, I), alkynes or azides, as described in Chapter 2.4, were used in conjunction with pre- and post-synthetic Sonogashira and CuAAC reactions.

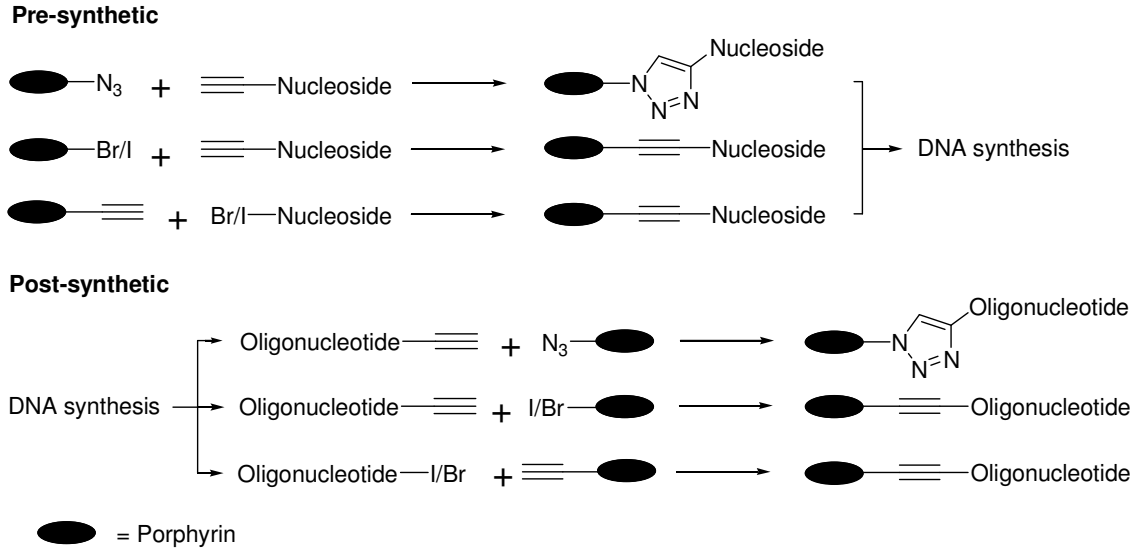

Figure 5.1 Synthetic outline for the development of DNA-porphyrin conjugates.

A pre-synthetic approach involves the attachment of a porphyrin to nucleosides which are then converted to the appropriate porphyrin phosphoramidites or H-phosphonates. These are then incorporated into the DNA structure during DNA synthesis. Due to their chemical nature, stability of porphyrin phosphoramidites as DNA building blocks is usually limited[46, 48] and is dependent on the structure of the molecule. H-Phosphonate porphyrin analogues have also been employed in DNA synthesis,[46, 55] however coupling yields are usually not satisfactory for their multiple incorporations. A pre-synthetic approach can allow for the incorporation of many functionalised nucleotides in a single DNA strand using automated DNA synthesis, only if high yielding reactions occur.

In this regard, a post-synthetic modification of DNA is a more versatile approach compared to the time-consuming preparation of phosphoramidites.[40] Post-synthetic modification, where a special functional group of the porphyrin reacts specifically with a pre-synthesised oligonucleotide carrying a complementary functional group, is particularly important for screening different substituents in nucleic acid structures.

5.2 Chapter Summary

This chapter investigates the pre-synthetic modification of oligonucleotides using both Sonogashira and CuAAC chemistry. Due to the problems accounted with pre-synthetic modification, focus switched to the development of a method for internal post-synthetic modification using alkyne containing ONs *via* CuAAC chemistry. We have screened porphyrin substituents using this method with ONs incorporating 2′-deoxy-5-ethynyluridine, 2′-*O*-propargyl uridine or 4-ethynylphenylmethylglycerol moieties. The synthesis of ONs possessing the internal porphyrin modifications allowed us to undertake UV-Vis and CD thermal stability studies on the resulting duplexes and triplexes.

5.3 Pre-synthetic Sonogashira and CuAAC Reactions

As discussed in Chapter 2 a number of precursors for the use in Sonogashira and CuAAC reactions were synthesised. These include compounds **32**, **35** and **40** (Figure 5.2) for use in Sonogashira chemistry and compounds **41**, **42**, **45** and **48-51** (Figure 5.3) for use in CuAAC chemistry. From these compounds we have synthesised a number of porphyrin possessing nucleosides and oligonucleotides using both pre- and post-synthetic approaches.

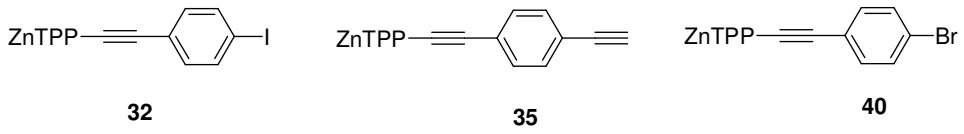

32 **35** **40**

Figure 5.2 Porphyrin precursors used in Sonogashira chemistry.

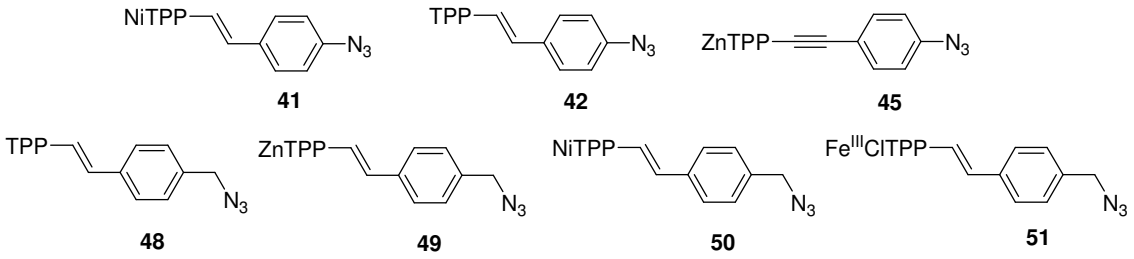

41 **42** **45**

48 **49** **50** **51**

Figure 5.3 Porphyrin precursors used in CuAAC chemistry.

5.3.1 Pre-synthetic Sonogashira Reaction

Pre-synthetic Sonogashira reactions focused on the modification of the commercially available 2′-deoxy-5′-*O*-DMT-5-iodouridine (**91**) and 5′-*O*-DMT-8-bromodeoxyguanosine (*N*-isobutyryl) (**92**) to create porphyrin modified nucleosides. Reaction of **92** with porphyrin **35** using various conditions involving CuI and $Pd(PPh_3)_4$ resulted in only the production of homodimer **34** as shown in Figure 5.4. This was not completely unexpected as Pd^0 coupling involving purines A and G are notoriously difficult due to the suspected interaction of the Pd with the purines.

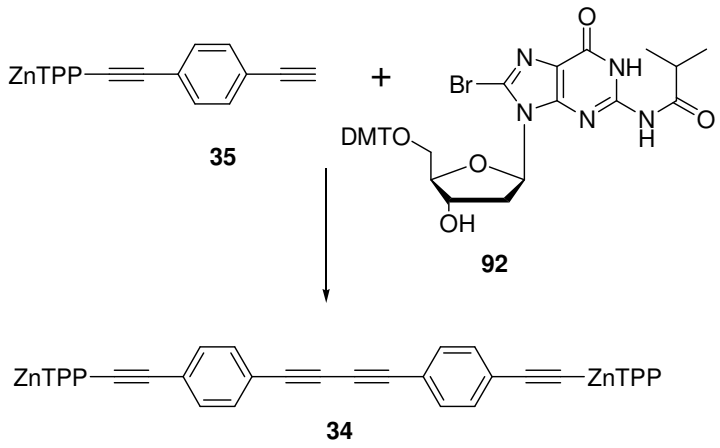

Figure 5.4 Attempted pre-synthetic Sonogashira coupling involving **35** and **92**.

The synthesis of the uridine porphyrin nucleoside **94** was achieved from 2-(4′-ethynylphenyl)ethynyl-5,10,15,20-tetraphenylporphyrinato zinc (II) (**35**) and pyrimidine 5′-*O*-DMT protected 2′-deoxy-5-iodouridine (**91**) in high yield (Figure 5.5). Crucial to the success of the Sonogashira coupling between **35** and **91** was the complete degassing of all solvents and the use of at least 4 equivalents of **35** to maximise the formation of compound **94**. It was also essential to mix both reactants in Et_3N before the addition of the Pd and Cu catalysts, failure to do so resulted in the exclusive formation of homodimer **34**. Although synthesis was successful, purification *via* silica gel chromatography was problematic and pure porphyrin nucleoside **94** was obtained in only 12% yield after subsequent methanol precipitation. Attempts to couple iodo porphyrin (**32**) and 2′-deoxy-5′-*O*-DMT-5-ethynyluridine (**93**) using the same reaction conditions showed only trace amounts of the desired product by TLC analysis of the reaction mixture. Similarly the reaction of bromo porphyrin **40** with **93** was unsuccessful.

The one step demetallation and DMT deprotection of **94** with trifluoroacetic acid provided compound **95** (Figure 5.5), whose spectroscopic properties were compared with the previously reported *meso* linked uridine nucleoside **96**.[43] In chloroform, the Soret band of the *meso* uridine **96** was observed at 420 nm while that for the *β*-pyrrolic functionalised **95** was detected at 429.5 nm. This 9.5 nm bathochromic shift in the Soret band is a result of a higher degree of conjugation occurring between the porphyrin core and the uracil in the *β*-pyrrolic linked **95** compared to the *meso* linked **96**. To the best of our knowledge, this is the first reported synthesis of a *β*-pyrrolic linked nucleoside.

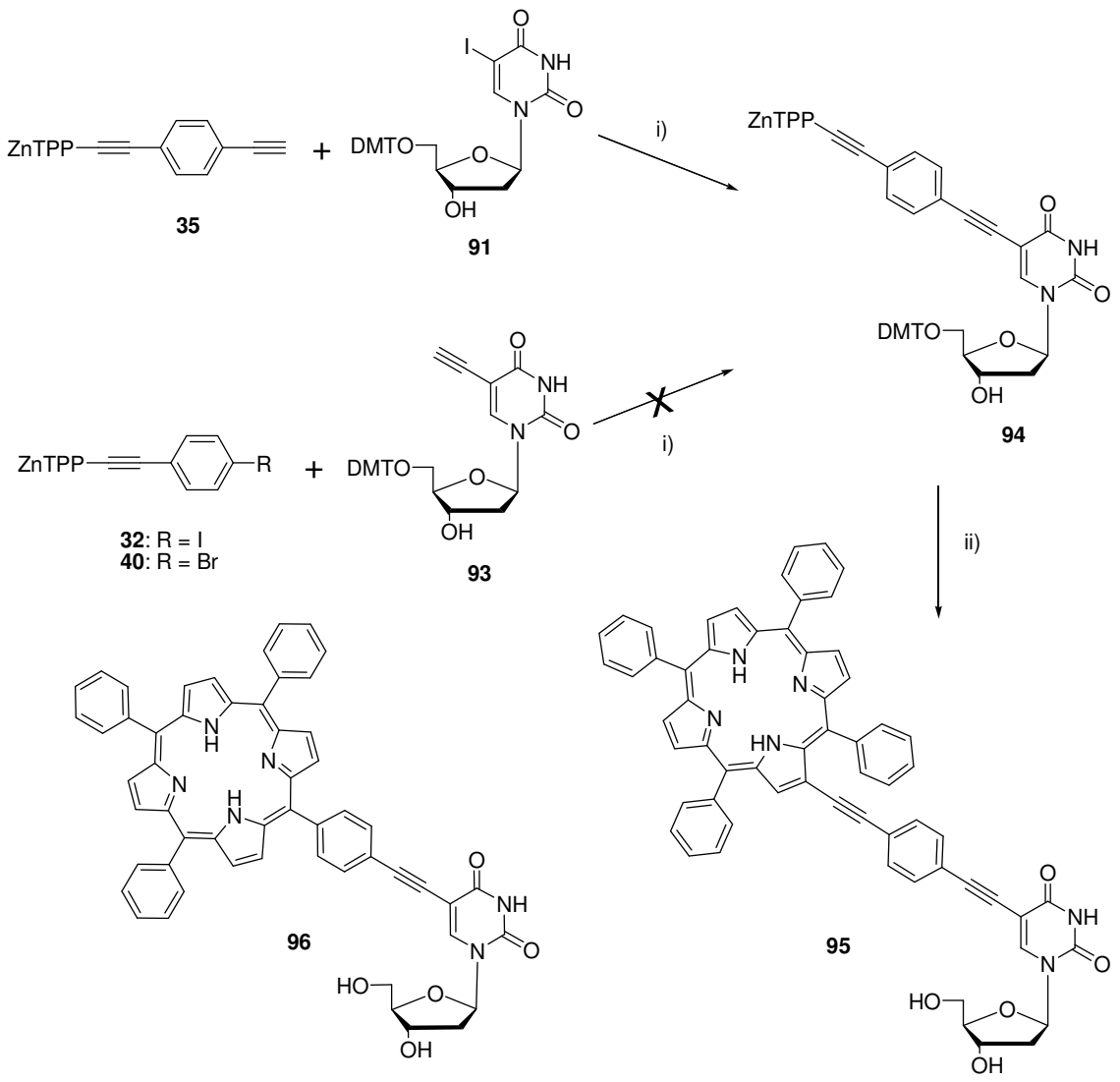

Figure 5.5 Pre-synthetic Sonogashira coupling reactions. Reagents and conditions: i) Et_3N, $Pd(PPh_3)_4$, CuI, 70 °C, overnight, 78% crude, 12% pure ii) DCM, TFA, RT, 2 min, 70%.

Due to the unexpectedly low quantities of compound **95** obtained, conversion of **95** to the corresponding phosphoramidite was not attempted and efforts were instead focused on pre- and post-synthetic CuAAC DNA modifications.

5.3.2 Pre-synthetic CuAAC Chemistry

Pre-synthetic CuAAC chemistry focused on the modification of 2′-deoxy-5-ethynyluridine with azido functionalised porphyrins discussed in Chapter 2.4.2. To investigate the versatility of the CuAAC reaction, reactions were performed with aromatic and aliphatic variants containing different metal ions.

The model triazoles **97-101** (Figure 5.6) containing Ni^{II}, Zn^{II}, Fe^{III} and Cu^{II} metal ions were synthesised from the corresponding azide and 2′-deoxy-5′-*O*-DMT-5-ethynyluridine **93** with 2 eq of $Cu(ACN)_4PF_6$, in THF. A copper catalyst that is soluble in organic solvents was used as it had previously shown positive results in comparison to aqueous $CuSO_4 \cdot 4H_2O$ or CuI in CuAAC reactions.[68] Silica TLC analysis of the reaction mixtures after two days showed the formation of a more polar material which either moved as one or two spots in MeOH:DCM (1:9). Further analysis showed that the addition of trifluoroacetic acid vapour to a sample of the crude reaction mixture before running the TLC resulted in only a single spot in MeOH:DCM (1:9). This suggested that the two polar TLC spots can be attributed to the complete or partial cleavage of the acid sensitive DMT protecting group during the CuAAC reaction. Conformation of the DMT cleavage was obtained on ^1H NMR spectroscopy (where possible) and ESI-MS spectrometry analysis of the polar material after silica gel column chromographic purification. Although it was possible to separate the desired triazoles from the unreacted azides using silica gel column chromatography, it was not possible to separate the DMT on and DMT off products from each other. As expected the copper catalysed reaction of the free base porphyrin azide **48** resulted in the quantitative isolation of the Cu^{II} metalled porphyrin azide **102**. Isolation and re-reaction of this Cu^{II} porphyrin azide resulted in the production of the desired triazole **101** in 44% yield.

The synthesis of **97-99** provided the opportunity to investigate and compare the spectroscopic properties of the porphyrin linked uracil derivatives. In the UV-Vis spectra of the triazole linked conjugate **99**, the porphyrin Soret band occurs at 435 nm. When compared to the ethynyl derivative **94** (Figure 5.5), which has a Soret band at 440 nm, we can conclude that the introduction of the triazole results in distruption of conjugation compared to the ethynyl linked **94**. Similarly, the comparison of the aromatic triazole **97** with the aliphatic triazole **98**, in which Soret bands were observed at 427.5 and 426 nm respectively, confirmed that the additional CH_2 group results in the disruption of conjugation between the porphyrin core and the uracil.

Although a number of 1,4-regioisomeric 1,2,3-triazoles were synthesised and characterised, which proves the possibility to link porphyrins to DNA using CuAAC chemistry, we focused on post-synthetic DNA modification.

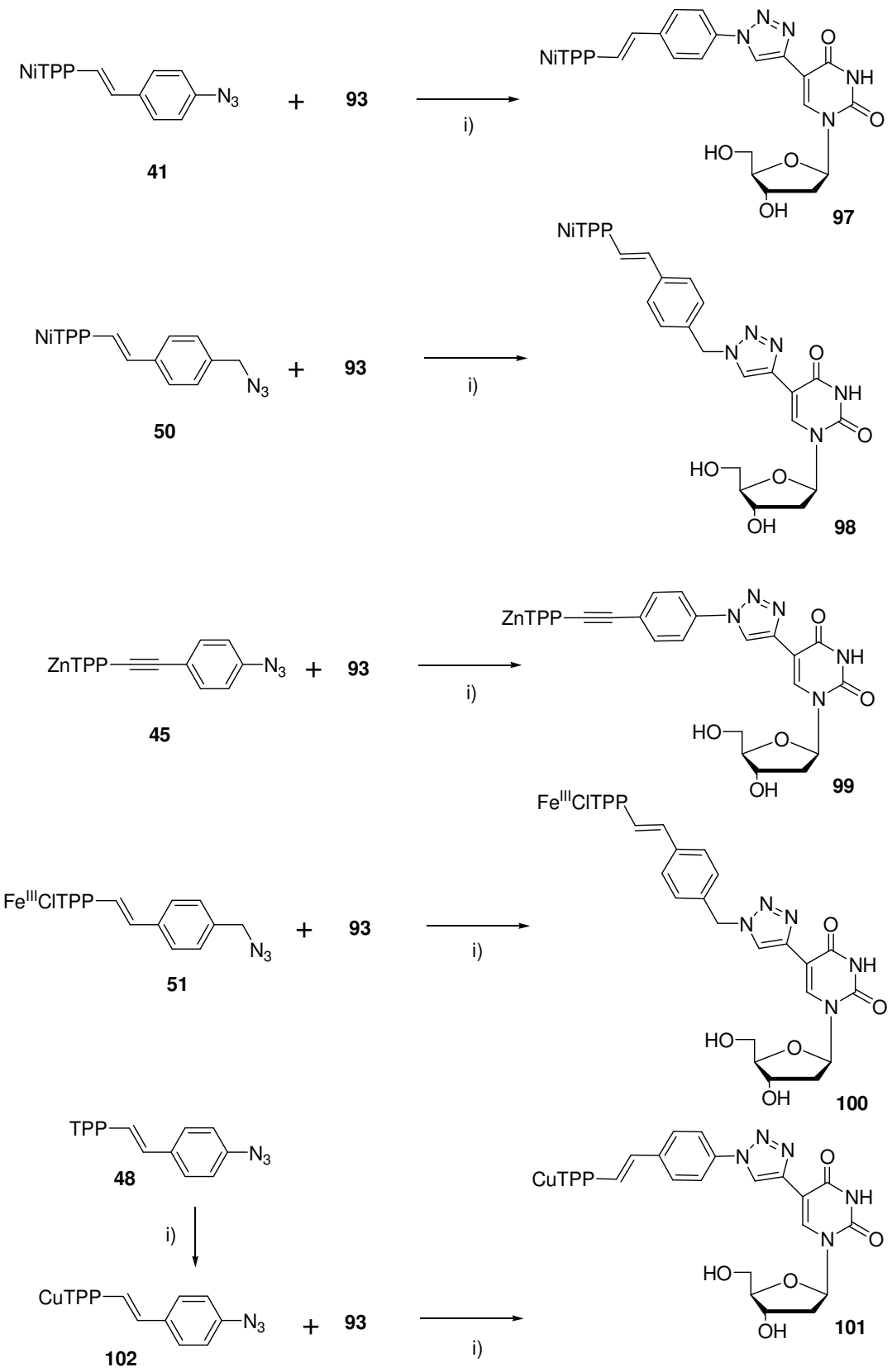

Figure 5.6 Synthesis of model triazole linked porphyrin nucleosides (shown as the DMT off structures). Reagents and conditions: i) THF, $Cu(ACN)_4PF_6$, RT, 2-4 days, 36% for **97**, 28% for **98**, 39% for **99**, 42% for **100** and 44% for **101**.

5.4 Post-synthetic Sonogashira and CuAAC Reactions

Post-synthetic oligonucleotide modification is an attractive alternative to the time-consuming preparation of multiple phosphoramidites. This is particularly important for screening various modifications of porphyrin possessing oligonucleotides. Post-synthetic modification is clearly an option for porphyrin derivatives because of the difficultly in synthesising the pre-synthetic analogues and the possibility of the decreased lifetime of porphyrin containing phosphoramidites.[43] We have therefore investigated post-synthetic Sonogashira and CuAAC reactions as a means to create porphyrin modified oligonucleotides.

5.4.1 Post-synthetic Sonogashira Reaction

For the post-synthetic Sonogashira reaction we prepared DMT on ONs using automated DNA synthesis containing a single internal insertion of one of the following DNA building blocks: 2′-deoxy-5-ethynyluridine (**V**), 2′-deoxy-8-bromoguanosine (**W**) or (*R*)-1-*O*-(2-iodobenzyl)glycerol (**X**). This gave **ON1-ON3** respectively (Figure 5.7). The phosphoramidites required for oligonucleotide synthesis were either prepared in the case of 2′-deoxy-5-ethynyluridine[136] and (*R*)-1-*O*-(2-iodobenzyl)glycerol[137] or purchased (2′-deoxy-8-bromoguanosine).

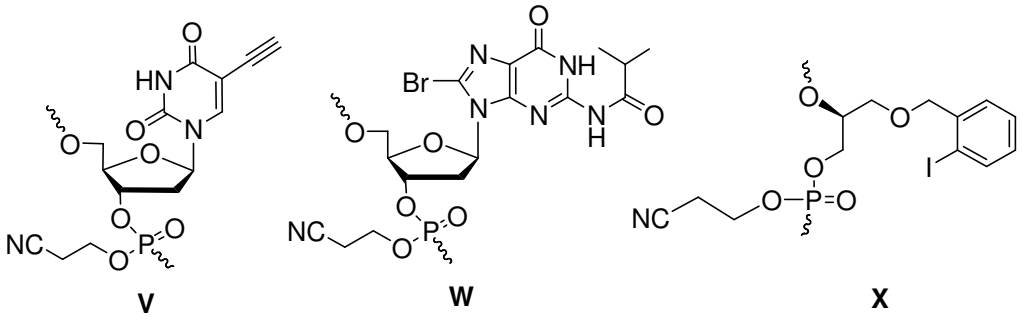

Figure 5.7 Post-synthetic Sonogashira reactions. Reagents and conditions: $Pd(PPh_3)_4$, CuI, DMF, Et_3N, 3 h.

Investigation into the Pd^0 catalysed Sonogashira reaction between CPG bound oligonucleotides **ON2** and **ON3** and ethylene functionalised porphyrin **35** was performed. Reactions were carried out using methods described earlier[138-142] followed by cleavage from the CPG support using 32% NH_4OH. TLC of the reaction mixture after the Sonogashira reaction showed the exclusive formation of the Glaser homodimer species **34** (Figure 2.23). UV-Vis spectroscopy of the oligonucleotides cleaved from the support CPG showed only traces of the porphyrin conjugates. Alternatively, the iodo (**32**) or the bromo (**40**) functionalised porphyrins were reacted with **ON1**, as under these conditions the formation of the homodimer porphyrin is infeasible. Unfortunately, reactions failed to produce any porphyrin functionalised oligonucleotides. Because of the failures of the Sonogashira reaction our focus switched to the CuAAC reaction.

5.4.2 Post-synthetic CuAAC Reaction

CuAAC reactions require a Cu^I catalyst that is usually produced from the *in situ* reduction of Cu^{II} with sodium ascorbate. Ni^{II} porphyrins were selected for the development of the post-synthetic procedure as these porphyrins are guaranteed to remain metallated throughout the CuAAC reaction. For the post-synthetic reactions ONs containing a single internal insertion of either 2′-deoxy-5-ethynyluridine (**V**), 2′-*O*-propargyl uridine (**Y**) or (*R*)-1-*O*-(4-ethynylbenzyl)glycerol (**Z**) were prepared using automated DNA synthesis (Figure 5.8). The phosphoramidites required for oligonucleotide synthesis were either prepared according to the published procedures in the case of 5-ethynyl-2′-deoxyuridine[136] and (*R*)-1-*O*-(4-ethynylbenzyl)glycerol[137] or purchased (2′-*O*-propargyl uridine). After the respective CuAAC reactions, these modifications will result in the positioning of the porphyrins in the major (**V**) or minor (**Y**) grooves of duplexes or as a bulged intercalating insertion (**Z**) in duplexes and triplexes.

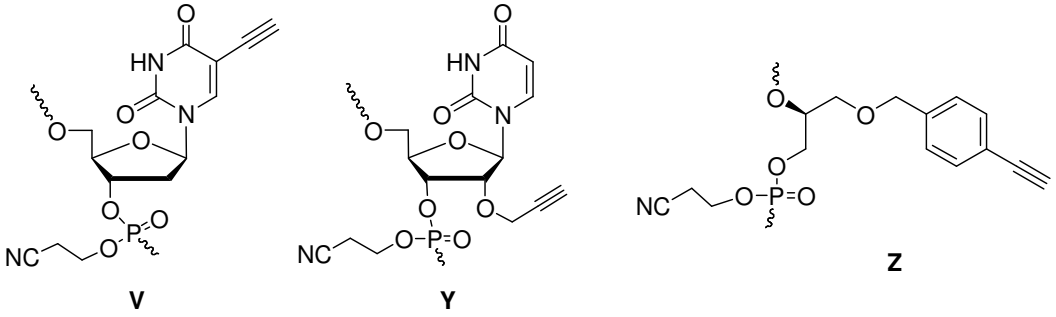

Figure 5.8 Acetylene containing nucleotides incorporated into DNA for use in CuAAC chemistry.

Numerous conditions have been used for the post-synthetic attachment of organic molecules to DNA using CuAAC chemistry.[61, 104, 143] Previous studies have shown that post-synthetic oligonucleotide based CuAAC reactions can be accelerated using microwave irradiation in a triethylammomium acetate buffer solution[144, 145] or on CPG support.[145, 146] Our attempts to achieve the coupling of nickel azido porphyrins **41** or **50** (Figure 5.3) using unfocused microwave irradiation (MicroSYNTH by Milestone Laboratory Systems) either on CPG or when the ON was in a buffer failed to produce any conjugates. The use of various combinations of Cu^{I} and Cu^{II} catalysts, solvents, and reducing agents at various temperatures did not improve the yields. Instead by increasing the reaction time and avoiding unfocussed microwave irradiation, porphyrin-DNA conjugates of **V**, **Y** and **Z** were produced in medium to high yields (**ON10-21**, Table 5.1 and Figure 5.9). These reactions were performed by shaking a reaction mixture containing CPG bound **ON10-21**, azido porphyrins **41** or **50**, $CuSO_4 \cdot 4H_2O$ and sodium ascorbate in DMSO:H_2O for 72 hours at RT. Alternatively, CuBr could be used, however, $CuSO_4 \cdot 4H_2O$ is easier to handle due to its greater solubility in water.

Oligonucleotide sequences were selected to position the porphyrin modifications internally, as apposed to a 5′ or 3′ molecular cap. Pure pyrimidine sequences (**ON4-6**) were designed to allow for antiparallel duplex or parallel triplex formation when combined with the appropriate complementary sequences. Mixed purine/pyrimidine sequences (**ON7-10**) were selected to investigate the versatility of the CuAAC reaction towards sequences containing purine nucleotides. These sequences also allowed for antiparallel duplex formation when combined with the appropriate complementary sequence.

Table 5.1 Oligonucleotides before and after CuAAC reactions with azides **41** or **50**.

No.	Oligonucleotide[c]	m/z [Da]		Retention	Conversion
		Calcd.	found	Times (min)[a]	(%)[b]
ON4	5' –CCCCTT**V**CTTTTTT	-	-	18.8	-
ON5	5' –CCCCTT**Y**CTTTTTT	-	-	18.2	-
ON6	5' –CCCCTT**Z**TCTTTTTT	-	-	17.8	-
ON7	5' –AGCT**V**GCTTGAG	-	-	20.8	-
ON8	5' –AGCT**Y**GCTTGAG	-	-	20.7	-
ON9	5' –CTCAAG**Z**CAAGCT	-	-	20.8	-
ON10	5' –CCCCTT**1**CTTTTTT	4958.9	4956.0	41.6	45
ON11	5' –CCCCTT**2**CTTTTTT	4972.9	4961.7	41.7	48
ON12	5' –CCCCTT**3**CTTTTTT	4988.9	4979.8	42.0	64
ON13	5' –CCCCTT**4**CTTTTTT	5002.9	4997.4	40.8	71
ON14	5' –CCCCTT**5**TCTTTTTT	5216.9	5202.8	43.2	60
ON15	5' –CCCCTT**6**TCTTTTTT	5231.0	5229.9	42.6	58
ON16	5' –AGCT**1**GCTTGAG	4497.8	4507.0	45.1	31
ON17	5' –AGCT**2**GCTTGAG	4511.9	4517.2	45.0	55
ON18	5' –AGCT**3**GCTTGAG	4527.8	4525.9	46.2	60
ON19	5' –AGCT**4**GCTTGAG	4541.8	4541.4	45.2	67
ON20	5' –CTCAAG**5**CAAGCT	4693.9	4697.2	47.0	19
ON21	5' –CTCAAG**6**CAAGCT	4707.9	4707.9	46.7	39

[a] HPLC retention times are ± 0.5 min, see methods for HPLC gradients. [b] Conversion % is determined from the HPLC peak integrals at 260 nm. [c]See Figure 5.9 for numbering.

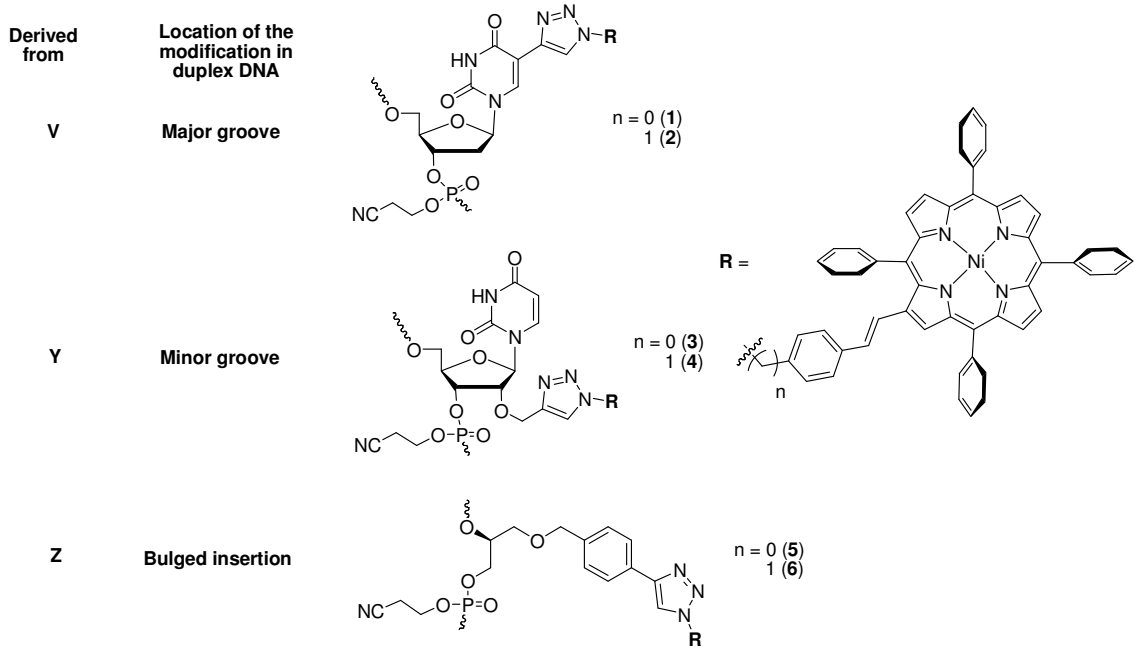

Figure 5.9 Porphyrin-DNA monomers obtained *via* the post-synthetic CuAAC chemistry.

CuAAC reactions (Figure 5.10) were achieved by mixing nickel containing porphyrin-azides **41** or **50** (7.67 μmol) and one of the alkyne CPG bound oligonucleotides **ON4-ON9** (0.33 μmol) in a micro-centrifuge vial, followed by the addition of DMSO (150 μL). Freshly prepared $CuSO_4 \cdot 4H_2O$ (0.2 μmol in 5 μL H_2O) and sodium ascorbate (1.0 μmol in 20 μL H_2O) solutions were added resulting in the partial precipitation of the porphyrin azide. The reactions were then sealed under argon, to avoid DNA cleavage caused by Cu^I ions in the presence of oxygen,[147] and shaken at RT for 72 hours.

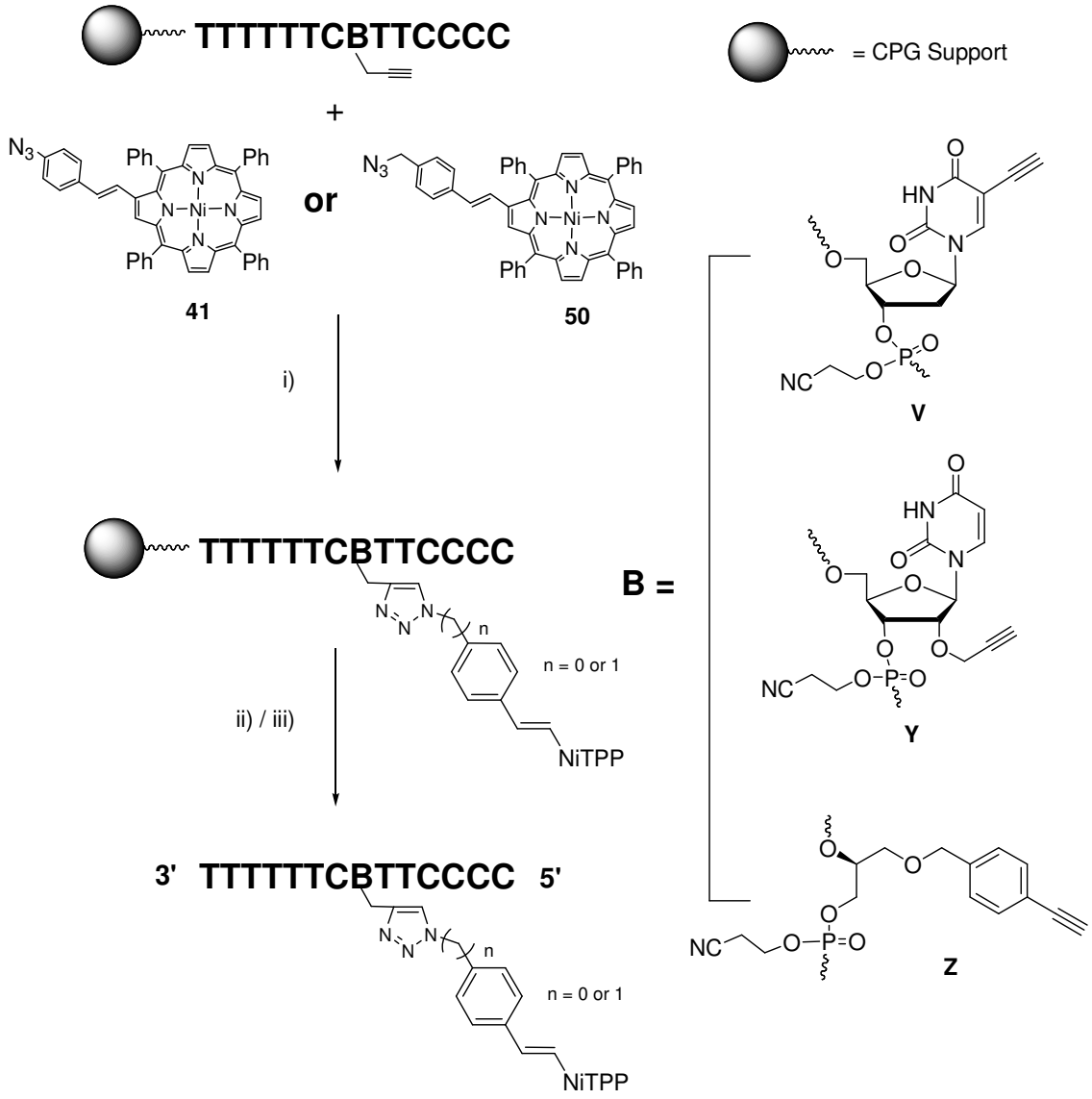

Figure 5.10 CuAAC reaction between azido porphyrins **41** or **50** and an oligonucleotide containing **V**, **Y** or **Z**. Reagents and conditions: i) $CuSO_4$, sodium ascorbate, DMSO, H_2O, RT, 72 h ii) 32% aq. NH_4OH, 55 °C, overnight iii) HPLC purification.

After shaking, the CPG supports were repeatedly washed with DCM to remove the unreacted azides. The resulting red coloured CPG support provided an indication of the progress of the reaction. The unreacted azide could be recovered in 80-90% yield for the use in future CuAAC reactions by washing the DCM solution containing the azide with H_2O, followed by drying over $MgSO_4$ and precipitation from DCM:MeOH. Oligonucleotides were then cleaved from the support using 32% aq NH_4OH, and purified using semi-preparative C_{18} HPLC monitored at both 260 and 427 nm (Figure 5.11). Porphyrin conjugated oligonucleotides showed appreciably increased retention times compared to unmodified oligonucleotides. As can be observed in Table 5.1, ONs possessing 2′-*O*-propargyl uridine (**Y**) had superior conversions in comparison to ONs containing 2′-deoxy-5-ethynyluridine (**V**) and (*R*)-1-*O*-(4-ethynylbenzyl)glycerol (**Z**). Mixed purine/pyrimidine sequences (**ON16-21**) were found to have lower conversions than pyrimidine sequences (**ON10-15**).

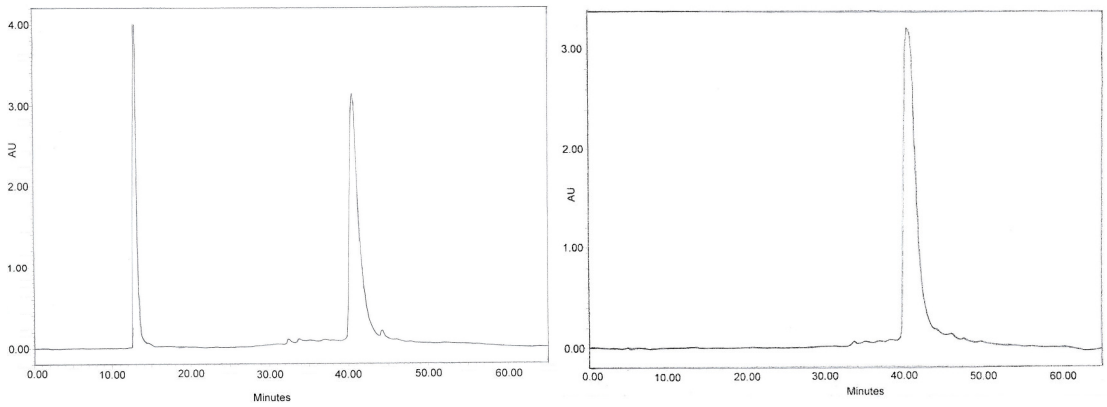

Figure 5.11. HPLC profiles of the reaction between azide **50** and **ON5** showing the significant increase in retention times for the porphyrin modified oligonucleotide (left: λ = 260 nm, right: λ = 427 nm).

Collected fractions were lyophilised, redissolved in 100 µL H_2O and precipitated from $LiClO_4$ and acetone to give deep red oligonucleotides. ONs were dissolved in 100 µL water to create stock solutions. Not all oligonucleotides could be completely solubilised and heating for several hours at 70 °C was required to increase solubility. Oligonucleotides were desalted using C_{18} zip-tips and then characterised by MALDI-TOF spectrometry (Table 5.1). It should be noted that the purchase and use of a new focused microwave system provided the conditions required for successful microwave accelerated CuAAC reactions to occur. Although not discussed here, this was used to produce porphyrin functionalised oligonucleotides in Chapter 6.

Purity of ONs was checked using 20% denaturing PAGE, showing a single red band with a significant retardation compared to the wild type oligonucleotide (Figure 5.12). This is in contrast to work published by Stulz *et al.*[43] which showed increased mobility of oligonucleotides possessing a single porphyrin moiety (based on the structure of porphyrin **96**, Figure 5.5) compared to the unmodified oligonucleotide.

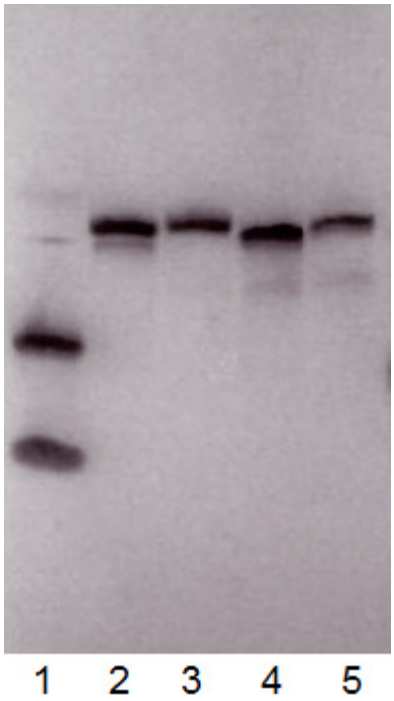

Figure 5.12 Denaturing 20% PAGE (7 M urea) of porphyrin modified oligonucleotides stained with Stains-All® dye and destained with H_2O. Porphyrin modified oligonucleotides were red before staining. Lane 1 is unmodified oligonucleotide **ONwt** (top) and a marker (bottom), lane 2 is **ON17**, lane 3 is **ON16**, lane 4 is **ON19** and lane 5 is **ON21**.

To summarise, Sonogashira and CuAAC chemistry have been shown to be useful methods for the creation of *β*-pyrrolic porphyrin functionalised nucleosides. More importantly, CuAAC reactions were found to be an effective method for the creation of post-synthetic and site-specific, internally modified porphyrin oligonucleotides. Reactions could be performed on aliphatic or aromatic azido Ni^{II} porphyrins and CPG bound ONs containing terminal alkyne modifications (**V**, **Y** and **Z**) in moderate to high yields (19-71% conversion).

This has allowed synthesis of a number of porphyrin possessing ONs for use in thermal stability studies on single stranded, duplex and triplex DNA.

5.5 UV-Vis and CD Studies of Porphyrin-DNA Conjugates

Optical and thermal stability properties of the oligonucleotides possessing Ni^{II} porphyrins were investigated using UV-Vis and CD spectroscopy. These methods were used to give an indication of the effect of a porphyrin modification on single stranded, duplex and triplex DNA possessing internal porphyrin modifications.

5.5.1 Single Stranded Oligonucleotides

Single stranded oligonucleotides **ON10-ON21** were prepared at a concentration of 1.0 μM in cacodylate buffer at various pH (5.0, 6.0 and 7.2). Samples were prepared by taking the appropriate quantity of oligonucleotide from the stock solution and diluting it to 1.0 μM with the appropriate pH buffer to obtain a 1.0 μM solution. CD spectra were then recorded at 20 °C from 220-500 nm.

CD spectra, at pH 6.0, of all porphyrin modified oligonucleotides showed DNA signals at 248 (negitive ellipticity) and 280 nm (positive ellipticity, not shown) and strong signals around the location of the porphyrin Soret band (Figure 5.13). Results showed, in general, a bisignate curve suggesting that either the porphyrin interacts with the chiral environment of the oligonucleotide or that dipole-dipole electronic interactions between two porphyrins occur.[38, 39, 47, 48, 50, 52, 54, 56]

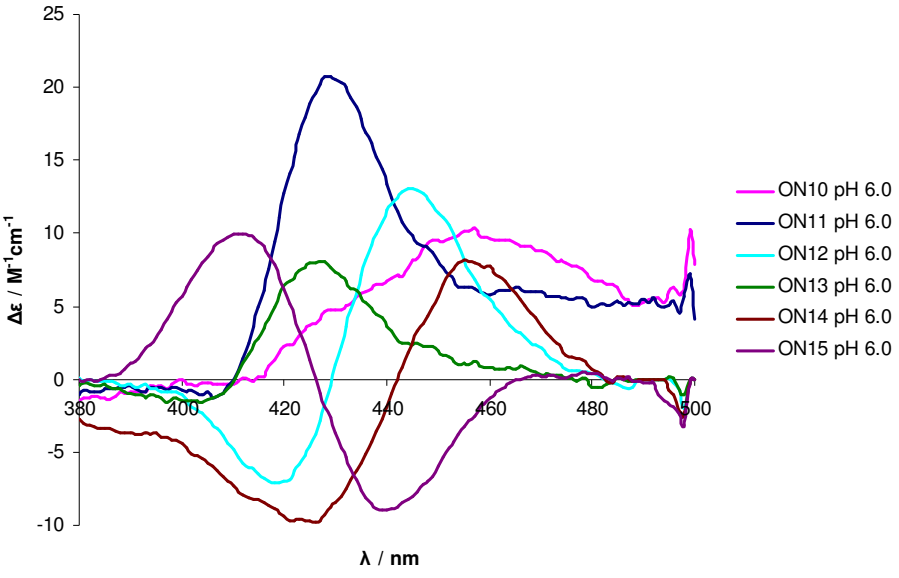

Figure 5.13 CD spectra of single stranded oligonucleotides **ON10-15** at pH 6.0.

Further analysis showed that CD signals were pH dependent for CT sequences (**ON10-15**) but not for mixmer sequences **ON16-21**. For example, the CT sequence **ON15** (Figure 5.14A) showed virtually no porphyrin CD signals at pH 7.2, while a strong bisignate curve was observed at pH 5.0 and 6.0. Along with this, CD intensity in the UV region decreased with increasing pH and was blue shifted by 6 nm. This is a characteristic signature of i-motif formation as a result of cytosine protonation (pK_a = 5.2) (Figure 5.14C).[148, 149] Increasing the pH resulted in cytosine deprotonation, i-motif unfolding and loss of the porphyrin-porphyrin interactions. It is possible that this structure allowed for the orientation of porphyrins in such a manner that porphyrin-porphyrin exciton coupling occurred through porphyrin stacking as shown in a possible i-tetraplex structure (Figure 5.14C). The unmodified oligonucleotide (**ONwt**, Table 5.2) did not show the characteristic pH dependent i-motif CD signals (Figure 5.15) suggesting that the porphyrin, rather than the ON sequence, triggers the formation of the i-motifs. Native PAGE (pH 5.0) confirmed the absence of an i-motif structure in **ONwt**. Porphyrin possessing ONs did not penetrate the native PAGE gel at pH 5.0. This significant retardation compared to that observed in denaturing gels confirmed the formation of a secondary structure. Although the molecularity of **ON10-15** could not be determined by native PAGE it may be possible using electrospray ionisation mass spectroscopy in pH 5.0 buffers. The pH independent CD spectra observed in mixmers (Figure 5.16) suggested the formation of aggregates rather than i-motifs in mixmer sequences **ON16-21**.

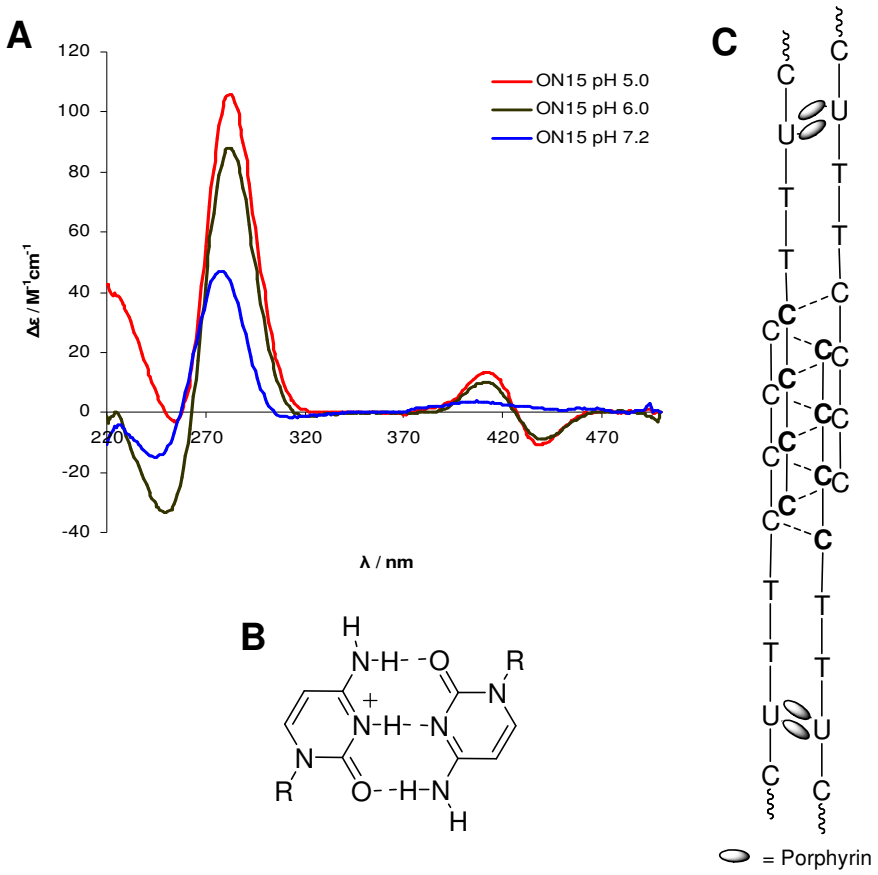

Figure 5.14 CD spectra of single stranded oligopyrimidine **ON15** at pH 5.0, 6.0 and 7.2 (A), cytosine+-cytosine base pair (B, R = furanose ring) and possible i-tetraplex of **ON13** (C).

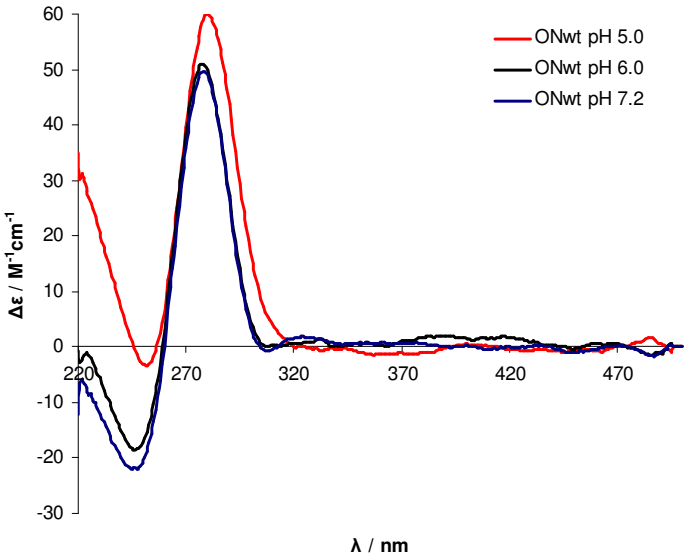

Figure 5.15 CD spectra of single stranded oligopyrimidine **ONwt** at pH 5.0, 6.0 and 7.2.

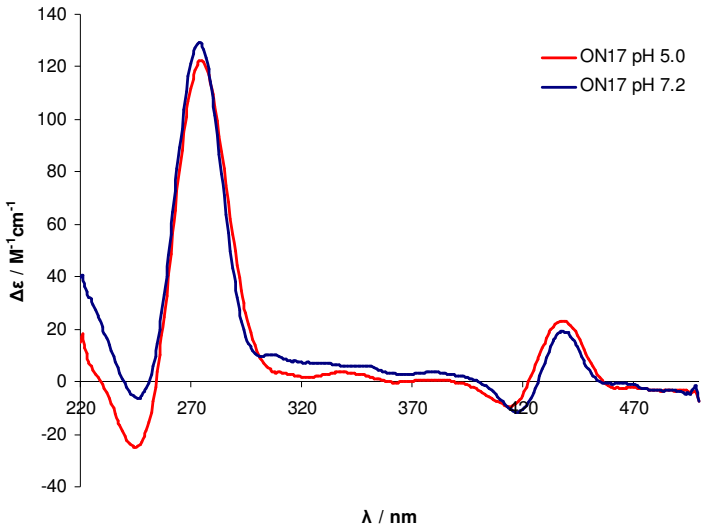

Figure 5.16 CD spectra of single stranded purine-pyrimidine oligonucleotide **ON17** at pH 5.0 and 7.2.

Thermal melting of the single stranded ONs resulted in the loss of the CD signal around 430 nm and reduced signal intensity at 280 nm (Figure 5.17), suggesting the melting of i-motifs (**ON10-ON15**) or the separation of aggregates. After melting, a CD signal for the porphyrin was only observed after incubation at 20 °C overnight and the intensity was significantly lower than for the unheated sequence. This suggested that the formation of aggregates or i-motifs was slow to occur at 1.0 μM concentration and that the i-motif or aggregates only form in the concentrated stock solution (*ca*. 300-1000 μM).

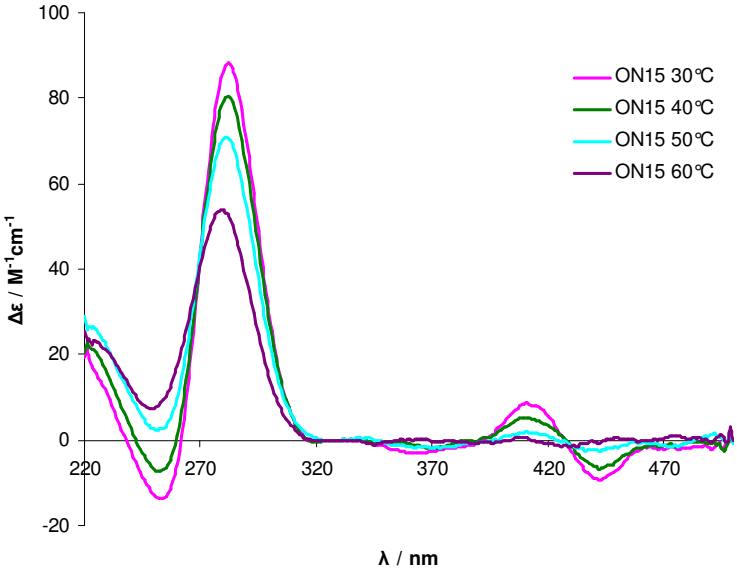

Figure 5.17 CD spectra showing the thermal melting of single stranded oligopyrimidine **ON15** from 30-60 °C at pH 5.0.

5.5.2 Triplexes and Duplexes Containing Internal Porphyrin Modifications

The thermal stability of triplexes and duplexes containing the synthesised oligonucleotides **ON10-ON21** was assessed by UV-Vis thermal denaturation experiments at 260 and 430 nm from 10-70 °C. The melting temperatures (T_m, °C) were determined as maxima of first derivatives of melting curves and are listed in Tables 5.2 and 5.4. Annealing temperatures are shown in Tables 5.3 and 5.5. The triplex forming oligonucleotide (TFO) sequences (**ONwt** and **ON10-15**) possessing different porphyrin modifications were studied in a parallel triplex towards the duplex **D1** (Table 5.2) and in antiparallel duplexes towards appropriate oligonucleotides **ON22-24** (Table 5.2-5.5). Triplexes were formed by mixing the TFO strand at 1.5 μM with 1.0 μM of each duplex strand (**D1**). Duplexes were formed from 1.0 μM of each strand in the appropriate buffer. Oligonucleotides were heated to 70 °C (triplexes) or 90 °C (duplexes) for 15 minutes then cooled to 10 °C an incubated for 30 minutes. Buffers were made to 20 mM sodium cacodylate, 100 mM NaCl and 50 mM $MgCl_2$ and adjusted to the required pH using dilute HCl according to the procedure described.[150] Modifications **1** and **2** (**ON10**, **ON11**, **ON16** and **ON17**) were designed to locate the porphyrin in major groove of the duplex, **3** and **4** (**ON12**, **ON13**, **ON18** and **ON19**) in the minor groove and modifications **5** and **6** (**ON14**, **ON15**, **ON20** and **ON21**) were inserted as an intercalating bulge in the middle of duplexes and triplexes.

5.5.2.1 Triplexes

A triple helix is formed when third single stranded oligonucleotide binds in the major groove of the duplex (Figure 1.7). This is achieved by forming T-A··T and C-G··C^+ Hoogsteen interactions (··), and requires the protonation of the cytosine in the TFO. The pK_a of the imino group of the cytosine is 5.2 thus triplex stability increases at a lower pH.

The thermal stability of triplexes was assessed by UV-Vis thermal melting at 260 and 430 nm (Table 5.2). At pH 6.0 two transitions were observed at 260 nm for parallel triplexes which correspond to the melting of the triplex at lower temperature and the duplex at 55 °C. At pH 5.0 triplex transitions occurred at higher temperatures (due to the increased protonation of cytosine) which resulted in the overlaid melting profiles for

duplexes and triplexes at 260 nm (**ON12-15/D1**). Sharp melting transitions for the triplexes were also visible at 430 nm, thus confirming the melting of the porphyrin containing TFO strands from the duplex.

As can be seen from the T_m data in Table 5.2, the internal insertion of a porphyrin resulted in increased T_m values of the Hoogsteen–type triplexes compared to the wild-type triplex (**ONwt/D1**). Stabilisation of all porphyrin modified triplexes was observed at pH 6.0 (ΔT_m = 3.0-12.0 °C). The TFO strands **ON10** and **ON14** containing aromatic porphyrins (modifications **1** and **5**, Figure 5.9) resulted in slightly higher stabilisation of the triplex at pH 6.0 than for TFO strands **ON11** and **ON15** containing the aliphatic linked porphyrins (modifications **2** and **6**). In the case of **ON14** and **ON15**, where the porphyrin is incorporated as a bulged insertion into the duplex strands, molecular modelling (AMBER* force field[151, 152]) suggested that stabilisation was most likely due to the intercalation of the porphyrin (Figure 5.18A-D). However, as shown in Figure 5.18 the porphyrin could either penetrate through the duplex DNA (A and B) or intercalate between bases in the duplex strands such that the *meso* phenyl rings are located in the grooves of the triplex (C and D). These two orientations were possible due to the long linker between the porphyrin and the phosphate backbone (19 Å). Intercalation, similar to that shown in TINA configurations[144, 153] (Figure 5.19), was found to be of higher energy (-20034 KJ/mol) than when the porphyrin penetrated the duplex strands and aligned itself in the minor groove (-20086 KJ/mol). This difference in energy is most likely a result of the destabilising bulge in the phosphate backbone of the TFO strand that is required for the porphyrin to intercalate between the bases of the duplex strands. Further thermal stabilisation might be possible by decreasing the linker length and thus reducing the bulge in the backbone of the TFO strand. Although not modelled, the aliphatic linked porphyrin in **ON15** is likely to be positioned in a similar manner to the aromatic porphyrin in **ON14**.

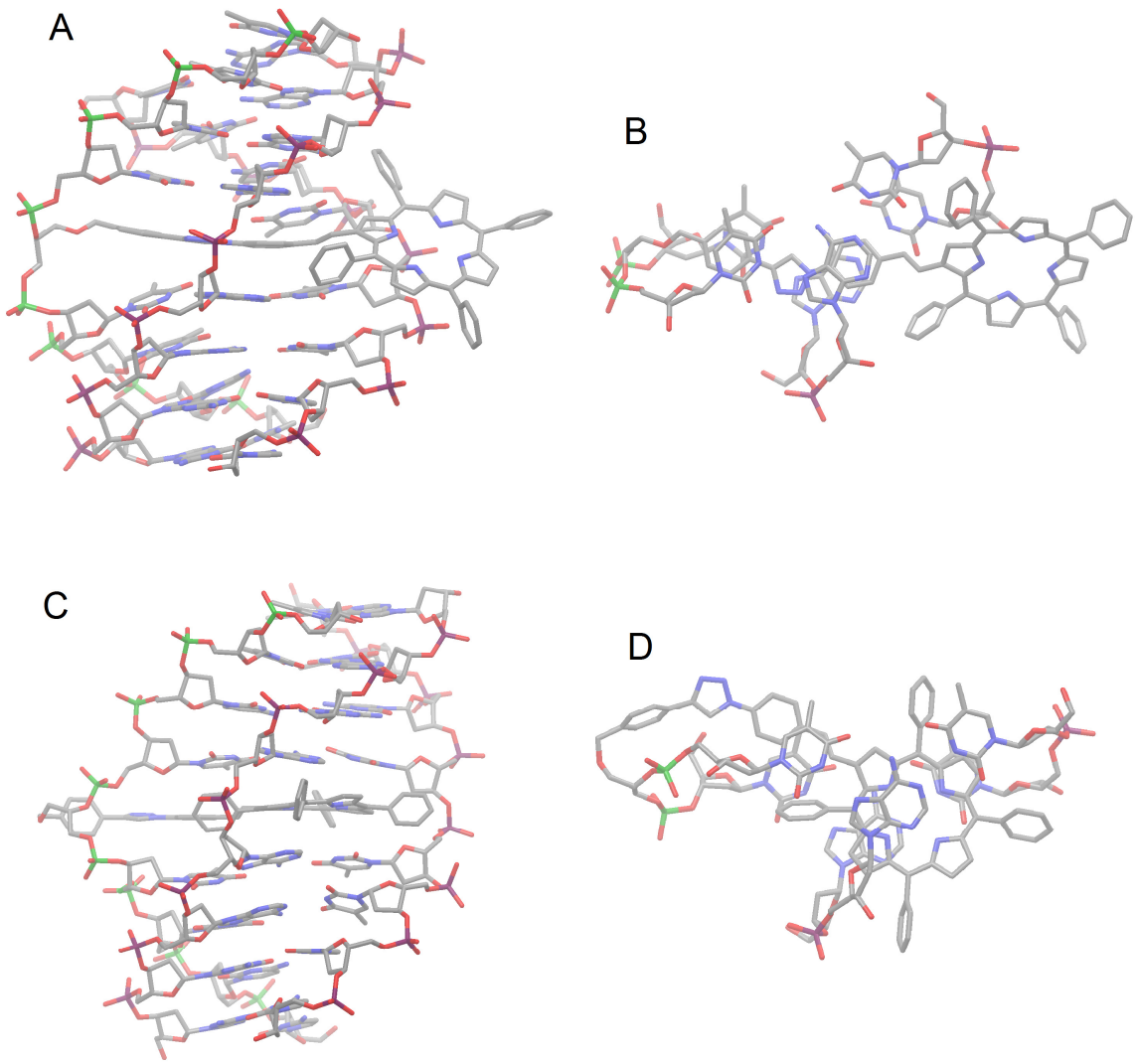

Figure 5.18 A representation of the AMBER* force field lowest energy minimised structures of the porphyrin possessing triplex **ON14/D1** showing two possible porphyrin orientations. Figures **A** (side) and **B** (top) show the porphyrin penetrating through the duplex **D1**. Figures **C** (side) and **D** (top) show the higher energy structure where the porphyrin intercalates between the bases of duplex **D1**. Phosphorus atoms in the TFO strand have been coloured green. In **B** and **D,** nucleotides not directly above or below the porphyrin modification have been removed for clarity.

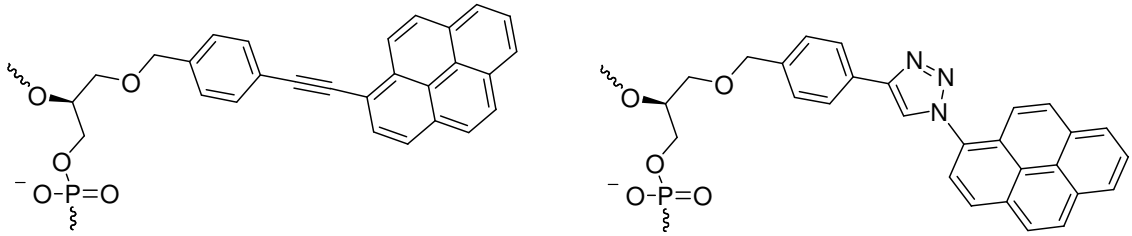

Figure 5.19 TINA structures incorporated into TFO strands used as bulged insertions to stabilise triplexes.[138, 144]

As expected, the T_m values of triplexes of **ON12-15/D1** increased at pH 5.0 due to the increased cytosine protonation. Surprisingly, the T_m values of **ON10-11** were almost unchanged. At pH 7.2 no triplex formation was observed above 10 °C. The lower T_m values for the triplexes at 430 nm suggested that the porphyrin was stabilising the triplex and the movement of the porphyrin resulted in the disruption of the triplex soon afterwards. The significantly lower annealing temperatures at 260 nm alludes to the possibility of different kinetics in the annealing and denaturing processes. The importance of the porphyrin in the stabilisation of the triplex strand is emphasised when we observe the previously reported T_m value for the bulged insertion of 1,2,3-triazole linked benzyl moiety (Figure 5.20) in the TFO strand.[144] Under identical conditions and using the sequence equivalent to **ON15**, destabilisation of the resulting triplex by greater than 23 °C was observed at pH 6.0.

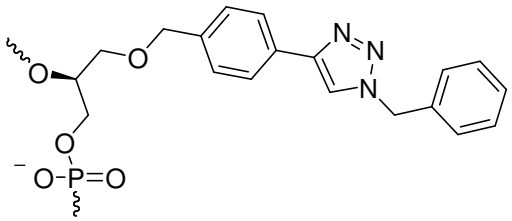

Figure 5.20 1,2,3-Triazole linked benzyl moiety incorporated into TFO strands.[144]

Table 5.2 Melting temperatures of parallel DNA triplexes and antiparallel DNA duplexes containing a single porphyrin modification.

		Parallel Triplex[a] 3'-CTGCCCCTTTCTTTTTT 5'-GACGGGGAAAGAAAAAA (**D1**)		Antiparallel Duplex[b] 3'-GGGGAAAGAAAAAA (**ON22**)	
		pH 5.0	pH 6.0	pH 6.0	pH 7.2
ONwt	5' –CCCCTTTCTTTTTT	54.0[c]	27.0	48.0	48.0
ON10	5' –CCCCTT**1**CTTTTTT	39.0 (39.0)	39.0 (37.0)	31.0 (30.0)	30.0 (30.3)
ON11	5' –CCCCTT**2**CTTTTTT	40.0 (39.5)	30.0 (37.7)	32.5 (29.0)	33.2 (33.7)
ON12	5' –CCCCTT**3**CTTTTTT	54.5[c] (53.5)	34.5 (29.3)	35.0 (28.5)	33.2 (33.7)
ON13	5' –CCCCTT**4**CTTTTTT	55.0[c] (54.0)[c]	34.5 (32.7)	41.5 (43.8)	41.7 (43.0)
ON14	5' –CCCCTT**5**TCTTTTTT	55.0[c] (53.0)	38.9 (37.0)	38.7 (24.0)	34.6 (37.0)
ON15	5' –CCCCTT**6**TCTTTTTT	55.0[c] (53.5)	36.3 (36.8)	33.3 (31.0)	34.3 (34.6)

Table 5.3 Annealing temperatures of parallel DNA triplexes and antiparallel DNA duplexes containing a single porphyrin modification.

		Parallel Triplex[a] 3'-CTGCCCCTTTCTTTTTT 5'-GACGGGGAAAGAAAAAA (**D1**)		Antiparallel Duplex[b] 3'-GGGGAAAGAAAAAA (**ON22**)	
		pH 5.0	pH 6.0	pH 6.0	pH 7.2
ONwt	5' –CCCCTTTCTTTTTT	54.0[c]	27.0	48.0	48.0
ON10	5' –CCCCTT**1**CTTTTTT	35.8 (35.0)	35.7 (37.0)	31.5 (31.8)	28.3 (28.1)
ON11	5' –CCCCTT**2**CTTTTTT	40.0 (38.9)	27.5 (30.8)	32.5 (29.0)	32.0 (33.0)
ON12	5' –CCCCTT**3**CTTTTTT	54.5[c] (47.3)	25.4 (25.4)	33.7 (28.7)	33.3 (31.6)
ON13	5' –CCCCTT**4**CTTTTTT	54.8 (50.9)[c]	18.0 (26.5)	42.8 (41.7)	42.5 (43.5)
ON14	5' –CCCCTT**5**TCTTTTTT	55.0[c] (53.3)	24.7 (36.7)	34.0 (24.0)	34.6 (36.4)
ON15	5' –CCCCTT**6**TCTTTTTT	55.0[c] (54.5)	32.0 (37.0)	33.5 (31.0)	34.9 (34.6)

T_m (°C) data for parallel triplex and antiparallel duplex melting, taking from the UV-Vis melting curves at 260 and 430 nm (shown in brackets). [a]C = 1.5 μM of **ON10-15** and **ONwt** and 1.0 μM of each strand of dsDNA **(D1)** in 20 mM sodium cacodylate, 100 mM NaCl and 5 mM $MgCl_2$, pH 5.0 and 6.0. [b]C = 1.0 μM of each strand in 20 mM sodium cacodylate, 100 mM NaCl and 5 mM $MgCl_2$, pH 6.0 and 7.2. [c]Third strand and duplex melting overlaid.

In order to confirm triplex formation, CD spectra of the triplexes was recorded at pH 5.0 (Figure 5.21) and 6.0 (Figure 5.22). A concentration of 1.0 μM of each oligonucleotide strand was used to avoid interference from any excess of the TFO strand. A negative band around 210 nm is considered to be a sign of parallel DNA triplexes.[154] As can be seen, a negative band exists at 209 nm, therefore confirming the formation of a triplex in porphyrin modified sequences. Although a negative band exists at 208 nm in duplex **D1** the intensity was significantly lower than for the triplex.

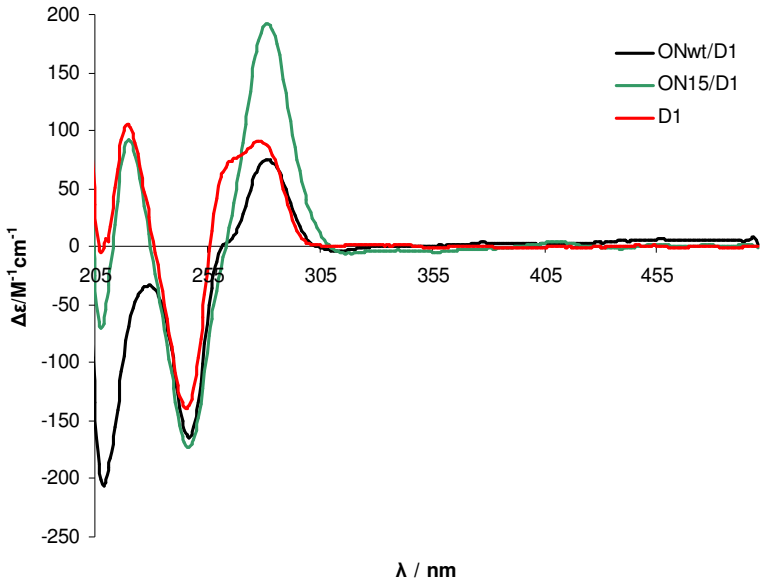

Figure 5.21 CD spectra of triplex **ONwt** and **ON15** with **D1**, and duplex **D1** alone at pH 5.0 (20 °C).

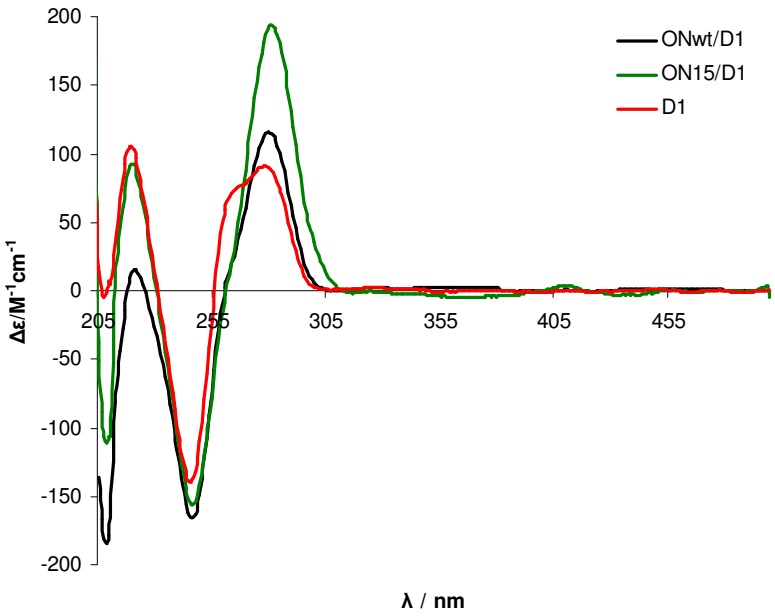

Figure 5.22 CD spectra of triplex **ONwt** and **ON15** with **D1** and duplex **D1** alone at pH 6.0 (20 °C).

5.5.2.2 Duplexes

It was observed (Table 5.2) that the single internal incorporation of a porphyrin in an antiparallel duplex (**ON10-15/ON22**) resulted in thermal destabilisation of the duplex compared to the unmodified duplex. Variation in the destabilisation depended on the porphyrin incorporated and its location in the duplex, remembering that modifications **1** and **2** were designed to locate the porphyrin in the major groove, **3** and **4** in the minor groove and **5** and **6** as an intercalating bulge in the middle of the duplex. Generalising the results we found that duplexes involving **ON10-11** and **ON14-15** showed significant thermal destabilisation between 13.4-18.0 °C. Molecular modelling (AMBER* force field) of the duplexes involving **ON10-11** (Figure 5.23A and B) and **ON14-15** (Figure 5.24A and B) suggested that the porphyrins had very little interaction with the nucleobases and were positioned in the major groove. Porphyrins **1** and **2** in **ON10** and **ON11** were located either in the major groove space (**ON10**) or positioned against the side of the major groove (**ON11**). Due to the linker length, porphyrins **5** and **6** protruded through the duplex, leaving just the phenyl and triazole moieties located in between bases in the duplex core and the porphyrin positioned in the major groove. This intercalation may account for the slight stabilisation of **ON14-15** over **ON10-11**. As the porphyrin is hydrophobic it could be expected that destabilisation is a result of a different hydration of the duplex compared to the wild type.

Significant differences were found in the melting temperatures of duplexes containing **ON12** and **ON13** where the porphyrin was positioned in the minor groove. Duplexes containing the aromatic porphyrin **ON12** showed ΔT_m of -13.0 to -14.8 °C, similar to the duplexes **ON10-11** and **ON14-15**, while duplex **ON12/ON22**, which contained the aliphatic porphyrin **4**, had a ΔT_m of -6.3 to -6.5 °C. Molecular modelling suggested that the aromatic (**ON12**, Figure 5.23C) and the aliphatic porphyrins (**ON13**, Figure 5.23D) follow the minor groove in a similar manner, however, the aliphatic porphyrin is less destabilising presumably as a result of rotational flexibility around the extra sp^3 carbon. The aromatic porphyrin in **ON12** is unable to fit as tightly in the minor grove and as a result lower T_m values were observed.

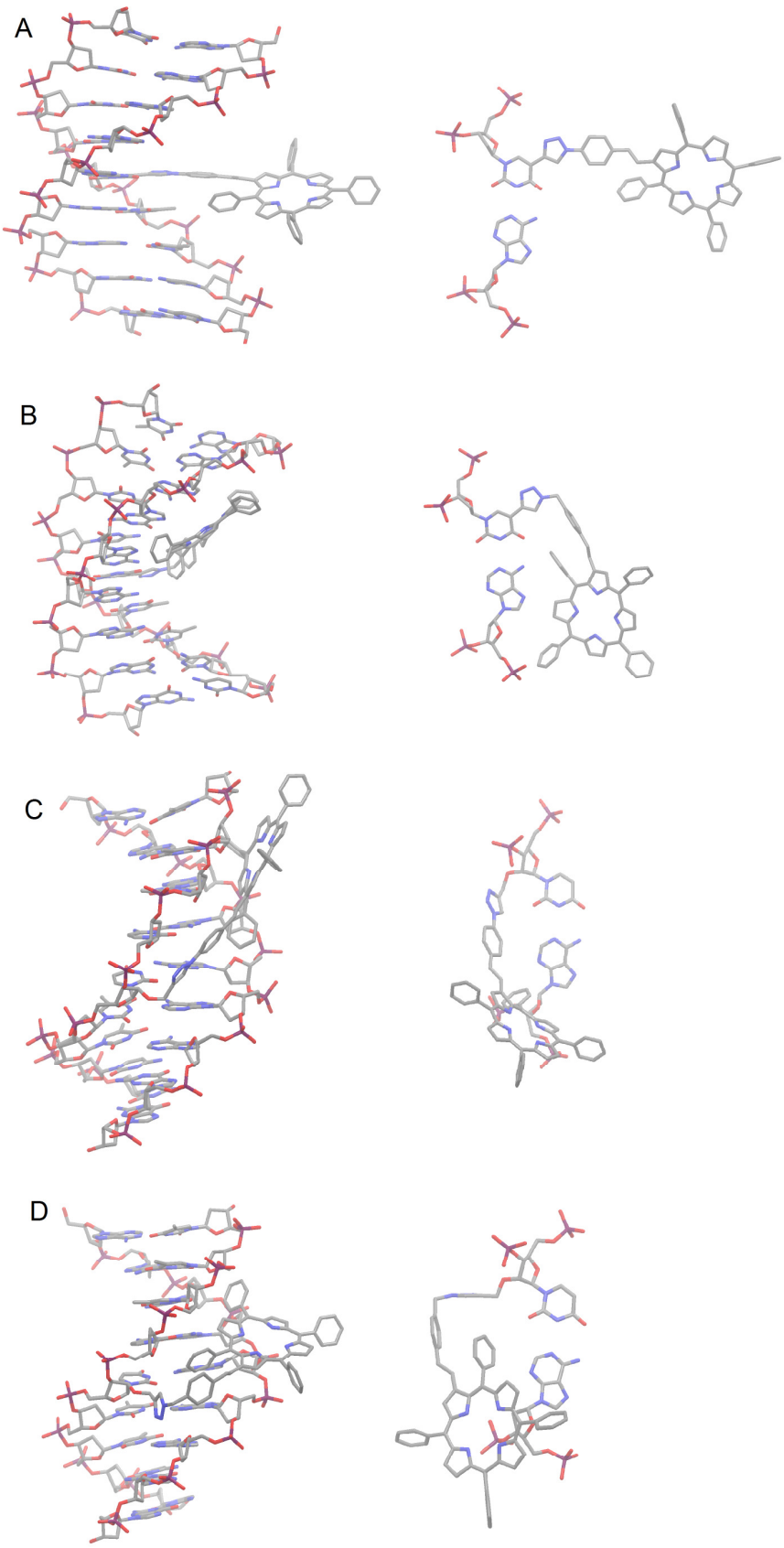

Figure 5.23 A representation of the lowest energy AMBER* force field minimised structures of duplexes involving **ON10** (A), **ON11** (B), **ON12** (C) and **ON13** (D). On the left is the side view and on the right is the top view (nucleotides above and below the porphyrin modification have been removed for clarity).

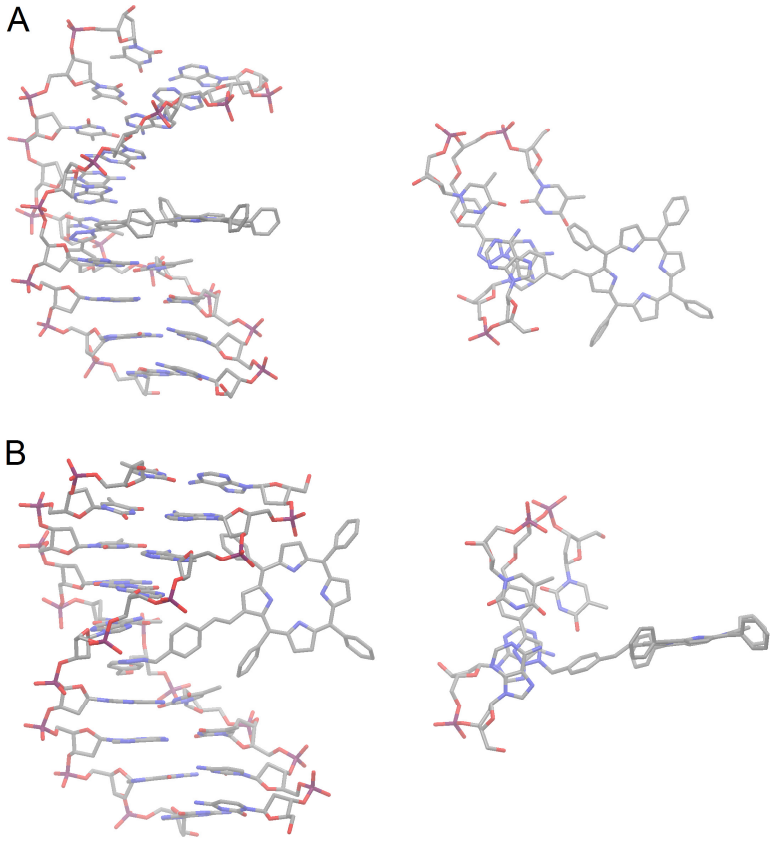

Figure 5.24 A representation of the lowest energy AMBER* force field minimised structure of duplexes involving **ON14** (A) and **ON15** (B). On the right is the side view and on the left is the top view (nucleotides not directly above or below the porphyrin modification have been removed for clarity).

Duplexes containing mixed purine/pyrimidine stands (Tables 5.4 and 5.5) showed T_m values consistent with that of the porphyrin modified CT sequences. Significant destabilisation was found in all duplexes especially those containing modifications of (*R*)-1-*O*-(4-ethynylbenzyl)glycerol (**ON20** and **ON21/ON24**). These duplexes showed ΔT_m of -16.3 to -18.0 °C for the duplexes containing the aromatic porphyrin **5** and even further destabilisation for the aliphatic porphyrin **6** (ΔT_m -21 to -22.1 °C). Duplexes containing a porphyrin in the minor groove (**ON18** and **ON19/ON23**) confirmed the melting trend shown in **ON10-15** – that being the additional flexibility of the aliphatic porphyrin **4** allows for that porphyrin to fit more comfortably in the minor groove of the duplex resulting in less destabilisation of the duplex. Additionally, the melting profiles showed virtually no hysteresis at either 260 or 430 nm for all duplexes indicating similar kinetics in both denaturing and annealing processes even with the introduction of a porphyrin.

Table 5.4 Melting temperatures of antiparallel duplexes containing mixed purine/pyrimidine oligodeoxynucleotides.

		Antiparallel Duplex 3'–TCGAACGAACTC (**ON23**)		Antiparallel Duplex 3'-GAGTTCGTTCGA (**ON24**)	
		pH 6.0	pH 7.2	pH 6.0	pH 7.2
ONwt$_m$	5' –AGCTTGCTTGAG	50.0	50.0	-	-
ON16	5' –AGCT**1**GCTTGAG	35.0 (32.0)	35.0 (34.0)	-	-
ON17	5' –AGCT**2**GCTTGAG	34.0 (33.5)	32.0 (NVT)	-	-
ON18	5' –AGCT**3**GCTTGAG	36.0 (36.0)	34.0 (35.0)	-	-
ON19	5' –AGCT**4**GCTTGAG	42.0 (39.0)	43.0 (NVT)	-	-
ON20	5' –CTCAAG**5**CAAGCT	-	-	32.0 (33.0)	33.3 (NVT)
ON21	5' –CTCAAG**6**CAAGCT	-	-	29.0 (28.0)	27.9 (29.1)

Table 5.5 Annealing temperatures of antiparallel duplexes containing mixed purine/pyrimidine oligodeoxynucleotides.

		Antiparallel Duplex 3'–TCGAACGAACTC (**ON23**)		Antiparallel Duplex 3'-GAGTTCGTTCGA (**ON24**)	
		pH 6.0	pH 7.2	pH 6.0	pH 7.2
ONwt$_m$	5' –AGCTTGCTTGAG	50.0	50.0	-	-
ON16	5' –AGCT**1**GCTTGAG	34.5 (31.5)	35.0 (34.0)	-	-
ON17	5' –AGCT**2**GCTTGAG	34.5 (NVT)	32.0 (NVT)	-	-
ON18	5' –AGCT**3**GCTTGAG	36.0 (36.5)	34.0 (35.0)	-	-
ON19	5' –AGCT**4**GCTTGAG	42.0 (38.5)	43.0 (NVT)	-	-
ON20	5' –CTCAAG**5**CAAGCT	-	-	33.6 (31.0)	32.2 (NVT)
ON21	5' –CTCAAG**6**CAAGCT	-	-	26.0 (27.5)	28.9 (27.0)

T_m (°C) data for antiparallel duplex melting taking from the UV melting curves at 260 and 430 nm (shown in brackets). C = 1.0 μM of each strand in 20 mM sodium cacodylate, 100 mM NaCl and 5 mM $MgCl_2$, pH 6.0 and 7.2. NVT = No visible transition.

The CD spectra of duplexes containing ONs **ON10-21** were recorded from 220-500 nm at 20 °C. CD spectra showed a negative band at around 245-250 nm and a positive band at 274-280 nm (Figure 5.25 and 5.26), clearly suggesting that the modified duplexes retained their overall B-form double helix structure. These oligonucleotides also showed, in general, a porphyrin CD signal as a bisignate curve around 430 nm. Similar bisignate curves have been assigned to exciton coupling between porphyrin molecules.[54, 56] As our structures possess only a single porphyrin modification these interactions would only be possible through duplex aggregation. Aggregation, which is thought to occur over longer time periods, was found to be unlikely as the porphyrin CD signal of a duplex that had been melted returned to the pre-melted level almost instantaneously (Figure 5.27). It was more likely that the porphyrin bisignate curve was a result of the porphyrin somehow interacting with the DNA grooves.

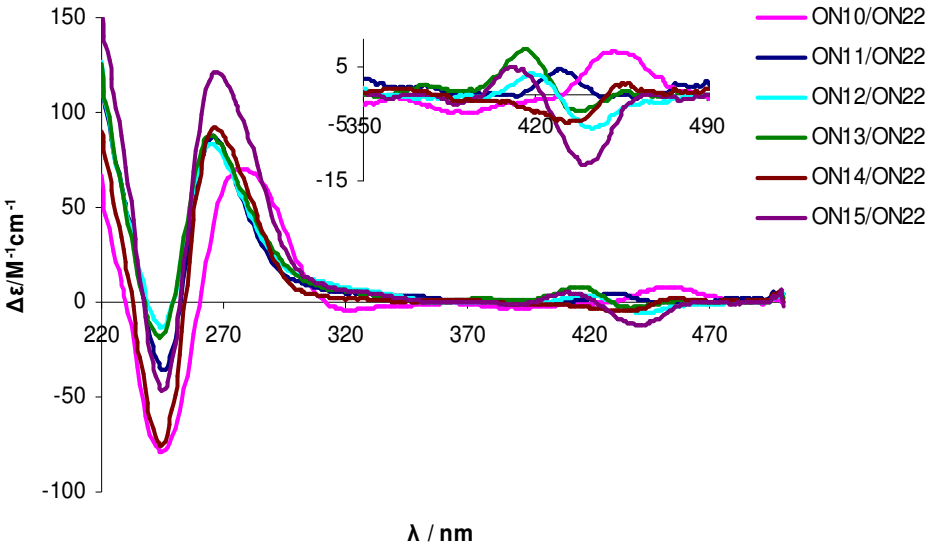

Figure 5.25 CD spectra of duplexes **ON10-15** with **ON22** at pH 6.0 (20 °C).

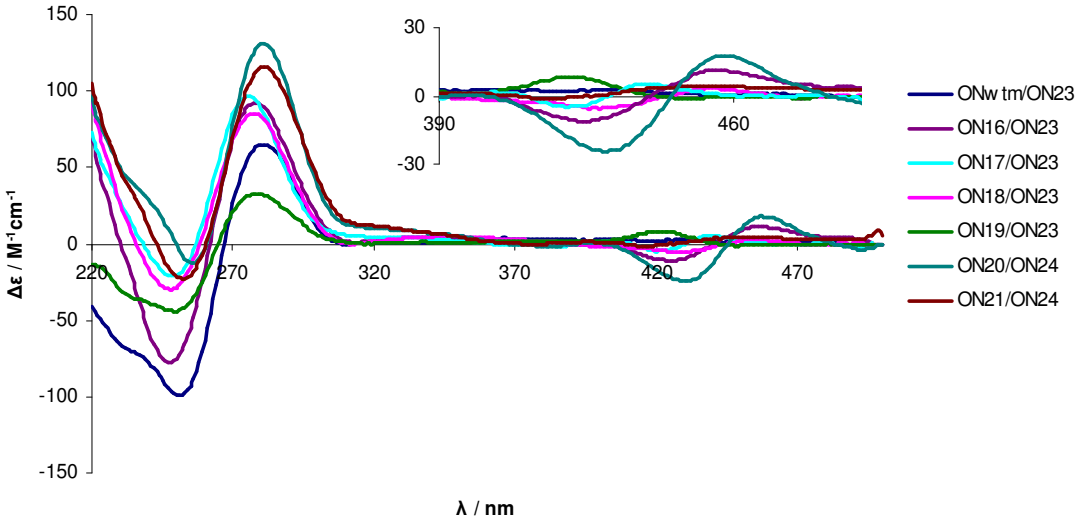

Figure 5.26 CD spectra of duplexes involving **ONwt$_m$** and **ON16-21** at pH 6.0 (20 °C).

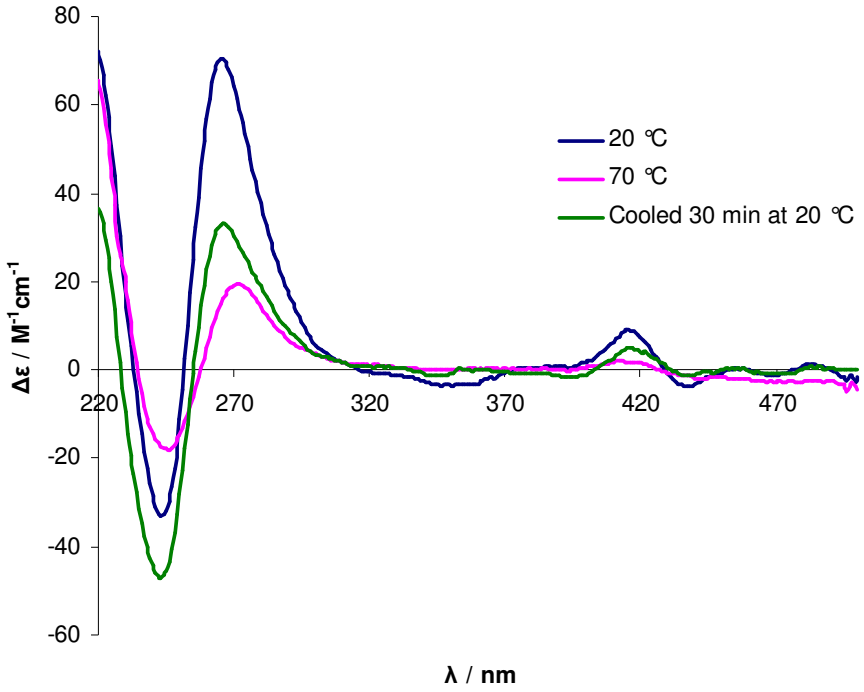

Figure 5.27 CD spectra of duplex **ON13/ON22** at 20 °C, 70 °C and after cooling and incubation at 20 °C for 30 minutes.

5.6 Conclusion

In conclusion we have developed both CuAAC and Sonogashira coupling methods for the pre-synthetic attachment of ethynyl and azidoporphyrins to 5-iodo and 5-ethynyl-2′-deoxyuridine respectively. From this we have gained an insight into the comparative levels of conjugation between the porphyrin cores and the nucleosides in ethynyl and 1,2,3-triazole linked porphyrin nucleosides.

More importantly, the CuAAC reaction was found to be is superior to Sonogashira chemistry for the post-synthetic construction of covalently linked porphyrin modified ONs. Using CuAAC chemistry, coupling of both aliphatic and aromatic Ni^{II} azidoporphyrins to ONs containing various terminal ethylnyl bonds was achieved. The effect of various single porphyrin modifications on the structure and thermal stability of single stranded, duplex and triplex DNA was screened. Single stranded ONs containing internal porphyrin modifications formed porphyrin driven i-motif structures in CT sequences and aggregates when the oligonucleotides did not posses the appropriate

sequence for i-motif formation. These aggregates and i-motifs were shown not to inhibit duplex and triplex formation. Thermal stability studies were performed on Hoogsteen-type triplexes containing porphyrin modified TFO strands and it was found that porphyrin modifications generally stabilise the triplex. Overall destabilisation was observed when a porphyrin was incorporated internally into a duplex, however, destabilisation was significantly lowered when the aliphatic porphyrin **50** was positioned in the minor groove.

Chapter 6 Porphyrin H-Aggregate Formation in the Minor Groove of the Duplex

6.1 Introduction

The helical self-assembled structure of nucleic acids provides the perfect template for the construction and development of functional π-systems with tunable optical properties.[4, 5, 15] Considerably different physico-chemical properties are often observed between chromophores that are closely packed on the same strand, in contrast to being attached to adjacent strands, of the duplex. Porphyrins have been widely studied as labels in a variety of applications such as light harvesting devices/electron transfer systems,[88, 89] low-power photon upconversion,[155] and the production of reactive oxygen species.[22, 156]

Covalent attachment of porphyrin moieties to DNA has been achieved using a variety of methodologies (see Chapter 1.7). Recently, the synthesis of a DNA containing 11 *meso*-functionalised porphyrins attached to 2′-deoxy-5-ethynyluridines was carried out from the corresponding phosphoramidites (Figure 1.22), however this showed a significant thermal destabilisation of the resulting duplex.[43] A stabilising effect of +0.5 °C per modification was observed when the porphyrins were placed adjacently in complementary strands.[44] Molecular modelling showed that porphyrins were arranged in a zigzag fashion and stacked in pairs in the major groove (Figure 1.23). Finally, an effective energy transfer between a zinc porphyrin and a free-base porphyrin in the major groove of the DNA duplex was observed.[44]

In this chapter we used a CuAAC chemistry approach developed in Chapter 5 to combine DNAs containing commercially available 2′-*O*-propargyl uridine or 2′-*O*-propargyl adenosine[157] with *β*-pyrrolic azido substituted porphyrins that allows us to place multiple functional entities in the *minor* groove of the DNA duplex.[158]

6.2 Chapter Summary

In this chapter we report the synthesis of oligonucleotides containing one or two internal porphyrin modifications *via* the post-synthetic microwave accelerated Cu^{I} catalysed Huisgen 1,3-dipolar azide alkyne cycloaddition reaction. In contrast to the single or double internal incorporations of porphyrins into one of the DNA strands of the duplex, the introduction of porphyrins into the second strand results in the formation of H-aggregates in the minor groove of the DNA helix. This also led to extraordinary enhancement of thermal stability to such an extent that duplexes with four adjacent porphyrins could only be dissociated at a low salt concentration. Molecular modelling indicated that porphyrins could accommodate a number of conformations including one in which the porphyrin sequence did not match the sequence of the nucleotides. Each stacking conformation resulted in a different duplex thermal stability and corresponding CD spectra.

6.3 Post-synthetic CuAAC Chemistry and Oligonucleotide Purification

As discussed in Chapter 5.5.2, the single incorporation of 1,2,3-triazole linked aliphatic Ni^{II} porphyrin in the minor groove of a duplex resulted in a thermal destabilisation of approximately 5.5-7.0 °C. This was significantly less than the equivalent aromatic linked porphyrin which showed a destabilisation of 14.7-16.0 °C. This was most likely due to the extra flexibility resulting from the additional sp^3 carbon. Therefore, investigation has continued further by incorporating multiple Ni^{II} aliphatic porphyrins (**50**, Figure 6.1) in a zipper fashion in the minor groove.

6.3.1 Microwave Accelerated Post-synthetic CuAAC Reaction

β-Pyrrolic functionalised azido porphyrin **50** (Figure 6.1) was synthesised from 5,10,15,20-tetraphenylporphyrin phosphonium salt[79, 87] as described in Chapter 2. The Ni^{II} ion was inserted into the porphyrin core to prevent the uptake of copper during the Cu^{I} catalysed CuAAC reaction. DMT-off ONs on CPG support were prepared containing single or double internal insertions of commercially available 2′-*O*-propargyl uridine or 2′-*O*-propargyl adenosine (Figure 6.2) using automated DNA synthesis.

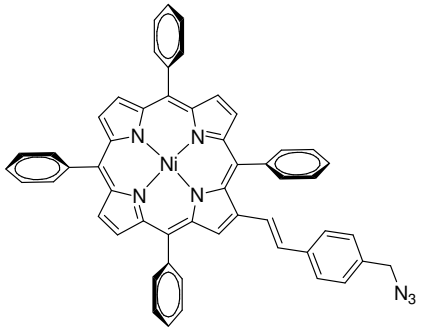

50

Figure 6.1 *β*-Pyrrolic functionalised azido porphyrin **50**.

As discussed in Chapter 5.4.2, the commonly used method involving the shaking of the reaction mixture containing azide **50**, $CuSO_4$, sodium ascorbate and an oligonucleotide bound to a CPG support at room temperature resulted in poor conversion of DNA to the desired product for mixmer sequences. It has been previously reported[144, 146] that microwave irradiation can be used to push the CuAAC reaction to completion,

especially for the ONs possessing several terminal alkynes in the sequence. In our case, focused microwave irradiation of CPG bound ONs possessing one or two propargyl nucleotides (Figure 6.2) for 20 minutes at 70 °C resulted in a full conversion of starting ONs as indicated by denaturing PAGE analysis of the cleaved ONs. This was in contrast to the results obtained when using unfocused microwave irradiation.

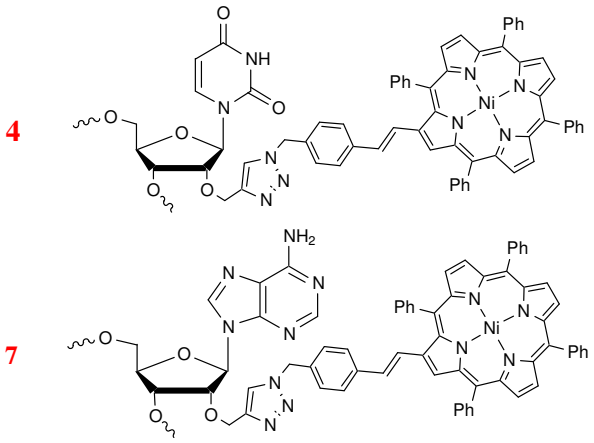

ON25	3' GTACGTATATATAGAGCG
ON26	5' CATGCATATATATCTCGC
ON27	3' GTACGTATA**4**ATAGAGCG
ON28	5' CATGCATATA**4**ATCTCGC
ON29	5' CATGCATAT**7**TATCTCGC
ON30	5' CATGCATA**4**ATATCTCGC
ON31	5' CATGCAT**7**TATATCTCGC
ON32	5' CATGCA**4**ATATATCTCGC
ON33	5' CATGC**7**TATATATCTCGC
ON34	3' GTACGTA**4**A**4**ATAGAGCG
ON35	5' CATGCATA**4**A**4**ATCTCGC
ON36	5' CATGCAT**7**T**7**TATCTCGC

Figure 6.2 Synthesised oligodeoxynucleotides.

DMT-off oligonucleotides on CPG (0.33 μmol) containing 2′-*O*-propargyl uridine or 2′-*O*-propargyl adenosine were removed from their corresponding columns and placed into a microwave reaction vessel together with compound **50** (7.67 μmol, 23 eq) in degassed DMSO (200 μL). Freshly prepared $CuSO_4 \cdot 5H_2O$ (0.32 μmol, 0.96 eq, 8 μL of a 40 μmol/mL solution in degassed H_2O) and sodium ascorbate (1.25 μmol, 3.8 eq, 25 μL of a 50 μmol/mL solution in degassed H_2O) were added. The reaction mixture was then irradiated in a microwave synthesiser (Discover, CEM Corporation, 70 °C, 100 watts, 20 min). The content of the reaction was transferred to a microcentrifuge tube and the CPG supports were repeatedly washed with DCM (1.5 mL) to remove any unreacted **50** followed by H_2O to remove any remaining copper. This resulted in a red coloured CPG, which was an indication of the progression of the reaction. Unreacted **50** was recovered in 80-90% yield by washing the DCM solution containing porphyrin with H_2O, drying over $MgSO_4$, and precipitating from DCM:MeOH. The obtained DMT-off oligonucleotides bound to CPG supports were cleaved with 32% aq NH_4OH (0.5 mL) at RT for 2 hours and then at 55 °C overnight.

6.3.2 Purification and Characterisation of Oligonucleotides Possessing Two Porphyrin Modifications

Cleaved porphyrin possessing ONs were purified using C_{18} puri-pak columns eluting single modifications in 20% $CH_3CN:H_2O$ and double modifications in 30-40% $CH_3CN:H_2O$. Oligonucleotides could be purified directly from the aq. NH_4OH solution using C_{18} puri-paks which was advantageous to the previously used HPLC purification method. It was observed that significant quantities of oligonucleotides containing two porphyrin modifications remained on the column during purification. After purification ONs were freeze dried, redissolved in H_2O (100 μL), precipitated from $LiClO_4$ and acetone (0.01 M lithium perchlorate in acetone (1.6 mL)) and dissolved in 100 μL of water to give a deep red solution of **ON27-ON36** (Table 6.1). Heating to 70 °C for 1 hour was required to dissolve some ONs. Oligonucleotides were characterised by MALDI-TOF MS in the negative mode using either 2′,4′,6′-trihydroxyacetophenone, 3-hydroxypicolinic acid or 6-azathiothymine as a matrix and dibasic ammonium citrate as a co-matrix (Table 6.1). Purity was checked using denaturing 20% PAGE, showing a red single band with a significant retardation compared to the wild type oligonucleotide. **ON34**-**ON36** containing two porphyrins did not penetrate into the gel (Figure 6.3).

Table 6.1 ONs synthesised and their mass spectroscopic analysis.

Strand	Sequence	m/z, calcd., Da	m/z, found, Da
ON25	3’ GTACGTATATATAGAGCG	5562.6	-
ON26	5’ CATGCATATATATCTCGC	5433.5	-
ON27	3’ GTACGTATA**4**ATAGAGCG	6431.2	6427.7
ON28	5’ CATGCATATA**4**ATCTCGC	6302.2	6297.6
ON29	5’ CATGCATAT**7**TATCTCGC	6316.2	6309.4
ON30	5’ CATGCATA**4**ATATCTCGC	6302.2	6297.0
ON31	5’ CAT GCAT**7**TATATCTCGC	6316.2	6316.7
ON32	5’ CATGCA**4**ATATATCTCGC	6302.2	6296.8
ON33	5’ CATGC**7**TATATATCT CGC	6316.2	6312.8
ON34	3’ GTACGTA**4**A**4**ATAGAGCG	7299.8	7305.1
ON35	5’ CATGCATA**4**A**4**ATCTCGC	7170.8	7167.5
ON36	5’ CATGCAT**7**T**7**TATCTCGC	7198.8	7199.1

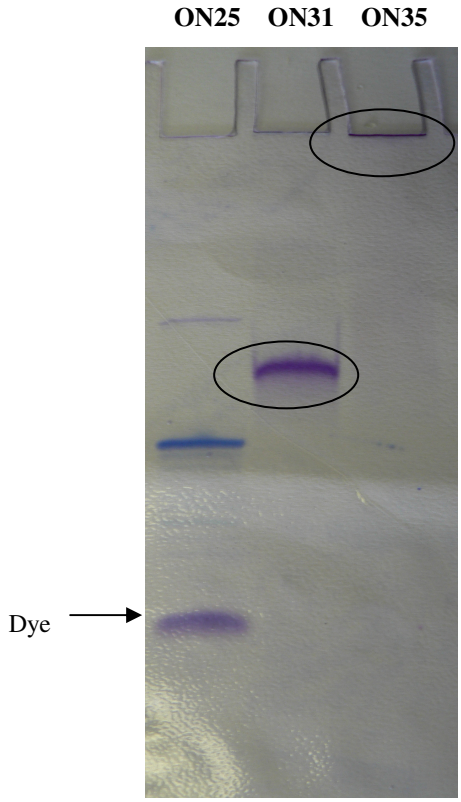

Figure 6.3 Representative PAGE (20% with 7 M urea) of unmodified oligonucleotide **ON25** and porphyrin modified oligonucleotides **ON31** and **ON35** captured using an Olympus digital camera after staining with Stains-All®. Porphyrin modified oligonucleotides are circled. Dyes were used for **ON25** only.

6.3.3 Application of the CuAAC Reaction to Zn^{II} and Fe^{III} Porphyrins

The development of the CuAAC reaction using Ni^{II} porphyrins allowed us to expand our investigation into Zn^{II} and Fe^{III} porphyrins (Figure 6.4). Zn^{II} porphyrins have been widely used in numerous applications involving light harvesting,[88, 89] electron transfer,[44, 159] fluorescence, reactive oxygen species production[156] *etc*. Additionally, they can be easily demetallated in acidic conditions to give the free base porphyrin which can be used to obtain various metalled species. Porphyrin containing Fe^{III} ions have been used in many biological applications such as oxygen transport and reaction catalysts.[160] The combination of porphyrins containing different metals in close proximity on a DNA could provided systems with very interesting photodynamic and electronic properties.

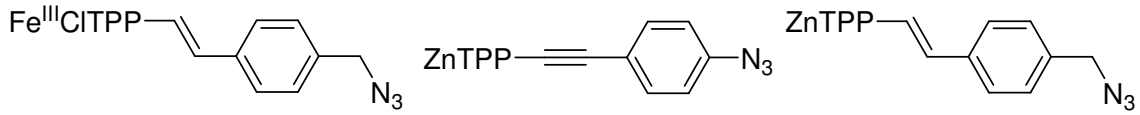

51 **45** **49**

Figure 6.4 Fe^{III} and Zn^{II} porphyrin azides.

Initial CuAAC reactions on Fe^{III} porphyrins failed to produce any sign of the desired conjugates using a Cu^{II} catalyst and sodium ascorbate. Comparing the redox potentials of Fe^{III} to Fe^{II} (~0.77 V) and Cu^{II} to Cu^{I} (~0.15 V)[161] led us to conclude that the Fe^{III} was being preferably reduced over the Cu^{II}. It should be noted that although these redox potentials are not specific to porphyrins they will be a close approximation to the actual redox values. Repeating the reaction using $Cu(ACN)_4PF_6$ in THF at RT for three days, followed by the cleavage of the oligonucleotides using aq NH_4OH, provided the desired conjugate as a light green solution. The solution was freeze dried and resulting solid was dissolved in H_2O. Purity was checked using 20% or 12% denaturing PAGE, however it was found that the oligonucleotide containing an iron porphyrin did not penetrate into the gel. Attempts to purify the oligonucleotide by C_{18} HPLC or C_{18} puri-pack columns failed to elute any of the desired oligonucleotide. Inspection of the puri-pack column showed that the porphyrin-ON complex was bound to the solid support. No mass spectra analysis was performed as the desired oligonucleotide could not be purified.

CuAAC reactions using Zn^{II} porphyrins **45** and **49** were problematic. In the primary experiment, in which porphyrin **49** and CPG bound ON with a sequence equivalent to the unmodified **ON28** were shaken for three days at RT, a green solution was obtained on cleavage with aq NH_4OH. Precipitation of the oligonucleotide using $LiClO_4$ and acetone resulted in a green coloured pellet. Denaturing 20% PAGE showed a single green band which migrated between Ni^{II} porphyrin-DNA and unmodified ONs.

Unfortunately, attempts to repeat this reaction using a second batch of **49** or using porphyrin **45** failed to produce any sign of the desired conjugates. Likewise, performing the reaction under microwave conditions was unsuccessful. On closer observation of the IR signals of **45** and **49**, differences were noticed that could account for the variations in reactivity observed. In the initial batch of compound **49** only a single azide asymmetric stretch was observed at 2097.2 cm^{-1}, however the second batch showed two independent

signals at 2097.1 and 2122.7 cm^{-1}. A similar trend was observed in the IR spectrum of compound **45**. This change in energy of the azide signal is consistent with the coordination of the azide to the fifth coordination site of Zn^{II} that occurs perpendicular to the plane of the porphyrin core (Figure 6.5).[162, 163] The addition of a stronger ligand such as pyridine to porphyrins **45** and **49** resulted in only a single IR signal at 2097.1 cm^{-1} and 2015.2 cm^{-1} respectively, suggesting azide coordination indeed occurred.

Although the addition of pyridine was not shown to inhibit the CuAAC reaction Ni^{II} porphyrin azides **50**, the addition of pyridine to the CuAAC reaction involving porphyrins **45** and **50** failed to produce any DNA conjugates.

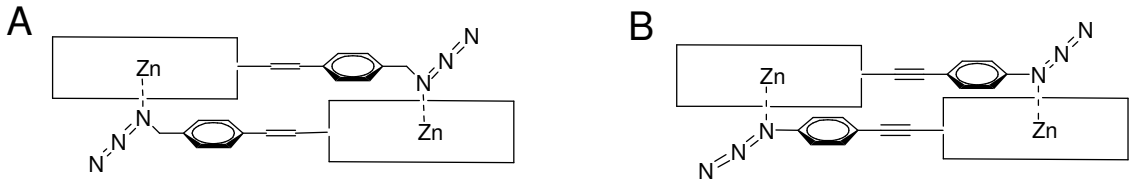

Figure 6.5 Possible modes for the coordination of **49** (A) and **45** (B).

6.4 UV-Vis and CD Spectroscopic Studies of DNA-Porphyrin Conjugates Containing Multiple Porphyrins

The thermal stability of the porphyrin modified DNA duplexes possessing one to four Ni^{II} porphyrins in various arrangements in the minor groove was accessed using UV-Vis thermal melting at 260 and 423 nm (Table 6.2, Figure 6.6). The interaction of the porphyrin moieties and DNA backbone structures were also examined by CD spectroscopy. In addition, molecular modelling calculations of plausible DNA structures were performed using the AMBER* force field.[151, 152]

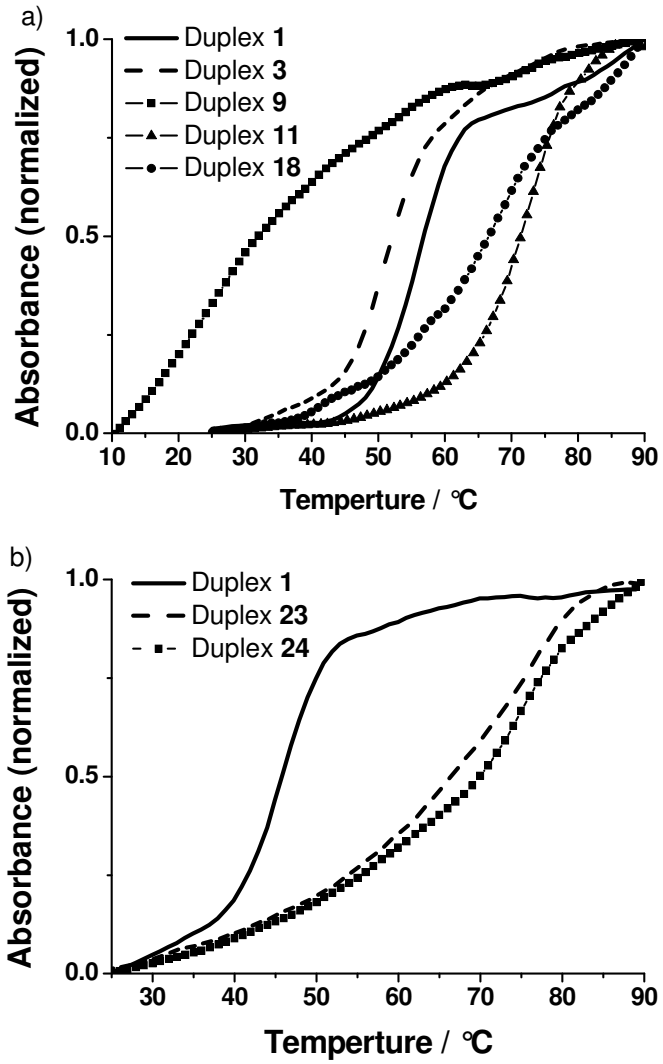

Figure 6.6 Representative UV melting profiles (260 nm) of unmodified and modified duplexes: a) duplex **1** and porphyrin modified duplexes **3**, **9**, **11** and **18**, C = 1.0 μM of each strand in 20 mM sodium cacodylate, 100 mM NaCl and 5 mM $MgCl_2$, pH 7.2; b) duplex **1** and porphyrin modified duplexes **23** and **24** at low salt concentrations, C = 1.0 μM of each strand in 20 mM sodium cacodylate, 6.25 mM NaCl, pH 7.2.

Table 6.2 Arrangement of porphyrins in DNA duplexes and their melting temperatures[a]

Duplex	Strands	Arrangement	$T_{d\ 260}$	$T_{a\ 260}$	$T_{d\ 423}$	$T_{a\ 423}$	$\Delta T_{m\ 260}$	ΔT_{260}/P
1	ON25/ON26	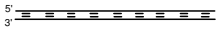	56.0 (46.1)[b]	56.0 (46.1)	----	----	----	----
2	ON27/ON26		51.2	51.0	52.0	50.0	-4.8	-4.8
3	ON25/ON28		51.2	50.8	53.3	52.7	-4.8	-4.8
4	ON25/ON29		50.0	50.0	49.2	48.0	-6.0	-6.0
5	ON25/ON30		53.5	53.5	53.8	53.7	-2.5	-2.5
6	ON25/ON31		50.8	50.8	52.0	50.7	-5.2	-5.2
7	ON25/ON32	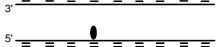	52.1	52.0	52.0	51.2	-3.9	-3.9
8	ON25/ON33		51.0	51.0	50.1	50.0	-5.0	-5.0
9	ON25/ON35		27.4	26.1	NVT[c]	NVT	-28.6	-14.3
10	ON25/ON36		25.0	25.0	NVT	NVT	-31.0	-15.5
11	ON27/ON28		71.8 (57.8)	72.6 (58.0)	72.2 (58.9)	74.5 (59.8)	+15.8 (+11.7)	+7.9 (+5.85)
12	ON27/ON29		71.2	71.0	72.6	72.3	+15.2	+7.6
13	ON27/ON30		71.1	71.7	72.3	73.5	+15.1	+7.55
14	ON27/ON31		69.2	68.0	71.8	71.4	+13.2	+6.6
15	ON27/ON32	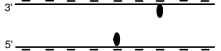	66.0	65.9	70.6	70.1	+10.0	+5.0
16	ON27/ON33	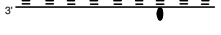	65.1	65.4	70.0	70.0	+9.1	+4.55

Table 6.2 cont. Arrangement of porphyrins in DNA duplexes and their melting temperatures[a]

Duplex	Strands	Arrangement	$T_{d\ 260}$	$T_{a\ 260}$	$T_{d\ 423}$	$T_{a\ 423}$	$\Delta T_{m\ 260}$	ΔT_{260}/P
17	ON34/ON28		71.2 (63.7)	68.8 (61.2)	73.0 (62.7)	70.8 (61.0)	+15.2 (+17.6)	+5.07 (+5.86)
18	ON34/ON30		70.8	66.2	73.2	70.0	+14.8	+4.93
19	ON34/ON31	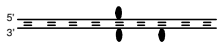	71.6	69.6	71.6	70.8	+15.6	+5.2
20	ON34/ON32		68.0	66.2	68.5	67.6	+12.0	+4.0
21	ON27/ON35		69.0	66.5	70.5	69.5	+13.0	+4.33
22	ON27/ON36	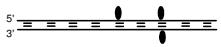	71.1	69.8	72.0	70.8	+15.1	+5.03
23	ON34/ON35	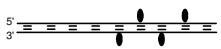	>90 (76.2)	>90 (74.8)	>90 (65.8)	>90 (65.3)	>34 (+30.1)	>8.5 (+7.53)
24	ON34/ON36		>90 (75.8)	>90 (77.5)	>90 (75.0)	>90 (76.0)	>34 (+29.7)	>8.5 (+7.43)

[a] T_m (°C) data for antiparallel duplex melting determined using the maximum of the first derivative of the UV-vis melting curves (λ = 260 and 423 nm, 0.5 °C/min). C = 1.0 μM of each strand in 20 mM sodium cacodylate, 100 mM NaCl and 5 mM $MgCl_2$, pH 7.2. [b] C = 1.0 μM of each strand in 20 mM sodium cacodylate, 6.25 mM NaCl, pH 7.2. [c]NVT = No visible transition.

The destabilisation of DNA duplexes that was observed in the cases of a single porphyrin substituent (Table 2, duplexes **2**-**8**, 2.5 to 6.0 °C) is consistent with that observed in Chapter 5. Molecular modelling indicated that the lowest energy structure of duplex **2** held the porphyrin within the minor groove (Figure 6.7A). This is most likely due to a combination of Van der Waals interactions between the porphyrin and the nucleobases and decreased entropy as the solvent cage around the porphyrin is partially removed (hydrophobic effect). Double modifications on the same strand (duplex **9** and **10**, Figure 6.7B) resulted in further destabilisation (ΔT_m –28.6-31.0 °C) compared to the unmodified duplex **1**.

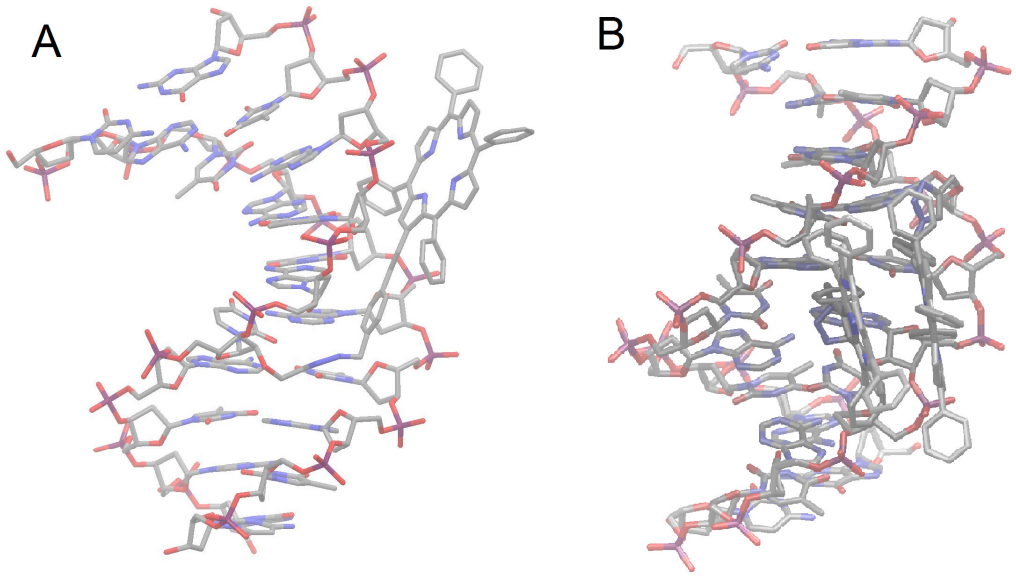

Figure 6.7 A representation of the lowest energy AMBER* force field minimised structures of duplex **2** (A) and duplex **10** (B).

To establish the effect on duplex stability of stacked porphyrins in the minor groove, duplexes **11**-**24** were prepared containing two, three or four alternating porphyrin substituents. Significantly enhanced thermal stability (ΔT_m +15.1-15.8 °C) was observed for duplexes in which the porphyrins were either attached to adjacent (*e.g.* duplexes **11** and **13**) or complementary bases (*e.g.* duplex **12**). It is well known that as a result of their highly planar aromatic structure porphyrins commonly form aggregates through π-π stacking.[164] During UV-Vis thermal meltings, recorded from 230 to 500 nm at 10 °C intervals, a bathochromic shift of 1.5-4.0 nm was observed for the Soret band (~420 nm) for duplexes **11**-**24** in which porphyrins were placed in both strands. In comparison, singly modified duplexes **2**-**8** did not exhibit this shift (Figure 6.8A). This

suggested the formation of H-aggregates between interlocked porphyrins bound to complementary strands of the duplex.[39] The observed shift in the Soret band upon the formation of H-aggregates is in a similar range to the previously studied DNA-based porphyrin dimers.[39] As the distance between the porphyrins on the complementary stands increased (duplexes **14**-**16**) the T_m decreases.

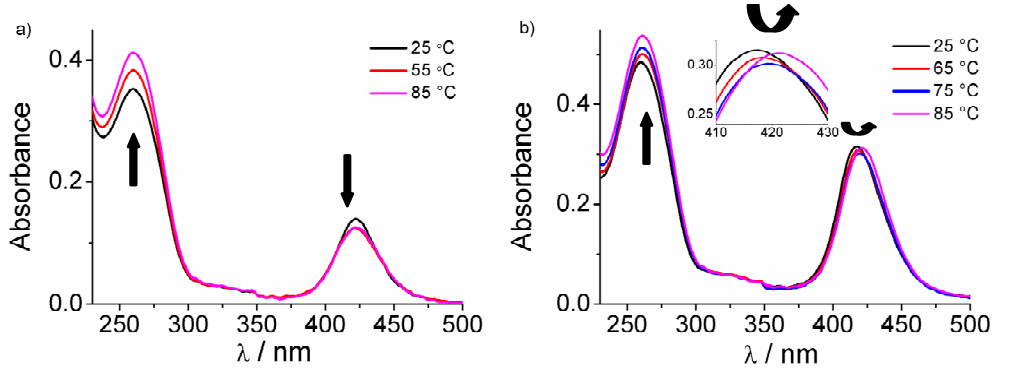

Figure 6.8 Representative UV-Vis annealing profiles: a) duplex **2** with a single modification showing an increase in absorbance at 260 nm and a decrease at 420 nm; b) duplex **11** with two interlocking modifications showing an increase in absorbance 260 nm and a bathochromic shift from 417-421 nm during melting.

It is interesting to note that for duplexes **11**-**16** the T_m values for the porphyrin region (423 nm) were slightly higher than those corresponding to the duplex DNA region (260 nm). The largest difference of 4.9 °C corresponded to duplex **16** that has three base-pairs in between overlapped porphyrins. This indicated that the porphyrins dissociate after the dissociation of the DNA duplex. According to molecular modelling, face-to-face π-π interactions between two porphyrins placed on opposite strands were observed for duplexes **11**, **12** and **13** and to some extent even in the case of duplex **16** due to the flexibility of the system (Figure 6.9).

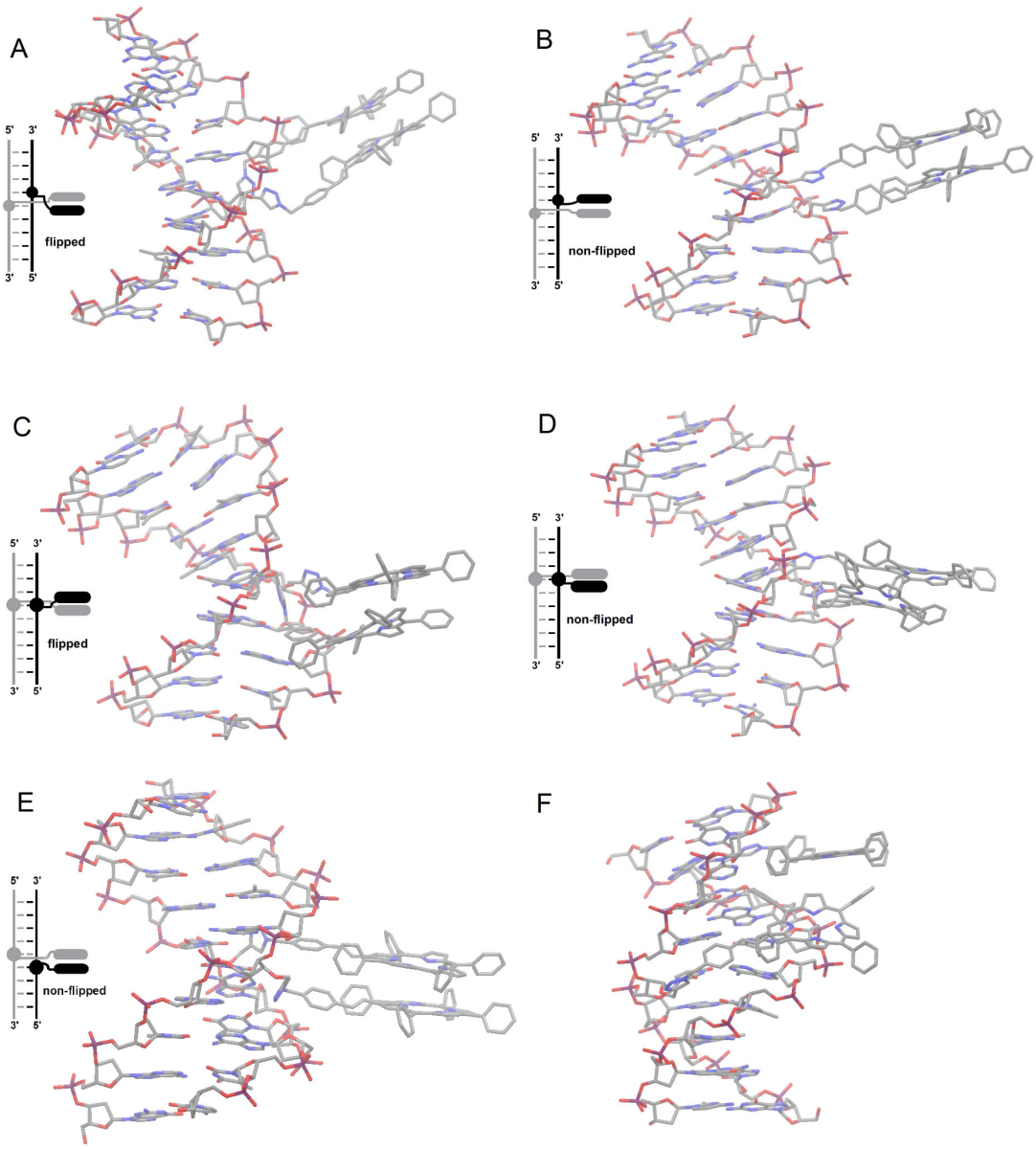

Figure 6.9 An AMBER* force field lowest energy minimised structures of porphyrin modified duplexes. A) Duplex **11** with flipped porphyrins, B) duplex **11** with non-flipped porphyrins, C) duplex **12** with flipped porphyrins, D) duplex **12** with non-flipped porphyrins, E) duplex **13** with non-flipped porphyrins and F) duplex **16**.

It is important to note that due to the flexible nature of the linker, numerous porphyrin conformations can be adopted relative to the DNA duplex, including a flipped conformation (Figure 6.10) in which porphyrins do not follow the sequence of the nucleotides in the duplex. The observed distances between O2′ atoms in duplexes **11** and **12** were between 6.1 - 7.7 Å and independent of the adopted conformation, *i.e.* flipped or non-flipped. However, the observed distance between O2′ atoms in duplex **13**

was significantly larger (11.3 Å), therefore, the non-flipped conformation was the preferred option. The orientation of the porphyrin moieties and the adopted conformations was confirmed by CD spectroscopy (Figure 6.11).

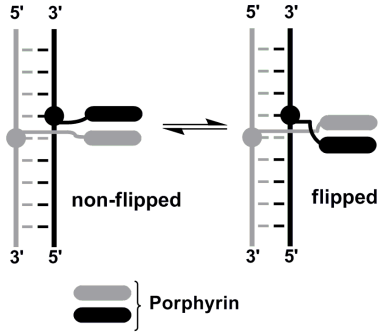

Figure 6.10 Plausible arrangement of porphyrins in duplex **11** showing the flipped and non-flipped conformations.

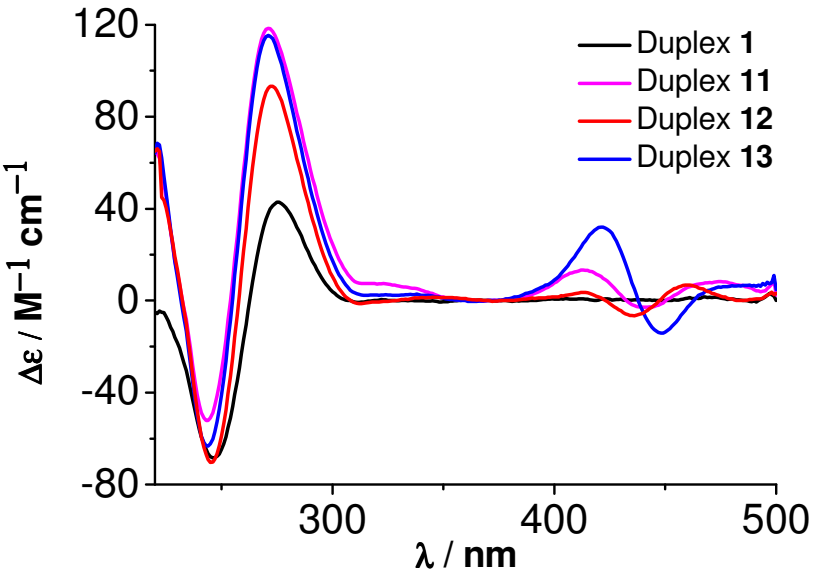

Figure 6.11 CD spectra of duplexes **1**, **11**, **12** and **13**.

In case of duplex **13**, strong positive and negative bands originating from the porphyrin's Soret band appeared at 422 and 448 nm, respectively. This negative CD exciton couplet (–/+ pattern) indicates the anticlockwise orientation of the transition dipoles of the porphyrins (Figure 6.12).[38, 49, 50] The flipping behaviour was confirmed by the different CD profiles in the region of the Soret band for duplexes **11** and **12**. Molecular modelling shows that in the non-flipped structures there is a clockwise orientation of the porphyrins' transition dipoles which should provide a positive CD

exciton couplet (+/– pattern). Contrary to this, an anticlockwise orientation is observed for the flipped structures which should give a rise to a negative CD exciton couplet. In fact the pattern of CD spectra for duplexes **11** and **12** in the Soret region is +/–/+ with maximum intensities at 474/441/413 and 460/436/413, respectively. This was attributed to the more dynamic interactions of the porphyrins and existence of both flipped and non-flipped porphyrins in duplexes **11** and **12**. A negative band at 245 nm and a positive band around 274 nm in CD spectra clearly suggested that the modified duplexes retain their overall B-form double helix structure. At 85 °C both the positive and negative bands in the Soret region of the CD spectra vanished which indicated that there is no contact between porphyrins when duplexes **11**-**13** are melted.

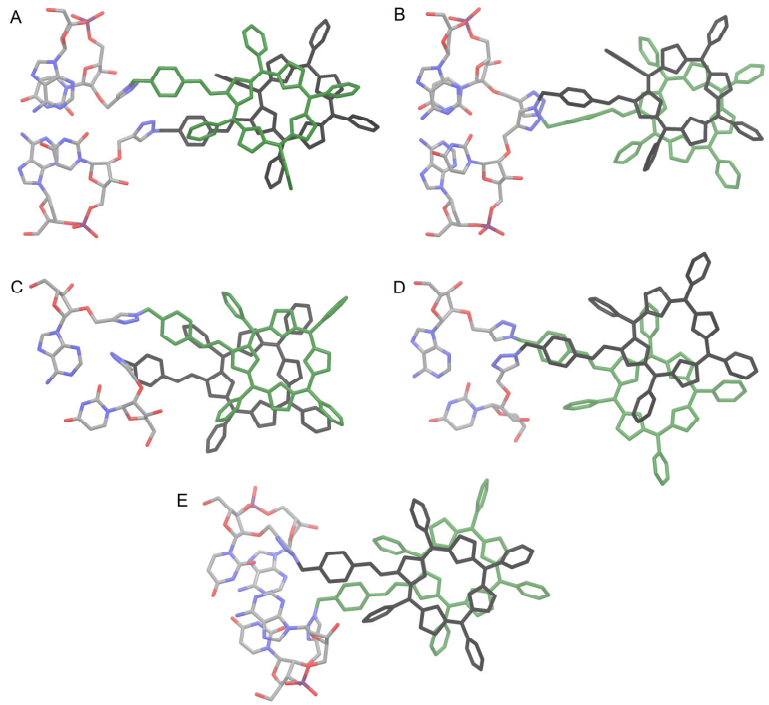

Figure 6.12 A representation the lowest AMBER* force field minimised structures of duplexes possessing two zipping porphyrins (nucleotides above and below have been removed for clarity). **A** and **C**: flipping porphyrins in duplexes **11** and **12** referring to the anticlockwise orientation of porphyrins' transition dipoles, respectively. **B** and **D**: non-flipping porphyrins with clockwise porphyrin orientation in duplexes **11** and **12**, respectively. **E**: duplex **13** with non-flipping porphyrins referring to the anticlockwise orientation of porphyrins.

The considerable difference in distances of O2′ atoms in the minor groove of DNA-RNA duplexes has been used in the construction of several nucleic acid zippers based on locked nucleic acids (LNA),[165-168] uridine-2′-carbamates[169] and O2′-pyrenylmethyl

nucleotides.[170-172] These systems implement multiple chromophore residues (generally pyrenes) which upon duplex formation results in a characteristic excimer fluorescence due to the interaction between pyrenes in electronically excited and ground states. Such systems have been implemented in signalling of full complimentarity (detection of mis-matches[165]) with the ultimate goal to create multichromophoric arrays. In these studies the strongest interactions between chromophores were ascribed for duplexes equivalent to structures **11** and **12**, however in our case an effective communication between porphyrins was also observed for structure **13**. The ability for porphyrins in duplex **13** to interact is most likely due to the long flexible linker which allows for ideal positioning of chromophores even when O2′ atoms are spaced further apart. This is supported by recent work by Wengel *et al.*[173] in which strong interactions between coronene moieties was observed in LNA duplexes equivalent to **11** and **13** when the coronene was tethered to 2′-amino-LNA by a long flexible linker (Figure 6.13A). Reducing the linker resulted in strong interactions only in structures equivalent to duplex **11** (Figure 6.13A).

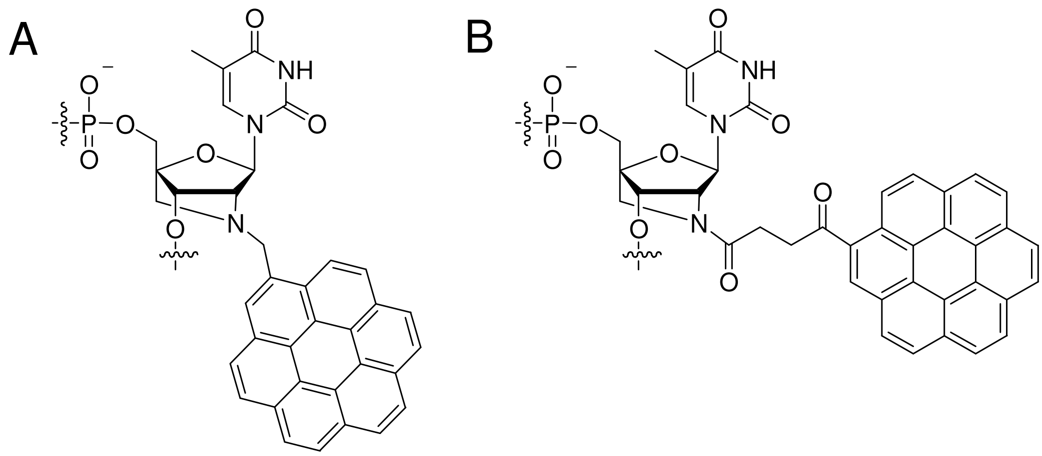

Figure 6.13 Coronene modified LNA possessing short (A) and long (B) linkers.

The introduction of a third porphyrin moiety into the duplex did not result in a further increase of the thermal stability (Table 6.2, duplexes **17**-**22**). It was observed that T_m values in the porphyrin region for duplexes **17** and **18** (73.0 and 73.2 °C, respectively) were higher than for duplex **20** (68.5 °C), in which flipping of the porphyrin substituents is unlikely to occur (see the discussion above for duplex **13**). This suggested the existence of two possible classes of stacking arrangements (Figure 6.14). The first in which the single porphyrin intercalated between the two porphyrins on the complementary strand (duplexes **17** and **18**), and the second in which the single

porphyrin was stacked either above or below the two porphyrins on the complementary strand (duplex **20**). This was made possible only by the flexibility of the porphyrin-linker combination which does not require the porphyrin sequence to follow the sequence of the nucleotides. In the second group we also included duplex **21** based on the the change in melting temperature per porphyrin (ΔT_{260}/P) which was very close to that of duplex **20**. The remaining duplexes with three porphyrins (**19** and **22**) were also included in the first group, in which all three porphyrins significantly contributed to the thermal stability of the complex. The lower values of ΔT_{260}/P for duplexes **17**-**22** might also be explained by the increased center-to-center distances between porphyrins (4.8 - 7.5 Å) in comparison with duplexes having double modifications (duplexes **11**-**13**, 4.4 - 5.0 Å) as observed in the molecular modelling studies. A more accurate conclusion about the flipping of porphyrins might be obtained upon combination of Ni^{II} porphyrins, which can serve as fluorescent quenchers,[174] with different fluorescent molecules attached in the similar manner to the duplex.

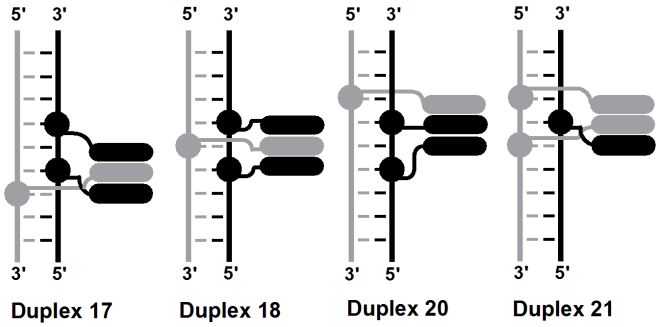

Figure 6.14 Plausible arrangements of porphyrins in duplexes with three modifications.

More dramatic increases in thermal stability were observed for duplexes containing four porphyrins (duplexes **23** and **24**). It should be noted that in order to measure the melting transitions of these very stable complexes the salt concentration had to be reduced from 100 mM to 6.25 mM NaCl and $MgCl_2$ excluded completely. Thus, duplex **23** with adjacent porphyrins had a ΔT_m of +30.1 °C and duplex **24** with overlapping porphyrins had a ΔT_m of +29.7 °C when compared to duplex **1** at low salt concentrations. This is a remarkable difference in thermal stability of ~65 °C between duplexes with four zipping porphyrins and duplexes with a double modification in one of the strands (duplexes **9** and **10**). Interestingly, a T_m value recorded at 423 nm for duplex **23** is lower than that for duplex **24**. This was thought to be a result of the different dynamic motions in the stack of porphyrins during melting. Indeed, molecular modelling showed that

porphyrins in duplex **23** could exist as a 2+2 stack while a contiguous stacking of all four porphyrins was observed for duplex **24** (Figure 6.15). Molecular modelling also showed that the introduction of the fourth closely attached chromophore leads to increased center-to-center distances between the inner porphyrins (9.6 Å) in duplex **23**. In the CD spectra for both duplexes **23** and **24**, broad negative bands were observed in the region of 400-450 nm, which can be ascribed to the complex interaction of four porphyrins in these structures (Figure 6.16). Further explaination may be proposed using calculated CD spectra[9, 56] based on the four porphyrin DNA models obtained with AMBER* force field molecular modelling.

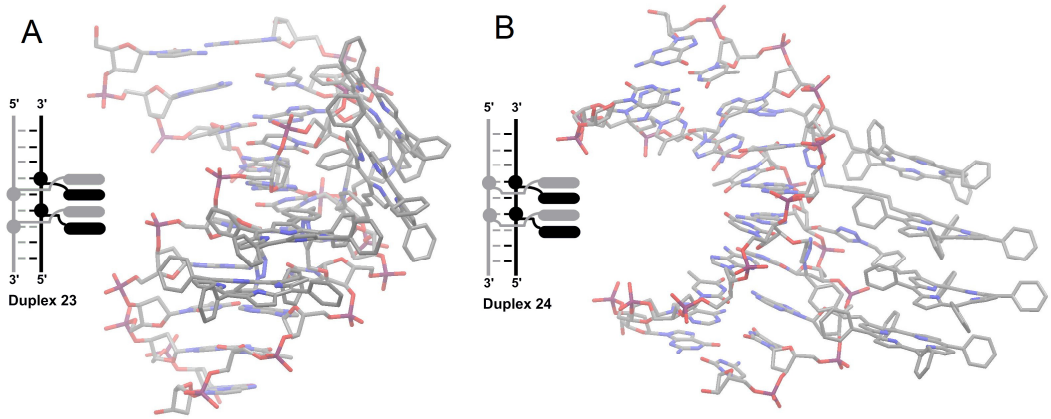

Figure 6.15 A representation of the lowest energy ABMER* force field minimised structures of duplexes **23** (A) and **24** (B) viewed into the minor groove. This clearly shows the 2+2 stack in duplex **23** and the continuous stacking of porphyrins in duplex **24**.

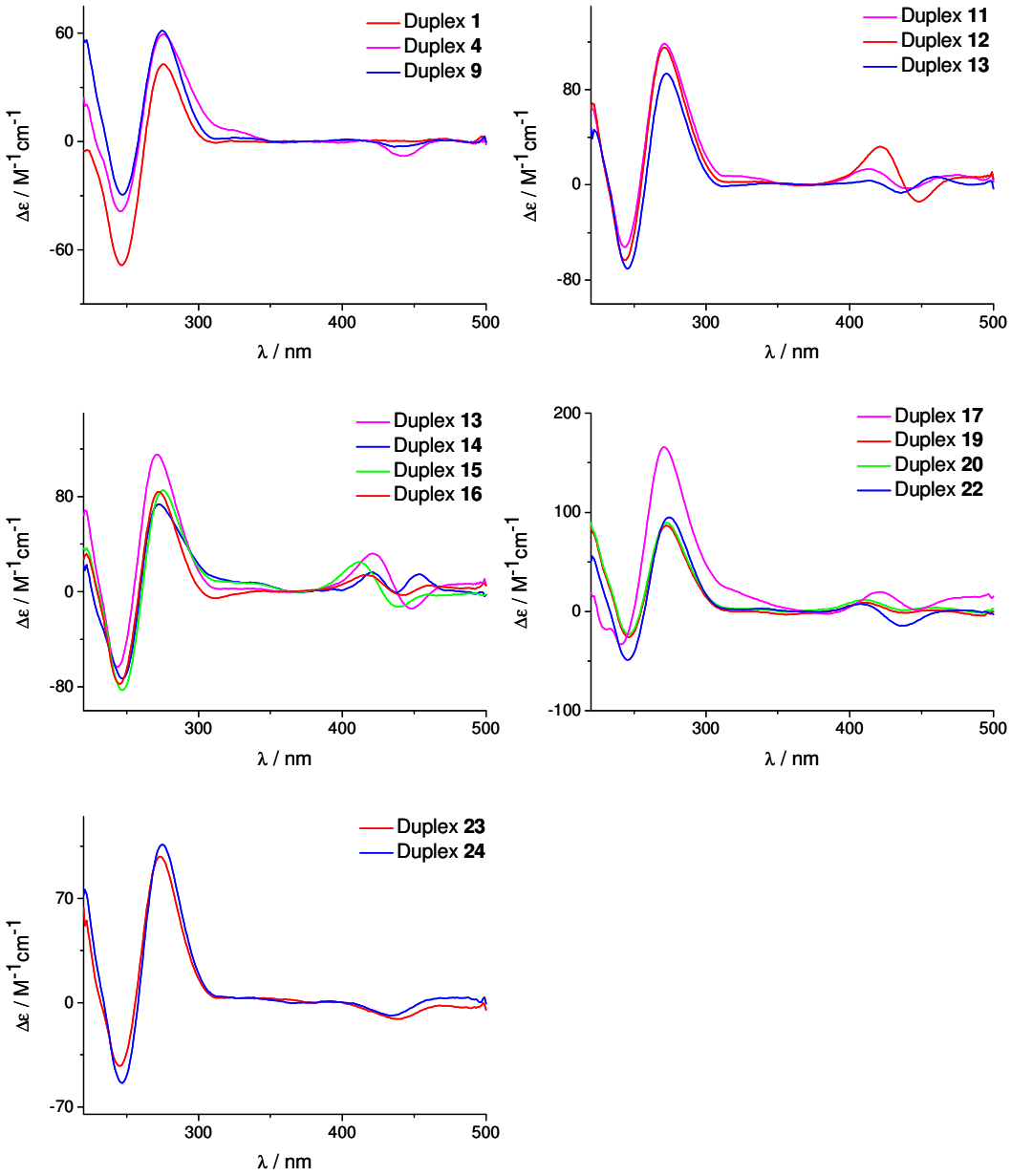

Figure 6.16 CD spectra of duplexes **1**, **4**, **9** and **11**-**24**.

The melting profiles showed virtually no hysteresis at either 260 or 423 nm for most of the duplexes studied including the four porphyrin zippers (Figure 6.17). This indicates that the denaturing-annealing kinetics was determined by the interaction of nucleic bases and not by the porphyrins. Also, the observed broadening of the melting curves for the four porphyrin duplexes **23** and **24** is thought to correspond to the unravelling of strands around the porphyrin aggregates. It is assumed that *β*-pyrrolic functionalisation of the porphyrins is vital as it prevents unfavourable interactions of the *meso* substituted

phenyl rings and allows for the easier accommodation of the porphyrins in the DNA environment.

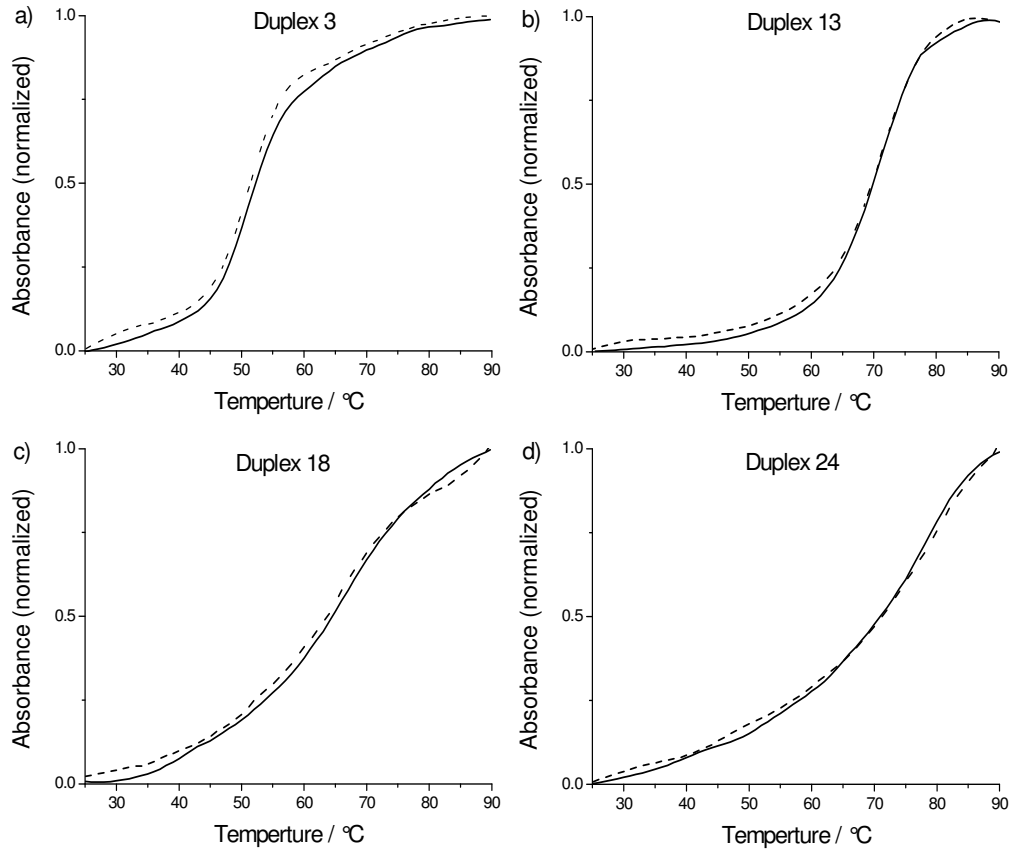

Figure 6.17 Representative UV melting profiles (260 nm) of duplexes **3** (a), **13** (b), **18** (c) and **24** (d) showing both denaturing (solid) and annealing (dashed) profiles. C = 1.0 μM of each strand in 20 mM sodium cacodylate, 100 mM NaCl and 5 mM $MgCl_2$, pH 7.2 for duplexes **3**, **13** and **18**. C = 1.0 μM of each strand in 20 mM sodium cacodylate, 6.25 mM NaCl, pH 7.2 for duplex **24**.

6.5 Conclusion

In conclusion, a quick and reliable microwave accelerated method for the post-synthetic attachment of azidoporphyrins to ONs containing the commercially available 2′-*O*-propargyl uridine and 2′-*O*-propargyl adenosine has been developed. The covalent attachment of adjacent porphyrin moieties into complementary strands of DNA led to the formation of face-to-face or H-aggregates in the minor groove, and resulted in a significant increase in the duplex thermal stability. The interaction of only two porphyrins led to thermal stabilisation of 7.55-7.9 °C per porphyrin with practically no

hysteresis between denaturing and annealing profiles. This is a significant improvement compared to previously studied DNA-porphyrin constructs.[38, 39, 42-44] Duplex thermal stability exceeded 90 °C when four porphyrins were stacked in the zipper motif. Based on molecular modelling and CD spectroscopy studies it was proposed that porphyrins may not necessarily follow the sequence of nucleotides in duplexes. However, duplex **13**, in which porphyrins actually followed the sequence of nucleotides, should be considered as a model for the DNA-based chromophoric assemblies possessing flexible linkers. We believe these findings in combination with previously published reports on porphyrin modified DNA duplexes lay a foundation for the future design of artificial DNA-chromophore supramolecular architectures and for their applications in material science and nanotechnology.

Chapter 7 Summary and Future Directions

The aim of this thesis was to create and study novel DNA-porphyrin supramolecular architectures, for use in nanotechnology, based on β-pyrrolic modified porphyrins. This has been achieved through the development of both covalently and non-covalently (lipophilic) linked porphyrin complexes.

During the synthesis of porphyrin precursors for DNA modification a modified Horner-Emmons reaction was developed for use in porphyrins. This enabled the creation of a versatile synthetic method for the construction of ethynyl linked β-pyrrolic porphyrin derivatives. This high yielding, scalable methodology improved on existing methodologies by negating the need of a metal catalyst and 2-bromo-5,10,15,20-tetraphenylporphyrin. Using the Horner-Emmons method, synthesis and evaluation of the performance of a number of porphyrin dyes in DSSCs applications was performed. To develop this chemistry further it would be advantageous to create a porphyrin modified phosphonate derivative. Such a modification may allow for the easy production of β-pyrrolic ethynyl linkers without the time consuming synthesis of multiple aromatic phosphonates.

Using the appropriate lipophilic building blocks, synthesis of non-covalently bound lipophilic complexes from short sequences of single stranded, duplex and GQ oligodeoxynucleotides was achieved. Loading studies on single stranded and duplex DNA showed slight overloading of porphyrins on DNA. Unfortunately, longer DNA sequences, which could be used for the construction of aligned DNA films, resulted in the formation of insoluble complexes. For future work it may be possible to create soluble complexes of large ONs by adapting the synthetic method to reduce the porphyrin loading ratio on DNA.

Using covalent modification techniques, methods for the pre-synthetic attachment of ethynylporphyrin and various azidoporphyrins to 5-iodo and 5-ethynyl-2′-deoxyuridine respectively, was achieved using Sonogashira and CuAAC chemistry. From insight into the comparative levels of conjugation between the porphyrin cores and the nucleosides was gained. More importantly, development of conventional and microwave accelerated

CuAAC reaction methods for the site specific, post-synthetic, internal attachment of Ni^{II} *β*-pyrrolic functionalised azidoporphyrins to ONs was accomplished. Reactions between azido porphyrins, possessing both aliphatic and aromatic linkages, and ONs containing various terminal alkynes allowed us to screen the effect of various single porphyrin modifications on single stranded, duplex and triplex DNAs. Single stranded porphyrin possessing ONs formed pH sensitive i-motifs or pH independent aggregates depending on the nucleotide sequence. Single internal duplex modification resulted in thermal destabilisation of 6.3-18.0 °C (in pyridimine sequences) depending on the location of the porphyrin in the duplex. Single porphyrin modification of a TFO strand led to thermal stabilisation of the resulting triplexes (ΔT_m = 3.0-9.0 °C at pH 6.0). Further stabilisation of a triplex possessing a porphyrinic bulged insertion may be possible by reducing the tether length.

Using the information gained from duplexes possessing single internal modifications, post-synthetically modified 2′-*O*-propargyl possessing duplexes with up to four aliphatic porphyrins were synthesised. This provided systems in which adjacent porphyrin moieties placed in complementary strands led to significantly increased duplex thermal stability as a result of face-to-face or H-aggregates formation in the minor groove of the duplex. The interaction of only two porphyrins resulted in thermal stabilisation of 7.55-7.9 °C per porphyrin and duplex thermal stability exceeded 90 °C when four porphyrins were stacked in the zipper motif. This was a significant improvement compared to previously studied DNA-porphyrin constructs, especially those in which the porphyrins are placed in the wider major groove.[44] Based on molecular modelling and CD spectroscopy studies it was proposed that porphyrins may not necessarily follow the sequence of nucleotides in duplexes.

Currently the post-synthetic CuAAC reaction is limited by the choice of metals within the porphyrin. It is important for the future development to incorporate porphyrins possessing various metal ions, particularly those ones leading to highly fluorescent porphyrins (*e.g.* Zn^{II}, Pt^{II}, Mg^{II} or H_2). If this is not achievable using CuAAC chemistry it may be possible to use ethynyl possessing DNA with porphyrins using alternative metal free ‘click reactions’ such as nitrile oxide chemistry (Figure 7.1).[175, 176] This chemistry would allow for the post-synthetic incorporation of free base porphyrins followed by the insertion of metal ions.

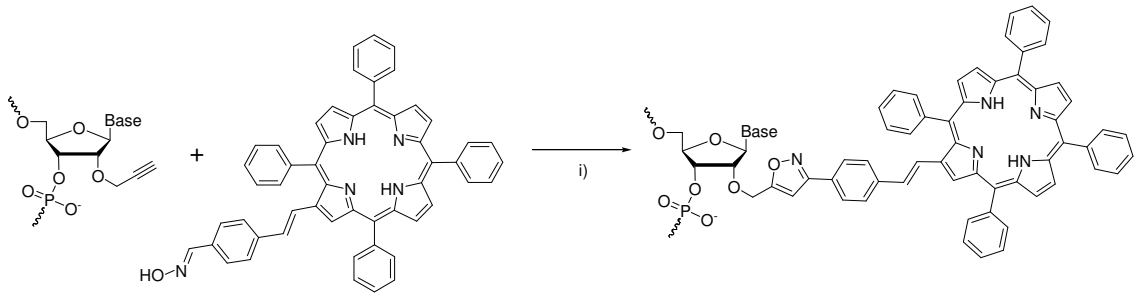

Figure 7.1 Possible metal free nitrile oxide post-synthetic chemistry. Reagents and conditions: Chloramine-T or NCS, $NaHCO_3$, DMSO, H_2O, RT.

Further development of a stacked arrangement of chromophores by incorporating a variety of moieties in the minor groove of DNA could be possible. Such chromophores may include fluorescent anthracene or pyrene moieties in combination with fluorescent quenching Ni^{II} porphyrins, which could confirm the flipped and non-flipped arrangement of chromophores in DNA. Further duplex thermal stabilisation and increased solubility may be possible by reducing the hydrophobicity of the porphyrin by incorporating charged groups in the *meso* positions of 5,10,15,20-tetraphenylporphyrins. This could be particularly interesting if the alternation of stack anionic (Figure 7.2A) and cationic (Figure 7.2B) porphyrins in the minor groove of the duplex was investigated. Possibilities also exist in 5,15-diphenylporphyrin derivatives (Figure 7.2C) where the porphyrin would be attached to DNA *via* the *meso* position but not in an orthogonal manner.

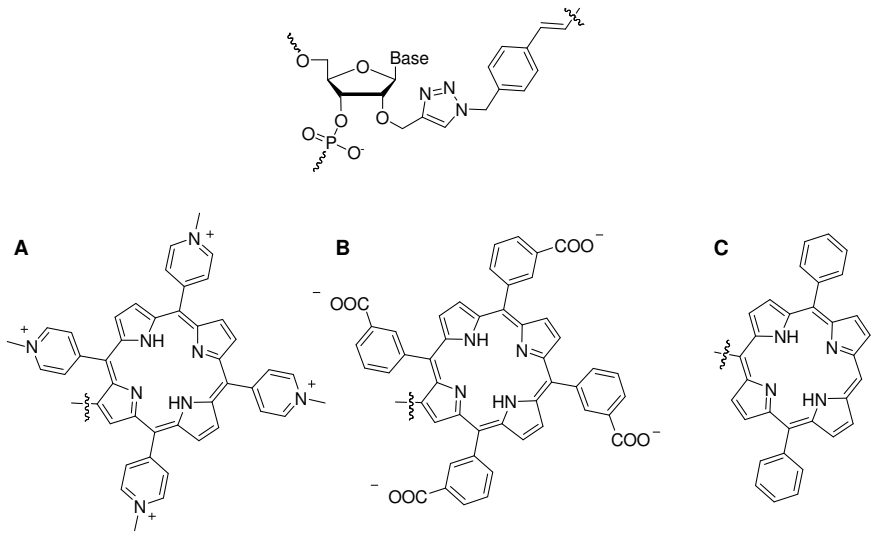

Figure 7.2 Incorporation of possible anionic (A), cationic (B) 5,10,15,20-tetraphenylporphyrins or 5,15-diphenylporphyrin derivatives.

By carefully choosing chromophores, such as combinations of Zn^{II} and free base porphyrins, creation of a molecular wire along the minor groove of the duplex may be possible. This could lead to interesting photonic properties. Of particular interest may be the development of systems for energy upconverstion.[155, 177, 178] Energy upconversion, which can occur *via* triplet-triplet annihilation where one higher energy singlet excited molecule is generated from two lower energy triplet excited molecules, has been shown to occur in solution involving Zn^{II}/Pt^{II} porphyrins and anthracene/pyrene moieties. It may be possible to place these moieties in complementary strands such that stacking in the minor groove occurs on duplex formation. This may allow for controllable energy upconversion on a duplex scaffold.

Chapter 8 Experimental Methods

8.1 Reagents and Equipment used for the Synthesis of Porphyrin Derivatives

Reagents

Solvents and reagents were supplied from many different sources, generally as AR grade. Chromatography solvents were distilled laboratory grade. H_2O used in porphyrin synthesis was of reverse osmosis grade. DMSO was dried over 4 Å molecular sieves and distilled at reduced pressure. THF was dried by passing argon degassed solvent through activated alumina columns. Dry DCM and DMF were prepared by distilling AR grade solvent over CaH_2 under N_2 atmosphere. $CHCl_3$ was dried over K_2CO_3 and distilled under N_2 atmosphere.

Reaction Monitoring and Chromatographic Purification

Due to the coloured nature of the chromophores, most of the reactions were easily monitored with thin layer chromatography (TLC) on silica TLC plates (60 F254) purchased from Merck and were visualised in UV light (254 nm) when necessary. The exception was the incomplete Horner-Emmons reaction where the halovinyl intermediate and the alkyne derivatives had the same R_f. In this case the reaction had to be worked up and the ratio of halovinyl intermediate to alkyne was determined by ^1H NMR spectroscopy.

Metallation of porphyrins with Zn^{II} generally resulted in compounds with a slightly lower R_f and metallation with Ni^{II} and Cu^{II} resulted in a higher R_f. Metallation with Fe^{III} resulted in a very polar compound that could only be moved on TLC using a 2-5% methanol in DCM. Malonic acid formation resulted in the production of very polar material that could only be separated from the decarboxylated acid on TLC in MeOH:acetic acid:DCM (5:1:94). Porphyrin nucleosides were very polar and moved as one or two spots in MeOH:DCM (1:9). Chromatographic purification of compounds,

when stated, was performed on the bench top using Silica 60 (230-400 mesh, SDS) or Al_2O_3 (Basic, 70-200 mesh, Scharlau). Various column diameters were used for the separation of different quantities of porphyrin: <50 mg (22 mm_{dia}), 50-100 mg (30 mm_{dia}), 100-200 mg (40 mm_{dia}) and >200 mg (60 mm_{dia}).

Precipitation of Porphyrins

The experimental methods in the following sections describe the purification of porphyrin derivatives by precipitation from DCM:MeOH. This involved the porphyrin residue being dissolved in DCM, filtered through clean cotton wool followed by the addition of a significant quantity of MeOH. The volume was then reduced *in vacuo* to approximately 5-10 mL. Additional MeOH was added and the process was repeated until a precipitate formed. An equivalent process was used to precipitate compounds from DCM:hexane.

NMR Spectroscopy

The primary characterisation technique for the porphyrin compounds was ^1H NMR spectroscopy. Porphyrin solutions of approximately 2 x 10^{-2} M in $CDCl_3$ or d_6-DMSO were prepared and ^1H NMR spectra were obtained on 400 or 500 MHz Brüker instruments using Topspin software. Chemical Shifts are given relative to TMS or the residual protium (d_6-DMSO, 2.51 ppm, pyridine 7.10 ppm) when TMS was not present. Although porphyrin compounds appear to have complex spectra, they are generally first order in nature and are easily assigned with the aid of short range COSY experiments.

A typical example of a β-pyrrolic modified TPP derivative (Figure 8.1) is described here. At high field, this spectrum shows the signals of two highly shielded nitrogen protons at the centre of the aromatic porphyrin core, as a broad singlet. This signal is lost on metallation. Moving up-field are the signals of the vinylic hydrogens ($H_{1'}$ and $H_{2'}$) as doublets with splitting of approximately 12.0 and 16.0 Hz for the *cis* and *trans* isomers respectively. Next come the aromatic hydrogens which are shown as doublets with a splitting of approximately 8.0 Hz. These are easily assigned from COSY spectra or coupling constants. The H_{ortho} of the *meso* functionalised phenyl rings are shown around 7.8 ppm as multiplets due the lack of symmetry in the porphyrin. Likewise, H_{meta}

and H_{para} hydrogens occur as multiplets around 7.4 ppm. The β-pyrrolic hydrogens are further down-field typically between 9.1 and 8.6 ppm. A typical coupling of 4.5 – 4.9 Hz can be observed for these protons but often they converge into overlapping chemical shifts. The furthest down-field signal is generally that of H_3 – the β-pyrrolic proton next to the β-pyrrolic substituent. The porphyrin ring current heavily deshields this proton, with an additive contribution from the β-pyrrolic substituent.

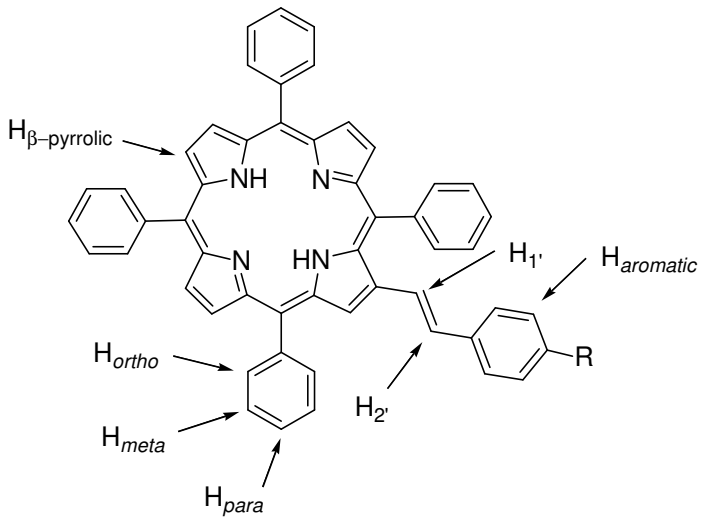

Figure 8.1 ^{1}H NMR spectroscopic assignments for β-pyrrolic functionalised porphyrins.

^{1}H NMR spectroscopy was the primary method for the determination of the presence of the halovinyl intermediate in the desired alkyne compound. The halovinyl could be observed by the presence of multiple NH signals (generally three) at approximately -2.70 ppm.

Mass Spectrometry

Low resolution mass spectrometry was used to confirm the identity of porphyrins. Masses were obtained as M^+ ions using a Waters Micromass MALDI in the positive ion mode. Molecular ions were generally obtained using a matrix free system and when a matrix was deemed necessary α-cyano-4-hydroxycinnamic acid, retinoic acid or 2-(4'-hydroxybenzeneazo)benzoic acid were used. Loss of N_2 was observed in all azido functionalised porphyrins. Low resolution mass spectra of porphyrin nucleosides could not be obtained.

High resolution mass spectrometry (HRMS) data for porphyrin compounds (excluding porphyrin nucleosides) were obtained by Raisa Imatdieva (University of Auckland) using a microTOF-Q ESI mass spectrometer or a VG-70SE FAB mass spectrometer with a *p*-nitrobenzyl alcohol matrix in the positive mode. Typically M^+ or $(M+H)^+$ ions were observed. High resolution mass spectrometry data for metallo porphyrin nucleosides was obtained by John Allen (Australian National University) using a Waters LCT ESI-TOF mass spectrometer in the negative mode and the free base porphyrin nucleoside on a Waters LCT Premier XE ESI-TOF mass spectrometer in the positive mode.

UV-Vis Absorption Spectroscopy

Solution UV-Vis spectroscopy was carried out for all free base and metallo porphyrin derivatives using a Shimadzu UV-3101PC UV-VIS-NIR-scanning spectrophotometer. The typical adsorption spectra were observed for all species, dominated by the Soret and Q bands as described in Chapter 1.

Infrared Spectroscopy

IR spectra were recorded when deemed necessary on a Nicolet 5700 FT-IR from Thermo Electron Corporation using an ATR attachment.

8.2 Reagents and Equipment used for the Synthesis of Porphyrin Possessing Oligonucleotides

Reagents

Solvents and reagents were supplied from many different sources, generally as AR grade. H_2O was used only after purification through a miliQ system. Unmodified short oligonucleotides were purchased from IDT (USA). Salmon testes DNA was purchased from Aldrich. Phosphoramidites used in automated DNA synthesis were commercially available from ChemGenes.

Synthesis of Oligonucleotides

DMT-off oligodeoxynucleotides were synthesised in a 1.0 μmol scale on 1000 Å CPG supports using a MerMade 4 Automated DNA Synthesiser from BioAutomation Corporation, using 4,5-dicyanoimidazole as an activator and 0.075 M solutions of the corresponding phosphoramidites in dry ACN. 2′-*O*-Propargyl uridine phosphoramidite or 2′-*O*-propargyl adenosine phosphoramidite (8 mg) was hand coupled by dissolving the amidite in the activator solution (1 mL) in a plastic syringe which was added to the support after the detritilation and washing cycles (coupling time of 5 minutes).

Purification

Porphyrin functionalised oligonucleotides were purified by HPLC or puri-pak columns. HPLC purification was achieved on a Waters 600 HPLC fitted with a Waters 2487 dual λ absorbance detector (260 and 427 nm) using a reverse-phase semipreparative Econosil C_{18} (10 μm, 10 × 250 mm) column. Puri-pak C_{18} purification cartridges were obtained from ChemGenes.

Mass Spectrometry

Molecular weights of the oligonucleotides were obtained using a Bruker Daltonics Autoflex MALDI TOF in the negative mode (University of Waikato) using either

2′,4′,6′-trihydroxyacetophenone, 3-hydroxypicolinic acid or 6-azathiothymine as a matrix and dibasic ammonium citrate as a co-matrix. Molecular weights of CT sequences were obtained using a Waters Micromass MALDI-TOF in the positive mode. Oligonucleotides were desalted using C_{18} zip-tips prior to loading on the MALDI plate.

Gel Electrophoresis

Purity of ON's was checked using denaturing 20% PAGE (7 M urea). Porphyrin modified oligonucleotides were observed as red bands for Ni^{II} containing porphyrins and as green bands for Zn^{II} and Fe^{III} porphyrins. Gels were stained with Stains-All® dye and destained with H_2O. Significant retardation of porphyrin modified oligonucleotides was observed compared to wild type oligonucleotides.

UV-Vis Spectroscopy

UV-Vis Spectroscopy and melting temperature measurements of oligonucleotides were performed on a CARY 100Bio UV-Vis spectrophotometer using a 2 × 6 multicell block with a Peltier temperature controller.

Extinction coefficients for porphyrin modified oligonucleotides were calculated using the extinction coefficients of each nucleoside at 260 nm. Extinction coefficients of unmodified nucleotides (L/(mol.cm)): dA (15400), dG (11700), dT (8800), dC (7300). Extinction coefficients for porphyrin modifications (L(mol.cm)): **1** (14800), **2** (14800), **3** (15900), **4** (15900), **5** (9000) , **6** (9000) and **7** (21400).

Circular Dichroism Spectroscopy

CD spectra were recorded using an Applied Photophysics Chirascan CD spectrophotometer (150 W Xe arc) with a Quantum Northwest TC125 temperature controller. Identical solutions were used for CD spectroscopy to that used for melting studies with the exception of triplex DNA where 1.0 μM of each oligonucleotide strand was used. An average of ten scans was recorded (1 nm intervals, 240 nm/min, 1 cm pathlength), baselined against the appropriate buffer solution then smoothed. Data was recorded in mdeg and converted to delta epsilon.

Molecular Modelling

Molecular modelling calculations and the construction of duplexes were performed using MacroModel v9.1 from Schrödinger. All calculations were conducted using AMBER* force field and the GB/SA water model.[151, 152] 11-Mer duplexes containing unmetallated tetraphenylporphyrin modified nucleotides were generated from a B type DNA-DNA duplex using Maestro v9.1 from Schrödinger. Parallel triplexes were built by the consecutive superimposition of triples CGC and TAT, which were generated with Insight II v9.72 from MSI and transported into MacroModel. Bulged insertions **5** and **6** were constructed in several steps. The unmodified duplex or triplex was constructed and the appropriate strand was disconnected by the deletion of the phosphate group at the location of the bulged insertion. Afterwards, the bulged insertion up to and including the triazole ring was built and placed between bases in the structure. The phosphate backbone was reconnected and minimisation was then performed, creating enough space for the bulged insertion. The appropriate porphyrin was then built off the triazole ring.

Constraints ensured the planarity of the porphyrins and were based on the metal complexed porphyrin available in the Maestro software (distances: N1-N3, N2-N4; 4.132 Å, force constant 100 and torsion angels: N1-C2-C3-C4, N2-C6-C7-C8, N3-C10-C11-C12, N4-C14-C15-C16; 0.0º, force constant 100). The stochastic dynamics calculations generating 250 structures were performed using an extended cut off potential with a SHAKE algorithm to constrain bond to hydrogen. Simulation temperature was 300 K, simulation time 500 ps and equilibration time 150 ps. All 250 structures were minimised using the PRCG method with convergence threshold of 0.05 KJ/mol and examined with Xcluster from Schrödinger to find representative low-energy structures.

8.3 Experimental Procedures for Chapter 2 - Synthesis of *β*-Pyrrolic Porphyrin Derivatives for DNA Modification

11-Bromoundecanal (4)

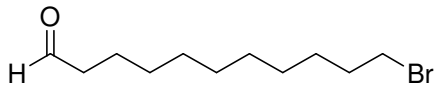

$C_{11}H_{21}BrO$
Exact Mass: 248.078
Mol. Wt.: 249.188

11-Bromoundecanol (500 mg, 2 mmol) was added to a mixture of PCC (644 mg, 3 mmol, 1.5 eq) in dry DCM (10 mL) under Ar and stirred at RT until the reaction was complete by TLC (4 hr). The crude reaction mixture was purified by silica gel column chromatography eluting the product with DCM as a colourless band. The solvent was removed *in vacuo* to give 11-bromoundecanal as a light yellow oil (416 mg, 83%). ^{1}H NMR (500 MHz, $CDCl_3$, TMS): δ 9.76 (t, 1H, *J* = 1.9 Hz CHO), 3.41 (t, 2H, *J* = 6.9 Hz, $CHO(CH_2)_9C\mathbf{H}_2Br$), 2.42 (td, 2H, *J* = 7.5 and 1.9 Hz, $CHOC\mathbf{H}_2(CH_2)_9Br$), 1.85 (dt, 2H, *J* = 7.7 and 6.9 Hz $CHO(CH_2)_8C\mathbf{H}_2CH_2Br$), 1.62 (q, 2H, *J* = 7.5 Hz, $CHOCH_2C\mathbf{H}_2(CH_2)_8Br$), 1.43-1.40 (m, 2H, $CHO(CH_2)_7C\mathbf{H}_2(CH_2)_2Br$), 1.30-1.28 (m, 10H, $CHO(CH_2)_2(C\mathbf{H}_2)_5(CH_2)_3Br$).

2-(12′-Bromododec-1′-*trans*-ene)-5,10,15,20-tetraphenylporphyrin (5)

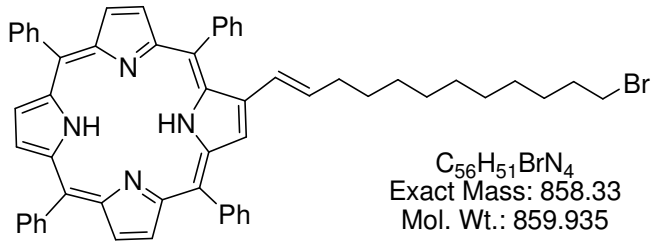

$C_{56}H_{51}BrN_4$
Exact Mass: 858.33
Mol. Wt.: 859.935

To a solution of TPPps (**3**, 400 mg, 0.43 mmol) and 11-bromoundecanal (**4**, 400 mg, 1.61 mmol, 3.75 eq) in dry DCM (20 mL), DBU (0.58 ml, 3.88 mmol, 9 eq) was added and the reaction was stirred under Ar at RT for 20 min. The resulting solution was passed down a plug of silica gel in DCM and the solvent was reduced *in vacuo*. The crude mixture was precipitated from DCM:MeOH and collected by filtration to give a purple solid (250 mg, 67%). ^{1}H NMR spectroscopic analysis showed a *cis/trans* mixture of the desired compound **5** and $TPPCH_3$ **7**. ^{1}H NMR key signals (500 MHz, $CDCl_3$, TMS): δ 6.20 (d, 1H, *J* = 11.7 Hz, H_{cis}), 6.07 (d, 2.5H, *J* = 15.7 Hz, H_{trans}), 2.58 (s, 1.5H, TPP-CH_3). This gave a ratio of **5***cis*:**5***trans*:TPP-CH_3 (**7**) of 2:5:1.

To the *cis/trans* mixture (33 mg, 38 μmol) in DCM (10 mL), I_2 (29 mg, 3 eq) was added and the mixture was stirred at RT under darkness for 3 hrs. The organic layer was then washed with a saturated solution of $Na_2S_2O_3$, separated, dried over $MgSO_4$, filtered and the solvent was removed *in vacuo*. The resulting solid was dissolved in DCM and purified by silica gel column chromatography eluting the product with DCM as a red band. The solvent was removed *in vacuo* and the *trans* product was precipitated from DCM:MeOH to give a purple powder (25 mg, 76%) that contained $TPPCH_3$ **7** (**5***trans*:**7** of 6:1). ^{1}H NMR (500 MHz, $CDCl_3$, TMS): δ 8.84 (s, 2.3H, **5** and **7** $H_{\beta\text{-pyrrolic}}$), 8.80-8.78 (m, 2.3H, **5** and **7** $H_{\beta\text{-pyrrolic}}$), 8.75-8.73 (m, 2.3H, **5** and **7** $H_{\beta\text{-pyrrolic}}$), 8.69 (m, 1.16H, **5** and **7** $H_{\beta\text{-pyrrolic}}$), 8.22-8.19 (m, 7H, H_{ortho}), 8.08-8.06 (m, 2.3H, H_{ortho}), 7.78-7.69 (m, 14H, $H_{meta,\ para}$), 6.42 (dt, 1H, J = 15.6 and 6.7 Hz, $H_{2'}$), 6.08 (d, 1H, J = 15.5 Hz, $H_{1'}$), 3.41 (t, 2H, J = 6.9 Hz, $(CH_2)_9C\mathbf{H}_2Br$), 2.58 (s, 0.45H, **7** $TPPCH_3$), 2.05-2.01, (m, 2H, $C\mathbf{H}_2(CH_2)_9Br$), 1.90 - 1.84 (m, 2H, $(CH_2)_8C\mathbf{H}_2CH_2Br$), 1.47-1.44 (m, 2H, $(CH_2)_7C\mathbf{H}_2(CH_2)_2Br$), 1.41-1.32 (m, 12H, $CH_2(C\mathbf{H}_2)_6(CH_2)_3Br$), -2.71 (br s, 2.33H, NH). UV-Vis (CH_2Cl_2): λ_{max} [nm] ($\varepsilon \times 10^{-3}$) 274 (42.3), 420.5 (138), 518.5 (8.57), 552.5 (3.98), 594.5 (2.69), 660 (2.29). ESI-LRMS: *m/z* (%, assignment) cluster at 859-864, 859 (90, $(M+H)^+$). HRMS: Calcd for $(M+H)^+$ ($C_{56}H_{52}BrN_4$): 859.3370, found: 859.3343.

2-(12′-Pyridiumyldodec-*trans*-1′-ene)-5,10,15,20-tetraphenylporphyrin bromide (6)

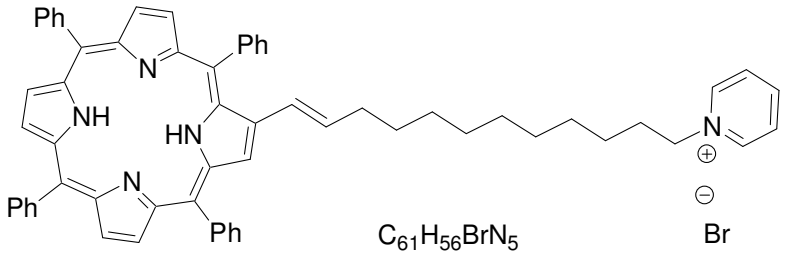

$C_{61}H_{56}BrN_5$
Exact Mass: 937.372
Mol. Wt.: 939.035

Compound **5***trans* (25 mg, 29 μmol) was refluxed in pyridine (2 mL) for two days after which the solvent was removed *in vacuo*. The crude solution was dissolved in DCM and purified through a plug of silica gel, eluting $TPPCH_3$ (4 mg) in DCM then the pyridinium salt in MeOH:DCM (3:20). The pyridinium salt was precipitated from DCM:hexane and collected by filtration. The resulting crystals were washed with a saturated aq. solution of NaBr to give a red solid (20 mg, 74%). ^{1}H NMR (500 MHz, d_6-DMSO): δ 9.06 (dd, 2H, J = 5.7 and 1.3 Hz, H_{Pyr}), 8.84-8.63 (m, 7H, $H_{\beta\text{-pyrrolic}}$), 9.56 (tt,

2H, *J* = 7.6 and 1.3 Hz, H_{Pyr}), 8.22-8.19 (m, 6H, H_{ortho}), 8.12 (t, 1H, *J* = 7.6 Hz, H_{Pyr}), 8.08-8.06 (m, 2H, H_{ortho}), 7.85-7.77 (m, 12H, $H_{meta, para}$), 6.44-6.41 (m, 1H, $H_{2'}$), 6.02 (d, 1H, *J* = 15.4 Hz, $H_{1'}$), 4.57 (t, 2H, *J* = 7.4 Hz, $(CH_2)_9CH_2PyrBr$), 2.00-1.98 (m, 2H, $CH_2(CH_2)_9PyrBr$), 1.93-1.88 (m, 2H, $(CH_2)_8CH_2CH_2PyrBr$), 1.30-1.23 (m, 14H, $CH_2(CH_2)_7(CH_2)_2PyrBr$), -2.69 (br s, 2H, NH). UV-Vis (CH_2Cl_2): λ_{max} [nm] ($\varepsilon \times 10^{-3}$) 272 (37.5), 423 (120), 519 (8.01), 556.5 (3.65), 594.5 (3.13), 673.5 (4.73). ESI-LRMS: *m/z* (%, assignment) cluster at 858-861, 858 (100, $(M-Br)^+$). HRMS: Calcd for $(M-Br)^+$ ($C_{61}H_{56}N_5$): 858.4530, found: 858.4480.

2-(12′-Bromododecane)-5,10,15,20-tetraphenylporphyrin (8)

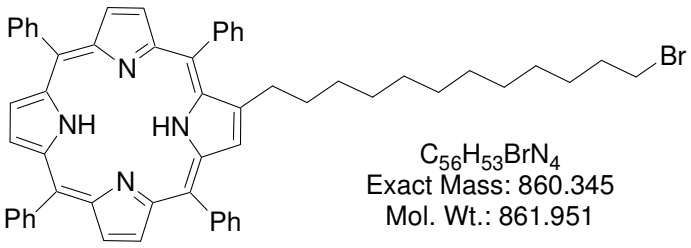

To a *cis/trans* mixture of **5** (210 mg, 0.24 mmol) in formic acid (21 mL), 10% palladium on carbon (210 mg) was added and the mixture was heated under H_2 atmosphere at 50˚C. After 3.5 hrs the reaction was halted by the addition of an aq. solution of NaOH (21 g in 150 mL H_2O) causing the porphyrin to precipitate from the solution. The resulting precipitate was collected by filtration then redissolved in DCM. The resulting solution was dried over $MgSO_4$, filtered and the solvent was removed *in vacuo*. The residue was purified by silica gel column chromatography collecting the major red fraction in DCM:hexane (1:1). The resulting solid was precipitated from DCM:MeOH to give a purple solid (85 mg, *ca.* 40%) in a 1:1 mixture of **8** and $TPPCH_3$ **7**. ^{1}H NMR (500 MHz, $CDCl_3$, TMS): δ 8.86 (s, 4H, **8** and **7** $H_{\beta\text{-pyrrolic}}$), 8.79 (d, 1H, *J* = 4.7 Hz, **7** $H_{\beta\text{-pyrrolic}}$), 8.78 (d, 1H, *J* = 4.7 Hz, **8** $H_{\beta\text{-pyrrolic}}$), 8.75 (d, 2H, *J* = 4.8 Hz, **7** $H_{\beta\text{-pyrrolic}}$), 8.73 (d, 2H, *J* = 4.9 Hz, **8** $H_{\beta\text{-pyrrolic}}$), 8.62 (d, 2H, *J* = 4.7 Hz, **7** $H_{\beta\text{-pyrrolic}}$), 8.60 (d, 2H, *J* = 4.7 Hz, **8** $H_{\beta\text{-pyrrolic}}$), 8.22-8.18 (m, 12H, **8** and **7** H_{ortho}), 8.10-8.09 (m, 2H, **8** H_{ortho}), 8.07-8.05 (m, 2H, **7** H_{ortho}), 7.78-7.66 (m, 24H, **8** and **7** $H_{meta, para}$), 3.39 (t, 2H, *J* = 6.9 Hz, **8** $(CH_2)_{11}CH_2Br$), 2.31 (t, 2H, *J* = 7.7 Hz, **8** $CH_2(CH_2)_{11}Br$), 2.58 (s, 3H, **7** $TPPCH_3$), 1.87-1.81 (m, 2H, **8** $(CH_2)_{10}CH_2CH_2Br$), 1.78-1.75 (m, 2H, **8** $CH_2CH_2(CH_2)_{10}Br$), 1.43-1.38 (m, 2H, **8** $(CH_2)_9CH_2(CH_2)_2Br$), 1.31-1.21 (m, 14H, **8** $(CH_2)_2(CH_2)_7(CH_2)_3Br$), -2.70 (4H, br s, NH). UV-Vis (CH_2Cl_2): λ_{max} [nm] ($\varepsilon \times 10^{-3}$)

274.5 (55.5), 417.5 (510), 514.5 (22.1), 549 (6.34), 588 (6.39), 643.5 (4.43). ESI-LRMS: *m/z* (%, assignment) cluster at 861-866, 861 (80, $(M+H)^+$). HRMS: Calcd for $(M+H)^+$ ($C_{56}H_{54}BrN_4$): 861.3526, found: 861.3503.

2-(12′-Pyridiumyldodecane)-5,10,15,20-tetraphenylporphyrin bromide (9)

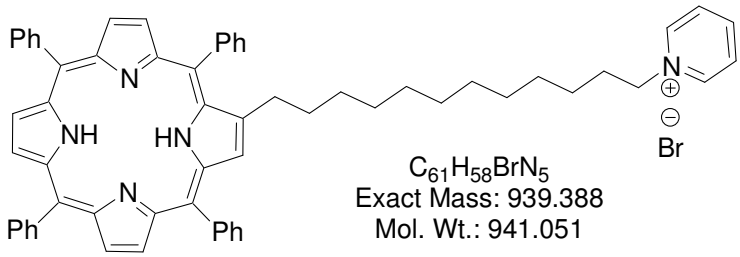

Compound **8** (80 mg, *ca*. 0.11 mmol) was refluxed in pyridine (20 mL) for two days, after which the solvent was removed *in vacuo*. The crude solid was dissolved in DCM and purified through a plug of silica gel, eluting $TPPCH_3$ (**7**, 34 mg) in DCM then the pyridinium salt in MeOH:DCM (1:4). The pyridinium salt was precipitated from DCM:hexane and collected by filtration. The resulting crystals were washed with a saturated aq. solution of NaBr to give a red solid (30 mg, *ca.* 30%). ^{1}H NMR (500 MHz, $CDCl_3$, TMS): δ 9.10 (d, 2H, *J* = 5.2 Hz, H_{Pyr}), 8.86 (s, 1H, $H_{\beta\text{-pyrrolic}}$), 8.86 (s, 1H, $H_{\beta\text{-pyrrolic}}$), 8.78 (d, 1H, *J* = 4.8 Hz, $H_{\beta\text{-pyrrolic}}$), 8.73 (d, 2H, *J* = 4.8 Hz, $H_{\beta\text{-pyrrolic}}$), 8.64 (s, 1H, $H_{\beta\text{-pyrrolic}}$), 8.61 (d, 1H, *J* = 4.8 Hz, $H_{\beta\text{-pyrrolic}}$), 8.21 (t, 1H, *J* = 1.3 Hz, H_{Pyr}), 8.20-8.18 (m, 6H, H_{ortho}), 8.09-8.07 (m, 2H, H_{ortho}), 7.81 (t, 2H, *J* = 6.6 Hz, H_{Pyr}), 7.79-7.67 (m, 12H, $H_{meta,\ para}$), 4.75 (t, 2H, *J* = 7.2 Hz, $C\mathbf{H}_2(CH_2)_{11}PyrBr$), 2.81 (t, 2H, *J* = 7.7 Hz, $(CH_2)_{11}C\mathbf{H}_2PyrBr$), 1.86 (m, 2H, $CH_2C\mathbf{H}_2(CH_2)_{10}PyrBr$), 1.76-1.80 (m, 2H, $(CH_2)_{10}C\mathbf{H}_2CH_2PyrBr$), 1.25-1.20 (m, 16H, $(CH_2)_2(C\mathbf{H}_2)_8(CH_2)_2PyrBr$), -2.81 (s br, 2H, NH). UV-Vis (CH_2Cl_2): λ_{max} [nm] ($\varepsilon \times 10^{-3}$) 418 (450), 515 (21.3), 549.5 (6.86), 587.5 (6.64), 643.5 (3.32). ESI-LRMS: *m/z* (%, assignment) cluster at 860-863, 860 (100, $(M-Br)^+$). HRMS: Calcd for $(M-Br)^+$ ($C_{61}H_{58}N_5$): 860.4678, found: 860.4687.

_N_-[(5,10,15,20-Tetraphenylporphinato-2-yl nickel II)methylene]ethanyl-1,2-diamine (11)

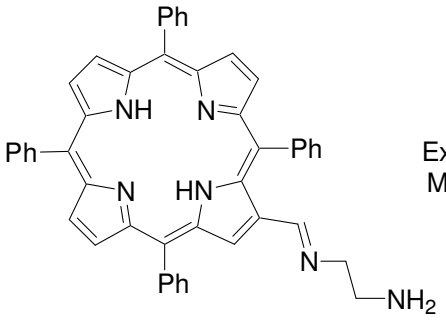

$C_{47}H_{36}N_6$
Exact Mass: 684.3
Mol. Wt.: 684.829

Ethylenediamine (**10**, 0.207 mL, 3.11 mmol, 10 eq) was added to a solution of TPPCHO (**2**, 200 mg, 0.311 mmol) in $CHCl_3$ (50 mL) and heated under Ar at 50 ˚C for 10 min. Acetic acid (1 drop) was added and heating was continued until TPPCHO was no longer visible by TLC (1 hr). The reaction was then precipitated from $CHCl_3$:MeOH and collected by filtration as a purple powder (202 mg).^{1}H NMR spectroscopy revealed the solid to be a 1:1 mixture of product (**11**) and TPPCHO (**2**). ^{1}H NMR (500 MHz, $CDCl_3$, TMS): δ 9.26 (s, 1H, CHO), 8.86-8.82 (m, 12H, **11** and **2** $H_{\beta\text{-pyrrolic}}$), 8.72 (d, 1H, J = 4.7 Hz, **11** or **2** $H_{\beta\text{-pyrrolic}}$), 8.57 (d, 1H, J = 4.7 Hz, **11** or **2** $H_{\beta\text{-pyrrolic}}$), 8.24-8.15 (12H, m, **11** and **2** H_{ortho}), 7.86-7.72 (m, 24H, **11** and **2** $H_{meta,\ para}$), 7.05 (d, 1H, J = 15.8 Hz, CH), 3.43 (t, 2H, J = 5.7 Hz, CH_2), 3.05 (t, 2H, J = 5.7 Hz, CH_2), -2.62 (2H, br s, **11** or **2** NH), -2.62 (2H,br s, **11** or **2** NH). ESI-LRMS: *m/z* (%, assignment) cluster at 685-688, 685 (100, $(M+H)^+$). ESI-HRMS: Calcd for $(M+H)^+$ ($C_{47}H_{37}N_6$): 685.3074, found: 685.3082.

2-Formyl-5,10,15,20-tetraphenylporphyrinato nickel II (14)

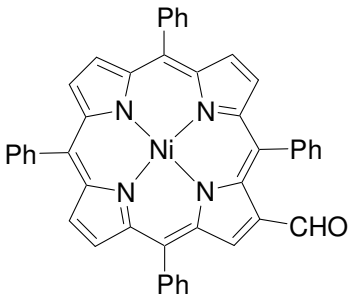

$C_{45}H_{28}N_4NiO$
Exact Mass: 698.162
Mol. Wt.: 699.423

To a solution of refluxing TPPCHO (**2**, 1.7 g, 2.64 mmol) in $CHCl_3$ (500 mL), $Ni(OAc)_2{\cdot}4H_2O$ (6.5 g, 26.4 mmol, 10 eq) in MeOH (50 mL) was added and refluxing was continued overnight. The solvent was removed *in vacuo*. The resulting solid was dissolved in hot $CHCl_3$ (50 °C, 100 mL) and purified through a plug of silica gel with hot $CHCl_3$ until colour was no longer eluted. The solvent was removed *in vacuo* and the

resulting solid was precipitated from DCM:hexane to give a red solid (1.8 g, 97%). Spectroscopic data is in agreement with Bonfantini *et al*.[87]

_N_-[(5′,10′,15′,20′-tetraphenylporphinato-2′-yl nickel II)methylene]benzene-1,4-diamine (15)

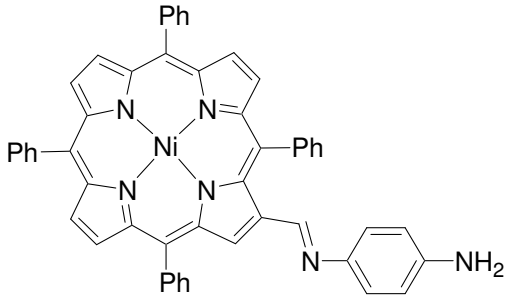

$C_{51}H_{34}N_6Ni$
Exact Mass: 788.22
Mol. Wt.: 789.549

p-Phenylenediamine (**13**, 77 mg, 0.71 mmol, 10 eq) was added to a solution of NiTPP-CHO (**14**, 50 mg, 71 μmol) in THF (15 mL), to this acetic acid (1 drop) was added and the reaction was stirred at RT overnight. The solvent was removed *in vacuo* to give a red solid which was purified by silica gel column chromatography eluting first the starting material with DCM (24 mg, 48%) then what was suspected to be the desired product with MeOH:DCM (1:9) (25 mg).

4-[*trans*-2′-(5″,10″,15″,20″-Tetraphenylporphyrin-2″-yl)ethen-1′-yl]nitrobenzene (19)

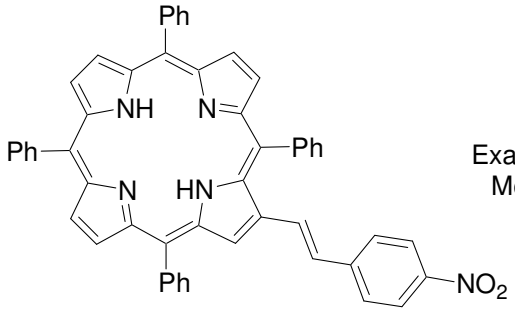

$C_{52}H_{35}N_5O_2$
Exact Mass: 761.279
Mol. Wt.: 761.867

DBU (315 μL, 2.10 mmol, 3.2 eq) was added to a solution of TPPps (**3**, 612 mg, 0.661 mmol) and 4-nitrobenzaldehyde (**18**, 297 mg, 1.98 mmol, 3 eq) in DCM (50 mL) and the reaction was stirred at RT under Ar for 30 min. Upon completion by TLC the solvent was reduced *in vacuo* and the resulting purple solid was precipitated from DCM:MeOH and collected by filtration as a *cis/trans* isomeric mixture (437 mg, 87%). The isomeric mixture was dissolved in $CHCl_3$ (30 mL) and I_2 (434 mg, 1.72 mmol, 3.0 eq) was added. After stirring under darkness at RT for 3 hrs a saturated aq. solution of $Na_2S_2O_3$ (100 mL) was added and stirring was continued for an additional 15 min. The

organic layer was separated, dried over $MgSO_4$, filtered and the solvent was reduced *in vacuo*. The resulting solid was precipitated from DCM:MeOH and collected by filtration to give pure *trans* product as a purple powder (430 mg, 85% overall). Spectroscopic data is in agreement with Bonfantini *et al.*[78]

4-[*trans*-2′-(5″,10″,15″,20″-Tetraphenylporphyrin-2″-yl)ethen-1′-yl]aminobenzene (20)

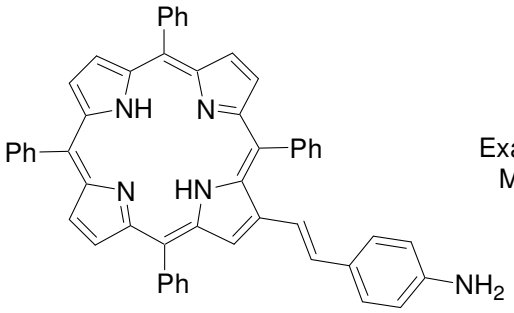

$C_{52}H_{37}N_5$
Exact Mass: 731.305
Mol. Wt.: 731.884

To a solution of compound **19** (120 mg, 0.157 mmol) in THF (100 mL), $SnCl_2 \cdot 2H_2O$ (1.42 g, 6.30 mmol, 40 eq) and conc. HCl (0.7 mL) were added and stirred in darkness under Ar for 24 hrs at RT. Afterwards, Et_3N (2.8 mL) was added forming a light brown coloured solid which was filtered through a glass sinter and washed with THF (20 mL). The filtrate solvent was removed *in vacuo*. The resulting solid was dissolved in DCM (37 mL), diluted with hexane (7 mL) and purified by alumina column chromatography (activity II, basic) eluting first the starting material with DCM:hexane (1:1) then the desired product with DCM (100 mg, 87%). ^{1}H NMR (500 MHz, $CDCl_3$, TMS): δ 8.98 (s, 1H, $H_{\beta\text{-pyrrolic}}$), 8.85 (s, 2H, $H_{\beta\text{-pyrrolic}}$), 8.81 (d, 1H, J = 4.6 Hz, $H_{\beta\text{-pyrrolic}}$), 8.77-8.76 (m, 2H, $H_{\beta\text{-pyrrolic}}$), 8.75 (d, 1H, J = 4.8 Hz, $H_{\beta\text{-pyrrolic}}$), 8.27-8.19 (m, 8H, H_{ortho}), 7.83-7.70 (m, 12H, $H_{meta,\ para}$), 7.25 (d, 1H, J = 16.0 Hz, $H_{1'\text{ or }2'}$), 7.10 (d, 2H, J = 7.8 Hz, $H_{aromatic}$), 6.80 (d, 1H, J = 16.0 Hz, $H_{1'\text{ or }2'}$), 6.68 (d, 2H, J = 7.8 Hz, $H_{aromatic}$), 3.80 (br s, 2H, NH_2), -2.57 (br s, 2H, NH). UV-Vis (CH_2Cl_2): λ_{max} [nm] ($\varepsilon \times 10^{-3}$) 278.5 (36.3), 421 (191), 524 (18.7), 568 (13.0), 600 (8.56), 654.0 (2.12). ESI-LRMS: *m/z* (%, assignment) cluster at 732-735, 732 (100, $(M+H)^+$). ESI-HRMS: Calcd for $(M+H)^+$ ($C_{52}H_{38}N_5$): 732.3122, found: 732.3118.

4-[*trans*-2′-(5″,10″,15″,20″-Tetraphenylporphyrinato-2″-yl nickel II)ethen-1′-yl]nitrobenzene (22)

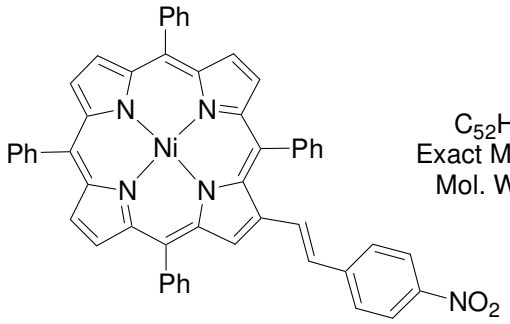

$C_{52}H_{33}N_5NiO_2$
Exact Mass: 817.199
Mol. Wt.: 818.544

$Ni(OAc)_2 \cdot 4H_2O$ (1.93 g, 7.81 mmol) in MeOH (6 mL) was added to a refluxing solution of compound **19** (425 mg, 0.56 mmol) in $CHCl_3$ (60 mL) and refluxing was continued overnight. The reaction mixture was taken to dryness, dissolved in DCM and purified through a plug of silica gel with DCM. The solvent was precipitated from DCM:MeOH and collected by filtration to give a red powder (455 mg, 100%). Spectroscopic data is in agreement with Bonfantini *et al.*[78]

4-[*trans*-2′-(5″,10″,15″,20″-Tetraphenylporphyrinato-2″-yl nickel II)ethen-1′-yl]aminobenzene (23)

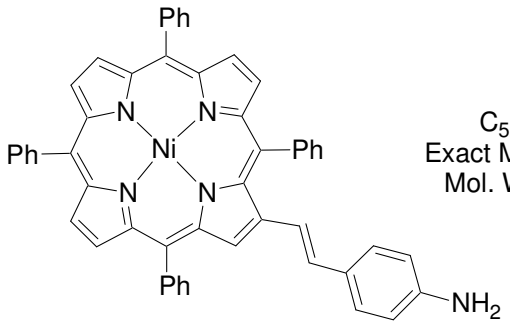

$C_{52}H_{35}N_5Ni$
Exact Mass: 787.225
Mol. Wt.: 788.561

To a solution of compound **22** (1.25 g, 1.52 mmol) in THF (830 mL), $SnCl_2 \cdot 2H_2O$ (14.7 g, 65 mmol, 42.8 eq) and conc. HCl (7.25 mL) were added and the reaction was stirred under Ar for 48 hrs at RT. Afterwards, Et_3N (29 mL) was added forming a light brown coloured solid which was filtered through a glass sinter and washed with THF (100 mL). The filtrate was concentrated *in vacuo*. The resulting red solid was dissolved in DCM (30 mL), diluted with hexane (30 mL) and purified by alumina column chromatography (activity II, basic) eluting first the starting material with DCM:hexane (1:1) (187 mg, 15%) then the desired product with DCM (940 mg, 78%). ^{1}H NMR (400 MHz, $CDCl_3$, TMS): δ 8.83 (s, 1H, $H_{\beta\text{-pyrrolic}}$), 8.71-8.66 (m, 6H, $H_{\beta\text{-pyrrolic}}$), 8.04-7.95 (m, 8H, H_{ortho}), 7.75-7.65 (m, 12H, $H_{meta,\ para}$), 7.05 (d, 1H, J = 15.8 Hz, $H_{1'\text{ or }2'}$), 7.02 (d,

2H, *J* = 8.2 Hz, $H_{aromatic}$), 6.67 (d, 2H, *J* = 8.1 Hz, $H_{aromatic}$), 6.65 (d, 1H, *J* = 16.0 Hz, $H_{1' \text{ or } 2'}$), 4.06 (br s, 2H, NH_2). UV-Vis (CH_2Cl_2): λ_{max} [nm] ($\varepsilon \times 10^{-3}$) 275 (109), 425 (175), 540 (21.5), 577 (16.8). ESI-LRMS: *m/z* (%, assignment) cluster at 788-794, 788 (100, $(M+H)^+$). ESI-HRMS: Calcd for $(M+H)^+$ ($C_{52}H_{36}N_5Ni$): 788.2304, found: 788.2139.

11-Bromoundecanoic acid (25)

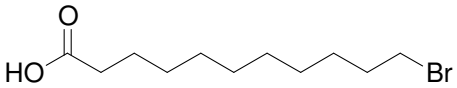

$C_{11}H_{21}BrO_2$
Exact Mass: 264.072
Mol. Wt.: 265.187

Chromium trioxide (1.8 g, 18.0 mmol, 1.5 eq) and H_2O (1.65 mL) was cooled to 0 °C and to this conc. H_2SO_4 (1.34 mL, 24.0 mmol, 2 eq) was added followed by H_2O (3 mL). After 5 minutes a solution of 11-bromoundecanol (**24**, 3.0 g, 12 mmol) in acetone (9 mL) was added dropwise over 1 minute. The reaction mixture was stirred for 2 hrs at 0 °C then stirred at RT for 12 hrs. Et_2O (100 mL) and H_2O (100 mL) were added and the aqueous layer was extracted with Et_2O (3 × 100 mL). The combined organic phases were then washed with brine (100 mL), the organic phase was dried over $MgSO_4$, filtered and reduced *in vacuo*. The resulting solid was purified by silica gel column chromatography eluting the product as a colourless band with DCM:0.5% AcOH affording the product as a white solid (1.30 g, 43%). ^1H NMR (500 MHz, $CDCl_3$, TMS): δ 10.18 (br s, 1H, COOH), 3.40 (t, 2H, *J* = 7.0 Hz, $COOH(CH_2)_9C\mathbf{H}_2Br$), 2.35 (t, 2H, *J* = 7.5, $COOHC\mathbf{H}_2(CH_2)_9Br$), 1.88-1.82 (m, 2H, $COOH(CH_2)_8C\mathbf{H}_2CH_2Br$), 1.66-1.60 (m, 2H, $COOHCH_2C\mathbf{H}_2(CH_2)_8Br$), 1.43-1.40 (m, 2H, $COOH(CH_2)_7C\mathbf{H}_2(CH_2)_2Br$), 1.35-1.28 (m, 10H, $CHO(CH_2)_2(C\mathbf{H}_2)_5(CH_2)_2Br$).

***trans*-1-{11-{4-[2-(5″,10″,15″,20″-Tetraphenylporphyrinato nickel II)vinyl]phenylamino}-11-oxoundecyl}bromide (26)**

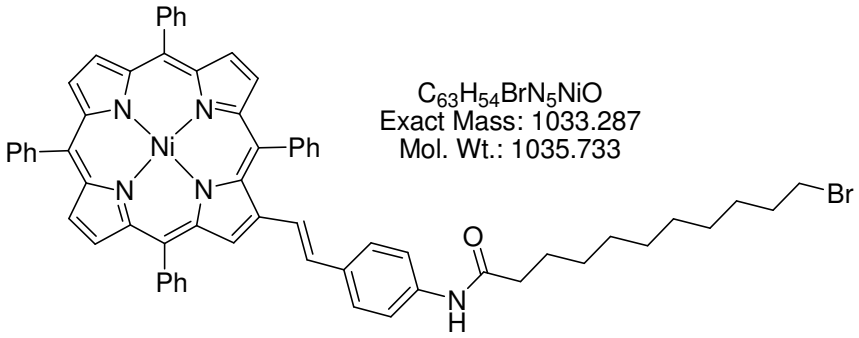

11-Bromoundecanoic acid (**25**, 2.01 g, 7.5 eq, 7.62 mmol) and DMAP (930 mg, 7.5 eq, 7.62 mmol) were dissolved in THF (600 mL) and cooled to 0 ˚C under Ar. To this EDC (1.18 g, 7.5 eq, 7.62 mmol) was added and the reaction mixture was stirred for 30 min at 0 ˚C followed by the addition of **23** (800 mg, 1.01 mmol). The reaction was stirred for 48 hrs at RT, diluted with DCM (300 mL) and washed with H_2O (3 × 300 mL). The organic layer was separated, dried over $MgSO_4$, filtered and the solvent was removed *in vacuo*. The resulting solid was purified by silica gel column chromatography eluting the product as the major red fraction in DCM. The solvent was removed *in vacuo* to give a purple solid (792 mg, 76%). ^{1}H NMR (400 MHz, d_6-DMSO): δ 9.92 (s, 1H, NH), 8.85 (s, 1H, $H_{\beta\text{-pyrrolic}}$), 8.67-8.62 (m, 6H, $H_{\beta\text{-pyrrolic}}$), 8.02-7.94 (m, 8H, H_{ortho}), 7.82-7.71 (m, 12H, $H_{meta,\ para}$), 7.55 (d, 2H, J = 8.5 Hz, $H_{aromatic}$), 7.17 (d, 1H, J = 16.0 Hz, $H_{1'}$), 7.11 (d, 2H, J = 8.5 Hz, $H_{aromatic}$), 6.98 (d, 1H, J = 16.0 Hz, $H_{2'}$), 3.51 (t, 2H, J = 6.9 Hz, $CO(CH_2)_9C\mathbf{H}_2Br$), 2.31 (t, 2H, J = 7.4 Hz, $COC\mathbf{H}_2(CH_2)_9Br$), 1.78 (dt, 2H, J = 7.3 and 6.8 Hz, $CO(CH_2)_8C\mathbf{H}_2CH_2Br$), 1.64-1.56 (m, 2H, $COCH_2C\mathbf{H}_2(CH_2)_8Br$), 1.38-1.27 (m, 12H, $CO(CH_2)_2(C\mathbf{H}_2)_6(CH_2)_2Br$). UV-Vis ($CH_2Cl_2$): λ_{max} [nm] ($\varepsilon \times 10^{-3}$) 425.5 (167), 539.5 (15.7), 576 (11.2). ESI-LRMS: *m/z* (%, assignment) cluster at 1033-1040, 1035 (100, M^+). HRMS: Calcd for M^+ ($C_{63}H_{54}BrN_5NiO$): 1035.2841, found: 1035.2804.

***trans*-1-{11-{4-[2-(5″,10″,15″,20″-Tetraphenylporphyrinato nickel II)vinyl]phenylamino}-11-oxoundecyl}pyridinium bromide (27)**

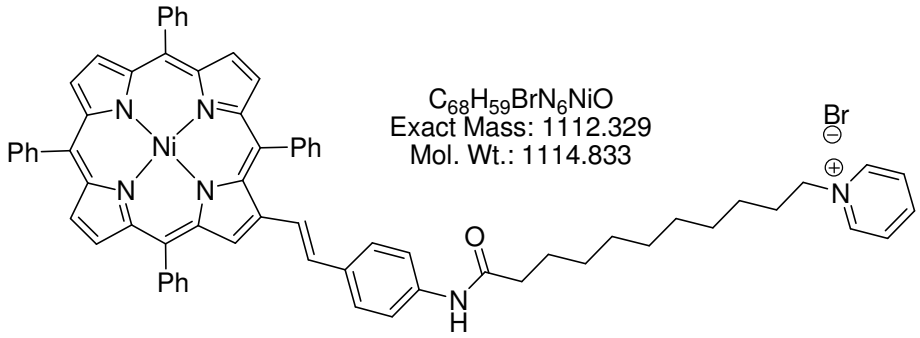

Compound **26** (560 mg, 0.542 mmol) was refluxed in pyridine (70 mL) overnight. Following this the solvent was removed *in vacuo* to give a purple solid which was dried under high vaccum for five days (603 mg, 100%). ^{1}H NMR (500 MHz, d_6-DMSO): δ 9.96 (s, 1H, NH), 9.10 (dd, 2H, J = 6.7 and 1.2 Hz, H_{pyr}), 8.86 (s, 1H, $H_{\beta\text{-pyrrolic}}$), 8.70-8.65 (m, 6H, $H_{\beta\text{-pyrrolic}}$), 8.61 (dt, 1H, J = 7.8 and 1.2 Hz, H_{pyr}), 8.17 (t, 2H J = 6.7 Hz, H_{pyr}), 8.04-7.96 (m, 8H, H_{ortho}), 7.83-7.74 (m, 12H, $H_{meta,\ para}$), 7.56 (d, 2H, J = 8.6 Hz, $H_{aromatic}$), 7.20 (d, 1H, J = 16.0 Hz, $H_{1'}$), 7.13 (d, 2H, J = 8.6 Hz, $H_{aromatic}$), 6.70 (d, 1H, J = 16.0 Hz, $H_{2'}$), 4.60 (t, 2H, J = 7.4 Hz, $CO(CH_2)_9C\mathbf{H}_2PyrBr$), 2.33 (t, 2H, J = 7.4 Hz, $COC\mathbf{H}_2(CH_2)_9PyrBr$), 1.95-1.89 (m, 2H, $CO(CH_2)_8C\mathbf{H}_2CH_2PyrBr$), 1.63-1.58 (m, 2H, $COCH_2C\mathbf{H}_2(CH_2)_8PyrBr$), 1.30-1.28 (m, 12H, $CO(CH_2)_2(C\mathbf{H}_2)_6(CH_2)_2PyrBr$). UV-Vis ($CH_2Cl_2$): λ_{max} [nm] ($\varepsilon \times 10^{-3}$) 425.5 (163), 538.5 (14.9), 575 (10.8). ESI-LRMS: *m/z* (%, assignment) cluster at 1033-1040, 1033 (100, $(M\text{-}Br)^+$). HRMS: Calcd for $(M\text{-}Br)^+$ ($C_{68}H_{59}N_6NiO$): 1033.4098, found: 1033.4062.

4-Iodobenzoyl chloride

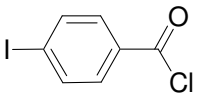

C7H4ClIO
Exact Mass: 265.900
Mol. Wt.: 266.464

4-Iodobenzoic acid (**28**, 5.0 g, 20 mmol) was refluxed overnight in $SOCl_2$ (25 mL). After cooling, the reaction mixture was diluted with H_2O (25 mL) and extracted into Et_2O (3 × 100 mL). The organic layer was separated, dried over $MgSO_4$, filtered and the solvent was removed *in vacuo*. The resulting solid was dissolved in Et_2O (200 mL), absorbed onto silica gel and purified by silica gel column chromatography, first eluting the product with DCM then eluting the starting material with ethylacetate (2.2 g, 44%). The product was taken to dryness to give a white solid (3.6 g, 47%). ^{1}H NMR (500

MHz, $CDCl_3$, TMS): δ 7.92 (d, 2H, J = 8.8 Hz, $H_{aromatic}$), 7.82 (d, 2H, J = 8.8 Hz, $H_{aromatic}$).

4-Iodobenzyl alcohol

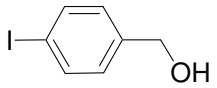

C_7H_7IO
Exact Mass: 233.954
Mol. Wt.: 234.034

4-Iodobenzyl alcohol was prepared using a method adapted from Ziyaei-Halimjani and Saidi.[102] 4-Iodobenzoyl chloride (3.6 g, 13.5 mmol) was dissolved in acetonitrile (20 mL) and to this $LiClO_4$ (1.43 g, 13.5 mmol) and $NaBH_4$ (1.35 g, 35.7 mmol) were added. The reaction then was stirred under Ar overnight at RT. The reaction was completed according to TLC after 24 hrs. The reaction mixture was diluted with H_2O (20 mL) and extracted into Et_2O (3 × 100 mL). The organic layer was separated, dried over $MgSO_4$, filtered and the solvent was removed *in vacuo*. The resulting white solid was purified by silica gel column chromatography eluting the product with DCM, which was taken to dryness to give a white solid (2.75g, 87%). Spectroscopic data is in agreement with Vassiliou *et al.*[179]

4-Iodobenzaldehyde

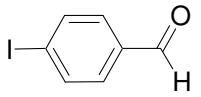

C_7H_5IO
Exact Mass: 231.939
Mol. Wt.: 232.018

4-Iodobenzaldehyde was prepared using a method adapted from De Mico *et al.*[101] To a solution of dry DCM (11 mL), 4-iodobenzyl alcohol (2.75 g, 11.7 mmol) and [bis(acetoxy)iodo]benzene (BIAB) (4.19 g, 13.0 mmol) were added and the reaction was stirred for 5 minutes at RT. Afterwards, TEMPO (177 mg, 1.17 mmol 0.1 eq) was added and stirring was continued for a further 2 hrs until reaction was completed according to TLC. The resulting mixture was diluted with DCM (20 mL), washed with an saturated aq solution of $Na_2S_2O_3$ (20 mL), $NaHCO_3$ (20 mL) then brine (20 mL), dried over $MgSO_4$, filtered and the solvent removed *in vacuo*. The resulting solid was purified by silica gel column chromatography first eluting any remaining alcohol with DCM:hexane (1:2) then the desired aldehyde with DCM. The colourless band was taken to dryness to give a white solid (2.30 g, 85%). ^1H NMR (500 MHz, $CDCl_3$, TMS): δ 9.98 (s, 1H, CHO), 7.94 (d, 2H, J = 8.5 Hz, $H_{aromatic}$), 7.61 (d, 2H, J = 8.5 Hz, $H_{aromatic}$).

Synthesis of compounds 29-32 are described in Chapter 8.4

2-[4′-(Trimethylsilyl)ethynylphenyl]ethynyl-5,10,15,20-tetraphenylporphyrinato zinc II (33)

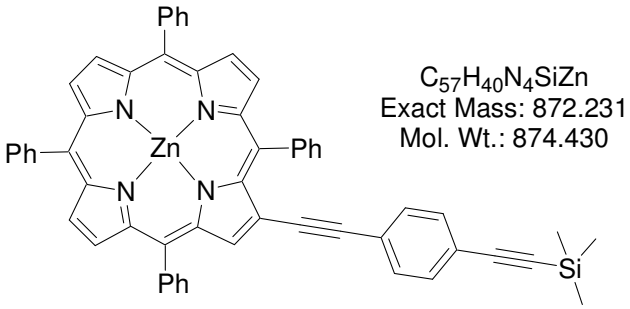

To a dry degassed solution of Et_3N (25 mL), 2-(4′-iodophenyl)ethynyl-5,10,15,20-tetraphenylporphyrinato zinc II (**32**, 500 mg, 0.55 mmol) was added and the reaction was stirred for 5 min at RT under Ar. Trimethylsilylacetylene (390 μL, 2.77 mmol, 5 eq) followed by $Pd(PPh_3)_4$ (191 mg, 0.16 mmol, 0.3 eq) and CuI (42 mg, 0.22 mmol, 0.5 eq) were added and the solution was refluxed under Ar for 3 hrs. After cooling to RT the solvent was removed *in vacuo*, the reaction mixture was dissolved in DCM (100 mL), washed with 5% aq. solution of Na_2EDTA (3 × 100 ml), 3 M aq. solution of NH_4OH (2 × 100 mL) and H_2O (100 mL). The organic layer was separated, dried over $MgSO_4$, filtered and the solvent was removed *in vacuo*. The crude purple solid was purified by silica gel column chromatography eluting the product with DCM:hexane (2:1) as a purple band which was taken to dryness to give a purple solid (446 mg, 93%). ^1H NMR (500 MHz, $CDCl_3$, TMS): δ 9.24 (s, 1H, $H_{\beta\text{-pyrrolic}}$), 8.95 (s, 2H, $H_{\beta\text{-pyrrolic}}$), 8.93 (s, 2H, $H_{\beta\text{-pyrrolic}}$), 8.90 (d, 1H, J = 4.7 Hz, $H_{\beta\text{-pyrrolic}}$), 8.79 (d, 1H, J = 4.7 Hz, $H_{\beta\text{-pyrrolic}}$), 8.25-8.20 (m, 8H, H_{ortho}), 7.81-7.60 (m, 12H, $H_{meta,\ para}$), 7.46 (d, 2H, J = 7.9 Hz, $H_{aromatic}$), 7.33 (d, 2H, J = 7.9 Hz, $H_{aromatic}$), 0.31 (s, 9H, CH_3). UV-Vis (CH_2Cl_2): λ_{max} [nm] ($\varepsilon \times 10^{-3}$) 431 (351), 556 (33.8), 593 (19.3). ESI-HRMS: Calcd for M^+ ($C_{57}H_{40}N_4SiZn$): 872.2308, found: 872.2305.

Glaser porphyrin homodimer (34)

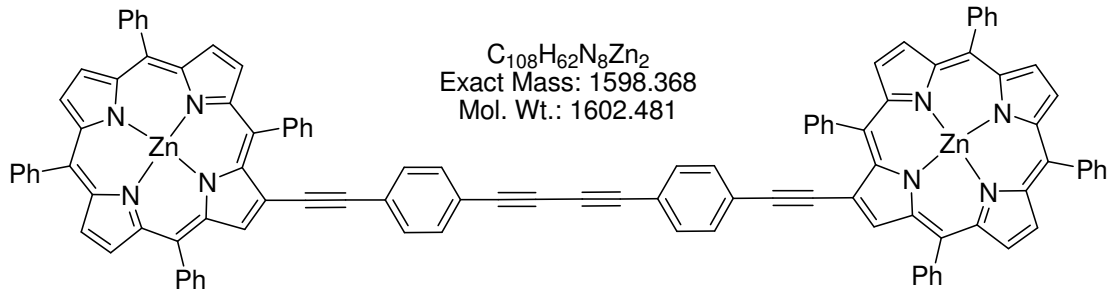

The unwanted homodimer was produced during the deprotection of **33** using TBAF when compound **33** was not adequately washed to remove Cu salts. ^{1}H NMR (500 MHz, $CDCl_3$, TMS): δ 9.27 (s, 2H, $H_{\beta\text{-pyrrolic}}$), 8.96 (s, 4H, $H_{\beta\text{-pyrrolic}}$), 8.93 (s, 4H, $H_{\beta\text{-pyrrolic}}$), 8.91 (d, 2H, J = 4.7 Hz, $H_{\beta\text{-pyrrolic}}$), 8.81 (d, 2H, J = 4.7 Hz, $H_{\beta\text{-pyrrolic}}$), 8.26-8.22 (m, 16H, H_{ortho}), 7.83-7.68 (m, 24H, $H_{meta,\ para}$), 7.54 (d, 4H, J = 8.2 Hz, $H_{aromatic}$), 7.38 (d, 4H, J = 7.9 Hz, $H_{aromatic}$). UV-Vis (CH_2Cl_2): λ_{max} [nm] ($\varepsilon \times 10^{-3}$) 432 (355), 558 (35.0), 593 (20.7). FAB-LRMS: *m/z* (%, assignment) cluster at 1599-1601, 1601 (100, M^+). HRMS: Calcd. for $(M+H)^+$ ($C_{108}H_{63}N_8{}^{64}Zn_2$): 1599.3758, found: 1599.3772.

2-(4′-Ethynylphenyl)ethynyl-5,10,15,20-tetraphenylporphyrinato zinc II (35)

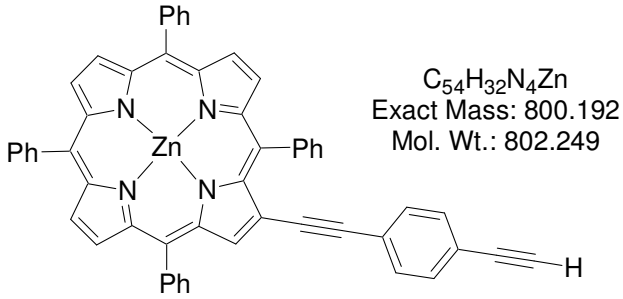

To a degassed solution of THF:DCM (2.5:1, 6 mL) 2-[4′-(trimethylsilyl)ethynylphenyl]ethynyl-5,10,15,20-tetraphenylporphyrinato zinc II (**34**, 200 mg, 0.230 mmol) was added and the reaction was stirred under Ar for 5 minutes at RT. Tetrabutylammonium fluoride (170 μL of a 1 M solution in THF, 0.74 eq) was added and stirring was continued for 5 minutes. The reaction mixture was diluted with DCM (50 mL), washed with degassed 20% aq. solution of $NaHCO_3$ (50 mL) then with degassed H_2O (50 mL). The organic layer was separated, dried over $MgSO_4$, filtered and taken to dryness to give a purple solid which was dissolved in DCM and purified through a plug of silica gel with DCM. The purple solution was taken to dryness to give a purple solid (178 mg, 97%). ^{1}H NMR (500 MHz, $CDCl_3$, TMS): δ 9.25 (s, 1H, $H_{\beta\text{-pyrrolic}}$), 8.95 (s, 2H, $H_{\beta\text{-pyrrolic}}$), 8.93 (s, 2H, $H_{\beta\text{-pyrrolic}}$), 8.89 (d, 1H, J = 4.6 Hz, $H_{\beta\text{-pyrrolic}}$),

8.79 (d, 1H, J = 4.6 Hz, $H_{\beta\text{-pyrrolic}}$), 8.25-8.21 (m, 8H, H_{ortho}), 7.84-7.63 (m, 12H, $H_{meta,\ para}$), 7.48 (d, 2H, J = 8.1 Hz, $H_{aromatic}$), 7.35 (d, 2H, J = 8.2 Hz, $H_{aromatic}$), 3.22 (s, 1H, CH). UV-Vis (CH_2Cl_2): λ_{max} [nm] ($\varepsilon \times 10^{-3}$) 286 (32.7), 431 (355), 556 (20.2), 591 (6.00). ESI-LRMS: *m/z* (%, assignment) cluster at 800-808, 800 (100, M^+). ESI-HRMS: Calcd for M^+ ($C_{52}H_{32}N_4Zn$): 800.1913 found: 800.1906.

Synthesis of compounds 36-40 are described in Chapter 8.4

4-[*trans*-2′-(5″,10″,15″,20″-Tetraphenylporphyrinato-2″-yl nickel II)ethen-1′-yl]azidobenzene (41)

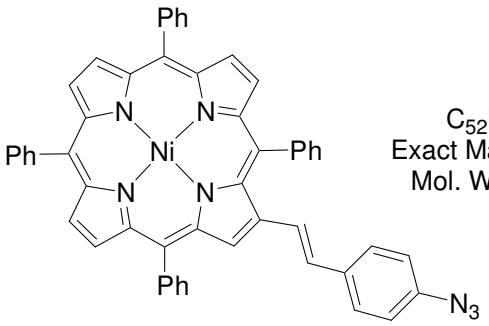

$C_{52}H_{33}N_7Ni$
Exact Mass: 813.215
Mol. Wt.: 814.559

To a solution of compound **23** (175 mg, 0.22 mmol) in THF (50 mL), $NaNO_2$ (122 mg, 1.76 mmol, 8 eq) in H_2O (400 μL) and H_2SO_4 (1 drop) were added and the mixture was stirred in darkness under Ar until no starting material was present by TLC (2 hrs). Afterwards NaN_3 (162 mg, 2.49 mmol, 11.3 eq) in H_2O (400 μL) was added and the reaction mixture was stirred for an additional 20 min. The resulting reaction mixture was diluted with DCM (150 mL), washed with H_2O (100 mL) then with a saturated aq. solution of $NaHCO_3$ (100 mL), dried over $MgSO_4$, filtered and the solvent was removed *in vacuo*. The resulting red solid was purified by silica gel column chromatography eluting the product with DCM:hexane (1:1) as a purple/red band. The resulting red solution was reduced *in vacuo* and the porphyrin was precipitated from DCM:MeOH giving a purple solid (175 mg, 98%). ^1H NMR (500 MHz, $CDCl_3$, TMS): δ 8.85 (s, 1H, $H_{\beta\text{-pyrrolic}}$), 8.70-8.66 (m, 6H, $H_{\beta\text{-pyrrolic}}$), 8.02-7.94 (m, 8H, H_{ortho}), 7.74-7.65 (m, 12H, $H_{meta,\ para}$), 7.15 (d, 2H, J = 8.5 Hz, $H_{aromatic}$), 7.06 (d, 1H, J = 16.2 Hz, $H_{1'\text{ or }2'}$), 6.96 (d, 2H, J = 8.5 Hz, $H_{aromatic}$), 6.78 (d, 1H, J = 16.2 Hz, $H_{1'\text{ or }2'}$). UV-Vis (CH_2Cl_2): λ_{max} [nm] ($\varepsilon \times 10^{-3}$) 426 (188), 538 (16.7), 572 (11.0). ESI-LRMS: *m/z* (%, assignment) cluster at 813-813, 818 (100, M^+). ESI-HRMS: Calcd for M^+ ($C_{52}H_{33}N_7Ni$): 813.2145, found: 813.2162. IR-ATR (cm^{-1}): 2116.0 (azide).

4-[*trans*-2′-(5″,10″,15″,20″-Tetraphenylporphyrin-2″-yl)ethen-1′-yl]azidobenzene (42)

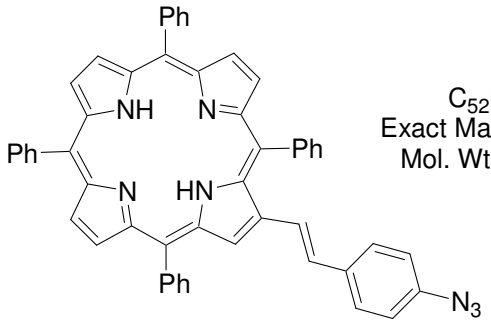

$C_{52}H_{35}N_7$
Exact Mass: 757.295
Mol. Wt.: 757.881

To a solution of compound **20** (70 mg, 96 μmol) in THF (100 mL), $NaNO_2$ (22 mg, 0.32 mmol, 33 eq) in H_2O (50 μL) and H_2SO_4 (1 drop) were added and the reaction was stirred in darkness under Ar until no starting material was present by TLC (3 hrs). Afterwards NaN_3 (27 mg, 0.41 mmol, 42 eq) in H_2O (100 μL) was added and the reaction mixture was stirred for an additional 10 min. The resulting reaction mixture was diluted with DCM (150 mL), washed with H_2O (100 mL) then with a saturated aq. solution of $NaHCO_3$ (100 mL), dried over $MgSO_4$, filtered and the solvent was removed *in vacuo* to give a purple solid (69 mg, 96%). ^{1}H NMR (500 MHz, $CDCl_3$, TMS): δ 9.02 (s, 1H, $H_{\beta\text{-pyrrolic}}$), 8.87 (s, 2H, $H_{\beta\text{-pyrrolic}}$), 8.85 (d, 1H, J = 4.9 Hz, $H_{\beta\text{-pyrrolic}}$), 8.81 (d, 2H, J = 4.8 Hz, $H_{\beta\text{-pyrrolic}}$), 8.75 (d, 1H, J = 4.7 Hz, $H_{\beta\text{-pyrrolic}}$), 8.29-8.21 (m, 8H, H_{ortho}), 7.86-7.76 (m, 12H, $H_{meta,\ para}$), 7.27 (d, 1H, J = 16.0 Hz, $H_{1'\text{ or }2'}$), 7.26 (d, 2H, J = 7.4 Hz, $H_{aromatic}$), 7.02 (d, 2H, J = 7.4 Hz, $H_{aromatic}$), 6.95 (d, 1H, J = 16.0 Hz, $H_{1'\text{ or }2'}$), -2.55 (br s, 2H, NH). UV-Vis (CH_2Cl_2): λ_{max} [nm] ($\varepsilon \times 10^{-3}$) 424.5 (168), 524.5 (15.2), 563.5 (8.68), 598.5, (5.67), 656.5 (1.94). ESI-LRMS: *m/z* (%, assignment) cluster at 758-761, 758 (100, $(M+H)^+$). HRMS: Calcd for $(M+H)^+$ ($C_{52}H_{35}N_7$): 758.3027, found: 758.3029. IR-ATR (cm^{-1}): 2115.7 (azide).

2-(4′-Azidophenyl)ethynyl-5,10,15,20-tetraphenylporphyrinato zinc II (45)

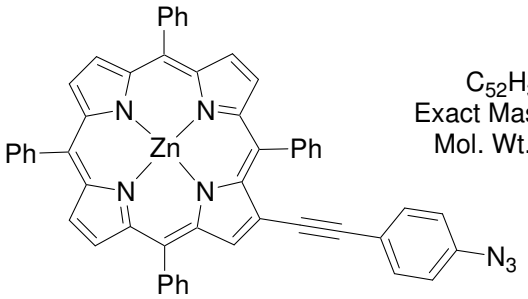

$C_{52}H_{31}N_7Zn$
Exact Mass: 817.193
Mol. Wt.: 819.239

To a solution of 2-(4′-iodophenyl)ethynyl-5,10,15,20-tetraphenylporphyrinato zinc II (**32**, 60 mg, 66 μmol) in dry DMSO (3 mL), NaN_3 (8.4 mg, 132 μmol, 2 eq), sodium ascorbate (1.2 mg, 6.6 μmol, 0.1 eq) and tetrakis(acetonitrile)copper(I) hexafluorophosphate (9.9 mg, 13.2 mmol, 0.2 eq) were added at once followed by *N*,*N*-DMEA (2.04 μL, 19.2 μmol, 0.3 eq). The reaction mixture was heated at 70 °C until TLC showed no starting material (48 hrs), cooled to RT, diluted with DCM (30 mL), washed with H_2O (30 mL) then with 5% aq. solution of Na_2EDTA (30 mL). The organic layer was separated, dried over $MgSO_4$, filtered and the solvent was removed *in vacuo*. The crude material was purified by silica gel column chromatography eluting the product in DCM:hexane (1:1) which was taken to dryness to give a purple solid (33 mg, 61%). ^{1}H NMR (500 MHz, $CDCl_3$, TMS): δ 9.24 (s, 1H, $H_{\beta\text{-pyrrolic}}$), 8.94 (s, 2H, $H_{\beta\text{-pyrrolic}}$), 8.93 (s, 2H, $H_{\beta\text{-pyrrolic}}$), 8.89 (d, 1H, J = 4.7 Hz, $H_{\beta\text{-pyrrolic}}$), 8.78 (d, 1H, J = 4.6 Hz, $H_{\beta\text{-pyrrolic}}$), 8.25-8.21 (m, 8H, H_{ortho}), 7.81-7.66 (m, 12H, $H_{meta,\ para}$), 7.38 (d, 2H, J = 8.5 Hz, $H_{aromatic}$), 7.01 (d, 2H, J = 8.8 Hz, $H_{aromatic}$). UV-Vis (CH_2Cl_2): λ_{max} [nm] ($\varepsilon \times 10^{-3}$) 281 (20.0), 430 (202), 556 (16.2), 593 (7.4). ESI-LRMS: *m/z* (%, assignment) cluster at 817-723, 817 (100, M^+). ESI-HRMS: Calcd for M^+ ($C_{52}H_{31}N_7Zn$): 817.1927, found: 817.1948. IR-ATR (cm^{-1}): 2105.2 (azide).

4-(Bromomethyl)benzonitrile

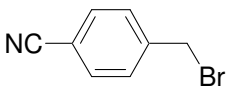

C_8H_6BrN
Exact Mass: 194.968
Mol. Wt.: 196.044

To a solution of *para*-tolunitrile (11.75 g, 0.1 mmol) in CCl_4 (100 mL), NBS (19.58 g, 0.11 mmol, 1.1 eq) was added and the reaction mixture was refluxed for 2 hrs with halogen lamp light irradiation. The reaction mixture was filtered while hot and the filtrate was taken to dryness to give a solid which was recrystallized twice from EtOH to give pure white needles (12.14g, 62%). ^{1}H NMR (400 MHz, $CDCl_3$, TMS): δ 7.64 (d, 2H, J = 8.4 Hz, $H_{aromatic}$), 7.50 (d, 2H, J = 8.4 Hz, $H_{aromatic}$), 4.47 (s, 2H, CH_2Br).

4-(Bromomethyl)benzaldehyde (46)

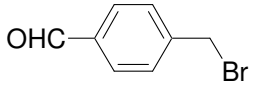

C_8H_7BrO
Exact Mass: 197.968
Mol. Wt.: 199.045

4-(Bromomethyl)benzaldehyde was synthesised from 4-(bromomethyl)benzonitrile according to the procedure described by Schlenoff *et al.*[105]

4-(Azidomethyl)benzaldehyde (47)

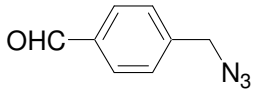

$C_8H_7N_3O$
Exact Mass: 161.059
Mol. Wt.: 161.161

4-(Azidomethyl)benzaldehyde was synthesised from 4-(bromomethyl)benzaldehyde according to the procedure described by Barbe *et al.*[106]

4-[*trans*-2′-(5″,10″,15″,20″-Tetraphenylporphyrin-2″-yl)ethen-1′-yl] azidomethylbenzene (48)

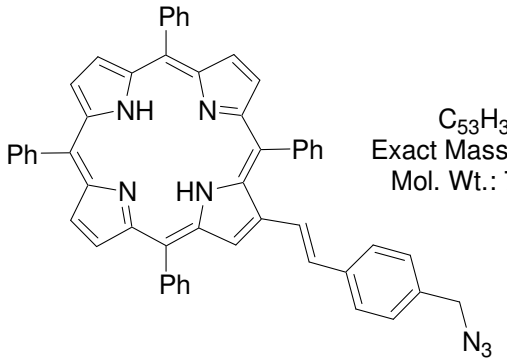

$C_{53}H_{37}N_7$
Exact Mass: 771.311
Mol. Wt.: 771.908

DBU (250 μL, 1.67 mmol, 3.1 eq) was added to a solution of TPPps (**3**, 500 mg, 0.54 mmol) and 4-(azidomethyl)benzaldehyde (**47**, 260 mg, 1.13 mmol, 3 eq) in DCM (100 mL) and the reaction was stirred at RT under Ar for 20 minutes. After TLC indicated that phosphonium salt had completely reacted, the solvent was reduced *in vacuo* and the resulting solid was precipitated from DCM:MeOH. The resulting purple solid was collected by filtration as a *cis/trans* (35:65) isomeric mixture (340 mg 76%) that also contained a small amount of $TPPCH_3$ (**7**) according to ^1H NMR spectroscopy. The isomeric mixture was dissolved in $CHCl_3$ (100 mL) and I_2 (103 mg, 0.41 mmol, 1.0 eq) was added. After stirring in darkness at RT overnight, saturated aq. solution of $Na_2S_2O_3$ (100 mL) was added and stirring was continued for an additional 15 minutes. The organic layer was separated, dried over $MgSO_4$, filtered and the solvent was removed *in vacuo* to give the *trans* product. The resulting purple solid was dissolved in DCM (20 mL), diluted with hexane (20 mL) and purified by silica gel column chromatography

first eluting traces of $TPPCH_3$ with DCM:hexane (1:1) then the desired product as a purple band with MeOH:DCM (1:19). The solvent was reduced *in vacuo* and the porphyrin was precipitated with DCM:MeOH. The porphyrin precipitate was collected by filtration to give pure *trans* product (270 mg, 60% overall) as a purple powder. ^{1}H NMR (400 MHz, d_6-DMSO): δ 9.02 (s, 1H, $H_{\beta\text{-pyrrolic}}$), 8.83-8.72 (m, 5H, $H_{\beta\text{-pyrrolic}}$), 8.67 (d, 1H, J = 4.8 Hz, $H_{\beta\text{-pyrrolic}}$), 8.26-8.18 (m, 8H, H_{ortho}), 7.89-7.80 (m, 12H, $H_{meta,\ para}$), 7.42 (d, 1H, J = 16.2 Hz, $H_{1'\text{ or }2'}$), 7.36 (d, 2H, J = 8.1 Hz, $H_{aromatic}$), 7.30 (d, 2H, J = 8.1 Hz, $H_{aromatic}$), 6.94 (d, 1H, J = 15.9 Hz, $H_{1'\text{ or }2'}$), 4.49 (s, 2H, CH_2N_3), -2.72 (br s, 2H, NH). UV-Vis (CH_2Cl_2): λ_{max} [nm] ($\varepsilon \times 10^{-3}$) 425 (172), 523 (12.4), 559 (7.60), 597 (4.83), 651 (1.79). ESI-LRMS: *m/z* (%, assignment) cluster at 772-775, 772 (100, $(M+H)^+$). ESI-HRMS: Calcd for $(M+H)^+$ ($C_{53}H_{38}N_7$): 772.3183, found: 772.3183. IR-ATR (cm^{-1}): 2096.6 (azide).

4-[*trans*-2′-(5″,10″,15″,20″-Tetraphenylporphyrinato-2″-yl zinc II)ethen-1′-yl] azidomethylbenzene (49)

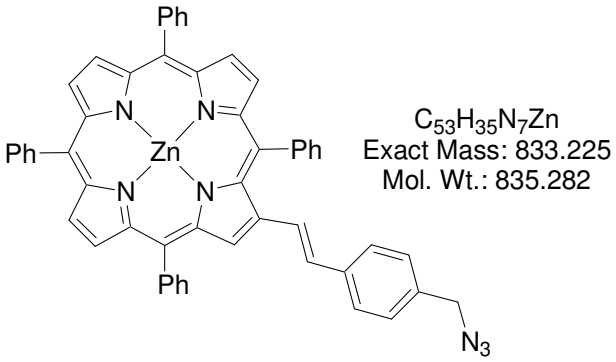

$Zn(OAc)_2 \cdot 2H_2O$ (31.3 mg, 0.14 mmol, 1.1 eq) in MeOH (2.5 mL) was added to a solution of porphyrin **48** (100 mg, 0.13 mmol) in DCM (25 mL) and the reaction was stirred at RT for 1 hr. The solvent was reduced *in vacuo* and the resulting solid was dissolved in DCM and purified through a plug of silica gel with DCM. The solvent was removed *in vacuo* to give a purple solid (105 mg, 97%). ^{1}H NMR (500 MHz, d_6-DMSO): δ 8.96 (s, 1H, $H_{\beta\text{-pyrrolic}}$), 8.76-8.71 (m, 5H, $H_{\beta\text{-pyrrolic}}$), 8.63 (d, 1H, J = 4.2 Hz, $H_{\beta\text{-pyrrolic}}$), 8.21-7.91 (m, 8H, H_{ortho}), 7.82-7.78 (m, 12H, $H_{meta,\ para}$), 7.35 (d, 2H, J = 7.3 Hz, $H_{aromatic}$), 7.29 (d, 2H, J = 7.4 Hz, $H_{aromatic}$), 7.27 (d, 1H, J = 16.0 Hz, $H_{1'\text{ or }2'}$), 6.98 (d, 1H, J = 16.0 Hz, $H_{1'\text{ or }2'}$), 4.48 (s, 2H, CH_2N_3). UV-Vis (CH_2Cl_2): λ_{max} [nm] ($\varepsilon \times 10^{-3}$) 428.5 (229), 556 (20.0), 591.5 (7.39). ESI-LRMS: *m/z* (%, assignment) cluster

at 833-842, 834 (100, $(M+H)^+$). HRMS: Calcd for $(M+H)^+$ ($C_{52}H_{36}N_7$): 834.2318, found: 834.2282. IR-ATR (cm^{-1}): 2097.1 (azide).

4-[*trans*-2′-(5″,10″,15″,20″-Tetraphenylporphyrinato-2″-yl nickel II)ethen-1′-yl] azidomethylbenzene (50)

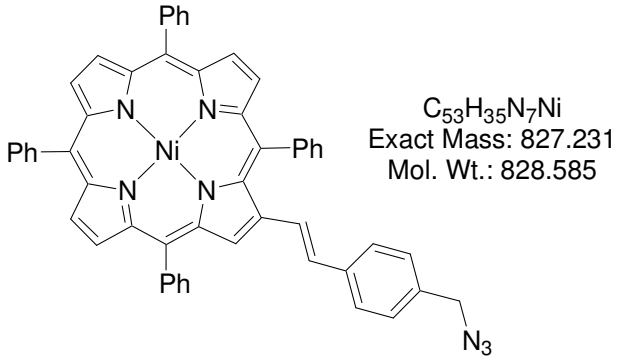

$Ni(OAc)_2 \cdot 4H_2O$ (240 mg, 0.96 mmol, 12.5 eq) in MeOH (10 mL) was added to a refluxing solution of porphyrin **48** (60 mg, 77.8 μmol) in $CHCl_3$ (90 mL) and refluxing was continued overnight. After cooling the solvent was reduced *in vacuo* and the porphyrin was precipitated from DCM:MeOH. The desired product was collected by filtration to give a red solid (60 mg, 99%). ^{1}H NMR (400 MHz, d_6-DMSO): δ 8.91 (s, 1H, $H_{\beta\text{-pyrrolic}}$), 8.68-8.63 (m, 6H, $H_{\beta\text{-pyrrolic}}$), 8.03-7.95 (m, 8H, H_{ortho}), 7.85-7.73 (m, 12H, $H_{meta,\ para}$), 7.32 (d, 2H, J = 8.3 Hz, $H_{aromatic}$), 7.27 (d, 1H, J = 16.3 Hz, $H_{1'\text{ or }2'}$), 7.21 (d, 2H, J = 8.4 Hz, $H_{aromatic}$), 6.81 (d, 1H, J = 16.0 Hz, $H_{1'\text{ or }2'}$), 4.46 (s, 2H, CH_2N_3). UV-Vis (CH_2Cl_2): λ_{max} [nm] ($\varepsilon \times 10^{-3}$) 425 (176), 538 (16.1), 570 (10.2). ESI-LRMS: *m/z* (%, assignment) cluster at 827-831, 828 (100, $(M+H)^+$).ESI-HRMS: Calcd for M^+ ($C_{53}H_{35}N_7Ni$): 827.2302, found: 827.2312. IR-ATR (cm^{-1}): 2096.1 (azide).

4-[*trans*-2′-(5″,10″,15″,20″-Tetraphenylporphyrinato-2″-yl iron III chloride)ethen-1′-yl] azidomethylbenzene (51)

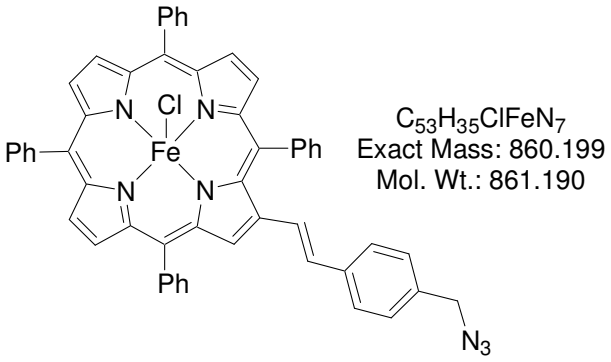

$C_{53}H_{35}ClFeN_7$
Exact Mass: 860.199
Mol. Wt.: 861.190

Spectroscopic grade acetonitrile (120 mL) was refluxed under argon for two hours to remove dissolved oxygen. The temperature was lowered to 70 °C and $FeCl_2 \cdot 4H_2O$ (320 mg, 1.61 mmol, 15.6 eq) was added. Porphyrin **48** (80 mg, 0.10 mmol) was dissolved in degassed chloroform (15 mL) and added slowly to the reaction mixture over 5 minutes. The temperature was increased and the solution was refluxed for a further 5 hours under Ar then overnight open to the air. The cooled solution was extracted with DCM (200 mL) and the organic layer was washed with 0.1 M HCl solution (6 × 100 mL) to extract the inorganic salts. The organic layer was separated, dried over $CaCl_2$ and the solvent was removed *in vacuo* to give a brown solid. The solid was dissolved in DCM and purified by silica gel column chromatography (3% MeOH:DCM) eluting the desired product as a brown band. The solvent was removed *in vacuo*, the purple solid dissolved in DCM (20 mL) and filtered through a #4 glass sinter. The solvent was removed *in vacuo* to give a purple solid (80 mg, 90%). UV-Vis (CH_2Cl_2): λ_{max} [nm] ($\varepsilon \times 10^{-3}$) 425 (132), 579 (10.1), 615 (6.80). ESI-LRMS: *m/z* (%, assignment) cluster at 825-827, 825 (100, M-Cl^+) and 860-865 (2, M^+). HRMS: Calcd for M^+ ($C_{53}H_{35}ClFeN_7$): 860.1986, found: 860.2002. IR-ATR (cm^{-1}): 2095.8 (azide).

8.4 Experimental Procedures for Chapter 3 - Synthesis of *β*-Pyrrolic Ethynyl Porphyrin Derivatives *via* the Modified Horner-Emmons Reaction

General Method for the Synthesis of Diphenyl hydroxyphenylmethylphosphonates

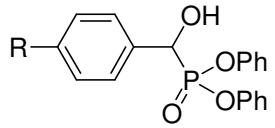

Diphenyl hydroxylphenylmethylphosphonates were prepared using the method from Kondo *et al.*[122] and Katritzky *et al.*[100] Aldehyde (*ca.* 40 mmol) was melted in a 250 mL round bottom flask using a heat gun if required. Diphenolphosphite (1 eq) followed by MgO (1 eq) were added and the reaction mixture was stirred overnight at RT to give a white solid. The solid was sonicated in $CHCl_3$ (200 mL) for 1 hr, filtered through fluted filter paper and washed with $CHCl_3$ until the eluent was clear by TLC. The solvent was removed *in vacuo* and the resulting solid was purified (if required) by silica gel column chromatography first eluting traces of the aldehyde then eluting the product. The solvent was removed *in vacuo*, the residue was dissolved in hot DCM, filtered through a #4 sinter and the solvent was removed *in vacuo* to give a white solid.

Diphenyl hydroxy(4-iodophenyl)methylphosphonate (29)

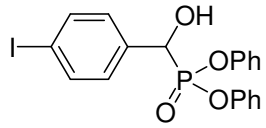

$C_{19}H_{16}IO_4P$
Exact Mass: 465.983
Mol. Wt.: 466.206

Compound **29** was isolated in 84% yield. Purified by silica gel column chromatography with MeOH:DCM (1:49). ^{1}H NMR (400 MHz, $CDCl_3$, TMS): δ 7.72 (dd, 2H, *J* = 8.6 and 0.7 Hz, $H_{aromatic}$), 7.32 (dd, 2H, *J* = 8.5 and 2.9 Hz, $H_{aromatic}$), 7.28-7.25 (m, 4H, $H_{aromatic}$), 7.18-7.13 (m, 2H, $H_{aromatic}$), 7.07-7.01 (m, 4H, $H_{aromatic}$), 5.28 (d, 1H, *J* = 9.3 Hz, CH), 3.40 (br s, 1H, OH). ESI-LRMS: *m/z* (%, assignment) cluster at 489-491, 489, (100, $(M+Na)^+$). ESI-HRMS: Calcd for $(M+Na)^+$ ($C_{19}H_{16}INaO_4P$): 488.9723, found: 488.9723.

Diphenyl hydroxy(4-bromophenyl)methylphosphonate (36)

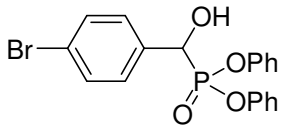

$C_{19}H_{16}BrO_4P$
Exact Mass: 417.997
Mol. Wt.: 419.206

Compound **36** was isolated in 90% yield. No chromatographic purification was required. ^{1}H NMR (500 MHz, $CDCl_3$, TMS): δ 7.49 (dd, 2H, *J* = 8.8 and 0.7 Hz, $H_{aromatic}$), 7.43 (dd, 2H, *J* = 8.8 and 2.9 Hz, $H_{aromatic}$), 7.29-7.24 (m, 4H, $H_{aromatic}$), 7.17-7.13 (m, 2H, $H_{aromatic}$), 7.06-7.01 (m, 4H, $H_{aromatic}$), 5.24 (d, 1H, *J* = 9.3 Hz, CH), 4.16 (br s, 1H, OH). FAB-LRMS: *m/z* (%, assignment) cluster at 419-422, 419, (100, $(M+H)^+$). HRMS: Calcd. for $(M+H)^+$ ($C_{19}H_{17}{}^{79}BrO_4P$): 419.0048, found: 419.0043.

Diphenyl hydroxyphenylmethylphosphonate (52)

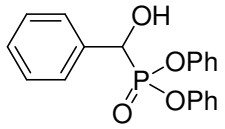

$C_{19}H_{17}O_4P$
Exact Mass: 340.086
Mol. Wt.: 340.31

Compound **52** was isolated in 73% yield. No chromatographic purification was required. Spectroscopic data is in agreement with Katritzky *et al.*[100]

Diphenyl hydroxy(4-methoxyphenyl)methylphosphonate (53)

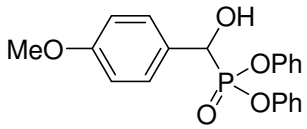

$C_{20}H_{19}O_5P$
Exact Mass: 370.097
Mol. Wt.: 370.336

Compound **53** was isolated in 90% yield. No chromatographic purification was required. Spectroscopic data is in agreement with Kondo *et al.* [122]

Diphenyl hydroxy(4-methoxycarbonylphenyl)methylphosphonate (54)

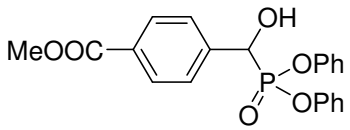

$C_{21}H_{19}O_6P$
Exact Mass: 398.092
Mol. Wt.: 398.346

Compound **54** was isolated in 82% yield. No chromatographic purification was required. ^{1}H NMR (500 MHz, $CDCl_3$, TMS): δ 8.08 (d, 2H, *J* = 8.1 Hz, $H_{aromatic}$), 7.67 (dd, 2H, *J* = 8.2, 2.2 Hz, $H_{aromatic}$), 7.32-7.03 (m, 10H, $H_{aromatic}$), 5.40 (d, 1H, *J* = 9.8 Hz, CH), 4.25 (br s, 1H, OH), 3.96 (s, 3H, CH_3). FAB-LRMS: *m/z* (%, assignment) cluster at 398-401, 399 (100, $(M+H)^+$). HRMS: Calcd for $(M+H)^+$ ($C_{21}H_{20}O_6P$): 399.0998, found: 399.0995.

Diphenyl hydroxy(4-pyridyl)methylphosphonate (55)

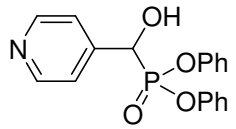

$C_{18}H_{16}NO_4P$
Exact Mass: 341.082
Mol. Wt.: 341.298

Reaction was preformed at 0 °C according to the procedure of Kondo *e. al.*[103] and compound **55** was isolated in 82% yield. No chromatographic purification was required. Spectroscopic data is in agreement with Kondo *et al*. [122]

Diphenyl hydroxy[4-(5′,5′-dimethyl-1′,3′-dioxane-2′-yl)phenyl]methyl phosphonate (56)

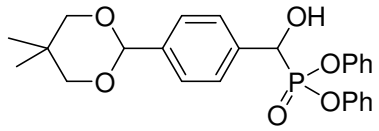

$C_{25}H_{27}O_6P$
Exact Mass: 454.155
Mol. Wt.: 454.452

Compound **56** was isolated in 88% yield. No chromatographic purification was required. ^{1}H NMR (500 MHz, $CDCl_3$, TMS): δ 7.61 (dd, 2H, *J* = 8.3, 2.2 Hz, $H_{aromatic}$), 7.56 (d, 2H, *J* = 8.3 Hz, $H_{aromatic}$), 7.31-7.13 (m, 6H, $H_{aromatic}$), 7.10-7.08 (m, 2H, $H_{aromatic}$), 7.06-7.03 (m, 2H, $H_{aromatic}$), 5.43 (s, 1H, CH), 5.27 (dd, 1H, *J* = 9.3, 5.0 Hz, C**H**OH), 3.81 (d, 2H, *J* = 11 Hz, CH_2), 3.81 (d, 2H, *J* = 11Hz, CH_2), 3.72 (br s, 1H, OH) 1.32 (s, 3H, CH_3), 0.84 (s, 3H, CH_3). FAB-LRMS: *m/z* (%, assignment) cluster at 453-457, 455 (100, $(M+H)^+$). HRMS: Calcd for $(M+H)^+$ ($C_{25}H_{28}O_6P$): 455.1623, found: 455.1621.

Diphenyl hydroxy(4-benzonitrile)methylphosphonate (57)

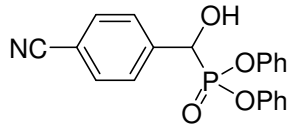

$C_{20}H_{16}NO_4P$
Exact Mass: 365.082
Mol. Wt.: 365.319

Compound **57** was isolated in 70% yield. Purified by silica gel column chromatography with DCM. ^{1}H NMR (500 MHz, $CDCl_3$, TMS): δ 7.65 (dd, 2H, *J* = 8.2, 1.7 Hz, $H_{aromatic}$), 7.56 (d, 2H, *J* = 8.2 Hz, $H_{aromatic}$), 7.37-6.99 (m, 10H, $H_{aromatic}$), 5.20 (d, 1H, *J* = 13.8 Hz, CH). ESI-LRMS: *m/z* (%, assignment) cluster at 366-368, 366, (100, $(M+H)^+$). ESI-HRMS: Calcd for $(M+H)^+$ ($C_{20}H_{17}NO_4P$): 366.8090, found: 366.0887.

Diphenyl hydroxy(4-nitrophenyl)methylphosphonate (58)

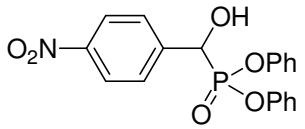

$C_{19}H_{16}NO_6P$
Exact Mass: 385.072
Mol. Wt.: 385.307

Compound **58** was isolated in 84% yield. No chromatographic purification was required. Spectroscopic data is in agreement with Kondo *et al.* [122]

General Method for the Synthesis of Diphenyl Chlorophenylmethylphosphonates

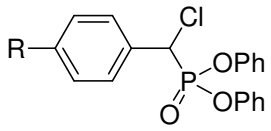

Diphenyl chlorophenylmethylphosphonates were prepared using the method from Kondo *et al.*[103] To the appropriate hydroxymethylphosphates, $POCl_3$ (2 mL/g of hydroxymethylphosphate) and *N,N*-diethylaniline (0.2 mL/g of hydroxymethylphosphate) was combined and heated at 90 °C for 1 hr. The resulting solution was cooled to RT then poured slowly into ice. The resulting solid was extracted into DCM (150 mL), the organic layer was separated and washed with saturated aq solution of $NaHCO_3$ solution (3 × 150 mL). The organic layer was separated, dried over $MgSO_4$, filtered and the solvent was removed *in vacuo*. The resulting solid was dissolved in DCM and filtered through a plug of silica gel with DCM. The solvent was removed *in vacuo* to give a white solid that solidified with time. Filtration of the solid gave the desired product.

Diphenyl chloro(4-bromophenyl)methylphosphonate (37)

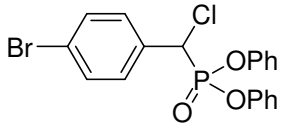

$C_{19}H_{15}BrClO_3P$
Exact Mass: 435.963
Mol. Wt.: 437.651

Compound **37** was isolated in 22% yield. ^{1}H NMR (500 MHz, $CDCl_3$, TMS): δ 7.56-7.50 (m, 4H, $H_{aromatic}$), 7.46-7.27 (m, 4H, $H_{aromatic}$), 7.23-7.15 (m, 4H, $H_{aromatic}$), 7.02 (d, 2H, J = 8.8 Hz, $H_{aromatic}$), 5.23 (d, 1H, J = 14.0 Hz, CH). FAB-LRMS: *m/z* (%, assignment) cluster at 436-441, 438 (100, $(M+H)^+$). HRMS: Calcd. for $(M+H)^+$ ($C_{19}H_{16}{}^{81}Br^{35}ClO_3P$): 438.9688, found: 438.9695.

Diphenyl chlorophenylmethylphosphonate (59)

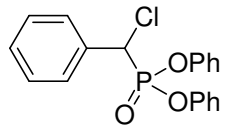

$C_{19}H_{16}ClO_3P$
Exact Mass: 358.053
Mol. Wt.: 358.755

Compound **59** was isolated in 19% yield. Spectroscopic data is in agreement with Katritzky *et al.*[100]

Diphenyl chloro(4-methoxyphenyl)methylphosphonate (60)

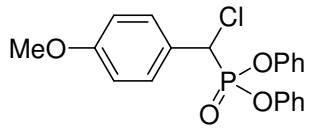

$C_{20}H_{18}ClO_4P$
Exact Mass: 388.063
Mol. Wt.: 388.781

Compound **60** was isolated in 25% yield. Spectroscopic data is in agreement with Kondo *et al.* [122]

Diphenyl chloro(4-methoxycarbonylphenyl)methylphosphonate (61)

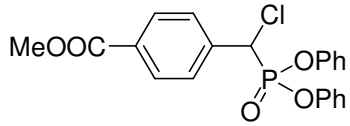

$C_{21}H_{18}ClO_5P$
Exact Mass: 416.058
Mol. Wt.: 416.791

Compound **61** was isolated in 17% yield. ^{1}H NMR (500 MHz, $CDCl_3$, TMS): δ 8.05 (d, 2H, J = 8.1 Hz, $H_{aromatic}$), 7.70 (dd, 2H, J = 8.6, 2.0 Hz, $H_{aromatic}$), 7.32-7.17 (m, 6H, $H_{aromatic}$), 7.13-7.10 (m, 2H, $H_{aromatic}$), 7.00-6.99 (m, 2H, $H_{aromatic}$), 5.30 (d, 1H, J = 14.0 Hz, CH), 3.93 (s, 3H, CH_3). FAB-LRMS: *m/z* (%, assignment) cluster at 416-420, 417 (100, $(M+H)^+$). HRMS: Calcd for $(M+H)^+$ ($C_{21}H_{19}O_5P^{35}Cl$): 417.0659, found: 417.0661.

Diphenyl chloro(4-pyridyl)methylphosphonate (62)

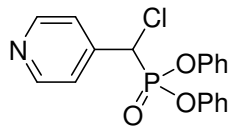

$C_{18}H_{15}ClNO_3P$
Exact Mass: 359.048
Mol. Wt.: 359.743

Compound **62** was isolated in 45% yield. Spectroscopic data is in agreement with Kondo *et al.*[103]

Diphenyl chloro(4-nitrophenyl)methylphosphonate (66)

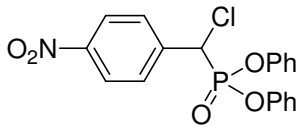

$C_{19}H_{15}ClNO_5P$
Exact Mass: 403.038
Mol. Wt.: 403.753

Compound **66** was isolated in 35% yield. Spectroscopic data is in agreement with Kondo *et al*. [122]

General Method for the Synthesis of Diphenyl Bromophenylmethylphosphonates

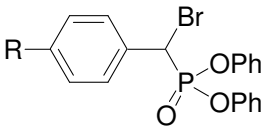

Diphenyl bromophenylmethylphosphonates were prepared using the method from Firouzabadi *et al.*[99] To a solution of DDQ (2 eq), PPh_3 (2 eq) and nBu$_4$NBr (2 eq) in dry DCM (30 mL/g of phosphonate), the appropriate hydroxymethylphosphates (1 eq) were added and the reaction was stirred overnight under Ar at RT. On completion, the reaction mixture was washed with H_2O (3 × 100 mL). The organic layer was separated, dried over $MgSO_4$, filtered and the solvent was removed *in vacuo*. The resulting oil was purified by silica gel column chromatography eluting the product as a colourless fraction with DCM unless otherwise stated. The solvent was removed *in vacuo* to give a slightly yellow oil that solidified on cooling

Diphenyl bromo(4-iodophenyl)methylphosphonate (30)

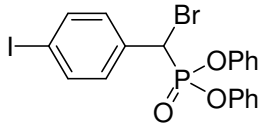

$C_{19}H_{15}BrIO_3P$
Exact Mass: 527.899
Mol. Wt.: 529.103

Compound **30** was isolated in 84% yield. ^{1}H NMR (500 MHz, $CDCl_3$, TMS): δ 7.73 (d, 2H, J = 8.2, Hz, $H_{aromatic}$), 7.40 (dd, 2H, J = 8.2 and 1.5 Hz, $H_{aromatic}$), 7.38-7.33 (m, 2H, $H_{aromatic}$), 7.27-7.15 (m, 6H, $H_{aromatic}$), 6.98 (d, 2H, J = 8.5 Hz , $H_{aromatic}$), 5.13 (d, 1H, J = 13.1 Hz, CH). ESI-LRMS: *m/z* (%, assignment) cluster at 529-533, 531, (100, $(M+H)^+$). ESI-HRMS: Calcd for $(M+H)^+$ ($C_{19}H_{16}BrIO_3P$): 528.9060, found: 528.9047.

Diphenyl bromo(4-bromophenyl)methylphosphonate (38)

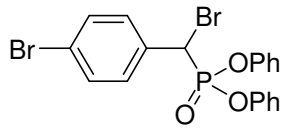

$C_{19}H_{15}Br_2O_3P$
Exact Mass: 479.913
Mol. Wt.: 482.102

Compound **38** was isolated in 84% yield. ^{1}H NMR (500 MHz, $CDCl_3$, TMS): δ 7.54-7.53 (m, 4H, $H_{aromatic}$), 7.37-34 (m, 2H, $H_{aromatic}$), 7.29-7.15 (m, 6H, $H_{aromatic}$), 7.00-7.15 (m, 6H, $H_{aromatic}$), 700-6.98 (m, 2H, $H_{aromatic}$), 5.16 (d, 1H, *J* = 13.0 Hz, CH). FAB-LRMS: *m/z* (%, assignment) cluster at 481-485, 483 (100, $(M+H)^+$). HRMS: Calcd. for $(M+H)^+$ ($C_{19}H_{16}{}^{79}Br^{81}BrO_3P$): 482.9183, found: 482.9179.

Diphenyl bromo[4-(5′,5′-dimethyl-1′,3′-dioxane-2′-yl)phenyl]methylphosphonate (64)

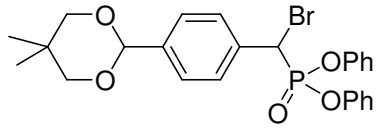

$C_{25}H_{26}BrO_5P$
Exact Mass: 516.07
Mol. Wt.: 517.349

Compound **64** was isolated in 64% yield. Purified by silica gel column chromatography with MeOH:DCM (1:49). ^{1}H NMR (500 MHz, $CDCl_3$, TMS): δ 7.65 (dd, 2H, *J* = 8.3, 1.8 Hz, $H_{aromatic}$), 7.56 (d, 2H, *J* = 8.3 Hz, $H_{aromatic}$), 7.37-7.10 (m, 8H, $H_{aromatic}$), 6.97-9.95 (m, 2H, $H_{aromatic}$), 5.39 (s, 1H, CH), 5.18 (d, 1H, *J* = 12.8 Hz, C**H**OH), 3.77 (d, 2H, *J* = 11.1 Hz, CH_2), 3.65 (d, 2H, *J* = 11.1 Hz, CH_2), 1.28 (s, 3H, CH_3), 0.80 (s, 3H, CH_3). FAB-LRMS: *m/z* (%, assignment) cluster at 515-521, 517 (50, $(M+H)^+$). HRMS: Calcd for $(M+H)^+$ ($C_{25}H_{27}{}^{79}BrO_5P$): 517.0779, found: 517.0764.

Diphenyl bromo(4-cyanophenyl)methylphosphonate (65)

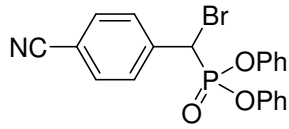

$C_{20}H_{15}BrNO_3P$
Exact Mass: 426.997
Mol. Wt.: 428.216

Compound **65** was isolated in 70% yield. ^{1}H NMR (500 MHz, $CDCl_3$, TMS): δ 7.65 (dd, 2H, *J* = 8.2, 1.7 Hz, $H_{aromatic}$), 7.56 (d, 2H, *J* = 8.2 Hz, $H_{aromatic}$), 7.37-6.99 (m, 10H, $H_{aromatic}$), 5.20 (d, 1H, *J* = 13.8 Hz, CH). FAB-LRMS: *m/z* (%, assignment) cluster at 427-433, 428 (100, $(M+H)^+$). HRMS: Calcd for $(M+H)^+$ ($C_{20}H_{16}{}^{81}BrNO_3P$): 430.0031, found: 430.0029.

2-(4′-Iodophenyl)ethynyl-5,10,15,20-tetraphenylporphyrin (31)

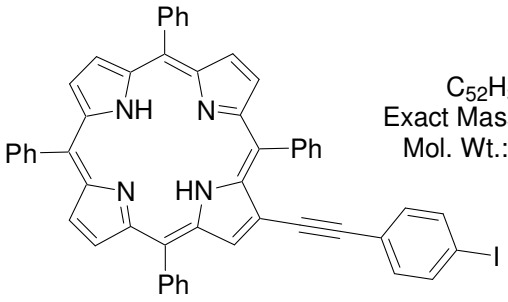

$C_{52}H_{33}IN_4$
Exact Mass: 840.175
Mol. Wt.: 840.750

TPP-CHO (**2**, 600 mg, 0.89 mmol) was dissolved in dry THF (80 mL). To this diphenyl bromo(4-iodophenyl)methylphosphonate (**30**, 1.41 mg, 2.67 mmol, 3 eq) and *t*-BuOK (8.0 g) were added and the reaction was stirred under Ar at RT for 3 hrs. Following this, DCM (50 mL) was added and the resulting purple solution was washed with H_2O (2 × 100 mL) then neutralised with dilute AcOH. The organic layer was separated, dried over $MgSO_4$ and filtered. The solvent was reduced *in vacuo* and the porphyrin was precipitated from DCM:MeOH to give a red powder that was collected by filtration (560 mg, 75%). ^{1}H NMR (500 MHz, $CDCl_3$, TMS): δ 9.08 (s, 1H, $H_{\beta\text{-pyrrolic}}$), 8.90 (s, 1H, $H_{\beta\text{-pyrrolic}}$), 8.84 (d, 1H, J = 4.8 Hz, $H_{\beta\text{-pyrrolic}}$), 8.79 (s, 1H, $H_{\beta\text{-pyrrolic}}$), 8.78 (s, 2H, $H_{\beta\text{-pyrrolic}}$), 8.75 (d, 1H, J = 4.8 Hz, $H_{\beta\text{-pyrrolic}}$), 8.25-8.21 (m, 8H, H_{ortho}), 7.85-7.65 (m, 14H, $H_{meta,\ para}$ and $H_{aromatic}$), 7.10 (d, 2H, J = 8.4 Hz, $H_{aromatic}$), -2.67 (br s, 2H, NH). UV-Vis (CH_2Cl_2): λ_{max} [nm] ($\varepsilon \times 10^{-3}$) 427 (167), 523 (13.9) 557 (4.46), 603 (3.62), 655 (2.87). ESI-LRMS: *m/z* (%, assignment) cluster at 841-843, 841 (100, $(M+H)^+$). ESI-HRMS: Calcd for $(M+H)^+$ ($C_{52}H_{34}IN_4$): 841.1823, found: 841.1777.

2-(4′-Bromophenyl)ethynyl-5,10,15,20-tetraphenylporphyrin (39)

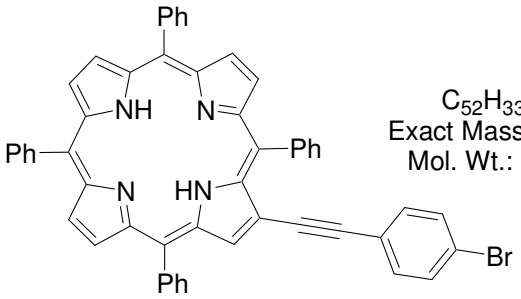

$C_{52}H_{33}BrN_4$
Exact Mass: 792.189
Mol. Wt.: 793.749

TPPCHO (**2**, 100 mg, 0.15 mmol) was dissolved in dry THF (15 mL). To this diphenyl bromo(4-bromophenyl)methylphosphonate (**38**, 223 mg, 0.46 mmol, 3 eq) or diphenyl chloro(4-bromophenyl)methylphosphonate (**37**, 202 mg, 0.46 mmol, 3 eq) and *t*-BuOK (1.5 g) were added and the reaction was stirred under Ar for 45 min at RT. Following this, DCM (25 mL) was added and the resulting purple solution was washed with H_2O

(2 × 50 mL) then neutralised with dilute glacial acetic acid. The organic layer was separated, dried over $MgSO_4$ and filtered. The solvent was reduced *in vacuo* and the porphyrin was precipitated from DCM:MeOH to give a red powder which was collected by filtration (48 mg, 40% from Br derivative **38**, 100 mg, 81% from Cl derivative **37**). ^{1}H NMR (500 MHz, $CDCl_3$, TMS): δ 9.09 (s, 1H, $H_{\beta\text{-pyrrolic}}$), 8.90 (s, 2H, $H_{\beta\text{-pyrrolic}}$), 8.85 (d, 1H, J = 4.7 Hz, $H_{\beta\text{-pyrrolic}}$), 8.79 (s, 1H, $H_{\beta\text{-pyrrolic}}$), 8.78 (s, 1H, $H_{\beta\text{-pyrrolic}}$), 8.76 (d, 1H, J = 4.8 Hz, $H_{\beta\text{-pyrrolic}}$), 8.25-8.21 (m, 8H, H_{ortho}), 7.83-7.64 (m, 12H, $H_{meta,\ para}$ and $H_{aromatic}$), 7.48 (d, 2H, J = 8.4 Hz, $H_{aromatic}$), 7.24 (d, 2H, J = 8.4 Hz, $H_{aromatic}$), -2.65 (br s, 2H, NH). UV-Vis (CH_2Cl_2): λ_{max} [nm] ($\varepsilon \times 10^{-3}$) 426.5 (345), 522.5 (29.2), 558 (9.06), 598.5 (8.13), 655 (5.87). FAB-LRMS: *m/z* (%, assignment) cluster at 792-795, 794 (70, M^+). HRMS: Calcd. for M^+ ($C_{52}H_{33}{}^{79}BrN_4$): 792.1888, found: 792.1874.

2-Phenylethynyl-5,10,15,20-tetraphenylporphyrin (67)

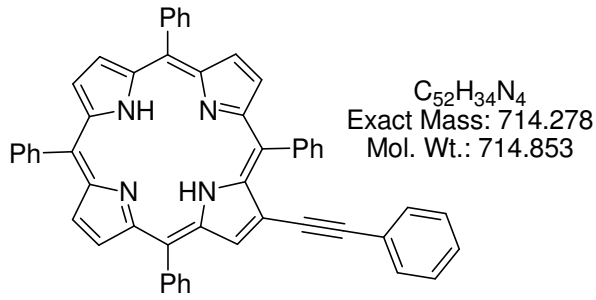

TPPCHO (**2**, 100 mg, 0.155 mmol) was dissolved in THF (15 mL). Compound **59** (151 mg, 0.47 mmol, 3 eq) and *t*-BuOK (1.5 g) were added and the reaction mixture was stirred under Ar for 1.5 hrs. The solvent was removed *in vacuo* and H_2O (20 mL) was added to the purple solid, resulting in a suspension. Glacial acetic acid was added slowly with stirring until the solution reached pH 5, and then the reaction mixture was extracted with $CHCl_3$ (50 mL). The organic layer was separated, dried over $MgSO_4$, filtered and the porphyrin was precipitated from DCM:MeOH to give a purple solid (60 mg, 54%). This was a mixture of halovinyl intermediate and ethynyl porphyrin **80** that appeared as one spot on TLC. To obtain a spectroscopically pure compound the solid (60 mg) was dissolved in dry THF (5 mL) and *t*-BuOK (0.25 g) was added. The solution was stirred under Ar at RT for 1 h. The solvent was removed *in vacuo* and H_2O (20 mL) was added. Glacial acetic acid was added slowly, with stirring, until pH 5 then the reaction mixture was extracted into $CHCl_3$ (50 mL). The organic layer was separated, dried over $MgSO_4$, filtered and the porphyrin was precipitated from DCM:MeOH to give a purple solid (30 mg, 50%). Spectroscopic data is in agreement with Ali *et al.*[130]

^{1}H NMR (500 MHz, $CDCl_3$, TMS): δ 9.10 (s, 1H, $H_{\beta\text{-pyrrolic}}$), 8.91 (s, 2H, $H_{\beta\text{-pyrrolic}}$), 8.86 (d, 1H, J = 5.0 Hz, $H_{\beta\text{-pyrrolic}}$), 8.81 (s, 2H, $H_{\beta\text{-pyrrolic}}$), 8.78 (d, 1H, J = 5.0 Hz, $H_{\beta\text{-pyrrolic}}$), 8.26-8.23 (m, 8H, H_{ortho}), 7.83-7.65 (m, 12H, $H_{meta,\ para}$), 7.40-7.34 (m, 5H, $H_{aromatic}$), -2.63 (br s, 2H, NH). ^{1}H NMR selected data for mixture of halovinyl intermediate **67a** and **67** (500 MHz, $CDCl_3$, TMS): δ -2.58, -2.64, -2.71. UV-Vis (THF): λ_{max} [nm] ($\varepsilon \times 10^{-3}$) 424 (324), 521 (21.8), 556 (5.60), 599 (5.00), 656 (2.54). FAB-LRMS: *m/z* (%, assignment) cluster at 713-716, 715 (100, $(M+H)^+$). HRMS: Calcd. for $(M+H)^+$ ($C_{52}H_{35}N_4$): 715.2862, found: 715.2857.

2-(4′-Methoxyphenyl)ethynyl-5,10,15,20-tetraphenylporphyrin (68)

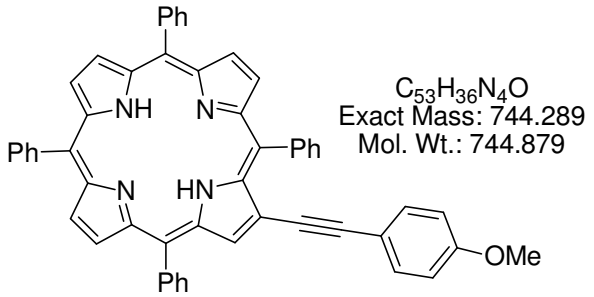

Compound **68** was prepared from **60** using the same method as used in compound **67** (97 mg, 84%). Spectroscopically pure compound was also obtained using the same method as for compound **67** (54 mg, 56%). ^{1}H NMR (500 MHz, $CDCl_3$, TMS): δ 9.04 (s, 1H, $H_{\beta\text{-pyrrolic}}$), 8.86 (s, 2H, $H_{\beta\text{-pyrrolic}}$), 8.81 (d, 1H, J = 4.9 Hz, $H_{\beta\text{-pyrrolic}}$), 8.77 (s, 2H, $H_{\beta\text{-pyrrolic}}$), 8.72 (d, 1H, J = 4.9 Hz, $H_{\beta\text{-pyrrolic}}$), 8.22-8.20 (m, 8H, H_{ortho}), 7.79-7.66 (m, 12H, $H_{meta,\ para}$), 7.29 (d, 2H, J = 8.7 Hz, $H_{aromatic}$), 6.86 (d, 2H, J = 8.7 Hz, $H_{aromatic}$), 3.86 (s, 3H, OCH_3), -2.69 (br s, 2H, NH). ^{1}H NMR selected data for mixture of halovinyl intermediate **68a** and compound **68** (400 MHz, $CDCl_3$, TMS): δ -2.60, -2.66, -2.72. UV-Vis (THF): λ_{max} [nm] ($\varepsilon \times 10^{-3}$) 422 (231), 521 (19.7), 558 (7.16), 599 (5.27), 656 (2.45). FAB-LRMS: *m/z* (%, assignment) cluster at 743-747, 745 (100, $(M+H)^+$). HRMS: Calcd. for $(M+H)^+$ ($C_{53}H_{37}N_4O$): 745.2967, found: 745.2970.

2-(4′-Pyridyl)ethynyl-5,10,15,20-tetraphenylporphyrin (70)

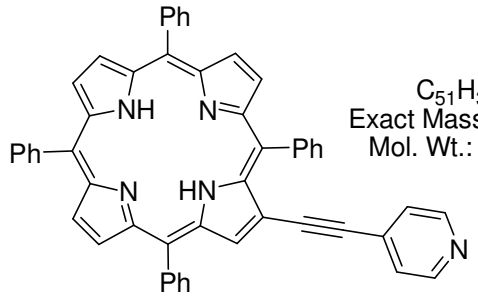

$C_{51}H_{33}N_5$
Exact Mass: 715.274
Mol. Wt.: 715.841

TPPCHO (**2**, 350 mg, 0.54 mmol) was dissolved in dry THF (20 mL). Compound **62** (215 mg, 0.60 mmol, 1.1 eq) and *t*-BuOK (112 mg, 0.68 mmol, 1.25 eq) were added and the reaction was stirred under Ar for 3 hrs. Following this, additional **62** (50 mg, 0.14 mmol) and *t*-BuOK (76 mg, 0.46 mmol) were added. On completion the solvent was removed *in vacuo* and the residue was redissolved in DCM (50 mL). The organic solution was washed with H_2O (50 mL), separated, dried over $MgSO_4$, filtered and the solvent was removed *in vacuo*. The residue was purified by silica gel column chromatography (28% aq. NH_4OH:MeOH:DCM 1:10:89) eluting the product as a brown band. The solvent was removed *in vacuo*, the reside was dissolved in DCM and the porphyrin was precipitated from DCM:MeOH to give a purple solid (275 mg, 70%). ^{1}H NMR (400 MHz, d_4-pyridine): δ 9.13 (s, 1H, $H_{\beta\text{-pyrrolic}}$), 8.92 (s, 2H, $H_{\beta\text{-pyrrolic}}$), 8.87 (d, 1H, J = 5.0 Hz, $H_{\beta\text{-pyrrolic}}$), 8.87 (m, 3H, $H_{\beta\text{-pyrrolic}}$), 8.58 (dd, 2H, J = 4.4 Hz, 1.6 Hz, $H_{aromatic}$), 8.25-8.20 (m, 8H, H_{ortho}), 7.84-7.63 (m, 12H, $H_{meta,\ para}$), 7.23 (dd, 2H, J = 4.4 Hz, 1.6 Hz, $H_{aromatic}$), -2.67 (br s, 2H, NH). UV-Vis (THF): λ_{max} [nm] ($\varepsilon \times 10^{-3}$) 427 (239), 521 (21.2), 556 (7.96), 599 (7.50), 656 (6.94). FAB-LRMS: *m/z* (%, assignment) cluster at 714-719, 716 (100, $(M+H)^+$). HRMS: Calcd for $(M+H)^+$ ($C_{51}H_{34}N_5O$): 716.2814, found: 716.2814.

2-[4′-(5,5-Dimethyl-1,3-dioxane-2-yl)phenyl]ethynyl-5,10,15,20-tetraphenylporphyrin (71)

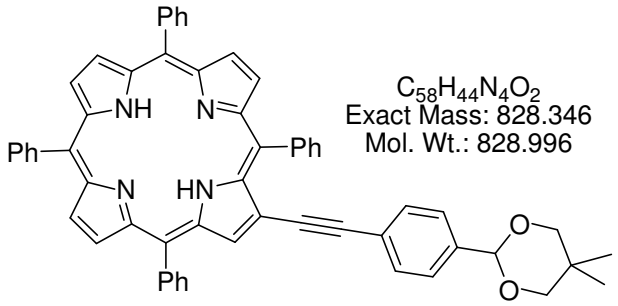

TPPCHO (**2**, 400 mg, 0.623 mmol) was dissolved in dry THF (53 mL). Compound **64** (900 mg, 1.74 mmol, 2.8 eq) and *t*-BuOK (5.3 g) were added and the reaction was stirred under Ar for 1 hr. Following this, DCM (150 mL) was added and the resulting purple solution was washed with H_2O (2 × 100 mL). The organic layer was separated, dried over $MgSO_4$ and filtered. The volume of the solvent was reduced to one third *in vacuo* and the porphyrin was precipitated from DCM:MeOH. The red powder was collected by filtration (453 mg, 88%). ^{1}H NMR (500 MHz, $CDCl_3$, TMS): δ 9.10 (s, 1H, $H_{\beta\text{-pyrrolic}}$), 8.90 (s, 2H, $H_{\beta\text{-pyrrolic}}$), 8.84 (d, 1H, J = 5.0 Hz, $H_{\beta\text{-pyrrolic}}$), 8.80 (s, 2H, $H_{\beta\text{-pyrrolic}}$), 8.76 (d, 1H, J = 5.0 Hz, $H_{\beta\text{-pyrrolic}}$), 8.25-8.21 (m, 8H, H_{ortho}), 7.82-7.63 (m, 12H, $H_{meta,\ para}$), 7.50 (d, 2H, J = 8.0 Hz, $H_{aromatic}$), 7.39 (d, 2H, J = 8.2 Hz, $H_{aromatic}$), 5.45 (s, 1H, CH), 3.85 (d, 2H, J = 11.0 Hz, CH_2), 3.72 (d, 2H, J = 11.0 Hz, CH_2), 1.38 (s, 3H, CH_3), 0.87 (s, 3H, CH_3), -2.65 (s, 2H, NH). UV-Vis (THF): λ_{max} [nm] ($\varepsilon \times 10^{-3}$) 424 (290), 521 (32.8), 556 (16.3), 599 (14.1), 656 (10.9). FAB-LRMS: *m/z* (%, assignment) cluster at 827-831, 829 (100, $(M+H)^+$). HRMS: Calcd. for $(M+H)^+$ ($C_{58}H_{45}N_4O_2$): 829.3542, found: 829.3531.

2-(4′-Cyanophenyl)ethynyl-5,10,15,20-tetraphenylporphyrin (73) and **2-(4′-benzamide)ethynyl-5,10,15,20-tetraphenylporphyrin (74)**

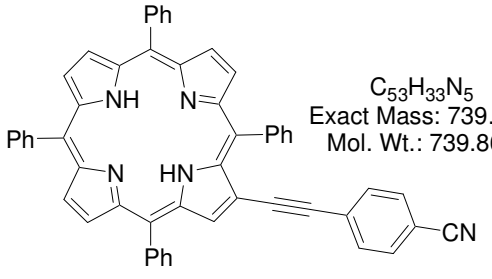

73

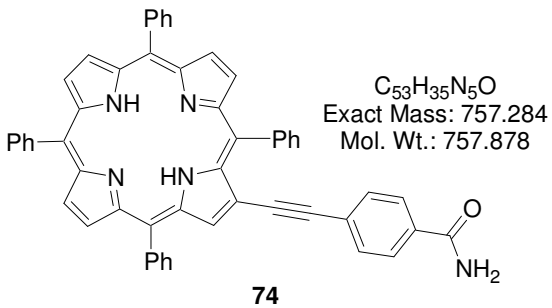

74

TPPCHO (**2**, 100 mg, 0.156 mmol) was dissolved in dry THF (15 mL). Compound **65** (132 mg, 0.31 mmol 2 eq) and *t*-BuOK (1.5 g) were added and the reaction mixture was

stirred under Ar for 3 hrs. H_2O (50 mL) and DCM (50 mL) were added forming an emulsion. To this glacial acetic acid was added slowly until the suspension cleared. The organic layer was separated, dried over $MgSO_4$, filtered and the solvent was removed *in vacuo*. The resulting solid was redissolved in DCM and purified through a plug of silica gel, first eluting **73** with DCM, then **74** with MeOH:DCM (1:20). Both **73** and **74** were precipitated as purple solids from MeOH (30 mg, 26%) and hexane (42 mg, 36%), respectively. Compound **73** ^{1}H NMR (500 MHz, $CDCl_3$, TMS): δ 9.13 (s, 1H, $H_{\beta\text{-pyrrolic}}$), 8.92 (s, 2H, $H_{\beta\text{-pyrrolic}}$), 8.87 (d, 1H, J = 4.9 Hz, $H_{\beta\text{-pyrrolic}}$), 8.79-8.78 (m, 3H, $H_{\beta\text{-pyrrolic}}$), 8.26-8.22 (m, 8H, H_{ortho}), 7.83-7.68 (m, 12H, $H_{meta,\ para}$), 7.63 (d, 2H, J = 8.1 Hz, $H_{aromatic}$), 7.45 (d, 2H, J = 8.1 Hz, $H_{aromatic}$), -2.64 (br s, 2H, NH). UV-Vis (THF): λ_{max} [nm] ($\varepsilon \times 10^{-3}$) 428 (200), 522 (19.2), 557 (7.08), 599 (6.68), 658 (5.83). FAB-LRMS: *m/z* (%, assignment) cluster at 738-742, 758 (100, M^+). HRMS: Calcd for M^+ ($C_{53}H_{33}N_5$): 739.2736, found: 739.2736. Compound **74** ^{1}H NMR (500 MHz, $CDCl_3$, TMS): δ 9.09 (s, 1H, $H_{\beta\text{-pyrrolic}}$), 8.88 (s, 2H, $H_{\beta\text{-pyrrolic}}$), 8.83 (d, 1H, J = 4.9 Hz, $H_{\beta\text{-pyrrolic}}$), 8.79 (s, 1H, $H_{\beta\text{-pyrrolic}}$), 8.74 (d, 2H, J = 4.9 Hz, $H_{\beta\text{-pyrrolic}}$), 8.23-8.18 (m, 8H, H_{ortho}), 7.79-7.59 (m, 14, $H_{meta,\ para}$ and $H_{aromatic}$), 7.41 (d, 2H, J = 8.0 Hz, $H_{aromatic}$), 6.04 (br s, 1H, NH_2), 5.60 (br s, 1H, NH_2), -2.67 (br s, 2H, NH). UV-Vis (THF): λ_{max} [nm] ($\varepsilon \times 10^{-3}$) 426 (229), 522 (20.9), 557 (7.34), 599 (6.37), 656 (4.68). FAB-LRMS: *m/z* (%, assignment) cluster at 757-761, 758 (100, $(M+H)^+$). HRMS: Calcd for $(M+H)^+$ ($C_{53}H_{36}N_5O$): 758.2920, found: 758.2911.

General Method for the Insertion of Zinc into the Porphyrins

A solution of $Zn(OAc)_2 \cdot 2H_2O$ (2 eq) in MeOH (10 mL) was added to solution of porphyrin (1 eq) in $CHCl_3$ (100 mL) and the reaction was stirred at RT. After stirring for 1 hr TLC analysis indicated that the reaction was complete. The solvent was removed *in vacuo* and the remaining solid was dissolved in DCM and purified through a plug of silica gel (DCM) if required. The solvent was removed *in vacuo* and the porphyrin was precipitated from DCM:MeOH to give a purple solid.

2-(4′-Iodophenyl)ethynyl-5,10,15,20-tetraphenylporphyrinato zinc II (32)

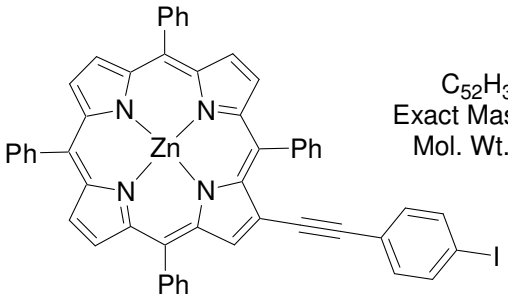

$C_{52}H_{31}IN_4Zn$
Exact Mass: 902.088
Mol. Wt.: 904.124

Compound **32** was isolated in 99% yield. ^{1}H NMR (500 MHz, $CDCl_3$, TMS): δ 9.25 (s, 1H, $H_{\beta\text{-pyrrolic}}$), 8.95 (s, 2H, $H_{\beta\text{-pyrrolic}}$), 8.93 (s, 2H, $H_{\beta\text{-pyrrolic}}$), 8.90 (d, 1H, J = 4.7 Hz, $H_{\beta\text{-pyrrolic}}$), 8.79 (d, 1H, J = 4.6 Hz, $H_{\beta\text{-pyrrolic}}$), 8.25-8.20 (m, 8H, H_{ortho}), 7.83-7.63 (m, 14H, $H_{meta,\ para}$ and $H_{aromatic}$), 7.12 (d, 2H, J = 7.1 Hz, $H_{aromatic}$). UV-Vis (CH_2Cl_2): λ_{max} [nm] ($\varepsilon \times 10^{-3}$) 272 (26.3), 430 (307), 556 (20.8), 592 (8.70). ESI-LRMS: *m/z* (%, assignment) cluster at 925-931, 925 (100, $(M+Na)^+$). ESI-HRMS: Calcd for $(M+Na)^+$ ($C_{52}H_{31}N_4NaZn$): 925.0777, found: 925.0730.

2-(4′-Bromophenyl)ethynyl-5,10,15,20-tetraphenylporphyrinato zinc II (40)

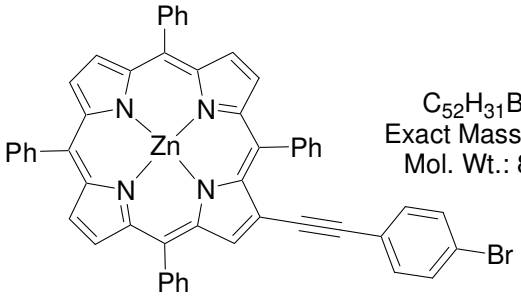

$C_{52}H_{31}BrN_4Zn$
Exact Mass: 854.102
Mol. Wt.: 857.123

Compound **40** was isolated in 92% yield. ^{1}H NMR (400 MHz, $CDCl_3$, TMS): δ 9.22 (s, 1H, $H_{\beta\text{-pyrrolic}}$), 8.93 (s, 2H, $H_{\beta\text{-pyrrolic}}$), 8.91 (s, 2H, $H_{\beta\text{-pyrrolic}}$), 8.87 (d, 1H, J = 4.8 Hz, $H_{\beta\text{-pyrrolic}}$), 8.76 (d, 1H, J = 4.8 Hz, $H_{\beta\text{-pyrrolic}}$), 8.22-8.18 (m, 8H, H_{ortho}), 7.79-7.60 (m, 12H, $H_{meta,\ para}$), 7.46 (d, 2H, J = 8.5 Hz, $H_{aromatic}$), 7.23 (d, 2H, J = 8.5 Hz, $H_{aromatic}$). UV-Vis (CH_2Cl_2): λ_{max} [nm] ($\varepsilon \times 10^{-3}$) 431 (279), 557 (18.3), 590.5 (7.83). FAB-LRMS: *m/z* (%, assignment) cluster at 853-860, 856 (100, M^+). HRMS: Calcd. for M^+ ($C_{52}H_{31}{}^{81}BrN_4{}^{64}Zn$): 856.1003, found: 856.1016.

2-Phenylethynyl-5,10,15,20-tetraphenylporphyrinato zinc II (75)

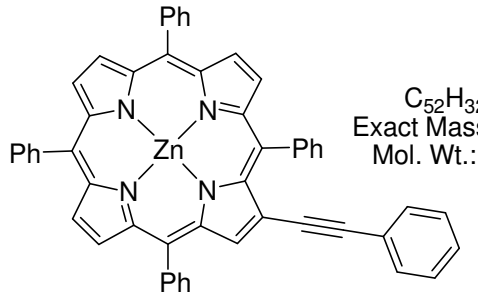

$C_{52}H_{32}N_4Zn$
Exact Mass: 776.192
Mol. Wt.: 778.227

Compound **75** was isolated in 92% yield. ^{1}H NMR (400 MHz, $CDCl_3$, TMS): δ 9.94 (s, 1H, $H_{\beta\text{-pyrrolic}}$), 8.94 (s, 2H, $H_{\beta\text{-pyrrolic}}$), 8.92 (s, 2H, $H_{\beta\text{-pyrrolic}}$), 8.89 (d, 1H, J = 4.8 Hz, $H_{\beta\text{-pyrrolic}}$), 8.79 (d, 1H, J = 4.8 Hz, $H_{\beta\text{-pyrrolic}}$), 8.24-8.20 (m, 8H, H_{ortho}), 7.80-7.63 (m, 12H, $H_{meta,\ para}$), 7.40-7.32 (m, 5H, $H_{aromatic}$). UV-Vis (CH_2Cl_2): λ_{max} [nm] ($\varepsilon \times 10^{-3}$) 430.5 (211), 557.5 (13.6), 588.5 (5.10). FAB-LRMS: *m/z* (%, assignment) cluster at 776-782, 776 (100, M^+). HRMS: Calcd. for M^+ ($C_{52}H_{32}N_4{}^{64}Zn$): 776.1918, found: 776.1913.

2-(4′-Methoxyphenyl)ethynyl-5,10,15,20-tetraphenylporphyrinato zinc II (76)

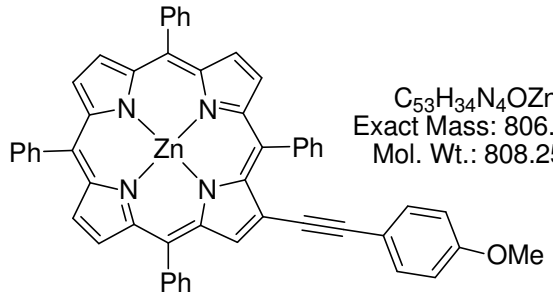

$C_{53}H_{34}N_4OZn$
Exact Mass: 806.202
Mol. Wt.: 808.253

Compound **76** was isolated in 86% yield. ^{1}H NMR (500 MHz, $CDCl_3$, TMS): δ 9.23 (s, 1H, $H_{\beta\text{-pyrrolic}}$), 8.96 (s, 2H, $H_{\beta\text{-pyrrolic}}$), 8.94 (s, 2H, $H_{\beta\text{-pyrrolic}}$), 8.90 (d, 1H, J = 4.7 Hz, $H_{\beta\text{-pyrrolic}}$), 8.79 (d, 1H, J = 4.7 Hz, $H_{\beta\text{-pyrrolic}}$), 8.26-8.22 (m, 8H, H_{ortho}), 7.83-7.68 (m, 12H, $H_{meta,\ para}$), 7.34 (d, 2H, J = 8.8 Hz, $H_{aromatic}$), 6.89 (d, 2H, J = 8.8 Hz, $H_{aromatic}$), 3.85 (s, 3H, OCH_3). UV-Vis (CH_2Cl_2): λ_{max} [nm] ($\varepsilon \times 10^{-3}$) 430 (214), 556 (16.9), 589 (6.61). FAB-LRMS: *m/z* (%, assignment) cluster at 806-812, 806 (100, M^+). HRMS: Calcd. for M^+ ($C_{53}H_{34}N_4O^{64}Zn$): 806.2024, found: 806.2033.

2-(4′-Pyridyl)ethynyl-5,10,15,20-tetraphenylporphyrinato zinc II (77)

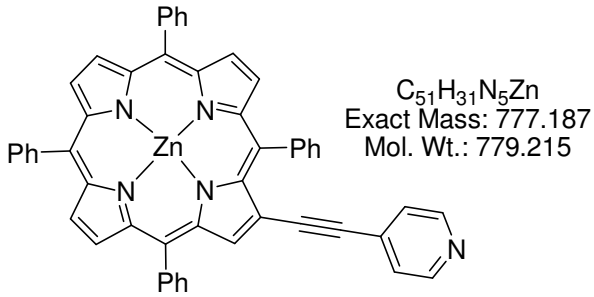

Compound **77** was isolated in 94% yield. ^{1}H NMR (500 MHz, d_4-pyridine): δ 9.55 (s, 1H, $H_{\beta\text{-pyrrolic}}$), 9.09 (s, 2H, $H_{\beta\text{-pyrrolic}}$), 9.08 (s, 2H, $H_{\beta\text{-pyrrolic}}$), 9.05 (d, 1H, J = 4.7 Hz, $H_{\beta\text{-pyrrolic}}$), 8.98 (d, 1H, J = 4.7 Hz, $H_{\beta\text{-pyrrolic}}$), 8.81 (d, 2H, J = 5.8 Hz, $H_{aromatic}$), 8.40-8.36 (m, 8H, H_{ortho}), 7.77-7.70 (m, 12H, $H_{meta,\ para}$), 7.42 (d, 2H, J = 5.7 Hz, $H_{aromatic}$), UV-Vis (CH_2Cl_2): λ_{max} [nm] ($\varepsilon \times 10^{-3}$) 433.5 (262), 560 (15.7), 609 (6.27). FAB-LRMS: *m/z* (%, assignment) cluster at 777-784, 778 (100, $(M+H)^+$). HRMS: Calcd. for $(M+H)^+$ ($C_{51}H_{32}N_5{}^{66}Zn$): 780.1918, found: 780.1922.

2-[4′-(5,5-Dimethyl-1,3-dioxane-2-yl)pheny]ethynyl-5,10,15,20-tetraphenylporphyrinato zinc II (78)

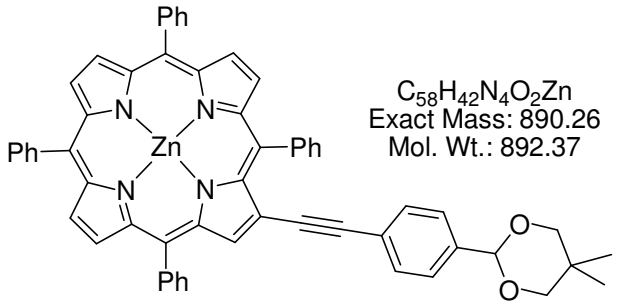

Compound **78** was isolated in 88% yield. ^{1}H NMR (500 MHz, $CDCl_3$, TMS): δ 9.26 (s, 1H, $H_{\beta\text{-pyrrolic}}$), 8.95 (s, 2H, $H_{\beta\text{-pyrrolic}}$), 8.94 (s, 2H, $H_{\beta\text{-pyrrolic}}$), 8.90 (d, 1H, J = 4.7 Hz, $H_{\beta\text{-pyrrolic}}$), 8.80 (d, 1H, J = 4.7 Hz, $H_{\beta\text{-pyrrolic}}$), 8.25-8.21 (m, 8H, H_{ortho}), 7.82-7.62 (m, 12H, $H_{meta,\ para}$), 7.50 (d, 2H, J = 8.1 Hz, $H_{aromatic}$), 7.41 (d, 2H, J = 8.2 Hz, $H_{aromatic}$), 5.45 (s, 1H, CH), 3.85 (d, 2H, J = 10.8 Hz, CH_2), 3.71 (d, 2H, J = 10.8 Hz, CH_2), 1.38 (s, 3H, CH_3), 0.86 (s, 3H, CH_3), UV-Vis (CH_2Cl_2): λ_{max} [nm] ($\varepsilon \times 10^{-3}$) 274 (137), 431 (244), 557.5 (15.7), 590.5 (6.15). ESI-LRMS: *m/z* (%, assignment) cluster at 891-896, 891 (100, $(M+H)^+$). ESI-HRMS: Calcd for $(M+H)^+$ ($C_{58}H_{43}N_4N_4O_2Zn$): 891.2672, found: 891.2663.

2-(4′-Formylphenyl)ethynyl-5,10,15,20-tetraphenylporphyrin (79)

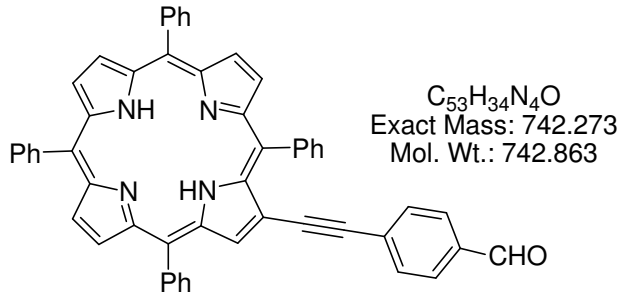

$C_{53}H_{34}N_4O$
Exact Mass: 742.273
Mol. Wt.: 742.863

Compound **71** (395 mg, 0.48 mmol) was added to a solution of CH_2Cl_2:TFA:H_2O (3:3:1, 46 mL total) and the reaction was stirred at RT for 1 h. The green solution was diluted with H_2O (50 mL) and DCM (50 mL) and neutralised with a saturated aq. solution of $NaHCO_3$. The red solution was separated, dried over $MgSO_4$, filtered and the solvent was removed *in vacuo*. The resulting solid was dissolved in DCM and purified by silica gel chromatography (DCM), eluting the product as a purple band. The solvent was reduced *in vacuo* and the porphyrin was precipitated from DCM:MeOH to give the aldehyde as a purple solid (286 mg, 81%). Spectroscopic data is in agreement with Guldi *et al.*[6] ^{1}H NMR (500 MHz, $CDCl_3$, TMS): δ 10.03 (s, 1H, CHO), 9.10 (s, 1H, $H_{\beta\text{-pyrrolic}}$), 8.88 (s, 2H, $H_{\beta\text{-pyrrolic}}$), 8.83 (d, 1H, J = 4.8 Hz, $H_{\beta\text{-pyrrolic}}$), 8.76 (s, 2H, $H_{\beta\text{-pyrrolic}}$), 8.74 (d, 1H, J = 4.8 Hz, $H_{\beta\text{-pyrrolic}}$), 8.23-8.18 (m, 8H, H_{ortho}), 7.83 (d, 2H, J = 8.2 Hz, $H_{aromatic}$), 7.80-7.61 (m, 12H, $H_{meta,\ para}$), 7.48 (d, 2H, J = 8.2 Hz, $H_{aromatic}$), -2.65 (s br, 2H, NH). UV-Vis (THF): λ_{max} [nm] ($\varepsilon \times 10^{-3}$) 428 (168), 522 (17.0), 558 (6.68), 600 (5.74), 658 (3.91). FAB-LRMS: *m/z* (%, assignment) cluster at 742-745, 743 (100, $(M+H)^+$). HRMS: Calcd for $(M+H)^+$ ($C_{53}H_{35}N_4O$): 743.2810, found: 743.2802.

2-(4′-Formylphenyl)ethynyl-5,10,15,20-tetraphenylporphyrinato zinc II (80)

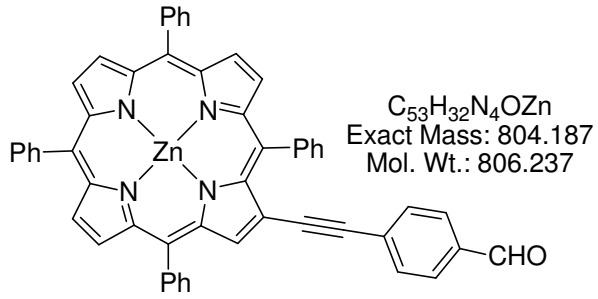

$C_{53}H_{32}N_4OZn$
Exact Mass: 804.187
Mol. Wt.: 806.237

A solution of $Zn(OAc)_2 \cdot 2H_2O$ (62 mg, 0.283 mmol, 1.27 eq) in MeOH (2 mL) was added to a solution of aldehyde **79** (165 mg, 0.222 mmol) in $CHCl_3$ (20 mL) and the reaction was stirred at RT. After 1 h, TLC analysis indicated that the reaction was complete. The solvents were removed *in vacuo* and the remaining residue was

precipitated from DCM:MeOH to give a purple powder (176 mg, 99%). Spectroscopic data is in agreement with Guldi *et al.*[6] ^{1}H NMR (500 MHz, $CDCl_3$, TMS): δ 10.02 (s, 1H, CHO), 9.27 (s, 1H, $H_{\beta\text{-pyrrolic}}$), 8.93 (s, 2H, $H_{\beta\text{-pyrrolic}}$), 8.915 (s, 2H, $H_{\beta\text{-pyrrolic}}$), 8.87 (d, 1H, J = 4.7 Hz, $H_{\beta\text{-pyrrolic}}$), 8.77 (d, 1H, J = 4.7 Hz, $H_{\beta\text{-pyrrolic}}$), 8.23-8.18 (m, 8H, H_{ortho}), 7.83 (d, 2H, J = 7.8 Hz, $H_{aromatic}$), 7.80-7.60 (m, 12H, $H_{meta,\ para}$), 7.51 (d, 2H, J = 8.2 Hz, $H_{aromatic}$). UV-Vis (THF): λ_{max} [nm] ($\varepsilon \times 10^{-3}$) 437 (185), 564 (10.2), 603 (6.63). FAB-LRMS: *m/z* (%, assignment) cluster at 804-810, 806 (100, M^+). HRMS: Calcd for M^+ ($C_{53}H_{32}N_4O^{64}Zn$): 804.1867, found: 804.1850.

2-(4′-Methoxycarbonylphenyl)ethynyl-5,10,15,20-tetraphenylporphyrinato zinc II (81)

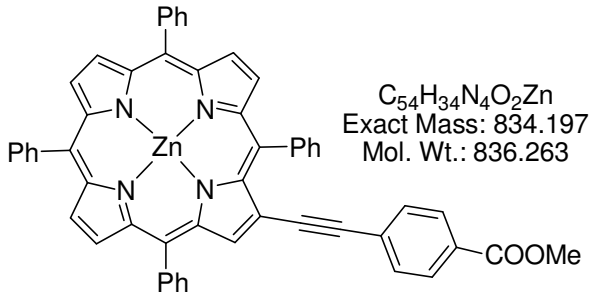

To a solution of aldehyde **80** (70 mg, 87μmol) in THF:MeOH (1:5, 21 mL), NaCN (85 mg, 3.0 mmol, 20 eq) was added and the reaction was stirred at RT, under Ar, for 30 min. Activated MnO_2 (560 mg, 6.5 mmol, 75 eq) was added and the reaction was refluxed for 18 hrs. On cooling to RT the reaction mixture was filtered through a plug of celite (DCM) and the solvent was removed *in vacuo*. The residue was purified by silica gel column chromatography (DCM) and taken to dryness *in vacuo* to give a purple solid (62 mg, 88%). ^{1}H NMR (500 MHz, $CDCl_3$, TMS): δ 9.24 (s, 1H, $H_{\beta\text{-pyrrolic}}$), 8.93 (s, 2H, $H_{\beta\text{-pyrrolic}}$), 8.91 (s, 2H, $H_{\beta\text{-pyrrolic}}$), 8.87 (d, 1H, J = 4.7 Hz, $H_{\beta\text{-pyrrolic}}$), 8.77 (d, 1H, J = 4.7 Hz, $H_{\beta\text{-pyrrolic}}$), 8.23-8.18 (m, 8H, H_{ortho}), 7.95 (d, 2H, J = 8.3 Hz, $H_{aromatic}$), 7.79-7.58 (m, 12H, $H_{meta,\ para}$), 7.42 (d, 2H, J = 8.2 Hz, $H_{aromatic}$), 3.91 (s, 3H, CO_2CH_3). UV-Vis (THF): λ_{max} [nm] ($\varepsilon \times 10^{-3}$) 437 (242), 531 (2.69), 566 (15.5), 603 (6.90). FAB-LRMS: *m/z* (%, assignment) cluster at 833-841, 836 (100, $(M+H)^+$). HRMS: Calcd for $(M+H)^+$ ($C_{54}H_{35}N_4O^{64}Zn$): 835.2051, found: 835.2049.

2-(4′-Carboxyphenyl)ethynyl-5,10,15,20-tetraphenylporphyrinato zinc II (82)

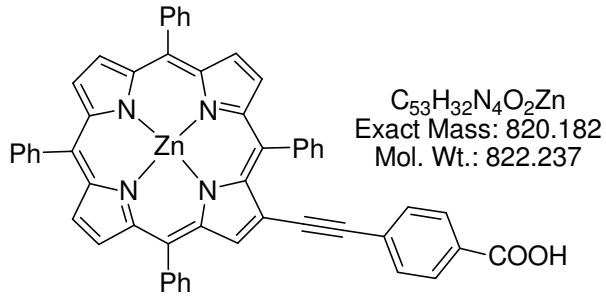

$C_{53}H_{32}N_4O_2Zn$
Exact Mass: 820.182
Mol. Wt.: 822.237

KOH (67 mg, 1.2 mmol, 20 eq) in a mixture of MeOH (16 mL) and H_2O (1.6 mL) was added to a solution of compound **81** (50 mg, 60 μmol) in THF (16 mL). The mixture was refluxed for 15 hrs under Ar. After cooling to RT, H_2O (10 mL), DCM (10 mL) and aq 2.0 M H_3PO_4 (0.63 ml, 21 eq) were added and the resulting organic layer was separated, dried over $MgSO_4$, filtered and the solvent was removed *in vacuo.* The residue was purified by silica gel column chromatography (Et_2O:DCM 1:4) and the porphyrin was precipitated from DCM:hexane to give a purple solid (36 mg, 73%). ^{1}H NMR (500 MHz, d_6-DMSO): δ 13.09 (br s, 1H, COOH), 9.02 (s, 1H, $H_{\beta\text{-pyrrolic}}$), 8.76 (s, 1H, $H_{\beta\text{-pyrrolic}}$), 8.76 (s, 1H, $H_{\beta\text{-pyrrolic}}$), 8.74 (s, 2H, $H_{\beta\text{-pyrrolic}}$), 8.71 (d, 1H, J = 4.5 Hz, $H_{\beta\text{-pyrrolic}}$), 8.77 (d, 1H, J = 4.5 Hz, $H_{\beta\text{-pyrrolic}}$), 8.32-8.21 (m, 8H, H_{ortho}), 7.94 (d, 2H, J = 8.3 Hz, $H_{aromatic}$), 7.84-7.72 (m, 12H, $H_{meta,\ para}$), 7.47 (d, 2H, J = 8.3 Hz, $H_{aromatic}$). UV-Vis (DMF): λ_{max} [nm] ($\varepsilon \times 10^{-3}$) 439 (253), 571 (13.4), 611 (4.45). FAB-LRMS: *m/z* (%, assignment) cluster at 818-826, 821 (100, $(M+H)^+$). HRMS: Calcd for $(M+H)^+$ ($C_{53}H_{33}N_4O_2{}^{64}Zn$): 821.1895, found: 821.1906.

2-[4′-(Ethen-1′′-yl-2′′-cyano-2′′carboxylic acid)phenyl]ethynyl-5,10,15,20-tetraphenylporphyrinato zinc II (83)

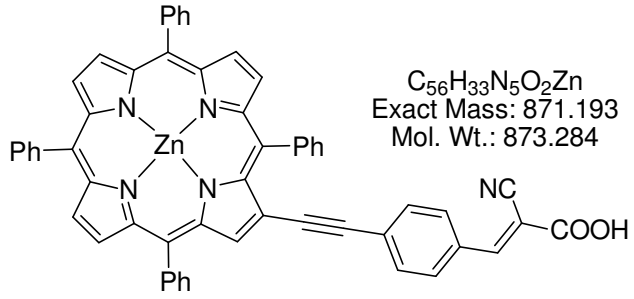

$C_{56}H_{33}N_5O_2Zn$
Exact Mass: 871.193
Mol. Wt.: 873.284

A mixture of porphyrin **80** (70 mg, 87 μmol), cyanoacetic acid (44.4 mg, 0.522 mmol, 6 eq) and ammonium acetate (40.2 mg, 0.52 mmol, 6 eq) in a solution of THF:acetic acid (1:1, 7 mL) was heated at 60°C for 5 hrs. Afterwards $Zn(OAc)_2{\cdot}2H_2O$ (76 mg, 0.35 mmol, 4 eq) was added and the solution was heated for an additional 15 min. On

cooling to RT the solution was filtered and sufficient H_2O was added to precipitate the product as a purple powder (68 mg, 97%). ^{1}H NMR (500 MHz, d_6-DMSO): δ 14.05 (s br, 1H, COOH), 9.05 (s, 1H, $H_{\beta\text{-pyrrolic}}$), 8.76 (s, 2H, $H_{\beta\text{-pyrrolic}}$), 8.74 (s, 2H, $H_{\beta\text{-pyrrolic}}$), 8.71 (d, 1H, J = 4.7 Hz, $H_{\beta\text{-pyrrolic}}$), 8.60 (d, 1H, J = 4.6 Hz, $H_{\beta\text{-pyrrolic}}$), 8.35 (s, 1H, $H_{acrylic}$), 8.21-8.15 (m, 8H, H_{ortho}), 8.06 (d, 2H, J = 8.4 Hz, $H_{aromatic}$), 7.86-7.70 (m, 12H, $H_{meta,\ para}$), 7.53 (d, 2H, J = 8.3 Hz, $H_{aromatic}$). UV-Vis (DMF): λ_{max} [nm] ($\varepsilon \times 10^{-3}$) 440.5 (243), 570 (19.8), 607 (10.3). FAB-LRMS: *m/z* (%, assignment) cluster at 871-877, 872 (100, M^+). HRMS: Calcd for M^+ ($C_{56}H_{33}N_5O_2{}^{64}Zn$): 871.1925, found: 871.1901.

2-[4′-(Ethen-1′′-yl-2′′,2′′-dicarboxylic acid)phenyl]ethynyl-5,10,15,20-tetraphenylporphyrinato zinc II (84) and **2-[4′-(ethen-1′′-yl-2′′-carboxylic acid)phenyl]ethynyl-5,10,15,20-tetraphenylporphyrinato zinc II (85)**

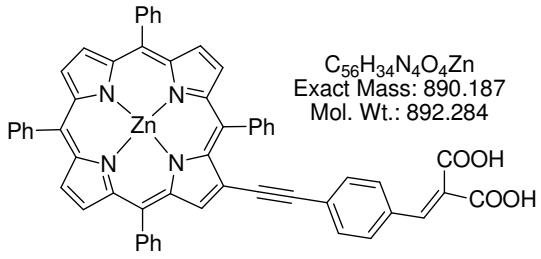

$C_{56}H_{34}N_4O_4Zn$
Exact Mass: 890.187
Mol. Wt.: 892.284

84

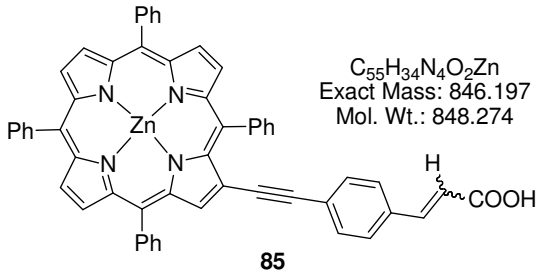

$C_{55}H_{34}N_4O_2Zn$
Exact Mass: 846.197
Mol. Wt.: 848.274

85

To a solution of aldehyde (**80**, 50 mg, 62.1 μmol) in THF:acetic acid (1:1, 5 mL total), malonic acid (258 mg, 2.48 mmol, 40 eq) and ammonium acetate (191.5 mg, 2.48 mmol, 40 eq) were added and the resulting solution was stirred at 40 °C for 4 hrs under Ar. TLC analysis of the reaction mixture showed the formation of the malonic acid derivative as well as the decarboxylated product. Afterwards, $Zn(OAc)_2 \cdot 2H_2O$ (50 mg, 0.22 mmol, 3.7 eq) was added and the reaction was stirred for an additional 15 minutes, filtered and sufficient H_2O was added to cause precipitation. The resulting solid was filtered and dried under reduced pressure to give a purple powder that was found to be 70:30 malonic acid (**84**):decarboxylated (**85**) material by ^{1}H NMR spectroscopy (*ca.* 96%). ^{1}H NMR (500 MHz, d_6-DMSO): δ 9.01 (s, 0.3H, **85**, $H_{\beta\text{-pyrrolic}}$), 8.99 (s, 0.7H, **84**, $H_{\beta\text{-pyrrolic}}$), 8.76 (s, 2H, **84** and **85**, $H_{\beta\text{-pyrrolic}}$), 8.74 (s, 2H, **84** and **85**, $H_{\beta\text{-pyrrolic}}$), 8.70 (d, 0.7H, J = 4.7 Hz, **84**, $H_{\beta\text{-pyrrolic}}$), 8.70 (d, 0.3H, J = 4.7 Hz, **85**, $H_{\beta\text{-pyrrolic}}$), 8.59 (d, 0.7H, J = 4.7 Hz, **84**, $H_{\beta\text{-pyrrolic}}$), 8.58 (d, 0.3H, J = 4.7 Hz, **85**, $H_{\beta\text{-pyrrolic}}$), 8.21-8.14 (m, 8H, **84** and **85**, H_{ortho}), 7.84-7.70 (m, 12.6H, **84** and **85**, $H_{meta,\ para}$, **84**, $H_{aromatic}$), 7.46 (d, 1.4H, J = 8.2 Hz, **84** $H_{aromatic}$), 7.38 (d, 1.4H, J = 8.2 Hz, **85**, $H_{aromatic}$), 7.31 (d, 0.6H, J = 8.3 Hz, **84** $H_{aromatic}$). Note: $H_{acrylic}$ and H_{acid} were not visible. ESI-LRMS **85**: *m/z* (%,

assignment) cluster at 847-854, 847 (100, $(M+H)^+$). ESI-HRMS: Calcd for $(M+H)^+$ ($C_{55}H_{35}N_4O_2Zn$): 847.2046, found: 847.2049. No HRMS could be obtained for compound **84**.

UV-Visible spectroscopic data for 2-(4′-carboxyphenyl)ethlyane-5,10,15,20-tetraphenylporphyrinato zinc II (**86**) and 4-(*trans*-2′-(2″-(5″,10″,15″,20″-tetraphenylporphyrinato zinc II yl)ethen-1′-yl))-1-benzoic acid (**87**). Compound **86**: UV-Vis (DMF): λ_{max} [nm] ($\varepsilon \times 10^{-3}$) 426 (426), 558.5 (14.8), 596.5 (4.42). Compound **87**: UV-Vis (DMF): λ_{max} [nm] ($\varepsilon \times 10^{-3}$) 437.5 (215), 567.5 (20.0), 605.5 (8.47).

DSSC Testing

DSSC were testing under conditions developed by Dr. Wayne Campbell. Solutions of acids were prepared in SDS AR BHT stabilised THF at 0.2 mM. To this, sintered TiO_2 on a ITO on a glass support (heated at 490 °C for 30 min) was added and soaked overnight at RT in darkness. The TiO_2 plates with bound porphyrins were removed from the dye solutions, rinsed, dried under high vacuum, placed in the cell holder containing a Pt counter electrode and I^-/I_3^- electrolyte was added. Four identical cells for each acid were irradiated under the intensity of 1 sun and the average values calculated excluding any outlying values.

Nanocrystalline screen printed TiO_2 plates were obtained form Dye-Sol. Electrolyte: 0.1 M LiI, 0.05 M I_2, 0.5 M 4-*tert*-butylpyridine, 0.6 M BMII, 0.5 M BHT in 1:1 valeronitrile:glutaronitrile

Dye loading studies

To perform the loading studies porphyrins were dissolved in THF (25 mL) at a concentration of approximately 1×10^{-5} M. 3 mL of this solution was added to a vial containing two TiO_2 plates that had previously been sintered at 490 °C for 30 min. The vials were sealed and the dye was left to be absorbed overnight (16 hrs) in the dark. The following day the cells were removed and washed with THF (10 × 1 mL) to remove the non-specifically bound porphyrins. In our case no non-specifically bound porphyrin was observed. The UV-Vis spectra of the initial and the final solutions were recorded from

220-800 nm (path length 0.1 cm) and the absorbance at λ_{max} was recorded. From this data the quantity of porphyrin bound to the surface of the TiO_2 for each dye was calculated.

8.5 Experimental Procedures for Chapter 4 - Construction of Lipophilic Porphyrin-DNA Complexes

2-(4′-*N*-Methylpyridiumyl)ethynyl-5,10,15,20-tetraphenylporphyrin iodine (90)

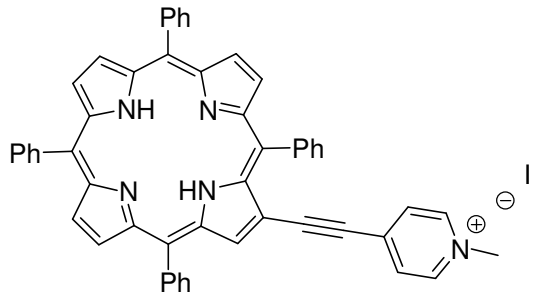

$C_{52}H_{36}IN_5$
Exact Mass: 857.202
Mol. Wt.: 857.78

To a solution of compound **70** (80 mg, 0.11 mmol) in dry DMF (4 mL) methyl iodide (36 μL, 0.56 mmol, 5 eq) was added and the reaction was stirred at 40 °C overnight under Ar. The solvent was removed *in vacuo* to give a brown solid which was dissolved in DCM and precipitated from DCM:hexane. The solid was collected by filtration and the crystals were washed with an aqueous solution of NaI to give a red solid (96 mg, 92%). ^{1}H NMR (400 MHz, $CDCl_3$, TMS): δ 9.26 (s, 1H, $H_{\beta\text{-pyrrolic}}$), 9.06 (d, 2H, J = 6.4 Hz, $H_{aromatic}$), 8.95 (d, 1H, J = 4.9 Hz, $H_{\beta\text{-pyrrolic}}$), 8.92 (d, 1H, J = 4.9 Hz, $H_{\beta\text{-pyrrolic}}$), 8.88 (d, 1H, J = 4.9 Hz, $H_{\beta\text{-pyrrolic}}$), 8.79 (d, 1H, J = 4.9 Hz, $H_{\beta\text{-pyrrolic}}$), 8.76 (d, 1H, J = 4.9 Hz, $H_{\beta\text{-pyrrolic}}$), 8.75 (d, 1H, J = 4.9 Hz, $H_{\beta\text{-pyrrolic}}$), 8.25-8.18 (m, 8H, H_{ortho}), 7.87-7.75 (m, 12H, $H_{meta,\ para}$), 7.72 (d, 2H, J = 6.6 Hz, $H_{aromatic}$), 4.46 (s, 3H, CH_3), -2.59 (br s, 2H, NH). UV-Vis (CH_2Cl_2): λ_{max} [nm] ($\varepsilon \times 10^{-3}$) 411 (176), 475 (103), 533 (23.1) 581 (14.9), 616 (10.9), 677 (9.52). ESI-LRMS: *m/z* (%, assignment) cluster at 730-733, 730 (100, $(M\text{-}I)^+$). ESI-HRMS: Calcd for $(M\text{-}I)^+$ ($C_{52}H_{36}N_5$): 730.2965, found: 730.2955.

General Synthetic Method for the Formation of Porphyrin-DNA Complexes

For the creation of lipophilic porphyrin DNA complexes we prepared a solution of oligonucleotide (Li^+ or Na^+ salt) in water (generally 100 μL, concentration of 100-500 μM). Porphyrin **9** or **27** (2.5 mg) was suspended in ACN (40 μL, sonicated for 15 minutes) then dissolved by the addition of water (40 μL). This porphyrin solution was further diluted to 1 mL with water. To the oligonucleotide solution the porphyrin solution was added in 2-5 μL fractions forming a red precipitate. Addition was continued until no more red precipitate is observed and a red colour developed in the

solution. To see if any more precipitate formed it was necessary to centrifuge the sample between additions of the porphyrin (5 sec at 13500 rpm). When no more precipitate was observed the sample was centrifuged to form a pellet of the porphyrin-DNA complex (15 min at 13500 rpm). The supernatant was removed and the pellet was washed with H_2O (2 × 1 mL) then dried under high vacuum for two days to remove any traces of H_2O or remaining solvent. The complex was dissolved in $CHCl_3$ (100 μL) to give a red solution.

8.6 Experimental Procedure for Chapter 5 - Covalent Attachment of Porphyrins to DNA and Chapter 6 - Porphyrin H-Aggregate Formation in the Minor Groove of the Duplex

2′-Deoxy-5′-*O*-dimethoxytrityl-5-[4-(5,10,15,20-tetraphenylporphyrinato-2-yl zinc II)ethynylphenyl]ethynyluridine (94)

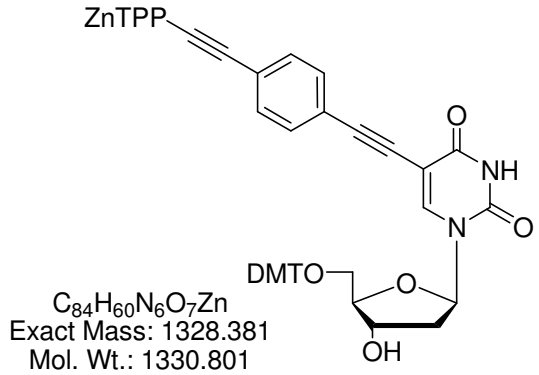

$C_{84}H_{60}N_6O_7Zn$
Exact Mass: 1328.381
Mol. Wt.: 1330.801

To a dry degassed solution of 2-(4′-ethynylphenyl)ethynyl-5,10,15,20-tetraphenylporphyrinato zinc II (**35**, 25 mg, 31.1 μmol) in Et_3N (1 mL), DMT protected 5-iodo-2′-deoxyuridine (**91**, 81 mg, 124 μmol, 4 eq) was added and the reaction mixture was stirred for 5 min at RT under Ar. $Pd(PPh_3)_4$ (3.6 mg, 3.1 μmol, 0.1 eq) and CuI (1.2 mg, 6.2 μmol, 0.2 mol %) were added and the reaction mixture was stirred under Ar at 70 °C overnight. TLC indicated that the reaction was almost complete. The reaction was diluted with DCM (25 mL), washed with a 5% aq. solution of Na_2EDTA (3 × 25 mL), then with a 3 M aq. solution of NH_4OH (2 × 25 mL) and finally with H_2O (25 mL). The organic layer was separated, dried over $MgSO_4$, filtered and the solvent was removed *in vacuo*. The resulting solid was dissolved in DCM and purified by silica gel column chromatography first eluting the Glaser homodimer (**34**) and trace starting material (**35**) with DCM as a red band followed by the desired product (**94**) with MeOH:DCM (1:9) as a crude mixture (32 mg, 78%). The crude mixture was precipitated from DCM:MeOH to give pure **94** which was collected by filtration as a purple solid (5 mg, 12%). ^{1}H NMR (500 MHz, d_6-DMSO): δ 11.83 (s, 1H, NH), 9.02 (s, 1H, $H_{\beta\text{-pyrrolic}}$), 8.77 (s, 2H, $H_{\beta\text{-pyrrolic}}$), 8.75 (s, 2H, $H_{\beta\text{-pyrrolic}}$), 8.72 (d, 1H, J = 4.6 Hz, $H_{\beta\text{-pyrrolic}}$), 8.60 (d, 1H, J = 4.6 Hz, $H_{\beta\text{-pyrrolic}}$), 8.23-8.16 (m, 8H, H_{ortho}), 7.85-7.75 (m, 14H, $H_{meta,\ para}$ and $H_{aromatic}$), 7.49 (d, 2H, J = 8.3 Hz, $H_{aromatic}$), 7.44-7.28 (m, 9H, H_{DMTO}), 6.95 (td, 4H, J = 7.0 and 1.9 Hz, H_{DMTO}), 6.48 (s, 1H, H_6), 6.18 (t, 1H, J = 5.4 Hz, $H_{1'}$), 5.47 (d, 1H, J = 4.7 Hz, OH), 4.46 (m, 1H, $H_{3'}$), 4.06 (m, 1H, $H_{4'}$), 3.76 (s, 3H, OCH_3), 3.75 (s, 3H,

OCH_3), 3.46-3.38 (m, 2H, $H_{5'}$), 2.56-2.52 (m, 1H, $H_{2'}$), 2.33-2.28 (m, 1H, $H_{2'}$). UV-Vis (CH_2Cl_2): λ_{max} [nm] ($\varepsilon \times 10^{-3}$) 440 (162), 570 (14.3), 605 (8.00). ESI-LRMS: *m/z* (%, assignment) cluster at 1363-1370, 1365, (100, $(M+Cl)^-$) ESI-HRMS: Calcd for $(M+Cl)^-$ ($C_{84}H_{60}N_6O_7Cl^{64}Zn$): 1363.3503, found: 1363.3505.

2′-Deoxy-5-[4-(5,10,15,20-tetraphenylporphyrin-2-yl)ethynylphenyl]ethynyluridine (95)

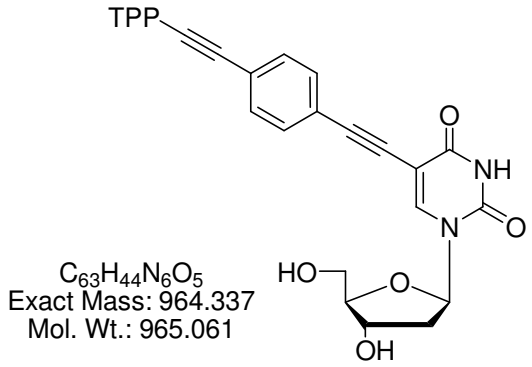

To a solution of crude porphyrin nucleoside **94** (15 mg, 11 μmol) in DCM (2 mL) trifluoroacetic acid (1.7 μL, 22 μmol, 2 eq) was added and the reaction mixture was stirred at RT for 2 minutes. To the resulting brown solution $CHCl_3$ (10 mL) was added and the solution was extracted with H_2O (5 × 10 mL) then basified with Et_3N (5 μL), dried over $MgSO_4$, filtered and the volume reduced to approximately 1 mL *in vacuo*. The porphyrin was precipitated from DCM:MeOH to give a brown solid which was collected by vacuum filtration (7.5 mg, 70%). ^{1}H NMR (400 MHz, d_6-DMSO): δ 12.02 (s, 1H, NH), 8.98 (s, 1H, $H_{\beta\text{-pyrrolic}}$), 8.92 (s, 2H, $H_{\beta\text{-pyrrolic}}$), 8.91 (s, 2H, $H_{\beta\text{-pyrrolic}}$), 8.86 (d, 1H, J = 4.7 Hz, $H_{\beta\text{-pyrrolic}}$), 8.73 (d, 1H, J = 4.7 Hz, $H_{\beta\text{-pyrrolic}}$), 8.27-8.21 (m, 8H, H_{ortho}), 7.87-7.79 (m, 14H, $H_{meta,\ para}$ and $H_{aromatic}$), 7.47 (d, 2H, J = 8.3 Hz, $H_{aromatic}$), 7.41 (s, 1H, H_6), 6.20 (t, 1H, J = 6.1 Hz, $H_{1'}$), 5.32 (d, 1H, J = 4.7 Hz, 3′OH), 5.22 (d, 1H, J = 5.6 Hz, 5′OH), 4.46 (m, 1H, $H_{3'}$), 3.95 (m, 1H, $H_{4'}$), 3.66 (m, 2H, $H_{5'}$), 2.20 (m, 2H, $H_{2'}$), -2.81 (br s, 2H, NH). UV-Vis ($CHCl_3$): λ_{max} [nm] ($\varepsilon \times 10^{-3}$) 429.5 (112), 524 (12.4), 560 (5.62), 600 (4.24), 659 (3.21). ESI-LRMS: *m/z* (%, assignment) cluster at 965-967, 965, (20, $(M+H)^+$) ESI-HRMS: Calcd for $(M+H)^+$ ($C_{63}H_{45}N_6O_5$): 965.3451, found: 965.3492.

General Synthetic Method for Porphyrin Nucleosides 97-101

Appropriate porphyrin azide (30 mg) was dissolved in dry THF (2.0 mL) and the reaction was degassed under Ar for 30 min. To this 2′-deoxy-5′-*O*-4″,4‴-dimethoxytrityl-5-ethynyluridine (**93**, 1 eq) was added followed by tetrakis(acetonitrile)copper(I)hexafluorophosphate (2 eq). The reaction was stirred at RT for 2 (**99-101**) to 4 (**97** and **98**) days at which point the solvent was removed *in vacuo* and the crude material was purified by silica gel column chromatography with MeOH:DCM (1:9) first eluting the starting azide followed by the product.

2′-Deoxy-5-{1-{4-[2-[4-(5,10,15,20-tetraphenylporphyrinato nickel II)vinyl]phenyl}-1,2,3-triazol-4-yl}uridine (97)

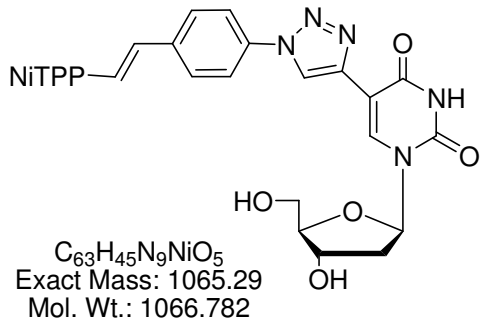

Characterisation and yields: Compound **97**, 13 mg, 36%. ^{1}H NMR (500 MHz, d_6-DMSO): δ 11.80 (br s, 1H, NH), 8.96 (s, 1H, $H_{\beta\text{-pyrrolic}}$), 8.93 (s, 1H, H_6 or $H_{triazole}$), 8.70-8.65 (m, 7H, $H_{\beta\text{-pyrrolic}}$ + H_6 or $H_{triazole}$), 8.05-7.99 (m, 8H, H_{ortho}), 7.93 (d, 2H, J = 8.6 Hz, $H_{aromatic}$), 7.91-7.74 (m, 12H, $H_{meta,\ para}$), 7.38 (d, 2H, J = 8.6 Hz, $H_{aromatic}$), 6.84 (d, 1H, J = 15.6 Hz, $H_{vinylic}$), 6.84 (d, 1H, J = 15.7 Hz, $H_{vinylic}$), 6.28 (t, 1H, J = 6.7 Hz, $H_{1'}$), 5.33 (d, 1H, J = 4.1 Hz, C3′OH), 5.10 (t, 1H, J = 4.9 Hz, CH_2OH), 4.34-4.30 (m, 1H, $H_{3'}$), 3.89 (m, 1H, $H_{4'}$), 3.66-3.63 (m, 2H, $H_{5'}$), 2.25-2.23 (m, 2H, $H_{2'}$). UV-Vis ($CHCl_3$): λ_{max} [nm] ($\varepsilon \times 10^{-3}$) 309 (20.7), 427.5 (119), 538 (9.48), 572 (6.87). ESI-LRMS: *m/z* (%, assignment) cluster at 1064-1070, 1064, (100, $(M-H)^-$). ESI-HRMS: Calcd for $(M-H)^-$ ($C_{63}H_{44}N_9O_5{}^{58}Ni$): 1064.2819, found: 1064.2828.

2′-Deoxy-5-{1-{4-[2-[4-(5,10,15,20-tetraphenylporphyrinato nickel II)vinyl]benzyl}--1,2,3-triazol-4-yl}uridine and **2′-deoxy-5′-*O*-dimethoxytrityl-5-{1-{4-[2-[4-(5,10,15,20-tetraphenylporphyrinato nickel II)vinyl]benzyl}-1,2,3-triazol-4-yl}uridine (98)**

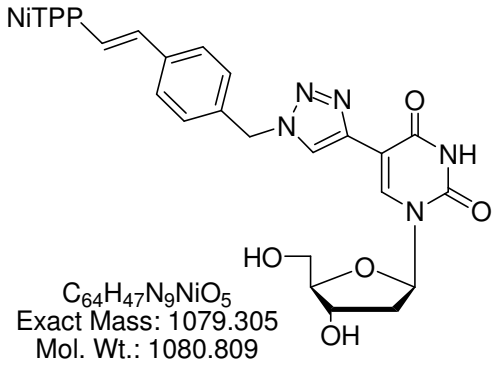

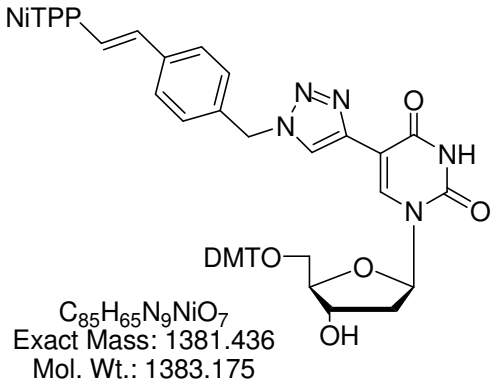

Compound **98**, in approximate ratio of 4:1 (DMT off: DMT on) 10 mg, 28%. ^{1}H NMR assigned for DMT off product in mixture (400 MHz, d_6-DMSO): δ 11.70 (br s, 1H, NH), 8.90 (s, 1H, $H_{\beta\text{-pyrrolic}}$), 8.67-8.63 (m, 6H, $H_{\beta\text{-pyrrolic}}$), 8.57 (s, 1H, H_6 or $H_{triazole}$), 8.44 (s, 1H, H_6 or $H_{triazole}$), 8.03-7.94 (m, 8H, H_{ortho}), 7.82-7.72 (m, 12H, $H_{meta,\ para}$), 7.27 (d, 2H, J = 8.2 Hz, $H_{aromatic}$), 7.25 (d, 1H, J = 16.1 Hz, $H_{vinylic}$), 7.19 (d, 2H, J = 8.2 Hz, $H_{aromatic}$), 6.79 (d, 1H, J = 16.1 Hz, $H_{vinylic}$), 6.24 (t, 1H, J = 7.0 Hz, $H_{1'}$), 5.64 (s, 2H, CH_2), 5.28 (d, 1H, J = 4.2 Hz, C3′OH), 5.02 (t, 1H, J = 4.9 Hz, C5′OH), 4.28 (m, 1H, $H_{3'}$), 3.85 (m, 1H, $H_{4'}$), 3.60 (m, 2H, $H_{5'}$), 2.18 (m, 2H, $H_{2'}$). UV-Vis ($CHCl_3$): λ_{max} [nm] ($\varepsilon \times 10^{-3}$) 309 (22.3), 426 (180), 540 (14.8), 576 (9.60). ESI-LRMS: *m/z* (%, assignment) cluster at 1078-1084, 1078, (100, DMT off, $(M-H)^-$) and 1380-1385, 1381, (15, DMT on, M^-). ESI-HRMS: DMT off; calcd for $(M-H)^-$ ($C_{63}H_{46}N_9O_5{}^{58}Ni$): 1078.2975, found: 1078.2991, DMT on; calcd for $(M)^-$ ($C_{85}H_{65}N_9O_7{}^{58}Ni$): 1381.4360, found: 1381.4333.

2′-Deoxy-5-{1-{4-[2-[4-(5,10,15,20-tetraphenylporphyrinato zinc II)ethynyl]benzyl}-1,2,3-triazol-4-yl}uridine and **2′-deoxy-5′-*O*-dimethoxytrityl-5-{1-{4-[2-[4-(5,10,15,20-tetraphenylporphyrinato zinc II)ethynyl]benzyl}-1,2,3-triazol-4-yl}uridine (99)**

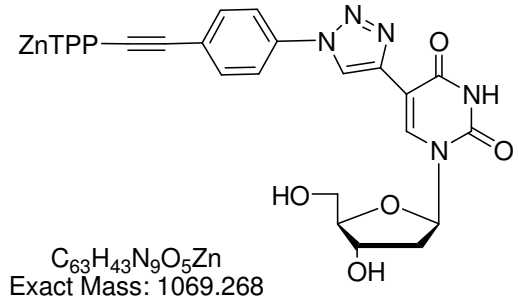

$C_{63}H_{43}N_9O_5Zn$
Exact Mass: 1069.268
Mol. Wt.: 1071.463

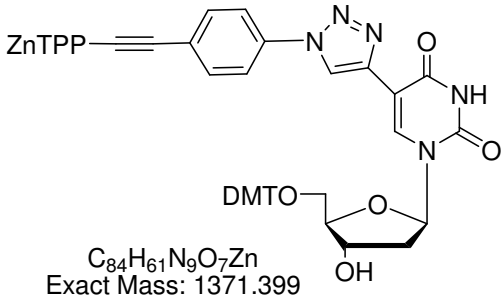

$C_{84}H_{61}N_9O_7Zn$
Exact Mass: 1371.399
Mol. Wt.: 1373.829

Compound **99**, in approximate ratio of 3:1 (DMT off: DMT on) 15 mg, 39%. ^{1}H NMR assigned for DMT off product in mixture (400 MHz, d_6-DMSO): δ 11.78 (br s, 1H, NH), 9.03 (s, 1H, $H_{\beta\text{-pyrrolic}}$), 8.89 (s, 1H, H_6 or $H_{triazole}$), 8.76 (s, 2H, $H_{\beta\text{-pyrrolic}}$), 8.74 (s, 2H, $H_{\beta\text{-pyrrolic}}$), 8.71 (d, 1H, J = 4.5 Hz, $H_{\beta\text{-pyrrolic}}$), 8.71 (s, 1H, H_6 or $H_{triazole}$), 8.59 (d, 1H, J = 4.5 Hz, $H_{\beta\text{-pyrrolic}}$), 8.22-8.15 (m, 8H, H_{ortho}), 7.85-7.74 (m, 12H, $H_{meta,\ para}$), 7.28 (d, 2H, J = 8.2 Hz, $H_{aromatic}$), 7.22 (d, 2H, J = 8.3 Hz, $H_{aromatic}$), 6.27 (t, 1H, J = 6.9 Hz, $H_{1'}$), 5.31 (d, 1H, J = 4.0 Hz, C3′OH), 5.09 (t, 1H, J = 5.0 Hz, C5′OH), 4.32 (m, 1H, $H_{3'}$), 3.89 (m, 1H, $H_{4'}$), 3.65 (m, 2H, $H_{5'}$), 2.24 (m, 2H, $H_{2'}$). UV-Vis ($CHCl_3$): λ_{max} [nm] ($\varepsilon \times 10^{-3}$) 435 (250), 563 (16.7) 603 (7.54). ESI-LRMS: *m/z* (%, assignment) cluster at 1068-1075, 1068, (100, DMT off, $(M-H)^-$) and 1370-1375, 1370, (20, DMT on, $(M-H)^-$). ESI-HRMS: DMT off; calcd for $(M-H)^-$ ($C_{63}H_{42}N_9O_5{}^{64}Zn$): 1068.2600, found: 1068.2600, DMT on; calcd for $(M-H)^-$ ($C_{84}H_{60}N_9O_7{}^{64}Zn$): 1370.3907, found: 1370.3933.

2′-Deoxy-5-{1-{4-[2-[4-(5,10,15,20-tetraphenylporphyrinato iron III chloride)vinyl]benzyl}--1,2,3-triazol-4-yl}uridine and **2′-deoxy-5′-*O*-dimethoxytrityl-5-{1-{4-[2-[4-(5,10,15,20-tetraphenylporphyrinato iron III chloride)vinyl]benzyl}-1,2,3-triazol-4-yl}uridine (100)**

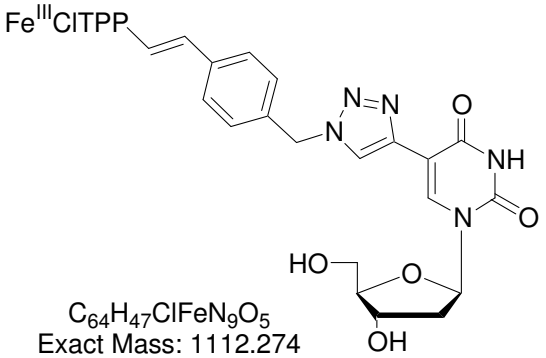

$C_{64}H_{47}ClFeN_9O_5$
Exact Mass: 1112.274
Mol. Wt.: 1113.413

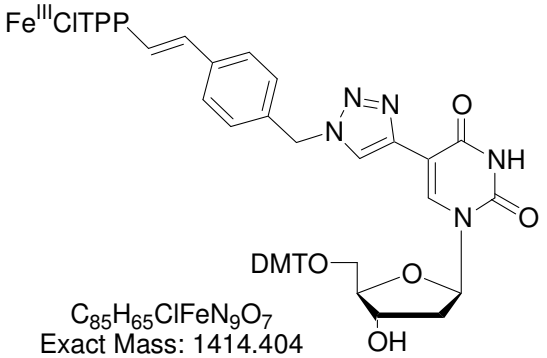

$C_{85}H_{65}ClFeN_9O_7$
Exact Mass: 1414.404
Mol. Wt.: 1415.78

Compound **100**, in unknown ratio of DMT off: DMT on, 15 mg, 42%. UV-Vis ($CHCl_3$): λ_{max} [nm] ($\varepsilon \times 10^{-3}$) 426 (120), 514 (16.6). ESI-LRMS: *m/z* (%, assignment) cluster at 1074-1079, 1077, (100, DMT off, $(M-Cl)^-$) ESI-HRMS: DMT off; calcd for $(M-HCl)^-$ ($C_{64}H_{46}N_9O_5{}^{56}Fe$): 1076.2971, found: 1076.2948, No HRMS could be obtained for the DMT on structure.

2′-Deoxy-5-{1-{4-[2-[4-(5,10,15,20-tetraphenylporphyrinato copper II)vinyl]phenyl}--1,2,3-triazol-4-yl}uridine and **2′-deoxy-5′-*O*-dimethoxytrityl-5-{1-{4-[2-[4-(5,10,15,20-tetraphenylporphyrinato copper II)vinyl]phenyl}-1,2,3-triazol-4-yl}uridine (101)**

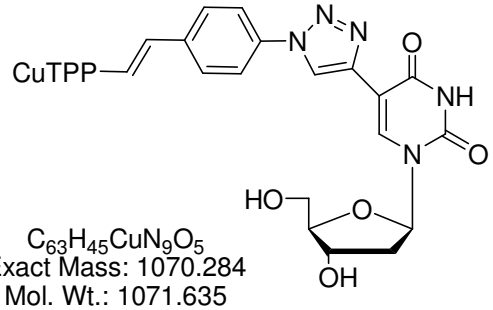

$C_{63}H_{45}CuN_9O_5$
Exact Mass: 1070.284
Mol. Wt.: 1071.635

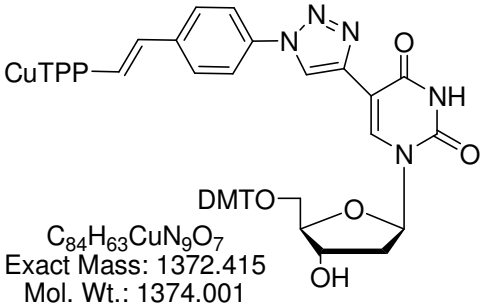

$C_{84}H_{63}CuN_9O_7$
Exact Mass: 1372.415
Mol. Wt.: 1374.001

Compound **101**, in unknown ratio of DMT off: DMT on, 15 mg, 44%. UV-Vis ($CHCl_3$): λ_{max} [nm] ($\varepsilon \times 10^{-3}$) 425 (182), 548 (13.7) 584 (5.94) ESI-LRMS: *m/z* (%, assignment) cluster at 1068-1075, 1068, (50, DMT off, $(M-H)^-$) and 1371-1075, 1371, (25, DMT on, $(M-H)^-$). ESI-HRMS: DMT off; calcd for $(M-H)^-$ ($C_{63}H_{44}N_9O_5{}^{63}Cu$): 1069.2761, found:

1069.2775, DMT on; calcd for $(M-H)^-$ ($C_{84}H_{62}N_9O_7{}^{63}Cu$): 1371.4068, found: 1371.4070.

4-[*trans*-2′-(5″,10″,15″,20″-Tetraphenylporphyrinato-2″-yl copper II)ethen-1′-yl]azidobenzene (102)

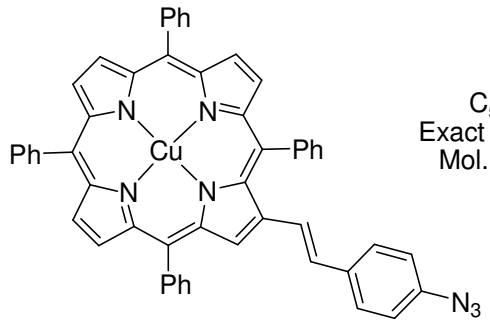

$C_{52}H_{33}CuN_7$
Exact Mass: 818.209
Mol. Wt.: 819.411

Compound **102** was produced as an unwanted product of the Cu^I catalysed CuAAC reaction between 4-[*trans*-2′-(5″,10″,15″,20″-tetraphenylporphyrin-2″-yl)ethene-1-yl]azidobenzene (**43**) and 2′-deoxy-5′-*O*-4″,4‴-dimethoxytrityl-5-ethynyluridine (**93**). UV-Vis ($CHCl_3$): λ_{max} [nm] ($\varepsilon \times 10^{-3}$) 422 (167), 547 (16.5), 584 (9.06). ESI-LRMS: *m/z* (%, assignment) cluster at 818-825, 818 (100, M^+). ESI-HRMS: Calcd for M^+ ($C_{52}H_{33}N_7Cu$): 818.2088, found: 818.2042. IR-ATR (cm^{-1}): 2114.1 (azide).

Experimental for the Synthesis of Porphyrin Oligonucleotides

Post-synthetic CuAAC Reaction

For the shaking reaction DMT-off **ON4-ON9** on CPG (0.33 μmol) containing the appropriate ethynyl modification were removed from their corresponding columns and added to a microcentifuge vial along with the appropriate azide (7.67 μmol, 23 eq) and degassed DMSO (150 μL). Freshly prepared $CuSO_4 \cdot 5H_2O$ (0.2 μmol, 0.6 eq, 5 μL of a 40 μmol/mL solution in degassed H_2O) and sodium ascorbate (1.0 μmol, 3 eq, 20 μL of a 50 μmol/mL solution in degassed H_2O) were added. The reaction mixture was shaken under Ar in darkness for three days.

For the microwave accelerated reaction DMT-off oligonucleotides on CPG (**ON25** or **ON26**, 0.33 μmol) containing 2′-*O*-propargyl uridine or 2′-*O*-propargyl adenosine were removed from their corresponding columns and placed into a microwave reaction vessel

together with appropriate azide (7.67 μmol, 23 eq) in degassed DMSO (200 μL). Freshly prepared $CuSO_4 \cdot 5H_2O$ (0.32 μmol, 0.96 eq, 8 μL of a 40 μmol/mL solution in degassed H_2O) and sodium ascorbate (1.25 μmol, 3.8 eq, 25 μL of a 50 μmol/mL solution in degassed H_2O) were added. The reaction mixture was then irradiated in a microwave synthesiser (Discover, CEM Corporation, 70 °C, 100 watts, 20 min).

The content of the reactions were transferred to a microcentrifuge tube. To the reaction mixture DCM (1.5 mL) was added and the CPG was centrifuged (14500 rpm for 1 minute). The DCM was removed and washing was repeated until the supernatant no longer showed any colour (see recovery of azides). The red CPG was then washed with H_2O (1.5 mL) to remove any remaining inorganic salts. Residual solvent was removed under reduced pressure and the obtained DMT-off oligonucleotides bound to CPG supports were treated with 32% aq NH_4OH (1 mL) at RT for 2 h and then at 55 °C overnight.

Recovery of Azides

To the combined DCM washings containing the appropriate reacted azide, H_2O (50 mL) was added and the resulting solution was vigorously stirred for 1 hr to remove DMSO and any remaining inorganic salts. The organic layer was extracted into DCM (2 × 50 mL), dried over $MgSO_4$, filtered and the porphyrin was precipitated from DCM:MeOH. The desired product was collected by filtration to give a red solid (approximately 80-90% recovery).

Purification of Oligonucleotides

Purification of porphyrin functionalised DMT off ONs by HPLC was accomplished using the following gradient. Buffer A [0.05 M triethylammonium acetate in H_2O (pH = 7.0)] and buffer B (75% ACN in H_2O), flow 2.5 mL min^{-1}. Gradients: 2 min 100% A, linear gradient to 70% B in 38 min, linear gradient to 100% B in 7 min, 100% B in 3 min and then 100% A in 10 min.

Purification of porphyrin functionalised DMT off ONs by puri-pak C_{18} cartridges was accomplished using the following method. Although it is recommended that the

solvents are allowed to drip through the column an increased flow rate of approximately 30 mL per min was found to be adequate for purification. Cartridges were first washed with ACN (2 × 2 mL) then activated with 1.0 M TEAA solution (3 × 2 mL). Crude porphyrin modified oligonucleotide was loaded on to the column in a 1:1 solution of conc. NH_4OH:H_2O (2 mL) with the eluent being reloaded and eluted until the eluent showed no colour. Cartridges were then flushed with 3% aq. NH_4OH solution (4 × 2 mL) followed by H_2O (4 × 2 mL). Oligonucleotides were then eluted with a gradient of ACN:H_2O (20% ACN to 100% ACN, 10% intervals) eluting single modifications in 20% ACN:H_2O and double modifications in 30-40% ACN:H_2O.

After purification ONs were lyophylised, dissolved in H_2O (100 μL, heating to 70 °C for 1 hr was required for some ONs), 0.01 M lithium perchlorate in acetone (1.6 mL) was added and the ONs were stored at -10 °C for 1 h. The precipitated ON pellet was centrifuged (15000 rpm for 30 min), the supernatant was removed and the pellet was washed with acetone (30 μL).

Melting Temperature Measurements

The triplexes were formed by first mixing the two strands of the Watson-Crick duplex, each at a concentration of 1.0 μM in the corresponding buffer solution followed by the addition of the third TFO strand at a concentration of 1.5 μM (total volume 1 mL). The solutions were then heated to 70 °C for 15 min, cooled and incubated at 10 °C for 30 min. The duplexes were formed by mixing the two strands each at a concentration of 1.0 μM in the appropriate buffer (total volume 1 mL). The solutions were heated at 90 °C for 15 min, cooled and incubated at 20 °C for 30 min. The melting temperatures were determined as the maxima of the first derivative plots of the melting curves obtained by measuring absorbance at 260 nm and 430/423 nm against increasing temperature (10 to 70 (or 90) °C, 1.0 °C per min for duplexes and 5 to 70 °C, 0.5 °C per min for triplexes). All melting temperatures are an average of two denaturing-annealing cycles.

Appendix A Crystallographic Data

Compound **80**

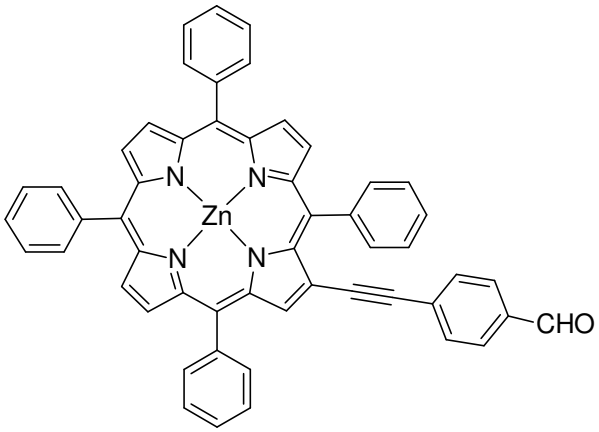

Empirical Formula	$C_{54}H_{35}N_4O_2Zn$	
Formula weight	910.15	
Temperature	106	
Wavelength	0.71073	
Crystal system	Monoclinic	
Space Group	P2 (1) /c	
Unit cell dimensions	a = 10.161(2) Å	α = 90.00 °
	b = 35.026(7) Å	β = 105.43(3) °
	c = 12.550(3) Å	γ = 90.00 °
Volume	4305.5(15) $Å^3$	
Z	4	
Density (calculated)	1.404 Mg/m^3	
Absorption Coefficient	0.744 mm^{-1}	
F(000)	1876	
Index ranges	-12<=h<=10, -43<=k<=39, -11<=l<=15	
Reflections collected	23230	
Independent reflections	8616	
Completeness to theta	0.978	
Refinement method	Shelxl-97	
Data/restraints/parameters	18	
Goodness-of-fit on F^2	1.052	
Largest diff. peak and hole	-1.167 e. $Å^{-3}$	
R factor (all)	0.0995	
R factor (gt)	0.0716	
wR factor (all)	0.1864	
wR factor (gt)	0.1713	

Compound **39a**

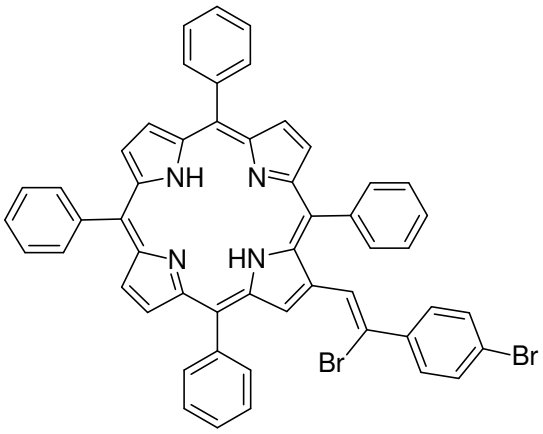

Empirical Formula	$C_{52}H_{34}Br_2N_4$	
Formula weight	890.65	
Temperature	106	
Wavelength	0.71073	
Crystal system	Triclinic	
Space Group	P-1	
Unit cell dimensions	a = 9.4970 (19) Å	α = 71.08 (3) °
	b = 13.337 (3) Å	β = 79.17 (3) °
	c = 19.031 (4) Å	γ = 74.07 (3) °
Volume	2179.7(8) $Å^3$	
Z	2	
Density (calculated)	1.357 Mg/m^3	
Absorption Coefficient	1.902 mm^{-1}	
F(000)	904	
Index ranges	-13<=h<=12, -19<=k<=18, -26<=l<=27	
Reflections collected	19407	
Independent reflections	12212	
Refinement method	Shelx-97	
Goodness-of-fit on F^2	1.098	
Largest diff. peak and hole	5.272 e. $Å^{-3}$	
R factor (all)	0.1380	
R factor (gt)	0.1020	
wR factor (all)	0.3325	
wR factor (gt)	0.2994	

References

1. Kadish, K. M.; Smith, K. M.; Guilard, R., *The Porphyrin Handbook*. Academic Press: London, **2000;** Vol. 4, p 345.
2. Lin, V. S. Y.; DiMagno, S. G.; Therien, M. J., Highly Conjugated, Acetylenyl Bridged Porphyrins: New Models for Light-Harvesting Antenna Systems, *Science* **1994,** 264, (5162), 1105-1111.
3. Campbell Wayne, M. *Porphyrins for Surface Modification.* Massey University, Palmerston North, **2001**.
4. Filichev, V. V.; Pedersen, E. B., DNA-Conjugated Organic Chromophores in DNA Stacking Interactions, *Wiley Encycl. Chem. Biol.* **2009,** 1, 493-524.
5. Varghese, R.; Wagenknecht, H.-A., DNA as a Supramolecular Framework for the Helical Arrangements of Chromophores: Towards Photoactive DNA-Based Nanomaterials, *Chem. Commun.* **2009**, (19), 2615-2624.
6. Wagenknecht, H.-A., Helical Arrangement of Porphyrins Along DNA: Towards Photoactive DNA-Based Nanoarchitectures, *Angew. Chem., Int. Ed.* **2009,** 48, (16), 2838-2841.
7. Neidle, S.; Balasubramanian, S., *Quadruplex Nucleic Acids*. The Royal Society of Chemsitry: London, **2006**.
8. Mergny, J.-L.; Lacroix, L., Analysis of Thermal Melting Curves, *Oligonucleotides* **2003,** 13, (6), 515-537.
9. Pescitelli, G.; Gabriel, S.; Wang, Y.; Fleischhauer, J.; Woody, R. W.; Berova, N., Theoretical Analysis of the Porphyrin-Porphyrin Exciton Interaction in Circular Dichroism Spectra of Dimeric Tetraarylporphyrins, *J. Am. Chem. Soc.* **2003,** 125, (25), 7613-7628.
10. Dos Santos, T.; Morandeira, A.; Koops, S.; Mozer, A. J.; Tsekouras, G.; Dong, Y.; Wagner, P.; Wallace, G.; Earles, J. C.; Gordon, K. C.; Officer, D.; Durrant, J. R., Injection Limitations in a Series of Porphyrin Dye-Sensitized Solar Cells, *J. Phys. Chem. C* **2010,** 114, (7), 3276-3279.
11. Earles, J. C.; Gordon, K.; Stephenson, A. W. I.; Partridge, A. C.; Officer, D. L., Manuscript under preperation.
12. Kasha, M.; Rawls, H. R.; El-Bayoumi, M. A., Exciton Model in Molecular Spectroscopy, *Pure Appl. Chem.* **1965,** 11, (3-4), 371-392.

13. Kypr, J.; Kejnovska, I.; Renciuk, D.; Vorlickova, M., Circular Dichroism and Conformational Polymorphism of DNA, *Nucleic Acids Res.* **2009,** 37, (6), 1713-1725.
14. Rodger, A.; Norden, B., *Circular Dichroism and Linear Dichroism*. Oxford University Press: **1997;** p 150.
15. Malinovskii, V. L.; Wenger, D.; Haner, R., Nucleic Acid-Guided Assembly of Aromatic Chromophores, *Chem. Soc. Rev.* **2010,** 39, (2), 410-422.
16. McMillin, D. R.; Shelton, A. H.; Bejune, S. A.; Fanwick, P. E.; Wall, R. K., Understanding Binding Interactions of Cationic Porphyrins with B-Form DNA, *Coord. Chem. Rev.* **2005,** 249, (13-14), 1451-1459.
17. Fiel, R. J.; Munson, B. R., Binding of Meso-Tetra (4-N-Methylpyridyl) Porphine to DNA, *Nucleic Acids Res.* **1980,** 8, (12), 2835-2842.
18. Carvlin, M. J.; Datta-Gupta, N.; Fiel, R. J., Circular Dichroism Spectroscopy of a Cationic Porphyrin Bound to DNA, *Biochem. Biophys. Res. Commun.* **1982,** 108, (1), 66-73.
19. Pasternack, R. F.; Gibbs, E. J.; Villafranca, J. J., Interactions of Porphyrins with Nucleic Acids, *Biochemistry* **1983,** 22, (23), 5409-5417.
20. Pasternack, R. F.; Gibbs, E. J.; Villafranca, J. J., Interactions of Porphyrins with Nucleic Acids, *Biochemistry* **1983,** 22, (10), 2406-2414.
21. O'Connor, A. E.; Gallagher, W. M.; Byrne, A. T., Porphyrin and Nonporphyrin Photosensitizers in Oncology: Preclinical and Clinical Advances in Photodynamic Therapy, *Photochem. Photobiol.* **2009,** 85, (5), 1053-1074.
22. Moreira, L. M.; dos Santos, F. V.; Lyon, J. P.; Maftoum-Costa, M.; Pacheco-Soares, C.; da Silva, N. S., Photodynamic Therapy: Porphyrins and Phthalocyanines as Photosensitizers, *Aust. J. Chem.* **2008,** 61, (10), 741-754.
23. Andrews, K.; McMillin, D. R., A Pared-Down Version of 5,10,15,20-Tetra(N-methylpyridinium-4-yl)porphyrin Intercalates into B-form DNA Regardless of Base Composition: Binding Studies of Tri(N-methylpyridinium-4-yl)porphyrins, *Biochemistry* **2008,** 47, (4), 1117-1125.
24. Chen, B.; Qin, W.; Wang, P.; Tian, T.; Ma, H.; Cao, X.; Wu, X.; Zhou, X.; Zhang, X.-L.; Liu, F.; Zheng, F.; Li, X., Synthesis of Beta-substituted Cationic Porphyrins and their Interactions with DNA, *Bioorg. Med. Chem. Lett.* **2003,** 13, (21), 3731-3733.

25. Dixon, I. M.; Lopez, F.; Tejera, A. M.; Esteve, J.-P.; Blasco, M. A.; Pratviel, G.; Meunier, B., A G-Quadruplex Ligand with 10000-Fold Selectivity over Duplex DNA, *J. Am. Chem. Soc.* **2007,** 129, (6), 1502-1503.

26. Zhang, H.-J.; Wang, X.-F.; Wang, P.; Pang, S.-P.; Ai, X.-C.; Zhang, J.-P., Interactions Between meso-Tetrakis(4-(N-methylpyridiumyl))porphyrin TMPyP4 and DNA G-quadruplex of Telomeric Repeated Sequence TTAGGG, *Sci. China, Ser. B: Chem.* **2008,** 51, (5), 452-456.

27. Lubitz, I.; Borovok, N.; Kotlyar, A., Interaction of Monomolecular G4-DNA Nanowires with TMPyP: Evidence for Intercalation, *Biochemistry* **2007,** 46, (45), 12925-12929.

28. Olaussen Ken, A.; Dubrana, K.; Domont, J.; Spano, J.-P.; Sabatier, L.; Soria, J.-C., Telomeres and Telomerase as Targets for Anticancer Drug Development, *Crit. Rev. Oncol. Hematol.* **2006,** 57, (3), 191-214.

29. Blasco, M. A., Telomeres and Human Disease: Ageing, Cancer and Beyond, *Nat. Rev. Genet.* **2005,** 6, (8), 611-622.

30. Neidle, S.; Parkinson, G., Telomere Maintenance as a Target for Anticancer Drug Discovery, *Nat. Rev. Drug Discovery* **2002,** 1, (5), 383-393.

31. Tanaka, K.; Okahata, Y., A DNA-Lipid Complex in Organic Media and Formation of an Aligned Cast Film, *J. Am. Chem. Soc.* **1996,** 118, (44), 10679-10683.

32. Sergeyev, V. G.; Pyshkina, O. A.; Lezov, A. V.; Melnikov, A. B.; Ryumtsev, E. I.; Zezin, A. B.; Kabanov, V. A., DNA Complexed with Oppositely Charged Amphiphile in Low-Polar Organic Solvents, *Langmuir* **1999,** 15, (13), 4434-4440.

33. Qu, J.; Morita, R.; Satoh, M.; Wada, J.; Terakura, F.; Mizoguchi, K.; Ogata, N.; Masuda, T., Synthesis and Properties of DNA Complexes Containing 2,2,6,6-Tetramethyl-1-piperidinoxy (TEMPO) Moieties as Organic Radical Battery Materials, *Chem. Eur. J.* **2008,** 14, (11), 3250-3259.

34. Qu, J.; Qiu, Z.; Chen, H.; Ogata, N.; Masuda, T., DNA-lipid Complexes Carrying Azobenzene Moieties: Preparation, Characterization, and Photoisomerization, *Polymer* **2009,** 50, (23), 5398-5405.

35. Fukushima, T.; Kawaguchi, M.; Hayakawa, T.; Takeda, S.; Inoue, Y.; Ohno, J.; Taniguchi, K., Drug Binding and Releasing Characteristics of DNA/lipid/PLGA Film, *Dent. Mater. J.* **2007,** 26, (6), 854-860.

36. Okahata, Y.; Kobayashi, T.; Tanaka, K.; Shimomura, M., Anisotropic Electric Conductivity in an Aligned DNA Cast Film, *J. Am. Chem. Soc.* **1998,** 120, (24), 6165-6166.

37. Mammana, A.; Asakawa, T.; Bitsch-Jensen, K.; Wolfe, A.; Chaturantabut, S.; Otani, Y.; Li, X.; Li, Z.; Nakanishi, K.; Balaz, M.; Ellestad, G. A.; Berova, N., Synthesis and Characterization of Water-soluble Free-Base, Zinc and Copper Porphyrin-Oligonucleotide Conjugates, *Bioorg. Med. Chem.* **2008,** 16, (13), 6544-6551.

38. Endo, M.; Fujitsuka, M.; Majima, T., Programmable Conformational Regulation of Porphyrin Dimers on Geometric Scaffold of Duplex DNA, *Tetrahedron* **2008,** 64, (8), 1839-1846.

39. Endo, M.; Fujitsuka, M.; Majima, T., Diastereochemically Controlled Porphyrin Dimer Formation on a DNA Duplex Scaffold, *J. Org. Chem.* **2008,** 73, (3), 1106-1112.

40. Weisbrod, S. H.; Marx, A., Novel Strategies for the Site-Specific Covalent Labelling of Nucleic Acids, *Chem. Commun.* **2008**, (44), 5675-5685.

41. Bouamaied, I.; Fendt, L.-A.; Haeussinger, D.; Wiesner, M.; Thoeni, S.; Amiot, N.; Stulz, E., Porphyrin-DNA: A Supramolecular Scaffold for Functional Molecules on the Nanometre Scale, *Nucleosides, Nucleotides Nucleic Acids* **2007,** 26, (10-12), 1533-1538.

42. Bouamaied, I.; Nguyen, T.; Ruhl, T.; Stulz, E., Supramolecular Helical Porphyrin Arrays using DNA as a Scaffold, *Org. Biomol. Chem.* **2008,** 6, (21), 3888-3891.

43. Fendt, L.-A.; Bouamaied, I.; Thoeni, S.; Amiot, N.; Stulz, E., DNA as Supramolecular Scaffold for Porphyrin Arrays on the Nanometer Scale, *J. Am. Chem. Soc.* **2007,** 129, (49), 15319-15329.

44. Nguyen, T. N.; Brewer, A.; Stulz, E., Duplex Stabilization and Energy Transfer in Zipper Porphyrin-DNA, *Angew. Chem., Int. Ed.* **2009,** 48, (11), 1974-1977.

45. Morales-Rojas, H.; Kool, E. T., A Porphyrin C-Nucleoside Incorporated into DNA, *Org. Lett.* **2002,** 4, (25), 4377-4380.

46. Sitaula, S.; Reed, S. M., Porphyrin Conjugated to DNA by a 2'-Amido-2'-deoxyuridine Linkage, *Bioorg. Med. Chem. Lett.* **2008,** 18, (2), 850-855.

47. Balaz, M.; Bitsch-Jensen, K.; Mammana, A.; Ellestad, G. A.; Nakanishi, K.; Berova, N., Porphyrins as Spectroscopic Sensors for Conformational Studies of DNA, *Pure Appl. Chem.* **2007,** 79, (4), 801-809.

48. Balaz, M.; Holmes, A. E.; Benedetti, M.; Proni, G.; Berova, N., Porphyrin Substituted Phosphoramidites: New Building Blocks for Porphyrin-Oligonucleotide Syntheses, *Bioorg. Med. Chem.* **2005,** 13, (7), 2413-2421.

49. Balaz, M.; Holmes, A. E.; Benedetti, M.; Rodriguez, P. C.; Berova, N.; Nakanishi, K.; Proni, G., Synthesis and Circular Dichroism of Tetraarylporphyrin-Oligonucleotide Conjugates, *J. Am. Chem. Soc.* **2005,** 127, (12), 4172-4173.

50. Balaz, M.; Li, B. C.; Jockusch, S.; Ellestad, G. A.; Berova, N., Tetraarylporphyrin as a Selective Molecular Cap for Non-Watson-Crick Guanine-Adenine Base-Pair Sequences, *Angew. Chem., Int. Ed.* **2006,** 45, (21), 3530-3533.

51. Balaz, M.; Li, B. C.; Steinkruger, J. D.; Ellestad, G. A.; Nakanishi, K.; Berova, N., Porphyrins Conjugated to DNA as CD Peporters of the Salt-Induced B to Z-DNA Transition, *Org. Biomol. Chem.* **2006,** 4, (10), 1865-1867.

52. Balaz, M.; Steinkruger, J. D.; Ellestad, G. A.; Berova, N., 5'-Porphyrin-Oligonucleotide Conjugates: Neutral Porphyrin-DNA Interactions, *Org. Lett.* **2005,** 7, (25), 5613-5616.

53. Berlin, K.; Jain, R. K.; Simon, M. D.; Richert, C., A Porphyrin Embedded in DNA, *J. Org. Chem.* **1998,** 63, (5), 1527-1535.

54. Onoda, A.; Igarashi, M.; Naganawa, S.; Sasaki, K.; Ariyasu, S.; Yamamura, T., Circular Dichroism of Neutral Zinc Porphyrin-Oligonucleotide Conjugates Modified with Flexible Linker, *Bull. Chem. Soc. Jpn.* **2009,** 82, (10), 1280-1286.

55. Li, H.; Fedorova, O. S.; Trumble, W. R.; Fletcher, T. R.; Czuchajowski, L., Site-Specific Photomodification of DNA by Porphyrin-Oligonucleotide Conjugates Synthesized via a Solid Phase H-Phosphonate Approach, *Bioconjugate Chem.* **1997,** 8, (1), 49-56.

56. Mammana, A.; Pescitelli, G.; Asakawa, T.; Jockusch, S.; Petrovic, A. G.; Monaco, R. R.; Purrello, R.; Turro, N. J.; Nakanishi, K.; Ellestad, G. A.; Balaz, M.; Berova, N., Role of Environmental Factors on the Structure and Spectroscopic Response of 5'-DNA-Porphyrin Conjugates Caused by Changes

in the Porphyrin-Porphyrin Interactions, *Chem. Eur. J.* **2009,** 15, (44), 11853-11866.

57. Huisgen, R., *1,3-Dipolar Cycloaddition Chemistry, Vol 1*. Wiley: New York, **1984;** p 1-176.
58. Tornoe, C. W.; Christensen, C.; Meldal, M., Peptidotriazoles on Solid Phase: [1,2,3]-Triazoles by Regiospecific Copper(I)-Catalyzed 1,3-Dipolar Cycloadditions of Terminal Alkynes to Azides, *J. Org. Chem.* **2002,** 67, (9), 3057-3064.
59. Rostovtsev, V. V.; Green, L. G.; Fokin, V. V.; Sharpless, K. B., A Stepwise Huisgen Cycloaddition Process: Copper(I)-Catalyzed Regioselective "ligation" of Azides and Terminal Alkynes, *Angew. Chem., Int. Ed.* **2002,** 41, (14), 2596-2599.
60. Amblard, F.; Cho, J. H.; Schinazi, R. F., Cu(I)-Catalyzed Huisgen Azide-Alkyne 1,3-Dipolar Cycloaddition Reaction in Nucleoside, Nucleotide, and Oligonucleotide Chemistry, *Chem. Rev.* **2009,** 109, (9), 4207-4220.
61. Gramlich, P. M. E.; Wirges, C. T.; Manetto, A.; Carell, T., Postsynthetic DNA Modification Through the Copper-Catalyzed Azide-Alkyne Cycloaddition Reaction, *Angew. Chem., Int. Ed.* **2008,** 47, (44), 8350-8358.
62. Maeda, C.; Yamaguchi, S.; Ikeda, C.; Shinokubo, H.; Osuka, A., Dimeric Assemblies from 1,2,3-Triazole-Appended Zn(II) Porphyrins with Control of NH-Tautomerism in 1,2,3-Triazole, *Org. Lett.* **2008,** 10, (4), 549-552.
63. Locos, O. B.; Heindl, C. C.; Corral, A.; Senge, M. O.; Scanlan, E. M., Efficient Synthesis of Glycoporphyrins by Microwave-Mediated "Click" Reactions, *Eur. J. Org. Chem.* **2010**, (6), 1026-1028.
64. Shetti, V. S.; Ravikanth, M., Synthesis of Triazole-Bridged Unsymmetrical Porphyrin Dyads and Porphyrin-Ferrocene Conjugates, *Eur. J. Org. Chem.* **2010**, (3), 494-508.
65. Palacin, T.; Khanh, H. L.; Jousselme, B.; Jegou, P.; Filoramo, A.; Ehli, C.; Guldi, D. M.; Campidelli, S., Efficient Functionalization of Carbon Nanotubes with Porphyrin Pendrons via Click Chemistry, *J. Am. Chem. Soc.* **2009,** 131, (42), 15394-15402.
66. Hao, E.; Jensen, T. J.; Vicente, M. G. H., Synthesis of Porphyrin-Carbohydrate Conjugates Using "Click" Chemistry and their Preliminary Evaluation in Human HEp2 cells, *J. Porphyrins Phthalocyanines* **2009,** 13, (1), 51-59.

67. Fazio, M. A.; Lee, O. P.; Schuster, D. I., First Triazole-Linked Porphyrin-Fullerene Dyads, *Org. Lett.* **2008,** 10, (21), 4979-4982.

68. Severac, M.; Le Pleux, L.; Scarpaci, A.; Blart, E.; Odobel, F., Synthesis of New Azido Porphyrins and their Reactivity in Copper(I)-Catalyzed Huisgen 1,3-Dipolar Cycloaddition Reaction with Alkynes, *Tetrahedron Lett.* **2007,** 48, (37), 6518-6522.

69. Shen, D.-M.; Liu, C.; Chen, Q.-Y., Synthesis and Versatile Reactions of Beta-Azidotetraarylporphyrins, *Eur. J. Org. Chem.* **2007**, (9), 1419-1422.

70. Jayawickramarajah, J.; Tagore, D. M.; Tsou, L. K.; Hamilton, A. D., Allosteric Control of Self-Assembly: Modulating the Formation of Guanine Quadruplexes Through Orthogonal Aromatic Interactions, *Angew. Chem., Int. Ed.* **2007,** 46, (40), 7583-7586.

71. Guckian, K. M.; Schweitzer, B. A.; Ren, R. X. F.; Sheils, C. J.; Tahmassebi, D. C.; Kool, E. T., Factors Contributing to Aromatic Stacking in Water: Evaluation in the Context of DNA, *J. Am. Chem. Soc.* **2000,** 122, (10), 2213-2222.

72. Guckian, K. M.; Schweitzer, B. A.; Ren, R. X. F.; Sheils, C. J.; Paris, P. L.; Kool, E. T., Experimental Measurement of Aromatic Stacking Affinities in the Context of Duplex DNA, *J. Am. Chem. Soc.* **1996,** 118, (34), 8182-8183.

73. gIsaksson, J.; Chattopadhyaya, J., A Uniform Mechanism Correlating Dangling-End Stabilization and Stacking Geometry, *Biochemistry* **2005,** 44, (14), 5390-5401.

74. Bouamaied, I.; Stulz, E., Porphyrin-Substituted Dinucleotides: Synthesis and Spectroscopy, *Chimia* **2005,** 59, (3), 101-104.

75. Bouamaied, I.; Stulz, E., Synthesis and Spectroscopic Properties of Porphyrin-Substituted Uridine and Deoxyuridine, *Synlett* **2004**, (9), 1579-1583.

76. Berman, A.; Izraeli, E. S.; Levanon, H.; Wang, B.; Sessler, J. L., Photoinduced Intraensemble Electron Transfer in a Base-Paired Porphyrin-Quinone System. Time-Resolved EPR Spectroscopy, *J. Am. Chem. Soc.* **1995,** 117, (31), 8252-8257.

77. Sessler, J. L.; Wang, B.; Harriman, A., Photoinduced Energy Transfer in Associated, but Noncovalently-Linked Photosynthetic Model Systems, *J. Am. Chem. Soc.* **1995,** 117, (2), 704-714.

78. Bonfantini, E. E.; Burrell, A. K.; Officer, D. L.; Reid, D. C. W.; McDonald, M. R.; Cocks, P. A.; Gordon, K. C., Synthesis, Characterization, Structure,

Electrochemistry, and Spectroscopy of Porphyrins that have a Conjugated Connection to Donor/Acceptor Groups, *Inorg. Chem.* **1997,** 36, (27), 6270-6278.

79. Bonfantini, E. E.; Officer, D. L., The Synthesis of Butadiene-Bridged Porphyrin Dimers and Styrylporphyrins using a Porphyrin-Derived Wittig Reagent, *Tetrahedron Lett.* **1993,** 34, (52), 8531-8534.
80. Stephenson, A. W. I.; Wagner, P.; Partridge, A. C.; Jolley, K. W.; Filichev, V. V.; Officer, D. L., An Alternative Synthesis of Beta-Pyrrolic Acetylene-Substituted Porphyrins, *Tetrahedron Lett.* **2008,** 49, (39), 5632-5635.
81. Lembo, A.; Tagliatesta, P.; Guldi, D. M., Synthesis and Photophysical Investigation of New Porphyrin Derivatives with beta-Pyrrole Ethynyl Linkage and Corresponding Dyad with [60]Fullerene, *J. Phys. Chem. A* **2006,** 110, (40), 11424-11434.
82. Nath, M.; Huffman, J. C.; Zaleski, J. M., Accelerated Bergman Cyclization of Porphyrinic-Enediynes, *Chem. Commun.* **2003**, (7), 858-859.
83. Nath, M.; Huffman, J. C.; Zaleski, J. M., Ambient Temperature Activation of Haloporphyrinic-Enediynes: Electronic Contributions to Bergman Cycloaromatization, *J. Am. Chem. Soc.* **2003,** 125, (38), 11484-11485.
84. Nath, M.; Pink, M.; Zaleski, J. M., Controlling Both Ground- and Excited-State Thermal Barriers to Bergman Cyclization with Alkyne Termini Substitution, *J. Am. Chem. Soc.* **2005,** 127, (2), 478-479.
85. Chandra, T.; Kraft, B. J.; Huffman, J. C.; Zaleski, J. M., Synthesis and Structural Characterization of Porphyrinic Enediynes: Geometric and Electronic Effects on Thermal and Photochemical Reactivity, *Inorg. Chem.* **2003,** 42, (17), 5158-5172.
86. Aihara, H.; Jaquinod, L.; Nurco, D. J.; Smith, K. M., Multicarbocycle formation Mediated by Arenoporphyrin 1,4-diradicals: Synthesis of Picenoporphyrins, *Angew. Chem., Int. Ed.* **2001,** 40, (18), 3439-3441.
87. Bonfantini, E. E.; Burrell, A. K.; Campbell, W. M.; Crossley, M. J.; Gosper, J. J.; Harding, M. M.; Officer, D. L.; Reid, D. C. W., Efficient Synthesis of Free-Base 2-Formyl-5,10,15,20-tetraarylporphyrins, their Reduction and Conversion to [(Porphyrin-2-yl)methyl]phosphonium Salts, *J. Porphyrins Phthalocyanines* **2002,** 6, (11 & 12), 708-719.

88. Campbell, W. M.; Burrell, A. K.; Officer, D. L.; Jolley, K. W., Porphyrins as Light Harvesters in the Dye-sensitized TiO_2 Solar Cell, *Coord. Chem. Rev.* **2004,** 248, (13-14), 1363-1379.

89. Campbell, W. M.; Jolley, K. W.; Wagner, P.; Wagner, K.; Walsh, P. J.; Gordon, K. C.; Schmidt-Mende, L.; Nazeeruddin, M. K.; Wang, Q.; Graetzel, M.; Officer, D. L., Highly Efficient Porphyrin Sensitizers for Dye-Sensitized Solar Cells, *J. Phys. Chem. C* **2007,** 111, (32), 11760-11762.

90. Duffy, P. E.; Quinn, S. M.; Roche, H. M.; Evans, P., Synthesis of Trans-Vaccenic Acid and cis-9-Trans-11-Conjugated Linoleic Acid, *Tetrahedron* **2006,** 62, (20), 4838-4843.

91. Reid, D. C. W. *A Building Block Approach to Porphyrin Arrays.* Massey University, Palmerston North, **1998**.

92. Campbell Wayne, M. *Ferrocene Functionalised Porphyrins.* Massey University, Palmerston North, **1997**.

93. Aksenova, E. A.; Mironov, A. F., The Synthesis of New Porphyrin-Quinone Dyad Systems, *Russ. J. Bioorg. Chem.* **2001,** 27, (1), 50-56.

94. Alonso, C. M. A.; Neves, M. G. P. M. S.; Tome, A. C.; Silva, A. M. S.; Cavaleiro, J. A. S., Beta-Imino-meso-tetraphenylporphyrin Derivatives in Hetero-Diels-Alder Reactions, *Eur. J. Org. Chem.* **2004**, (15), 3233-3239.

95. Silva, A. M. G.; Lacerda, P. S. S.; Tome, A. C.; Neves, M. G. P. M. S.; Silva, A. M. S.; Cavaleiro, J. A. S.; Makarova, E. A.; Lukyanets, E. A., Porphyrins in 1,3-Dipolar Cycloaddition Reactions. Synthesis of New Porphyrin-Chlorin and Porphyrin-Tetraazachlorin Dyads, *J. Org. Chem.* **2006,** 71, (22), 8352-8356.

96. Zhu, J.; Zhao, X.; Gao, Y.; Cao, S., Synthesis of Asymmetric meso-Tetraphenylporphyrin Mono-Substituted with a Formyl-Ferrocene Schiff-Base at the Beta-Position, *Huaxue Tongbao* **2005,** 68, (9), 101-105.

97. Baldwin, J. E.; Crossley, M. J.; DeBernardis, J., Efficient Peripheral Functionalization of Porphyrins, *Tetrahedron* **1982,** 38, (5), 685-692.

98. Lee, J.; Kim, Y.; Kang, S. K.; Choi, I.; Yi, J., Synthesis of trans-Substituted Porphyrin Building Blocks Containing Two S-trityl or Thiol Groups, *Korean J. Chem. Eng.* **2006,** 23, (3), 512-515.

99. Firouzabadi, H.; Iranpoor, N.; Sobhani, S., PPh_3/DDQ as a Neutral System for the Facile Preparation of Diethyl Alpha-Bromo, Alpha-Iodo and Alpha-

Azidophosphonates from Diethyl Alpha-Hydroxyphosphonates, *Tetrahedron* **2004,** 60, (1), 203-210.

100. Katritzky, A. R.; Rogovoy, B. V.; Mitrokhin, A. Y., The Preparation of Diarylacetylenes via Diphenyl (Benzotriazol-1-yl)(aryl)methylphosphonates, *ARKIVOC* **2002**, (13), 17-27.
101. De Mico, A.; Margarita, R.; Parlanti, L.; Vescovi, A.; Piancatelli, G., A Versatile and Highly Selective Hypervalent Iodine(III)/2,2,6,6-Tetramethyl-1-piperidinyloxyl-Mediated Oxidation of Alcohols to Carbonyl Compounds, *J. Org. Chem.* **1997,** 62, (20), 6974-6977.
102. Halimjani, A.; Saidi, M., Sodium Borohydride-solid $LiClO_4$. An Effective Reagent for Reducing Aldehydes and Ketones in Aprotic Solvent, *Synth. Commun.* **2005,** 35, (17), 2271-2276.
103. Kondo, K.; Ohnishi, N.; Takemoto, K.; Yoshida, H.; Yoshida, K., Synthesis of Optically Quadratic Nonlinear Phenylpyridylacetylenes, *J. Org. Chem.* **1992,** 57, (5), 1622-1625.
104. El-Sagheer, A. H.; Brown, T., Click Chemistry with DNA, *Chem. Soc. Rev.* **2010,** 39, (4), 1388-1405.
105. Wen, L.; Li, M.; Schlenoff, J. B., Polyporphyrin Thin Films from the Interfacial Polymerization of Mercaptoporphyrins, *J. Am. Chem. Soc.* **1997,** 119, (33), 7726-7733.
106. Barbe, J.-M.; Canard, G.; Brandes, S.; Guilard, R., Synthesis and Physicochemical Characterization of meso-Functionalized Corroles: Precursors of Organic-Inorganic Hybrid Materials, *Eur. J. Org. Chem.* **2005**, (21), 4601-4611.
107. Mozer, A. J.; Griffith, M. J.; Tsekouras, G.; Wagner, P.; Wallace, G. G.; Mori, S.; Sunahara, K.; Miyashita, M.; Earles, J. C.; Gordon, K. C.; Du, L.; Katoh, R.; Furube, A.; Officer, D. L., Zn-Zn Porphyrin Dimer-Sensitized Solar Cells: Toward 3-D Light Harvesting, *J. Am. Chem. Soc.* **2009,** 131, (43), 15621-15623.
108. Annoni, E.; Pizzotti, M.; Ugo, R.; Quici, S.; Morotti, T.; Bruschi, M.; Mussini, P., Synthesis, Electronic Characterization and Significant Second-Order Non-Linear Optical Responses of meso-Tetraphenylporphyrins and their ZnII Complexes Carrying a Push or Pull Group in the Beta-Pyrrolic Position, *Eur. J. Inorg. Chem.* **2005**, (19), 3857-3874.

109. Vail, S. A.; Schuster, D. I.; Guldi, D. M.; Isosomppi, M.; Tkachenko, N.; Lemmetyinen, H.; Palkar, A.; Echegoyen, L.; Chen, X.; Zhang, J. Z. H., Energy and electron transfer in beta -alkynyl-linked porphyrin-[60]fullerene dyads, *J. Phys. Chem. B* **2006,** 110, (29), 14155-14166.

110. Chinchilla, R.; Najera, C., The Sonogashira reaction: a booming methodology in synthetic organic chemistry, *Chem. Rev.* **2007,** 107, (3), 874-922.

111. Gao, G.-Y.; Ruppel, J. V.; Allen, D. B.; Chen, Y.; Zhang, X. P., Synthesis of Beta-Functionalized Porphyrins via Palladium-Catalyzed Carbon-Heteroatom Bond Formations: Expedient Entry into Beta-Chiral Porphyrins, *J. Org. Chem.* **2007,** 72, (24), 9060-9066.

112. Zhang, C.; Suslick, K. S., Syntheses of Boronic-Acid-Appended Metalloporphyrins as Potential Colorimetric Sensors for Sugars and Carbohydrates, *J. Porphyrins Phthalocyanines* **2005,** 9, (9), 659-666.

113. Liu, C.; Shen, D.-M.; Chen, Q.-Y., Unexpected Bromination Ring-Opening of Tetraarylporphyrins, *Chem. Commun.* **2006**, (7), 770-772.

114. Takanami, T.; Hayashi, M.; Chijimatsu, H.; Inoue, W.; Suda, K., Palladium-Catalyzed Cyanation of Porphyrins Utilizing Cyanoethylzinc Bromide as an Efficient Cyanide Ion Source, *Org. Lett.* **2005,** 7, (18), 3937-3940.

115. Ali, H.; Van Lier, J. E., Phenylselenyl Halides: Efficient Reagents for the Selective Halogenation and Nitration of Porphyrins, *Tetrahedron Lett.* **1991,** 32, (38), 5015-5018.

116. Anderson, H. L.; Sanders, J. K. M., Synthesis of a Cyclic Porphyrin Trimer with a Semi-Rigid Cavity, *J. Chem. Soc.* **1989**, (22), 1714-1715.

117. Ljungdahl, T.; Pettersson, K.; Albinsson, B.; Maartensson, J., Solvent and Base Dependence of Copper-Free Palladium-Catalyzed Cross-Couplings between Terminal Alkynes and Arylic Iodides: Development of Efficient Conditions for the Construction of Gold(III)/Free-Base Porphyrin Dimers, *J. Org. Chem.* **2006,** 71, (4), 1677-1687.

118. Nazeeruddin, M. K.; Pechy, P.; Renouard, T.; Zakeeruddin, S. M.; Humphry-Baker, R.; Comte, P.; Liska, P.; Cevey, L.; Costa, E.; Shklover, V.; Spiccia, L.; Deacon, G. B.; Bignozzi, C. A.; Graetzel, M., Engineering of Efficient Panchromatic Sensitizers for Nanocrystalline TiO_2-Based Solar Cells, *J. Am. Chem. Soc.* **2001,** 123, (8), 1613-1624.

119. Nazeeruddin, M. K.; Humphry-Baker, R.; Officer, D. L.; Campbell, W. M.; Burrell, A. K.; Graetzel, M., Application of Metalloporphyrins in Nanocrystalline Dye-Sensitized Solar Cells for Conversion of Sunlight into Electricity, *Langmuir* **2004,** 20, (15), 6514-6517.

120. Schmidt-Mende, L.; Campbell Wayne, M.; Wang, Q.; Jolley Kenneth, W.; Officer David, L.; Nazeeruddin Md, K.; Gratzel, M., Zn-Porphyrin-Sensitized Nanocrystalline TiO_2 Heterojunction Photovoltaic Cells, *ChemPhysChem* **2005,** 6, (7), 1253-1258.

121. Wang, Q.; Campbell, W. M.; Bonfantani, E. E.; Jolley, K. W.; Officer, D. L.; Walsh, P. J.; Gordon, K.; Humphry-Baker, R.; Nazeeruddin, M. K.; Graetzel, M., Efficient Light Harvesting by Using Green Zn-Porphyrin-Sensitized Nanocrystalline TiO_2 Films, *J. Phys. Chem. B* **2005,** 109, (32), 15397-15409.

122. Kondo, K.; Fujitani, T.; Ohnishi, N., Synthesis and Non-Linear Properties of Disubstituted Diphenylacetylene and Related Compounds, *J. Mat. Chem.* **1997,** 7, (3), 429-433.

123. Gallagher, M. J.; Noerdin, H., The Synthesis and Photochemistry of p-Dimethylamino-p'-nitrodiphenylethyne: a Push-Pull Acetylene, *Aust. J. Chem.* **1985,** 38, (6), 997-1005.

124. Kusurkar, R.; Goswami, S.; Vyas, S., Reactions of Vilsmeier-Haack Reagent with Aromatic and Heterocyclic Aldoximes, *Indian J. Chem., Sect. B: Org. Chem. Incl. Med. Chem.* **2003,** 42B, (12), 3148-3151.

125. Rao, K. V. V. P.; Dandala, R.; Handa, V. K.; Rao, I. V. S.; Rani, A.; Shivashankar, S.; Naidu, A., A Novel Approach for the Conversion of Primary Amides into Tetrazoles by using Tributyltin Chloride and Aodium azide in the Presence of DMF, *Synlett* **2007**, (8), 1289-1293.

126. Su, J.; McKittrick, B. A.; Tang, H.; Burnett, D. A.; Clader, J. W.; Greenlee, W. J.; Hawes, B. E.; O'Neill, K.; Spar, B.; Weig, B.; Kowalski, T.; Sorota, S.; Li, C.; Liu, T., SAR Study of Bicyclo[4.1.0]heptanes as Melanin-Concentrating Hormone Receptor R1 Antagonists: Taming hERG, *Bioorg. Med. Chem.* **2007,** 15, (16), 5369-5385.

127. Earles, J. C., Otago University, Dunedin, Manuscript in preparation.

128. Wang, Q.; Campbell Wayne, M.; Bonfantani Edia, E.; Jolley Kenneth, W.; Officer David, L.; Walsh Penny, J.; Gordon, K.; Humphry-Baker, R.; Nazeeruddin Mohammad, K.; Gratzel, M., Efficient Light Harvesting by Using

Green Zn-Porphyrin-Sensitized Nanocrystalline TiO_2 Films, *J. Phys Chem B* **2005,** 109, (32), 15397-15409.

129. Walsh, P. J.; Gordon, K. C.; Wagner, P.; Officer, D. L., Resonance Raman Studies of Beta-substituted Porphyrin Systems with Unusual Electronic Absorption Properties, *ChemPhysChem* **2006,** 7, (11), 2358-2365.
130. Ali, H.; van Lier, J. E., Synthesis of Beta-substituted Porphyrins using Palladium Catalyzed Reactions, *Tetrahedron* **1994,** 50, (41), 11933-11944.
131. Burrell, A. K.; Officer, D. L.; Reid, D. C. W., Aldehyde-Appended Tetraphenylporphyrin: a New Building Block for Porphyrin Arrays, *Angew. Chem., Int. Ed.* **1995,** 34, (8), 900-902.
132. Walsh, P. J.; Gordon, K. C.; Officer, D. L.; Campbell, W. M., A DFT study of the Optical Properties of Substituted Zn(II)TPP complexes, *Theochem* **2006,** 759, (1-3), 17-24.
133. Okahata, Y.; Tanaka, K., Oriented Thin Films of a DNA-Lipid Complex, *Thin Solid Films* **1996,** 284-285, 6-8.
134. Okahata, Y.; Kobayashi, T.; Nakayama, H.; Tanaka, K., DNA-Aligned Cast Film and its Anisotropic Electron Conductivity, *Supramol. Sci.* **1998,** 5, (3-4), 317-320.
135. Paramasivan, S.; Rujan, I.; Bolton, P. H., Circular Dichroism of Quadruplex DNAs: Applications to Structure, Cation Effects and Ligand Binding, *Methods* **2007,** 43, (4), 324-331.
136. Graham, D.; Parkinson, J. A.; Brown, T., DNA Duplexes Stabilized by Modified Monomer Residues: Synthesis and Stability, *J. Chem. Soc., Perkin Trans. 1* **1998**, (6), 1131-1138.
137. Geci, I.; Filichev, V. V.; Pedersen, E. B., Synthesis of Twisted Intercalating Nucleic Acids Possessing Acridine Derivatives. Thermal Stability Studies, *Bioconjugate Chem.* **2006,** 17, (4), 950-957.
138. Filichev, V. V.; Pedersen, E. B., Stable and Selective Formation of Hoogsteen-Type Triplexes and Duplexes Using Twisted Intercalating Nucleic Acids (TINA) Prepared via Postsynthetic Sonogashira Solid-Phase Coupling Reactions, *J. Am. Chem. Soc.* **2005,** 127, (42), 14849-14858.
139. Khan, S. I.; Grinstaff, M. W., Palladium(0)-Catalyzed Modification of Oligonucleotides during Automated Solid-Phase Synthesis, *J. Am. Chem. Soc.* **1999,** 121, (19), 4704-4705.

140. Beilstein, A. E.; Grinstaff, M. W., On-Column Derivatization of Oligodeoxynucleotides with Ferrocene, *Chem. Commun.* **2000**, (6), 509-510.

141. Rist, M.; Amann, N.; Wagenknecht, H.-A., Preparation of 1-Ethynylpyrene-Modified DNA via Sonogashira-type Solid-Phase Couplings and Characterization of the Fluorescence Properties for Electron-Transfer sStudies, *Eur. J. Org. Chem.* **2003**, (13), 2498-2504.

142. Mayer, E.; Valis, L.; Wagner, C.; Rist, M.; Amann, N.; Wagenknecht, H.-A., 1-Ethynyl-Pyrene as a Tunable and Versatile Molecular Beacon for DNA, *ChemBioChem* **2004,** 5, (6), 865-868.

143. Meldal, M.; Tornoe, C. W., Cu-Catalyzed Azide-Alkyne Cycloaddition, *Chem. Rev.* **2008,** 108, (8), 2952-3015.

144. Geci, I.; Filichev, V. V.; Pedersen, E. B., Stabilization of Parallel Triplexes by Twisted Intercalating Nucleic Acids (TINAs) Incorporating 1,2,3-Triazole Units and Prepared by Microwave-Accelerated Click Chemistry, *Chem. Eur. J.* **2007,** 13, (22), 6379-6386.

145. Lietard, J.; Meyer, A.; Vasseur, J.-J.; Morvan, F., New Strategies for Cyclization and Bicyclization of Oligonucleotides by Click Chemistry Assisted by Microwaves, *J. Org. Chem.* **2008,** 73, (1), 191-200.

146. Bouillon, C.; Meyer, A.; Vidal, S.; Jochum, A.; Chevolot, Y.; Cloarec, J.-P.; Praly, J.-P.; Vasseur, J.-J.; Morvan, F., Microwave Assisted "Click" Chemistry for the Synthesis of Multiple Labeled-Carbohydrate Oligonucleotides on Solid Support, *J. Org. Chem.* **2006,** 71, (12), 4700-4702.

147. Weller, R. L.; Rajski, S. R., DNA Methyltransferase-Moderated Click Chemistry, *Org. Lett.* **2005,** 7, (11), 2141-2144.

148. Mathur, V.; Verma, A.; Maiti, S.; Chowdhury, S., Thermodynamics of i-Tetraplex Formation in the Nuclease Hypersensitive Element of Human c-myc Promoter, *Biochem. Biophys. Res. Commun.* **2004,** 320, (4), 1220-1227.

149. Manzini, G.; Yathindra, N.; Xodo, L. E., Evidence for Intramolecularly Folded i-DNA Structures in Biologically Relevant CCC-Repeat Sequences, *Nucleic Acids Res.* **1994,** 22, (22), 4634-4640.

150. Boutorine, A. S.; Escude, C., Biophysical Analysis of Triplex-Helix Formation, *Current Protocols in Nucleic Acid Chemistry* **2007**, Unit 7.12.

151. Weiner, S. J.; Kollman, P. A.; Case, D. A.; Singh, U. C.; Ghio, C.; Alagona, G.; Profeta, S., Jr.; Weiner, P., A New Force Field for Molecular Mechanical

Simulation of Nucleic Acids and Proteins, *J. Am. Chem. Soc.* **1984,** 106, (3), 765-784.

152. Weiner, S. J.; Kollman, P. A.; Nguyen, D. T.; Case, D. A., An All Atom Force Field for Simulations of Proteins and Nucleic Acids, *J. Comput. Chem.* **1986,** 7, (2), 230-252.
153. Filichev, V. V.; Gaber, H.; Olsen, T. R.; Jorgensen, P. T.; Jessen, C. H.; Pedersen, E. B., Twisted Intercalating Nucleic Acids - Intercalator Influence on Parallel Triplex Stabilities, *Eur. J. Org. Chem.* **2006**, (17), 3960-3968.
154. Manzini, G.; Xodo, L. E.; Gasparotto, D.; Quadrifoglio, F.; van der Marel, G. A.; van Boom, J. H., Triple Helix Formation by Oligopurine-Oligopyrimidine DNA Fragments. Electrophoretic and Thermodynamic Behavior, *J. Mol. Biol.* **1990,** 213, (4), 833-843.
155. Sugunan, S. K.; Tripathy, U.; Brunet, S. M. K.; Paige, M. F.; Steer, R. P., Mechanisms of Low-Power Noncoherent Photon Upconversion in Metalloporphyrin-Organic Blue Emitter Systems in Solution, *J. Phys. Chem.* **2009,** 113, (30), 8548-8556.
156. Kolarova, H.; Nevrelova, P.; Tomankova, K.; Kolar, P.; Bajgar, R.; Mosinger, J., Production of Reactive Oxygen Species after Photodynamic Therapy by Porphyrin Sensitizers, *Gen. Physiol. Biophys.* **2008,** 27, (2), 101-105.
157. Grotli, M.; Douglas, M.; Eritja, R.; Sproat, B. S., 2'-O-Propargyl Oligoribonucleotides: Synthesis and Hybridization, *Tetrahedron* **1998,** 54, (22), 5899-5914.
158. Berndl, S.; Herzig, N.; Kele, P.; Lachmann, D.; Li, X.; Wolfbeis, O. S.; Wagenknecht, H.-A., Comparison of a Nucleosidic vs. Non-Nucleosidic Postsynthetic "Click" Modification of DNA with Base-Labile Fluorescent Probes, *Bioconjugate Chem.* **2009,** 20, (3), 558-564.
159. Kadish, K. M.; Smith, K. M.; Guilard, R., *The Porphyrin Handbook*. Academic Press: London, **2000;** Vol. 8, p 205.
160. Li, T.; Wang, E.; Dong, S., G-quadruplex-based DNAzyme for Facile Colorimetric Detection of Thrombin, *Chem. Commun.* **2008**, (31), 3654-3656.
161. *CRC Handbook of Chemistry and Physics*. 70 ed.; CRC Press: Florida, **1989**.
162. Cenini, S.; Gallo, E.; Caselli, A.; Ragaini, F.; Fantauzzi, S.; Piangiolino, C., Coordination Chemistry of Organic Azides and Amination Reactions Catalyzed

by Transition Metal Complexes, *Coord. Chem. Rev.* **2006,** 250, (11+12), 1234-1253.

163. Dori, Z.; Ziolo, R. F., Chemistry of Coordinated Azides, *Chem. Rev.* **1973,** 73, (3), 247-254.
164. Hunter, C. A.; Sanders, J. K. M., The Nature of π-π Interactions, *J. Am. Chem. Soc.* **1990,** 112, (14), 5525-5534.
165. Astakhova, I. V.; Korshun, V. A.; Wengel, J., Highly Fluorescent Conjugated Pyrenes in Nucleic Acid Probes: (Phenylethynyl)pyrenecarbonyl-Functionalized Locked Nucleic Acids, *Chem. Eur. J.* **2008,** 14, (35), 11010-11026.
166. Kalek, M.; Madsen, A. S.; Wengel, J., Effective Modulation of DNA Duplex Stability by Reversible Transition Metal Complex Formation in the Minor Groove, *J. Am. Chem. Soc.* **2007,** 129, (30), 9392-9400.
167. Babu, B. R.; Hrdlicka, P. J.; McKenzie, C. J.; Wengel, J., Optimized DNA Targeting using N,N-Bis(2-pyridylmethyl)-beta-alanyl 2'-Amino-LNA, *Chem. Commun.* **2005**, (13), 1705-1707.
168. Hrdlicka, P. J.; Babu, B. R.; Sorensen, M. D.; Wengel, J., Interstrand Communication Between 2'-N-(Pyren-1-yl)methyl-2'-amino-LNA Monomers in Nucleic Acid Duplexes: Directional Control and Signalling of Full Complementarity, *Chem. Commun.* **2004**, (13), 1478-1479.
169. Dioubankova, N. N.; Malakhov, A. D.; Shenkarev, Z. O.; Korshun, V. A., Oligonucleotides Containing New Fluorescent 1-Phenylethynylpyrene and 9,10-Bis(phenylethynyl)anthracene Uridine-2'-Carbamates: Synthesis and Properties, *Tetrahedron* **2004,** 60, (21), 4617-4626.
170. Nakamura, M.; Murakami, Y.; Sasa, K.; Hayashi, H.; Yamana, K., Pyrene-Zipper Array Assembled via RNA Duplex Formation, *J. Am. Chem. Soc.* **2008,** 130, (22), 6904-6905.
171. Nakamura, M.; Shimomura, Y.; Ohtoshi, Y.; Sasa, K.; Hayashi, H.; Nakano, H.; Yamana, K., Pyrene Aromatic Arrays on RNA Duplexes as Helical Templates, *Org. Biomol. Chem.* **2007,** 5, (12), 1945-1951.
172. Nakamura, M.; Ohtoshi, Y.; Yamana, K., Helical Pyrene-Array along the Outside of Duplex RNA, *Chem. Commun.* **2005**, (41), 5163-5165.
173. Gupta, P.; Langkjaer, N.; Wengel, J., Synthesis and Biophysical Studies of Coronene Functionalized 2'-Amino-LNA: A Novel Class of Fluorescent Nucleic Acids, *Bioconjugate Chem.* **2010,** 21, (3), 513-520.

174. Pasternack, R. F.; Caccam, M.; Keogh, B.; Stephenson, T. A.; Williams, A. P.; Gibbs, E. J., Long-Range Fluorescence Quenching of Ethidium Ion by Cationic Porphyrins in the Presence of DNA, *J. Am. Chem. Soc.* **1991,** 113, (18), 6835-6840.

175. Gutsmiedl, K.; Fazio, D.; Carell, T., High-density DNA Functionalization by a Combination of Cu-Catalyzed and Cu-Free Click Chemistry, *Chem. Eur. J.* **2010,** 16, (23), 6877-6883.

176. Singh, I.; Vyle, J. S.; Heaney, F., Fast, copper-free click chemistry: A Convenient Solid-Phase Approach to Oligonucleotide Conjugation, *Chem. Commun.* **2009**, (22), 3276-3278.

177. Tanaka, K.; Inafuku, K.; Chujo, Y., Environment-Responsive Upconversion Based on Dendrimer-Supported Efficient Triplet-Triplet Annihilation in Aqueous Media, *Chem. Commun.* **2010,** 46, (24), 4378-4380.

178. Baluschev, S.; Miteva, T.; Yakutkin, V.; Nelles, G.; Yasuda, A.; Wegner, G., Up-Conversion Fluorescence: Noncoherent Excitation by Sunlight, *Phys. Rev. Lett.* **2006,** 97, (14), 143903.

179. Vassiliou, S.; Xeilari, M.; Yiotakis, A.; Grembecka, J.; Pawelczak, M.; Kafarski, P.; Mucha, A., A Synthetic Method for Diversification of the P1' Substituent in Phosphinic Dipeptides as a Tool for Exploration of the Specificity of the S1' Binding Pockets of Leucine Aminopeptidases, *Bioorg. Med. Chem.* **2007,** 15, (9), 3187-3200.